National Library of Canada
Acquisitions and Bibliographic Services Branch
395 Wellington Street
Ottawa, Ontario
K1A 0N4

Bibliothèque nationale du Canada
Direction des acquisitions et des services bibliographiques
395, rue Wellington
Ottawa (Ontario)
K1A 0N4

Your file Votre référence

Our file Notre référence

NOTICE

The quality of this microform is heavily dependent upon the quality of the original thesis submitted for microfilming. Every effort has been made to ensure the highest quality of reproduction possible.

If pages are missing, contact the university which granted the degree.

Some pages may have indistinct print especially if the original pages were typed with a poor typewriter ribbon or if the university sent us an inferior photocopy.

AVIS

La qualité de cette microforme dépend grandement de la qualité de la thèse soumise au microfilmage. Nous avons tout fait pour assurer une qualité supérieure de reproduction.

S'il manque des pages, veuillez communiquer avec l'université qui a conféré le grade.

La qualité d'impression de certaines pages peut laisser à désirer, surtout si les pages originales ont été dactylographiées à l'aide d'un ruban usé ou si l'université nous a fait parvenir une photocopie de qualité inférieure.

Canada

High speed deflagration and its transition to detonation

by

Randy Shek-Ming Chue

A thesis submitted to the
Faculty of Graduate Studies and Research
in partial fulfillment of the requirements for the degree of
Doctor of Philosophy
in
Mechanical Engineering

Department of Mechanical Engineering
McGill University
Montréal, Québec
June 1993

ISBN 0-315-91875-6

Canada

Abstract

The transition from deflagration to detonation is studied by focusing on the actual final process, i.e. the onset of detonation itself. The high speed deflagration prior to transition is obtained by suppressing the oscillatory structure of a detonation first. A theoretical model is developed to analyze the resulting deflagration complex which shows that it propagates close to half the CJ detonation velocity with the deflagration slowly separating from the leading shock. These high speed deflagrations thus obtained just prior to transition to detonation as well as the highly turbulent fast deflagrations that have been observed prior to transition in earlier studies are shown to be CJ deflagrations where the propagation velocities are governed by energetics rather than the flow structure.

To understand how the nonsteady behavior of detonations may affect the transition process, the one-dimensional pulsating detonation is analyzed by computational studies. The time averaged solution of the non-overdriven detonation over a cycle is found to recover the steady CJ solution and the independence of the far rearward boundary condition is demonstrated for the activation energies studied. The self-oscillatory nature of the detonation also plays a key role in the maintenance, failure, and re-establishment of the detonation structure. To study the onset of detonation, the high speed deflagration obtained by failing the detonation is subsequently perturbed with periodic disturbances to stimulate transition. The numerical simulations show that the perturbations undergo a frequency selective amplification process to accelerate transition where the optimal frequency is related to the chemical reaction time of the detonation. The existence of optimal perturbation frequencies to stimulate transition is also observed in the experimental investigation carried out, although its value appears to depend on the channel dimension. Based on the oscillatory and frequency selective nature of the detonation phenomena, an oscillator model is proposed. An equation that has the basic features of a mechanical oscillator has been derived for the pulsating detonation. The proposed oscillator concept indicates the need to examine detonation phenomena from the point of view of a resonant oscillator.

Résumé

La transition déflagration-détonation a été étudié en se concentrant sur la phase finale, c'est à dire l'établissement de la détonation elle-même. La déflagration rapide avant le régime de transition est obtenue en supprimant la structure oscillatoire de la détonation. Un model théorique a été developpé dans le but d'analyser le mécanisme complexe de cette déflagration se propageant a une célérité prôche de la moitié de la célérité de détonation Chapman-Jouguet (CJ), tout en se découplant de l'onde de choc de tête. Il a pu être démontré que les déflagrations rapides et les déflagrations très turbulentes précèdant la transition vers la détonation sont en fait des déflagrations CJ dont les célérités de propagation sont determinées par l'énergétique plutôt que par l'hydro-dynamic.

Afin de comprendre l'influence du comportement instable de la détonation sur le processus de transition, une détonation uni-dimensionelle oscillante a été modèlisée lors d'une étude numérique. La moyenne de la solution dans le temps sur un cycle pour une détonation non-surdétonative tend vers la solution stable CJ et s'avère indépendente des conditions aux limites loin en amont dans la gamme d'énergie d'activation étudiée. La nature auto-oscillatoire de la détonation joue un rôle clé dans l'entretient, l'amortissement, et le re-établissement de la structure de la détonation. Afin d'étudier l'établissement de la détonation, une déflagration rapide obtenue en amortissant une détonation est soumise à des perturbations périodiques pour exciter la transition. Les simulations numériques ont montré que les perturbations subissaient un processus d'amplification fréquentiellement sélectif permettant d'accèlerer la transition vers la détonation. La fréquence optimale est liée au temps de réaction chimique. Les résultats experimentaux ont aussi montré l'existence d'une fréquence optimale de perturbation stimulant la transition, même s'il apparait que sa valeur semble dépendre des dimensions du tube. Un model théorique a été présenté sur la base d'un mécanisme de détonation oscillatoire et fréquentiellement selectif. Une équation ayant les caractèristiques d'un oscillateur mécanique a été dérivée dans le cadre d'une détonation pulsatoire. Le concept oscillatoire proposé indique clairement le besoin d'examiner le phenomène de la détonation d'un point de vue d'un oscillateur résonant.

To
Patricia
my love

Acknowledgements

I would like to express my sincere gratitude to Professor John Lee, my supervisor, for his continuous support and invaluable guidance throughout the course of this work. I have gained much from his keen physical insights and enthusiasm in science and education. I am also grateful to Professor David Frost for providing me guidance and support in many ways over the years. I would like to express my sincere thanks to Professor Rom Knystautas for his encouragement, stimulating discussions, and assistance on various aspects of the work.

Special thanks are due to Dr. Fan Zhang for the stimulating scientific exchanges, friendship, and moral support. I am also indebted to Professor Georgii Makhviladze of the Russian Academy of Sciences in Moscow, who during his visit at McGill University in 1991 to 1992 has worked very closely with me. I have benefited much from his overwhelming enthusiasm, valuable discussions, and friendship.

I would also like to thank Professor Anatoli Papyrin (Russian Academy of Sciences, Novosibirsk) for helping with the experimental set-up. A special thanks to Dr. Paul Thibault (Combustion Dynamics Ltd.) for making available his computer code and for the valuable discussions on the research materials. Many thanks to Mr. Julian Lee and Dr. Olivier Peraldi for the translation of the abstract into French.

The assistance and encouragement from all members of the Shock Wave Physics Group, past and present, during my stay at McGill is gratefully acknowledged.

Finally, I wish to express my deepest appreciation to my wife, Patricia, who must bear with my constant "non-existence" during the course of my doctoral studies.

Table of Contents

List of Figures

List of Tables

Nomenclature

A	Area
a	Acceleration (a_p = acceleration of piston)
c	Sound speed
D	Shock velocity; channel diameter (Chapter 5)
D_1	Fluctuating component of shock velocity divided by D_{CJ}
E	Activation energy
e	Specific energy, internal plus kinetic
e_i	Specific internal energy
F	Fluctuating component of shock displacement
f	Degree of overdrive, $f = (D/D_{CJ})^2$
I	Nondimensional volume-averaged energy in the detonation complex
k	Pre-exponential factor for Arrhenius reaction rate law
L	Length
L^*	Transition distance (Chapter 5)
l	Length of periodic perturbation (Chapter 4)
l_h	Hydrodynamic thickness of the pulsating detonation
M	Mach number
P	Pressure fluctuation in eqn. (6.6)
p	Pressure
Q	Heat of reaction
q	Normalized heat release in eqn. (2.21)
$\dot{q}$	Rate of heat release per unit mass
R	Specific gas constant
$\dot{R}_F$	Flame propagation velocity
$\dot{R}_S$	Shock propagation velocity
s	Obstacle spacing
T	Temperature
t	Time

t^* Time for re-transition, in units of $t_{1/2}$

t_0 Time at which periodic perturbations are placed ahead of the shock (Chapter 4)

$t_{1/2}$ Half reaction time

u Particle velocity

v Specific volume

V Volume

W Nondimensional volume averaged reaction rate in eqn. (6.20)

W_1 Fluctuating component of W

w Rate of consumption of reactant mass; phase parameter in eqn. (6.6)

x Spatial coordinate (Eulerian); ratio of initial to final volume (Chapter 2)

y Ratio of final to initial pressure (Chapter 2)

Greek symbols

α Reactant mass fraction. $\alpha = 1$ before reaction, $\alpha = 0$ when reaction is complete

β Parameter in Hugoniot equation (Chapter 2); constant in Duffing's equation

δ Constant in Duffing's equation

η $1/M^2$

γ Ratio of specific heats

Λ Wavelength of perturbation

λ Detonation cell size

μ Small parameter

ω Frequency

ρ Density

σ Constant in Duffing's equation

τ Period of pulsating detonation

τ_p Period of perturbation

ξ Lagrangian space parameter; nondimensional space variable $\xi = x/l_h$

Subscripts

$(\,)_0$ Initial undisturbed state

$(\,)_1$ Shocked state

$(\,)_2$ Burnt gas state

$(\,)_{1/2}$ Half-reaction in the steady-state ZND detonation

$(\,)_{CJ}$ Chapman-Jouguet state; steady ZND solution

$( )_F$ Flame

$( )_p$ Piston condition; perturbation parameter

$( )_s$ Shock (Chapter 2)

$( )_{sh}$ Shocked state

Superscripts

$( )^*$ Nondimensional quantities

$( )^0$ Steady state solution

Chapter 1

Introduction

1.1 Background

The propagation velocity of combustion waves can vary over a wide spectrum. A gaseous combustible mixture can propagate as a deflagration or as a detonation. In the deflagration regime, in the limit it can burn as a laminar flame that propagates at a velocity of the order of 0.5 m/s, or it may accelerate to a turbulent flame with velocities potentially orders of magnitude higher. The turbulent flame may also undergo transition to a detonation wave and propagate at velocities of about 2000 m/s. It is not surprising that a diverse variety of propagation mechanisms may possibly be involved corresponding to the observed four orders of magnitude of wave velocity. There are still numerous gaps in the knowledge of the vast family of combustion waves and every progress in understanding these phenomena will have considerable theoretical interest. In this thesis, I will concentrate my study on the high velocity regimes specifically to examine transition to detonation.

The ability to predict the occurrence and characteristics of detonation waves is also of great practical value. As the fastest mode of combustion and with its large power-density, detonation poses both a great concern for safety of possible explosion accidents as well as a challenge in harnessing it for potential future applications in propulsion systems. The feasibility of using oblique detonation waves in ram-jets is under current investigation for application to propulsion of a new generation of hypersonic vehicles.

1.2 The Genesis of Detonation

The basic goal of detonation research is to gain insight into the different aspects of the detonation phenomena, namely, its development, steady propagation, and failure. By now, it has been established that even the steady propagation of detonation waves involves periodic formation and failure of individual wavelets. No doubt, advances in the understanding of the formation process will contribute to a better description of the general behavior of detonations.

The formation of detonations can be realized in two ways: direct or blast initiation and transition from deflagration to detonation. Direct initiation will occur if a blast or shock wave is strong enough to auto-ignite the combustible mixture processed by it to form a detonation. For direct initiation, the energy of the source plays a key role in determining whether initiation is successful or not. If a sufficient amount of energy is released by the igniter, rapid auto-ignition takes place immediately behind the generated blast wave and the reaction coupled shock wave quickly becomes a Chapman-Jouguet (CJ) detonation. Below a certain critical value of igniter energy, the reaction front decouples from the leading shock wave and direct initiation is not achieved. For direct initiation, since the initiation is accomplished directly without first propagating as a deflagration, it has been appropriately referred to as direct initiation. Bach, Knystautas, and Lee (1969, 1971) have developed a theoretical model to treat direct initiation using reacting blast waves. A subsequent theory was later established by Lee, Knystautas, and Guirao (1982) to predict the minimum initiation energy for direct initiation. A comprehensive review of the blast initiation theory is given by Lee (1977).

Alternately, the combustible mixture can be ignited by a low energy igniter and burn as a slow deflagration. Under appropriate conditions, it can accelerate and undergo transition to detonation. This process is referred to as deflagration to detonation transition,

or DDT. Despite significant progress in studying DDT through many experimental as well as theoretical efforts, the underlying physics of this complex phenomena remains unclear.

1.3 Previous Works

Deflagration to detonation transition has been a subject of intense study for a long time.[1] From previous experimental works, the qualitative description of the processes of transition are quite well established: starting with weak ignition and the subsequent acceleration of the laminar flame to turbulent, all the way to the final stage of detonation onset. The photographic studies by the research group of Oppenheim are particularly noteworthy in elucidating the genesis of detonation. The details of the actual onset of detonation in smooth confined tubes have been revealed with unsurpassed clarity by their stroboscopic laser Schlieren photographic records (Urtiew and Oppenheim 1965, 1966, 1967, 1968; Meyer and Oppenheim 1971). The onset of detonation was observed to originate from localized regions in the turbulent flame brush (so-called hot spots). Localized explosions from these hot spots then become spherical detonation "bubbles" which grow to catch up with the leading shock front of the deflagration (Urtiew and Oppenheim 1965). The effect of compression waves emitted by the accelerating flame to induce onset was illustrated by their experiments and by analytical calculations (Laderman and Oppenheim 1961) which was derived from the work of Chu (1956). A numerical simulation of the flame acceleration process was later performed by Kurylo et al. (1979). The role of the leading shock in triggering auto-ignition and subsequent onset of detonation is also revealed where shock strengthening is accomplished by merging of compression waves and shocks ahead of the flame front (Urtiew and Oppenheim 1965, 1966), and by shock reflection at the closed end of a tube (Meyer and Oppenheim 1971, Laderman and Oppenheim 1961).

[1] The comprehensive review of the gaseous detonation and transition phenomena can be found in the recent papers by Lee (1991) and Shepherd and Lee (1992).

Although the events that lead to the final onset of detonation may vary, Oppenheim pointed out that the transition process observed essentially consists of an "explosion within explosion", as he has labeled the localized explosion center. This has remained the most plausible mechanism that leads to the onset of detonation and many theoretical studies have evolved around this concept. Modern asymptotic analyses have now been developed to investigate the formation of the explosion centers (e.g., Clarke 1978, 1979; Jackson, Kapila, and Stewart 1989; Almgren, Majda, and Rosales 1990). In essence, these analytical studies are concerned with the evolution of hot spots due to rapid shock wave development or localized pressure buildup in an explosive medium. Although these do indicate the possibility of explosion center formation, their physical interpretations are often handicapped amidst complex mathematics, and the results are dependent on the initial spatial inhomogeneities in the system which must be provided by other means. Moreover, the nature of these asymptotic analyses restricts the predictions to the initial growth, while the final development of detonation cannot be analyzed.

The physics of rapid shock wave amplification in detonation formation was more clearly elucidated by the studies of Zel'dovich and independently by Lee. Zel'dovich demonstrated that by controlling the temperature (or induction time) gradient of an initially quiescent reactive atmosphere, one can determine whether or not the resulting reaction wave will evolve into detonation (Zel'dovich et al. 1970, Zel'dovich 1980). Lee pointed out that the rapid shock amplification can be explained by the fact that the chemical energy release in the reaction front is synchronized with the propagation of the compression (or shock) wave (Lee et al. 1978, Yoshikawa 1980). The suggested interpretation was based upon the Rayleigh criterion of instability due to unsteady heat input which stated that "If heat be given to the air at the moment of greatest condensation, or taken from it at the moment of greatest rarefaction, the vibration is encouraged". The Shock Wave Amplifica-

tion by Coherent Energy Release (SWACER)[2] mechanism was proposed in their study of photo-chemical initiation of detonation where an induction time gradient field in an initially quiescent photo-dissociating gas mixture is generated by strong UV light irradiation. These theories have provided significant insight regarding the role of inhomogeneities and phase relations between the heat source and the gasdynamic flow field that may lead to rapid shock development. However, the initial flow conditions investigated in these studies are clearly different from those observed during transition and it remains difficult to relate these theories with the generally observed transition phenomena. For instance, the actual flow before onset is not quiescent, and the question of how the initial inhomogeneities are set up remains unanswered. In order to analyze the onset of detonation, these analyses must be advanced further together with realistic initial conditions commonly observed prior to onset of detonation.

On another front, the use of wall obstacles (or so-called Shchelkin's spiral) to stimulate transition to detonation has been studied by Laffite (1928) and Shchelkin (1940). The transition process in similar experiments is largely associated with the intense interaction between the flame and the obstacles. The mechanism by which transition is facilitated had been credited to the generation of turbulence by the obstacles, hence promoting flame acceleration (Lee and Moen 1980, Lee 1986). However, more recent experiments by Teodorczyk (1989) have demonstrated that the transition to detonation may have been facilitated by the transverse pressure waves generated by the obstacles rather than by the turbulence. By placing acoustic absorbing materials underneath wall obstacles, Teodorczyk observed that the damping of the transverse pressure waves inhibited transition. Hence turbulence alone, without transverse pressure waves, has thereby been demonstrated to be insufficient for detonation to form.

[2]The acronym SWACER was introduced to emphasize the similarity of the amplification mechanism to the well known LASER mechanism which is based on light amplification due to coherent energy release by stimulated emission in a resonant cavity.

As a whole, the experimental studies performed so far have revealed a variety of mechanisms for transition to take place, yet the criteria for transition have not been fully understood. While the qualitative descriptions of the transition process is quite established, the quantitative understanding of transition is incomplete. It is still not possible to predict "a priori" for a given system, i.e., for a prescribed mixture in a prescribed tube geometry, if a deflagration can accelerate to detonation or not. Neither is it possible to predict the time (or distance) it would take for transition to occur for systems where transition is known to be possible. Experimental measurements in one system (e.g., fixed tube diameter) cannot be correlated with another, nor can transition data for one mixture be linked to other mixtures.

It is useful to note that the transition phenomenon can be classified into two phases, the initial flame acceleration and the final onset of detonation (Shephard and Lee 1992). Perhaps foremost amongst the reasons that the transition process remains unclear is that most of the experiments carried out to study the transition from deflagration to detonation inevitably mixed the initial flame acceleration phase with the eventual onset once the maximum deflagration velocity is achieved. The initial phase involves a complex phenomena of flame acceleration mechanisms, from laminar through the compressible turbulent regimes which are strongly influenced by initial and boundary conditions. It is unlikely that a general quantitative description of this phase may be achieved. Moreover, due to the random nature of the formation of the explosive centers, it is very difficult to experimentally obtain repeatable and controllable initial conditions at which the onset of detonation can be studied.

On the other hand, it is important to recognize that the key step of transition is the onset phase and the phenomenon does appear to have certain universal characteristics. In general, the deflagration prior to onset always involves a quasi-steady unstable regime

which propagates at a velocity near 1000 m/s, about half the CJ detonation velocity (Lee, Soloukhin, and Oppenheim 1969), and the onset usually undergoes an abrupt event as detonation is formed. The onset process is directly associated with the final establishment of detonation and much clarification is still needed. It thus seems that a fruitful approach to study transition is to direct attention to the onset phase, yet this had not been feasible in previous experiments.

In order to progress further in studying the transition process, it is important to establish clearly the initial conditions at which the onset of detonation will occur, and to recognize the essential characteristics of detonation which the transition process must establish. The recent results of Dupré et al. (1988) have provided some directions in fulfilling these requirements. Their experiments have shown that when the transverse waves of a detonation are damped out, the detonation will fail where the leading shock is decoupled from the reaction zone. The resulting structure is more or less a one-dimensional deflagration with a shock/reaction-front complex which propagates also at about half the CJ detonation velocity for some distance prior to transition back to detonation. The significance of Dupré's results is two fold. First, by removing the transverse waves of a detonation, the wave will fail and the quenched wave decelerates to a propagation velocity commonly obtained prior to transition to detonation. The shock-flame complex is also very similar to the quasi-steady regime which occurs at critical conditions in different initiation experiments such as direct initiation (Bach et al. 1969, Edwards et al. 1978) and critical tube diameter experiments (Edwards et al. 1979). Lee and Ramamurthi (1976) have concentrated on this quasi-steady regime to build a theory to describe blast initiation. In the propagation of galloping detonations, the wave intermittently travels in the failed mode for some time before re-transition to detonative condition and then decays to repeat the cycle (Dupré et al. 1990). Just prior to the establishment of the high velocity regime, a shock-deflagration

structure has been observed which has similar characteristics as the quenched wave obtained by failing a detonation. Thus, the quasi-steady shock-reaction structure just prior to the establishment of detonation is a well-observed entity. It would be of great theoretical and practical interest to investigate the nature of the wave and determine whether it recovers the maximum velocity deflagration. If it does, this simple one-dimensional structure can be used as a well-defined initial condition to examine detonation onset which is then free of the flame acceleration process so dominant in many previous experiments.

Secondly, detonation is demonstrated to require transverse waves for its propagation. Transverse waves are indeed a manifestation of the unsteady coupling between the chemical reactions and the gasdynamic flow field, which forms a rather well-organized cellular structure behind the detonation front. The nonsteady nature of detonations have been revealed in many experimental and theoretical investigations to be in contrast with the classical theory of Zel'dovich (1940), von Neumann (1942), and Döring (1943) (ZND) which postulates a steady "laminar" detonation structure with a shock followed by a reaction front. Theoretical analyses have shown that for high enough activation energies, detonations are inherently oscillatory even in the one dimensional framework (Erpenbeck 1962, 1964; Fickett and Wood 1966). Without the oscillatory structure, a detonation will not sustain itself. The intrinsic oscillatory nature of detonation has therefore suggested that the transition to detonation can be considered as the establishment of this form of organized structure. Hence, the understanding of the transition process cannot be complete unless this aspect has been examined. In this sense, the explosion center or hot spot concept seems to be incomplete. The amplification of the explosion center may provide a static criterion for the onset of detonation (e.g., critical temperature gradient, critical shock strength, etc). What is required, however, may be a dynamic criterion that controls the formation of the organized cellular pattern. Consequently, the oscillatory behavior of detonation should be

examined more closely. It may be fruitful to consider its similarities with classical oscillators since the properties of classical oscillators are well known—their natural frequencies and the physical mechanisms for maintaining the periodic behavior can be easily identified. The excitation or start-up of an oscillator is also closely linked to its frequency. All these should help to shed light on the formation of detonation which may be likened to an oscillator.

1.4 Current State of the Art

In summary, in spite of the extensive efforts to study the transition from deflagration to detonation thus far, the understanding remains qualitative. This stems largely from the fact that the associated phenomena are highly complex and involve many aspects of combustion and wave processes. It is not always possible to distinguish experimentally the initial flame acceleration phase from the final onset of detonation. Neither is the possible influence of the oscillatory nature of the resulting detonation on the transition process fully understood, since the obtained detonation is not a steady state wave. Hence, it is sometimes difficult to define precisely what the transition process refers to. (In other words, the transition from what to what?)

The onset phase of detonation is indeed the final establishment of the detonation. However, because of the difficulty in distinguishing the flame acceleration phase from the final phenomenon of onset, the initial conditions for the onset of detonation are hard to control and the quantitative understanding of the process remains unclear. The work of Dupré et al. (1988) has indicated that when a detonation is quenched, a shock-flame structure is obtained which has characteristics very similar to the quasi-steady regime observed in many different experiments just prior to the establishment of detonation. Because of its apparent universal behavior, the quasi-steady shock-reaction complex just prior to the establishment of detonation may represent a unique class of combustion wave that deserves

better understanding. More importantly, this has given a new impetus to examine the transition process by concentrating on the onset phase which can be accomplished by using the quasi-steady structure as a well-controlled initial condition for the study.

At the other end of the transition process, it is well known that the final detonation formed is not a steady ZND wave, but one with oscillatory characteristics. However, the role of the establishment of the organized structure has not been fully realized in the current understanding of the transition from deflagration to detonation. Existing criteria for transition to take place usually involve the generation of critical shock strength for auto-ignition to occur. These qualitative conditions are inadequate since the question of the formation of the dynamic structure, which may or may not be a stable one, has not been addressed. In order to better understand the transition of detonation, it may be necessary to incorporate the oscillatory characteristics attained in the establishment of the final structure.

In the following section, the objective of the present work will be described and a brief outline of the thesis will be provided.

1.5 Scope and Outline of the Present Work

The principal objective of the thesis is to elucidate on the process of transition from deflagration to detonation by focusing on the events during the onset of detonation where the deflagration prior to transition has already attained a maximum velocity. The present work aims at achieving a quantitative description of the events that lead to the final establishment of detonation through theoretical and experimental investigations. To devote attention to the onset phase, the initial condition for the study will be obtained by inducing failure of an established detonation wave. The subsequent re-transition to detonation will be examined to determine the key factors that control the genesis of detonation.

In order to define more clearly the starting and ending conditions for the transition

process to take place, Chapters 2 and 3 will aim to provide a quantitative description of the initial quasi-steady shock-flame complex and the final oscillatory detonation.

The thesis will start by examining the high speed deflagration just prior to transition to detonation. In spite of the fact that the quasi-steady regime is a universal metastable state that occurs just prior to onset of detonation, it is not well understood. The purpose of Chapter 2 is to determine the nature of the wave and to develop a quantitative model to calculate its properties. In view of the approximate one-dimensional shock-flame structure observed in Dupré's experiments (Dupré et al. 1988), a quasi-steady one-dimensional model will be developed to analyze the obtained fast deflagration. The propagation velocity will be derived and the predicted values will be compared with experiments. These fast deflagrations will be shown to be the maximum velocity deflagrations prior to transition to detonation and will thus be served as a well-defined initial state for the present examination of deflagration to detonation transition. The relation between the quasi-steady regime and other high speed deflagrations observed prior to transition to detonation in various experiments for different boundary conditions (i.e., tube geometries or wall roughness) will be discussed.

The final product of the transition process, that is the self-sustained detonation, will be examined in Chapter 3. Since the final detonation obtained is inherently a nonsteady wave rather than a steady ZND detonation, it is necessary to understand its properties before proceeding to study the transition process. A one dimensional computational study will be carried out using the reactive Euler equations to elucidate the dynamic behavior of the one-dimensional pulsating detonation. Numerical simulations will be performed to examine how the detonation is initiated using a piston. The periodic and oscillatory behavior of the established solution and its relation to the steady Chapman-Jouguet solution will be studied. The similarity of the behavior of the pulsating detonation to other oscillators will

also be pointed out to indicate the possibility of understanding the oscillatory mechanisms of detonation waves using classical oscillator concepts. The response of the pulsating wave to different perturbations and its subsequent failure will be analyzed. The detailed structure of the resulting metastable wave and its ability for re-transition to detonation will be examined to help understand the transition process itself.

The transition process will be investigated in Chapter 4 using one-dimensional computational analysis. The high speed deflagration complex obtained by quenching an established one-dimensional pulsating detonation will serve as the initial condition for transition to start. This quasi-steady shock-reaction structure will be subsequently perturbed with periodic disturbances to induce transition to detonation. Numerical experiments will be carried out to determine the optimal condition for transition using periodic disturbances and the sensitivity of the process to the frequency of the applied perturbation will be examined. To support this approach, an experimental investigation will be described in Chapter 5 to examine the formation of real multi-dimensional detonations. The initial condition for transition will be obtained by damping out the transverse waves of a self-sustained CJ detonation using acoustic absorbing walls to produce a maximum velocity deflagration. Transition will be induced by placing periodic wall obstacles along the channel to generate artificial transverse pressure waves to facilitate the formation of the natural transverse wave structure of the detonation. The optimal perturbation frequencies that will facilitate transition to detonation will be examined.

In Chapter 6, an attempt will be made to establish the analogy of the pulsating detonation to nonlinear oscillators by deriving the equivalent oscillator equation. The oscillator concept may provide a means for the mechanism of pulsation and the oscillatory structure of detonations to be interpreted. The possibility of treating the establishment of the self-organized pulsating detonation (i.e., transition) as the self-excitation of an oscillator

will be discussed.

Chapter 2

The Quasi-Steady Regime Prior to Transition

2.1 Introduction

The purpose of this chapter is to define clearly the high speed deflagration obtained just prior to the onset of detonation. In the present research, we propose to generate the initial condition for the transition study by inducing failure of an established detonation. A one-dimensional analytical model will therefore be developed to analyze the quasi-steady regime and to provide a quantitative description of its properties. The predicted velocities will be compared with the experimentally obtained quasi-steady waves as well as with other maximum velocities deflagrations. The nature of the quasi-steady regime will be discussed in light of the analysis.

2.1.1 Experimentally Observed Quasi-Steady Regime

The generation of the quasi-steady regime by failing an established detonation wave was first demonstrated by the experimental study of Dupré et al. (1988). The quenching process is illustrated by the high speed framing photographs taken by Teodorczyk (1989) from a similar experiment shown in Fig. 2.1. In the figure, a Chapman-Jouguet (CJ) detonation wave is first generated and enters from the left. As it traverses the damping

section, the transverse waves are damped out by the acoustic absorbing walls and the reaction zone gradually decouples from the leading shock while the velocity decreases. The resulting reaction front is an approximate one-dimensional deflagration which propagates at a slightly lower velocity than the leading shock. Unlike a detonation, this complex is uncoupled since the shock slowly separates from the flame. Nevertheless, each element seems to be at a quasi-steady state with approximately constant speeds. Furthermore, this one dimensional shock/reaction-front complex propagates at about half the original CJ detonation velocity for some distance prior to transition back to detonation.

2.1.2 Other Fast Flames Observed

Many experimental observations have indicated that the maximum propagation velocity of deflagrations appears to be also at approximately half the CJ detonation velocity. Some of the examples will be pointed out below.

Fast Deflagrations Just Prior to Transition

The fast deflagrations observed just prior to the transition from deflagration to detonation in smooth tubes have generally attained this velocity before the final onset (Lee, Soloukhin, and Oppenheim, 1969). Above a velocity of approximately 1000 m/s, transition to detonation is imminent. In smooth tubes, these high speed deflagrations consist of a shock (or a family of compression waves) ahead of a reaction zone. The separation distance between the leading shock and the flame front is much larger than that for detonations, indicating that the propagation mechanism is not one of shock-induced auto-ignition. The fast deflagration prior to the onset of detonation has been obtained in the computational studies by Clarke et al. (1986, 1990). Using a one-dimensional Navier-Stokes model with the addition of large amount of thermal power at $x = 0$ to the half space $x > 0$, a strong precursor shock wave followed by a fast deflagration was obtained that propagates in a

metastable state for some time before the appearance of a ZND detonation (Clarke et al. 1986, 1990).

In galloping detonations, the combustion wave intermittently propagates in a failed mode before re-transition to detonative condition and then decouples again to repeat the process (Dupré et al. 1990). The shock-deflagration complex in the failed mode shares similar characteristics as fast deflagration obtained by damping out the transverse waves of a detonation.

Quasi-Steady Regime Under Critical Blast Initiation

Although direct or blast initiation of detonation does not involve the acceleration of a deflagration to undergo transition to detonation, a quasi-steady regime that also has a similar shock-reaction front structure has been observed to occur at the critical conditions just before the initiation of detonation and is found to propagate at about half the CJ detonation velocity (Bach et al. 1969; Edwards et al. 1978). The quasi-steady regime has also been observed in computational studies. A quasi-steady shock-reaction front complex in a slowly evolving configuration was obtained when the energy input to initiate the detonation is supplied by a mechanical piston (Singh and Clarke 1992). The nature of this metastable regime has not been fully clarified although it has sometimes been referred to as "low velocity detonation" because of its sub-CJ propagation velocity. The low velocity has been speculated to be a result of incomplete combustion which decreases the effective energy available to sustain the wave at the CJ detonation velocity (Edwards et al. 1978). This conjecture was based on the experimental observations that unburnt gas can escape the more intense combustion regions at the transverse shocks (Edwards et al. 1978). However, all experimental evidences have shown that the transverse wave system is absent in these quasi-steady regimes, it is unlikely that the low velocity detonation with a partial energy

release can provide a meaningful explanation of the sub-CJ wave.

Turbulent High Speed Deflagrations—Choking Regime

In general, the propagation velocities of high speed deflagrations can range from about 600m/s to 1000m/s which are dependent on the turbulent transport rates, and thus the detailed flow structure. However, for turbulent high speed deflagrations in rough tubes, it is found possible to obtain a steadily propagating deflagration at about 1000 m/s without it undergoing transition to detonation, whereas in smooth tubes transition to detonation usually occurs when the deflagration has accelerated to such velocities. This maximum deflagration velocity is again close to half the CJ detonation velocity, although the detailed flow structure is far more complex than that observed in other conditions (i.e., the quasi-steady regime and fast flames in smooth tubes, etc). The flow structure of a turbulent high speed deflagration is illustrated in Fig. 2.2, which is a time sequence of high speed framing schlieren photographs of such propagation for a hydrogen-oxygen mixture in a channel where the walls are roughened with obstacles. The structure consists of a series of compression waves in the front, followed by a highly turbulent reaction zone. The leading compression waves are not strong enough to cause auto-ignition so that the trailing reaction zone propagates at a slightly lower velocity than the leading compression waves.

Figure 2.3 displays a streak photograph obtained by Wagner (1981), which is a trace of the trajectory of a deflagration where equally-spaced orifice plates are placed along the wall. The deflagration is seen to accelerate initially and eventually attains a steady velocity. The important feature to note from the photograph is that the trajectory of the steady state deflagration front is quite parallel to the the c^+ characteristics in the product gases, which can be identified by the streak lines that propagate in the direction of the deflagration. These steady high speed turbulent deflagration velocities are found

to be quite close to the sound speed in the burnt gases and has prompted Lee (1986) to refer to this regime of combustion as the "choking" regime. Since the sound speed is only a function of temperature, it indicates that thermodynamics play a key role in these deflagrations. Comparing the velocities of the quasi-steady regimes just prior to the establishment of detonation (in direct initiation, in transition, and in galloping detonations), and the highly turbulent choking regime, it appears that they are similar and depend mainly on the energetics of the mixture rather than on the details of the flow structure.

In the following section, the analytical model for the quasi-steady regime will be developed and the predicted theoretical propagation velocities will be compared with the extensive experimental data that is available for some of these high speed deflagrations.

2.2 Analytical Model

The high speed photographs in Fig. 2.1 have thus indicated that the quasi-steady regime resulting from failing a detonation can be modeled by a one-dimensional shock followed by a reaction front as shown in Fig. 2.4. Upstream of the complex, the gas is stationary so the initial velocity u_0 vanishes. The velocity behind the flame, u_2, is assumed to vanish to satisfy the end-tube boundary condition. We shall assume that the deflagration is a maximum velocity wave that propagates at the sound speed of the burnt gas, that is it satisfies the Chapman-Jouguet (CJ) condition. This kind of configuration has always been a topic for theoretical study, not least because of the availability of elementary solutions for its component parts, in this case, a shock wave and a subsonically-propagating deflagration. The text by Shchelkin and Troshin (1964) contains a lengthy chapter under the heading of "Double Discontinuities", and refers to an earlier work by Oppenheim (1953). Shchelkin and Troshin describe the propagation of separate discontinuities as dictated by the relevant Hugoniot relationships, either adiabatic or nonadiabatic as the case may be. Oppenheim

derived the locus of possible states 2 that may exist downstream of a given upstream region 0 on the hypothesis that the deflagration is of the CJ-type (i.e., it is propagating at exactly sonic speed relative to the burnt gas in region 2). Oppenheim called this particular locus a Q-curve, while Shchelkin and Troshin described it as a generalized Hugoniot curve.

There is one particular point on Oppenheim's Q-curve that corresponds to $u_2 = 0$ in Fig. 2.4. Since the form of this special result, which was not noted by the earlier writers, is particularly relevant to the present study we derive it here from first principles. Deflagrations in the experiments travel along tubes in the direction away from a solid end wall. While u_2 is certainly equal to zero at such an end wall, observations suggest that the condition $u_2 = 0$ will also be encountered throughout the domain between the wall and the flame. In the one-dimensional numerical computations made by Clarke et al. (1986, 1990) of the Navier-Stokes model of events that follow from the initial addition of thermal power to a simple combustible gas, the shock wave and the fast-flame predicted by the Navier-Stokes solution prior to the appearance of a ZND detonation follow paths on an x, t-diagram that are very similar to the ones sketched in Fig. 2.4 here, and the computed gas velocity in region 2 is, for all practical purposes, equal to zero, as proposed in the present case.

A further indication that u_2 vanishes is illustrated by the streak photograph obtained by Wagner (1981) in Fig. 2.4. Since the velocity of the deflagration front is close to the sound speed of the burnt gas (c_2), while the c^+ characteristics propagate with velocity $u_2 + c_2$ and are parallel to the deflagration front, the photograph demonstrates that the particle velocity in the burnt gas is indeed small.

The key fact in the present study is the insensitivity of the broad flow-field pattern (of shock followed by deflagration) to any details of behavior within any particular deflagration.

2.2.1 Governing Equations

The governing equations for the deflagration model is derived as follows. The conservation laws across the shock may be written as

$$\rho_0 \dot{R}_S = \rho_1(\dot{R}_S - u_1) \tag{2.1}$$

$$p_0 + \rho_0 \dot{R}_S^2 = p_1 + \rho_1(\dot{R}_S - u_1)^2 \tag{2.2}$$

$$h_0 + \frac{\dot{R}_S^2}{2} = h_1 + \frac{(\dot{R}_S - u_1)^2}{2} \tag{2.3}$$

and similarly for the flame

$$\rho_1(\dot{R}_F - u_1) = \rho_2 \dot{R}_F \tag{2.4}$$

$$p_1 + \rho_1(\dot{R}_F - u_1)^2 = p_2 + \rho_2 \dot{R}_F^2 \tag{2.5}$$

$$h_1 + \frac{(\dot{R}_F - u_1)^2}{2} + Q = h_2 + \frac{\dot{R}_F^2}{2} \tag{2.6}$$

Assuming a perfect gas, the enthalpy h can be expressed as a function of p and ρ as

$$h = \frac{\gamma}{\gamma - 1}\frac{p}{\rho} \tag{2.7}$$

In the above equations, subscript 0 denotes the initially undisturbed state ahead of the shock, subscript 1 denotes the shocked gas between the shock and the flame, and subscript 2 denotes the burned products behind the flame.

Let us first consider the solution for the flame. From the conservation of mass (2.4) the density ratio can be expressed in terms of the velocity ratio as

$$x = \frac{\rho_1}{\rho_2} = \frac{\dot{R}_F}{\dot{R}_F - u_1} \tag{2.8}$$

Using the conservation of mass and momentum (2.4) and (2.5) the pressure ratio can be expressed in terms of the density ratio and the flame velocity as:

$$y = 1 + \gamma_1 \left(\frac{\dot{R}_F^2}{c_1}\right)^2 \frac{1 - x}{x^2} \tag{2.9}$$

where $y = p_2/p_1$. Equations (2.8) and (2.9) can be used to eliminate the velocities in the energy equation (2.6). By using equation (2.7) for h, the energy equation becomes

$$(x - \alpha)(y + \alpha) = \beta \tag{2.10}$$

where

$$\alpha = \frac{\gamma_2 - 1}{\gamma_2 + 1} \qquad \beta = \frac{\gamma_2 - 1}{\gamma_2 + 1}\left[\left(\frac{\gamma_1 + 1}{\gamma_1 - 1} + \frac{2\gamma_1 Q}{c_1^2}\right) - \frac{\gamma_2 - 1}{\gamma_2 + 1}\right]$$

with $c_1^2 = \gamma_1 p_1/\rho_1$ being the sound speed of the reactants immediately ahead of the flame front. Equation (2.10) represents the Hugoniot curve on a pressure-density plot which is the locus of downstream states (p_2, ρ_2) for a given initial state (p_1, ρ_1) and chemical energy release Q of the mixture. For a perfect gas, the Hugoniot curve is a rectangular hyperbola as illustrated by equation (2.10).

The locus of possible solutions across the shock can be obtained similarly from the conservation equations (2.1) to (2.3). Since the mixture is non-reactive across the shock (i.e., $Q = 0$), the Hugoniot equation for $\gamma_0 = \gamma_1 = \gamma$ is then

$$(\hat{x} - \hat{\alpha})(\hat{y} + \hat{\alpha}) = \hat{\beta} \tag{2.11}$$

$$\hat{x} = \frac{\rho_0}{\rho_1} \qquad \hat{y} = \frac{p_1}{p_0}$$

$$\hat{\alpha} = \frac{\gamma - 1}{\gamma + 1} \qquad \hat{\beta} = \frac{4\gamma}{(\gamma + 1)^2}$$

Furthermore, the downstream state across the shock can be obtained using equations (2.1) to (2.3) to give the usual Rankine-Hugoniot relations for a normal shock in a perfect gas, i.e.,

$$\frac{\rho_1}{\rho_0} = \frac{\gamma + 1}{\gamma - 1 + 2\eta} \tag{2.12}$$

$$\frac{p_1}{p_0} = \frac{2\gamma - (\gamma - 1)\eta}{(\gamma + 1)\eta} \tag{2.13}$$

$$\frac{c_1}{c_0} = \sqrt{\frac{[2\gamma - (\gamma - 1)\eta][2\eta + (\gamma - 1)]}{(\gamma + 1)^2 \eta}} \tag{2.14}$$

$$\frac{u_1}{c_0} = \frac{2(1 - \eta)}{\gamma + 1}\eta^{-\frac{1}{2}} \tag{2.15}$$

where

$$\eta M_S^2 = 1; \qquad c_0 M_S = \dot{R}_S; \tag{2.16}$$

M_S is the shock Mach number.

The solution to the conservation equations for the shock/reaction-zone complex can be represented graphically using a Hugoniot diagram, which is a plot of pressure versus the specific volume (i.e., $1/\rho$) as displayed in Fig. 2.5. Given an initial state 0, the shocked state 1 lies on the Shock-Hugoniot given by equation (2.11). The straight line that connects the initial state and intersects the Shock-Hugoniot at state 1 is the Rayleigh line, which is given by the conservation of mass and momentum equations. Since there is no energy addition across a shock ($Q = 0$), both the initial and shocked states lie on the Shock-Hugoniot. The solution behind the deflagration (state 2) lies on the Hugoniot for the deflagration given by equation (2.10). For a Chapman-Jouguet deflagration, the solution is obtained by the intersection of the Rayleigh line from the shocked state to the lower tangency point on the Hugoniot curve.

2.2.2 Approximate Solution for Constant γ

If γ is further considered to be constant across the flame as well as across the shock, then the downstream states across the flame front can be solved for in terms of the upstream conditions using equations (2.8), (2.9) and (2.10). For example the density ratio can be written as

$$\frac{\rho_2}{\rho_1} = \frac{\gamma + 1}{\gamma + \eta_F \pm S} \tag{2.17}$$

where

$$S = \sqrt{(\eta_F - 1)^2 - 2(\gamma^2 - 1)Q\frac{\eta_F}{c_1^2}} \tag{2.18}$$

and

$$\eta_F M_F^2 = 1; \quad c_1 M_F = \dot{R}_F - u_1. \tag{2.19}$$

Similar expressions can be written for the other quantities (e.g. pressure ratio). The two signs in front of S in equation (2.17) denote the two possible solutions for a given flame speed. For a Chapman-Jouguet deflagration, the two solutions coincide, i.e. $S = 0$, and we obtain

$$\frac{\rho_2}{\rho_1} = \frac{\gamma + 1}{\gamma + \eta_F} \tag{2.20}$$

where η_F (for the Chapman-Jouguet condition) is now given by equation (2.18) for $S = 0$. Thus, the Mach number of the deflagration relative to the flow between the shock and reaction front is related to the energy release by:

$$\left(\frac{1}{M_F} - M_F\right)^2 = 2q\left(\frac{c_0}{c_1}\right)^2, \quad q = (\gamma^2 - 1)\frac{Q}{c_0^2} \tag{2.21}$$

From the conservation of mass across the shock and the flame (i.e., eqns. 2.1 and 2.4) the flow Mach number relative to the deflagration can be related to that behind the shock:

$$M_F\left(\frac{\rho_1}{\rho_2} - 1\right) = M_1\left(\frac{\rho_1}{\rho_0} - 1\right) \tag{2.22}$$

where $M_1 = \frac{\dot{R}_s - u_1}{c_1}$ is the Mach number of the flow behind the shock relative to the shock. Utilizing the Rankine-Hugoniot relationships across a normal shock (eqns. 2.12, 2.14) equation (2.22) can be expressed as the following relationship for the Mach number M_F of the flow in front of the flame with respect to the flame, and the shock Mach number M_S:

$$\left(\frac{1}{M_F} - M_F\right) = 2\left(\frac{1}{M_1} - M_1\right) = 2\frac{c_0}{c_1}\left(\frac{1}{M_S} - M_S\right). \tag{2.23}$$

Substituting equation (2.14) for c_0/c_1, equation (2.21) can be reduced to

$$\left(\frac{1}{M_S} - M_S\right)^2 = \frac{1}{2}q \tag{2.24}$$

The solution for M_S^2 is

$$M_S^2 = 1 + \frac{q}{4} + \sqrt{(1 + \frac{q}{4})^2 - 1} \tag{2.25}$$

For $q \gg 1$, which in general is the case for explosive gas mixtures (since q is typically of order 20) the approximate value of M_S is

$$M_S \simeq \sqrt{\frac{q}{2}} \tag{2.26}$$

The propagation velocity of the flame can be obtained using the mass conservation across the flame and the shock to yield

$$\begin{aligned} \dot{R}_F &= (\dot{R}_F - u_1) + u_1 \\ \frac{\dot{R}_F}{c_0} &= M_F \frac{c_1}{c_0} + M_S \left(1 - \frac{\rho_0}{\rho_1}\right) \end{aligned} \tag{2.27}$$

Using the Rankine-Hugoniot relations across the normal shock (i.e., eqns. 2.12, 2.14) and equation (2.21), for $q \gg 1$, the flame velocity relative to the fixed tube can be approximated by:

$$\frac{\dot{R}_F}{c_0} \simeq \frac{\gamma(\gamma-1) + 2(\gamma+1)}{2(\gamma+1)^2} \sqrt{2q} \tag{2.28}$$

The CJ detonation Mach number $M_D = \dot{R}_D/c_0$ for the same mixture can be expressed as a function of the heat release q as:

$$\left(\frac{1}{M_D} - M_D\right)^2 = 2q \tag{2.29}$$

The solution for the quadratic equation for M_D^2 is

$$M_D^2 = 1 + q + \sqrt{(1+q)^2 - 1} \tag{2.30}$$

For $q \gg 1$, the CJ Mach number is approximately

$$M_D \simeq \sqrt{2q} \tag{2.31}$$

Upon comparing equations (2.26) and (2.31), we see that

$$\begin{aligned} M_S &\simeq \frac{1}{2} M_D \\ \text{or} \quad \dot{R}_S &\simeq \frac{1}{2} \dot{R}_D \end{aligned} \tag{2.32}$$

The precursor shock velocity of a CJ deflagration is thus about one half the corresponding CJ detonation speed for the same mixture. For $\gamma = 1.4$, the flame velocity of the CJ deflagration is

$$\frac{\dot{R}_F}{c_0} \simeq 0.655\sqrt{q} \tag{2.33}$$

and from equation (2.31), we obtain

$$\dot{R}_F \simeq 0.465\dot{R}_D \tag{2.34}$$

The comparison of $\dot{R}_F$ with $\dot{R}_D$ for various γ is given in Table 2.1. It can be seen that the CJ deflagration velocity (relative to a fixed coordinate) is about one half the corresponding CJ detonation velocity $\dot{R}_D$. This is precisely what the experimental results of Dupré et al. (1988) showed.

Table 2.1: Comparison of CJ deflagration with CJ detonation velocities for various γ

γ	$\frac{\dot{R}_F}{\dot{R}_D} = \frac{\gamma(\gamma-1)+2(\gamma+1)}{2(\gamma+1)^2}$
1.4	0.465
1.3	0.472
1.2	0.479
1.1	0.489

2.2.3 Exact Solution for Arbitrary q

In order to compare quantitatively the theoretical model with experimental results, a more exact analysis is required. In this analysis, the assumption that γ is constant across the flame is relaxed, although the change in γ across the shock is still assumed negligible. The assumption that $q \gg 1$ is not necessary as q will be computed directly in the analysis.

Because γ changes across the flame front, the state downstream of the flame can no longer be represented by the simple expression of equation (2.17), although the numerical

values can still be computed. The solution across the flame will be obtained using the Hugoniot equation. Given the state upstream of the flame, for a perfect gas, the Hugoniot equation for the downstream state is represented by equation (2.10) which can be rewritten in the following forms:

$$x = \frac{\beta}{y+\alpha} + \alpha \tag{2.35}$$

$$y = \frac{\beta}{x-\alpha} - \alpha \tag{2.36}$$

The unknowns across the flame are the density and pressure ratios (x, y) and the flame velocity $\dot{R}_F$. The pressure ratio y can be solved for in the following manner. The mass conservation equation (2.8) is first rewritten as:

$$\dot{R}_F = \frac{x u_1}{x-1} \tag{2.37}$$

Using the alternate form of the Hugoniot equation (2.35), the density ratio x can be eliminated:

$$\dot{R}_F = \frac{\frac{\beta}{y+\alpha} + u_1 + \alpha u_1}{\frac{\beta}{y+\alpha} + \alpha - 1}$$

$$\dot{R}_F = \frac{\beta u_1 + \alpha u_1 (y+\alpha)}{\beta + (\alpha-1)(y+\alpha)} \tag{2.38}$$

Substituting equation (2.35) for x, and equation (2.38) for $\dot{R}_F$ into the momentum equation (2.9), the pressure ratio across the flame is:

$$y = \frac{p_2}{p_1} = \frac{B - \sqrt{B^2 + 4(\alpha-1)[\beta + \alpha(\alpha-1) - \alpha\gamma_1(\frac{u_1}{c_1})^2]}}{2(1-\alpha)} \tag{2.39}$$

where $B = \beta + (\alpha-1)^2 + \gamma_1(\frac{u_1}{c_1})^2$. If the coefficients α and β are known, the pressure ratio y can be determined. Equations (2.35) and (2.38) can then be used to calculate the density ratio and the flame speed, respectively.

Note that since the Hugoniot equation (2.10) contains only two coefficients (α, β), if any two states on the Hugoniot curve are known, α and β can be evaluated and the

downstream state can be determined. The two states chosen here are the constant volume combustion and the Chapman-Jouguet detonation. Standard equilibrium combustion codes (e.g. STANJAN) are available to calculate these states so that α and β are obtained. Once the coefficients are known, for a given state ahead of the flame, equation (2.39) will give the general solution for the pressure ratio that satisfies the boundary condition $u_2 = 0$.

Because the condition ahead of the flame front depends on the strength of the precursor shock, the Chapman-Jouguet deflagration must be solved as an interdependent shock-flame complex. The Chapman-Jouguet complex can be solved by finding the unique shock velocity $\dot{R}_S$ that would satisfy the Chapman-Jouguet condition. The procedure for computing the flow field is illustrated as follows. The calculation proceeds from an assumed value of the shock velocity $\dot{R}_s$. The shocked state 1 is calculated using the Rankine-Hugoniot relations for the shock, i.e. equations (2.12), (2.13), (2.14) and (2.15). To relate the states across the flame, the Hugoniot relation across the flame and the solution for the pressure are applied (i.e., eqns. 2.39, 2.35, and 2.37).

The coefficients (α, β) in these equations are evaluated using the chemical equilibrium code STANJAN (Reynolds 1987) to fit the Hugoniot equation to two states—constant volume combustion and CJ detonation, for the given shocked state. The entire flow field is then calculated for the assumed shock velocity. The flame velocity is tested to see whether the Chapman-Jouguet condition is satisfied. If it is not, a new shock velocity is assumed and the iteration continues until the CJ deflagration is obtained.

2.3 Results and Discussion

Following the calculation procedures for CJ deflagration, the propagation velocity of the reaction front is calculated. The theoretical velocities will be compared with the approximate one-dimensional deflagration obtained by damping out the transverse waves

of an established detonation (Dupré et al. 1988) and with the rough tube experiments in Lee (1986).

2.3.1 The Quasi-Steady Regime Following Failure

In Figs. 2.6 to 2.8, the theoretical CJ deflagration velocities are compared with the velocities of the quasi-steady shock-reaction complex from Dupré. In the figures, the flame velocities are plotted against the initial pressure for three different mixtures—ethylene (C_2H_4), acetylene (C_2H_2), and hydrogen (H_2) in stoichiometric concentration with oxygen. For C_2H_4, Fig. 2.6 shows that the calculated flame velocity is about 1100 m/s which increases slightly with the initial pressure. The theoretical values of flame velocity agree quite well with the experimental data. For acetylene (Fig. 2.7), the theoretical deflagration velocity is about 1000m/s which also increases slightly with initial pressure. The calculated flame velocities again exhibit good agreement with the measured values. The calculated flame velocity for the hydrogen-oxygen mixture (Fig. 2.8) is about 1400 m/s and is slightly higher than the measured data, which are at about 1200 m/s. Note that because hydrogen is a very light gas, it has a high sound speed. As a result it is difficult to maintain strong shocks in hydrogen so that the transverse waves in the original detonation are more easily damped than for the other mixtures. It is possible that the hydrogen deflagration may have decayed further to propagate at a sub-CJ deflagration velocity.

Although the structure of the approximate one-dimensional deflagration from Dupré's experiments may seem very similar to the idealized model so that the agreement between the theoretical and experimental propagation velocities is expected, there is nevertheless some fundamental difference between the two structures. The idealized deflagration is in effect a steady "laminar" reaction front that is free of any flow fluctuations. On the other hand, the experimental deflagration, although quite one-dimensional, can still be seen to contain turbulence. Thus, even for the one-dimensional case, the agreement between

theoretical and experimental results indicates that these high speed deflagrations are quite independent of the detailed flow structure.

As a whole, the theoretical flame velocities are very close to the measured flame velocities. It is important to note that for the same energy input Q, the CJ deflagration obtained exhibits a velocity decrease of approximately 50 percent from that of the original detonation. This sub-CJ detonation velocity wave is thus not due to a partial heat release as may have previously been suggested (Edwards et al. 1978), but to the change in propagation mode. Moreover, the observed quasi-steady shock-reaction front structure is also not that of an induction process as it is for detonation waves. Otherwise the separation distance between the shock and the deflagration front would have remained constant, as it is dictated by a constant velocity leading shock. The presented deflagration model clearly demonstrates that the quasi-steady regime obtained by damping the transverse waves of a detonation is not that of detonation, but one that is equivalent to a Chapman-Jouguet deflagration.

Thus by removing the transverse waves of a detonation, the detonation fails and the maximum velocity deflagration is obtained. This maximum velocity deflagration is a Chapman-Jouguet deflagration which lies on the tangency point of the Hugoniot curve (Fig. 2.5), as is well established from classical theory.[1] Yet, CJ deflagrations had been believed previously not to be readily observable in reality. Such a deflagration was unachievable in previous experiments of flame propagation in smooth tubes because deflagrations usually undergo a transient state of acceleration due to turbulent interaction which inevitably destroys the one-dimensional structure and also quickly leads to transition to detonation. Thus, the high speed deflagrations observed in previous experiments would likely undergo a highly transient passage through the CJ state.

[1] For example, see the discussion of the CJ deflagration by Taylor and Tankin (1958) and the analysis of steady flames by Kuhl, Kamel, and Oppenheim (1973).

2.3.2 The Highly Turbulent Choking Regime

Although the structure of the high speed deflagrations observed in rough tube experiments (Lee 1986) are much more complex than the one dimensional deflagration of Dupré, the fact that the flame velocities are also about one half the CJ detonation velocity, and that the flame propagates at about the sound speed of the burnt gas indicate that energetics, rather than the detailed flow structure, is the key factor. Thus, when the deflagration has achieved the maximum possible velocity without undergoing transition to detonation in rough tubes, the velocity obtained would be insensitive to the detailed flow structure and the deflagration would be equivalent to a Chapman-Jouguet deflagration. Let us investigate this by calculating the CJ deflagration velocities for the rough tube experiments and see how they compare with the measured flame velocities. The experimental results in Lee (1986) are obtained for five different mixtures—$C_2H_4, H_2, C_3H_8, C_2H_2$ and CH_4, all in air and initially at atmospheric pressure and room temperature, where the measurements are taken for tube diameters of 15cm and 5cm, with the respective blockage ratio (B.R.=obstacle area over channel area) of 0.39 and 0.43.

The calculated CJ deflagration velocities and the measured terminal flame velocities, which are near the maximum velocities achieved in the rough tube without undergoing transition to detonation, are compared in Figs. 2.9 to 2.13. In the figures, the flame velocities are plotted against mixture concentration expressed in terms of equivalence ratio. Also plotted in the figures are the corresponding CJ detonation velocities for reference. From these figures, it can be seen that the calculated flame velocities are about one half the CJ detonation speed and are indeed very close to the measured flame velocities. Note that even though there is a large change in the tube diameter and blockage ratio (B.R.), which represents drastically different turbulent transport rates in the flow, the measured flame speeds are not significantly affected. The agreement between theoretical and experimental flame

velocities are especially good for C_2H_4, H_2, and C_3H_8 (Figs. 2.9, 2.10, 2.11). For C_2H_2 and CH_4 (Figs. 2.12, 2.13), the measured flame velocities are near, but consistently below the maximum possible velocities prior to transition to detonation. Therefore, the measured flame velocities for C_2H_2 and CH_4 are slightly lower than the calculated CJ deflagration velocities. Also to be noted in Figs. 2.12 and 2.13 is that the measured flame velocities for the smaller tube diameter and larger blockage ratio are slightly lower than those for larger tube diameter and smaller blockage ratio, since the losses associated with the former condition are expected to be larger so that the velocities are decreased. This effect is more pronounced for C_2H_2 and CH_4 because their velocities are below the maximum deflagration velocity so the influence due to the different transport rates becomes more apparent.

Because the theoretical CJ deflagration velocity is simply the sound speed of the burnt gas which depends only on the temperature (sound speed is proportional to $\sqrt{T}$ or $\sqrt{Q}$, the square root of energy addition) the agreement between the theoretical results with the experimental data strongly supports the premise that the propagation velocities of these multi-dimensional high speed deflagrations are determined by energetics rather than the detailed flow structure. Indeed, these combustion processes are governed by thermodynamics and are quite independent of the flow structure.

The similarity between the seemingly different forms of high speed deflagration can obtain further support upon consideration of the Chapman-Jouguet detonation. The latter is widely known to be inherently three-dimensional and unsteady due to the propagation of transverse waves normal to the direction of propagation of the detonation. Yet, the average wave velocity agrees well with one dimensional theory. For a CJ detonation, which is the minimum velocity detonation, it is not the detailed flow structure, but the energetics that plays the dominant role. For the CJ deflagration, which is the maximum-velocity deflagration, a similar argument applies.

Since the high speed deflagrations under examination are energetics dependent, it is worthwhile to examine the possible energy losses associated with the turbulent deflagrations in rough tubes to see whether they can affect the propagation velocity. First, there may be heat transfer from the deflagration complex because the combustion process will generate significantly higher temperatures than its surroundings. However, the time scale associated with the diffusion of heat from the gas to the tube is several orders of magnitude larger than the characteristic time associated with the propagation of the deflagration. Therefore, the energy loss due to heat transfer should be quite negligible. Another mechanism for energy deficit involves the turbulent nature of the deflagration. The turbulence generated by the rough walls will cause scattering of the kinetic energy of the main propagation to velocity fluctuations in the other dimensions. Strictly speaking, no energy is lost from the deflagration complex, yet the distribution of the multi-dimensional velocity fluctuations does "lock up" part of the useful kinetic energy. However, because the propagation velocity is only proportional to the square root of the energy (eqns. 2.26 or 2.28), it is insensitive to such deficit. Hence, although the high speed deflagrations in the rough tubes are highly turbulent and multi-dimensional, their propagation velocities still exhibit good agreement with the theoretical values.

Therefore, the turbulent high speed deflagrations in the choking regime, as classified by Lee (1986), are indeed Chapman-Jouguet deflagrations. One can now identify these on the Hugoniot curve as one of the four combustion processes (together with constant volume combustion, constant pressure combustion, and CJ detonation) that are uniquely determined by thermodynamics. And in contrast to previous belief, Chapman-Jouguet deflagrations can be readily observed in the propagation of fast deflagrations in rough channels.

2.4 Summary

In the present research, it is proposed that a maximum velocity deflagration can be used for the study of onset of detonation by inducing failure of an established detonation. To clearly define the initial condition, the resulting approximate one-dimensional fast deflagration is analyzed using a simple model that satisfies the Chapman-Jouguet condition. The analytical solution obtained for constant γ and large heat release demonstrates that the propagation velocity is close to one half the CJ detonation propagation velocity corresponding to the same mixture, as have been shown by previous experiments. The numerical calculations of the propagation velocities and the comparison with experimental data have successfully demonstrated that the quasi-steady regime obtained by damping out the transverse waves of a detonation is a Chapman-Jouguet deflagration.

Moreover, the propagation velocity of the seemingly very different form of high speed deflagration—the highly turbulent deflagration in the choking regime observed in rough tube experiments, is also found to have excellent agreement with their one-dimensional counter-part. The comparisons with the extensive experimental data that are available have demonstrated that these maximum velocity deflagrations, which propagate at the sound speed of the product gases, are energetics governed and are insensitive to the detailed flow structure. The present analysis strongly indicates that the the quasi-steady deflagration just prior to the establishment of detonation and the highly turbulent choking regime, are indeed Chapman-Jouguet deflagrations where the propagation velocities are uniquely determined by thermodynamics.

The success in generating a one-dimensional fast deflagration has also opened up new opportunities to study the onset of detonation. Because the fast deflagration obtained by removing the transverse waves of a detonation is a CJ deflagration, one can perturb this and study the reverse process of the re-establishment of the transverse wave structure

and the re-birth of the detonation. In many previous experimental studies of the transition process, the deflagration under observation is generated from ignition and undergoes an acceleration phase prior to transition. In such studies, the observations are always complicated by the wide variation of propagation velocity and flow structure of the deflagration prior to the onset of detonation. By using a CJ deflagration to study the transition process, one can have a clear control of the initial condition of transition that is free from the effects due to the acceleration process and can thus concentrate on the onset phenomenon.

Chapter 3

The One-dimensional Pulsating Detonation

The purpose of this chapter is to examine the final product of the transition process, i.e., the detonation. Unlike the classical steady state ZND model, real detonation waves are inherently nonsteady and this behavior may influence the establishment of the detonation itself. It is therefore important to examine the properties of the unsteady detonation before proceeding to study how this entity is formed during transition.

The characteristics of one-dimensional detonations, in particular, the intrinsic oscillatory behavior, will be reviewed through direct numerical simulation. The initiation of the detonation using a piston and its self-sustained propagation will be analyzed. The study of the response of the oscillatory wave to perturbations, its failure and the subsequent natural re-transition will also provide insight for understanding the transition problem.

The usefulness of numerical experiments cannot be over-emphasized. There are limitations as to what can be experimentally measured in order to describe the events of the formation, steady propagation, and failure of the highly transient detonation phenomena. Numerical experiments can, on the other hand, provide the freedom to probe the unsteady process to obtain detailed and insightful information that may otherwise be difficult to measure in real experiments.

3.0.1 The One-Dimensional Representation

Unlike deflagrations, the combustion process in a detonation is coupled with the shock wave that it generates. The system propagates as an integral structure with the same velocity. The one-dimensional ZND model is the simplest description of detonation propagation. It consists of a steady-state structure with a leading shock coupled with a fast reaction front. The ZND model provides a mechanism for the propagation of the detonation wave where gas particles are adiabatically compressed and heated by the leading shock. Following an induction period, intense chemical reaction occurs and the expansion of the products provide the feedback of energy to maintain the shock propagation. A unique feature of the steady state wave is that the products in the wake of the detonation satisfies the Chapman-Jouguet (CJ) condition with the burnt gas particles travel at sonic velocity relative to the wave. The sonic CJ plane isolates the detonation from the products and permits the detonation to be independent of back boundary and initial conditions once the steady state wave is established. However, the ZND model is unstable and the coupling between chemical reactions and the gasdynamic flow field is invariably nonsteady. Experimental and theoretical studies have shown that, in general, detonation waves possess a three dimensional oscillatory structure which manifests itself as a complex pattern of transverse shock waves at the detonation front. Hence, it is necessary to recognize that the resulting detonation following transition will not be a steady ZND wave, but one that involves an oscillatory and unstable structure.

Although direct numerical simulations are now capable of reproducing two- and three-dimensional detonations (e.g., Oran and Boris 1987, Taki and Fujiwara 1978, 1981, 1984, Bourlioux et al. 1992), the one dimensional dynamics of the reactive Euler equations remain a simple and powerful tool to study the underlying physics that governs the oscillatory propagation. The dynamic structure in the one-dimensional treatment manifests

as a longitudinal pulsating wave that, in essence, maintains the same unstable behavior as obtained in multi-dimensions.

The first computational investigation of the instability of piston driven (or so-called overdriven) detonations was carried out by Fickett and Wood (1966). Using the method of characteristics and a single-step Arrhenius law for the reaction rate, they demonstrated that the unstable one-dimensional detonation evolves into an oscillatory wave for high enough activation energies. The calculated stability boundary and the frequency of the oscillations obtained by varying the activation energy agreed well with the linearized theory of Erpenbeck (1962, 1964). Similar nonlinear oscillatory behavior was again obtained when the simple Arrhenius law was replaced by a chain branching reaction mechanism (Fickett et al. 1972). In a later study, Abouseif and Toong (1982) used the first order finite difference method of Rusanov and a simple Arrhenius law to examine the instability of one-dimensional detonations. By decreasing the degree of piston overdrive, while holding the activation energy constant, they demonstrated that the shock pressure is transformed from a regular periodic pattern into irregular oscillatory motion in which the dominant mode is distorted and overlapped by higher modes. Moen et al. (1984) used a second order MacCormack algorithm with FCT anti-diffusion scheme and fine mesh resolution to perform similar computations as those of Abouseif and Toong. They reported that the periodic pattern breaks up completely into an irregular pattern before the degree of overdrive approaches one. Large pockets of unburnt gas was found in the product region and they speculated that the explosions of these pockets may provide the flow perturbations resulting in the high level of instability patterns observed. More recently, Bourlioux et al. (1991) used a second order extension of Godunov's method (PPM) with conservative shock tracking and adaptive mesh refinement to examine the effects of the degree of piston overdrive on the unstable detonation. Near the instability boundary, the pulsating detonation

oscillates at a well defined frequency as predicted by the more recently developed linearized theory of Lee and Stewart (1990). As the instability pattern grows, their results seem to indicate that the transformation process follows a period doubling sequence before the higher modes appear as the degree of overdrive is reduced. Naturally, the detailed features of the oscillatory behavior and their subsequent break up would depend on the specifics of the numerical methods and the resolution used. Nevertheless, the numerical results obtained have indicated that the nonsteady one-dimensional detonation manifests itself in an oscillatory manner controlled by chemical kinetics and gasdynamics (such as activation energy, the degree of piston overdrive, heat of reaction, and specific heats ratio).

The previous works have clearly shown that the pulsating detonation manifests as an self-organized oscillatory wave. In this chapter, we will attempt to provide an overview of the different aspects of the pulsating wave to help understand how the self-oscillatory behavior may influence the formation of the detonation itself. We will first describe the governing equations used to carry out the direct numerical simulation of the pulsating detonation.

3.1 Governing Equations

The detonation to be studied will be obtained in a manner similar to that treated by Fickett and Wood (1966) and by Abouseif and Toong (1982). Consider the space initially filled with a quiescent combustible mixture bounded at $x = 0$ with a piston. The piston moves with velocity $u_p(t)$ generates a strong shock wave to initial a detonation (see Fig. 3.1). After the detonation has established a regular oscillatory pattern, its detailed behavior will be analyzed.

Dissipative processes such as viscous and heat losses are assumed negligible in the present analysis. The chemical reaction is assumed to take place in a one-step ir-

reversible process that follows the Arrhenius law. In a piston-fixed reference frame, the one-dimensional equations of motion describing the reactive flow can be expressed as follows:

$$\text{Mass Conservation:} \quad \frac{\partial \rho}{\partial t} + \frac{\partial (\rho u)}{\partial x} = 0 \tag{3.1}$$

$$\text{Momentum Conservation:} \quad \frac{\partial u}{\partial t} + u\frac{\partial u}{\partial x} = -\frac{1}{\rho}\frac{\partial p}{\partial x} - a_p \tag{3.2}$$

$$\text{Energy Conservation:} \quad \frac{\partial p}{\partial t} + u\frac{\partial p}{\partial x} + \gamma p\frac{\partial u}{\partial x} = \rho(\gamma - 1)\dot{q} \tag{3.3}$$

$$\text{Reactant Consumption:} \quad \frac{\partial \alpha}{\partial t} + u\frac{\partial \alpha}{\partial x} = -k\alpha e^{-E/RT} \tag{3.4}$$

$$\text{State Equation:} \quad p = \rho RT \tag{3.5}$$

The above symbols are defined as follows: t is time, x distance, p pressure, T temperature, u velocity, ρ density, α reactant mass fraction, γ and R are the specific heats ratio and the specific heat constant, respectively, and E the specific activation energy, k the reaction rate constant, a_p is the piston acceleration du_p/dt, and $\dot{q}$ is the heat release rate where the $(\dot{})$ signifies time derivative.

The flow variables are then nondimensionalized with respect to the initial undisturbed state (p_0, ρ_0, T_0), and the velocity with respect to the initial sound speed (c_0), while the energy quantities are nondimensionalized with respect to RT_0. The independent variable of time is nondimensionalized with respect to the half-reaction time $(t_{1/2})$, which is defined as the time for half of the reactants to be consumed (i.e., α depleted from 1.0 before reaction starts to 0.5 when half reacted) in the steady-state ZND detonation. The space variable is nondimensionalized with respect to $c_0 t_{1/2}$, while the pre-exponential constant (k) is also normalized with respect to $t_{1/2}$. Thus:

$$\begin{aligned} p^* &= \frac{p}{p_0},\ r^* = \frac{\rho}{\rho_0},\ T^* = \frac{T}{T_0},\ u^* = \frac{u}{c_0} \\ E^* &= \frac{E}{RT_0},\ q^* = \frac{q}{RT_0} \end{aligned} \tag{3.6}$$

$$t^* = \frac{t}{t_{1/2}},\ x^* = \frac{x}{c_0 t_{1/2}},\ k^* = k t_{1/2} \tag{3.7}$$

Accordingly, the acceleration of the piston in equation (3.2) is nondimensionalized as:

$$a_p^* = \frac{t_{1/2}}{c_0}\frac{du_p}{dt} \tag{3.8}$$

The normalized value of k^* supplies the correspondence of $t^* = 1$ to the time for half of the reactant mass to react and form products for the ZND solution. In the present work, all time units are measured in half-reaction times.

Furthermore, the governing equations are written in the Lagrangian form. This procedure has two advantages, first, it permits the history of each gas particles to be followed to facilitate the examination of shock-reaction interactions. Numerically, the Lagrangian approach of following the gas particles also allows an accurate description of the flow near shock waves—as particles are compressed behind shocks, the grid spacing is decreased directly with the gas volume. This characteristic alleviates the need (to some extent) of using adaptive grids. The nondimensionalized governing equations in Lagrangian form is given as follows:

$$\text{Mass Conservation:} \quad \frac{\partial v}{\partial t} - \frac{\partial u}{\partial \xi} = 0 \tag{3.9}$$

$$\text{Momentum Conservation:} \quad \frac{\partial u}{\partial t} + \frac{\partial p/\gamma}{\partial \xi} = -a_p \tag{3.10}$$

$$\text{Energy Conservation:} \quad \frac{\partial e}{\partial t} + \frac{\partial pu/\gamma}{\partial \xi} = -\frac{Q}{\gamma}\dot{\alpha} - a_p u \tag{3.11}$$

$$\text{Reactant Consumption:} \quad \dot{\alpha} = \frac{d\alpha}{dt} = -w(\alpha, t),\ \ w(\alpha, t) = k\alpha e^{-E/T} \tag{3.12}$$

$$\text{State Equation:} \quad p = \rho T \ \ (\rho = \frac{1}{v}) \tag{3.13}$$

where e is the sum of the internal and kinetic energies given by:

$$e = \frac{1}{\gamma(\gamma-1)}\frac{p}{\rho} + \frac{u^2}{2} \tag{3.14}$$

Q is the nondimensional heat of reaction and ξ is the Lagrangian space coordinate defined by $d\xi = \rho(dx - udt)$. Note that all variables are now expressed in the nondimensional form, and hence the (*)'s will be omitted in all subsequent expressions.

The algorithm of the present computation is originally developed by Yoshikawa (1980) and later by Moen et al. (1984) and has been adapted for more detailed investigation of the flow structure in the present work. The governing equations are solved using a 2-step MacCormack algorithm with the flux-corrected transport anti-diffusion scheme. A detailed description of the numerical scheme is given in Appendix A. In order to start the calculation, the steady one-dimensional ZND detonation is first calculated to obtain the time scale and the shocked and burned gas velocities which are used to prescribe the initial motion of the piston in the unsteady problem. The present results are calculated using a spatial resolution that is equivalent to 50 numerical cells for determining the half-reacted region in the steady ZND solution. It should be stressed that the overall resolution is amongst the highest used compared with previous works. The Courant number used is 0.5.

3.1.1 Parameters used in the studies

In the present calculations, the gas mixture is taken to have a nondimensional heat of reaction Q of 50, and γ is assumed constant at 1.2. The so-called degree of piston overdrive f, as defined in Fickett and Wood (1966) to be:

$$f = \left(\frac{D}{D_{CJ}}\right)^2 \tag{3.15}$$

is taken to be 1, where D is the detonation velocity. Thus, $f = 1$ corresponds to a CJ detonation wave at steady state. For the parameters chosen in the present study, the ZND detonation is characterized by a shock pressure of 42.06, shock temperature of 4.813, while the pressure and temperature in the burnt products are 21.53 and 12.00, respectively. The detonation velocity is at 6.216, the shocked gas velocity at 5.505 , and the products are at

2.752, all measured in the absolute laboratory frame. The activation energy will be varied in the study while keeping the degree of overdrive at 1.

3.2 Initiation and Oscillatory Characteristics

The formation of the pulsating detonation by the action of a piston will first be examined. In the following calculations, the velocity of the piston to initiate the detonation is given in Fig. 3.2. At time zero, the piston is set to move into the fresh mixture ($x > 0$) at the von Neumann shocked gas velocity ($u_p = u_{sh}$) and is maintained for 1.8 half-reaction times ($t = 1.8$), after which it decelerates linearly to the steady state CJ burnt gas velocity (u_{CJ}) at 2 half-reaction times ($t = 2$), and remains at this level afterwards. The value of u_{sh} and u_{CJ} is obtained from the steady ZND solution.

The transient initiation of the detonation for activation energy ranging from 20 to 30 is displayed in Fig. 3.3 where the evolution of the shock pressure is plotted with time. Due to the sudden and high initial velocity of the piston, the gas near the piston surface is compressed rapidly to form a shock wave which initiates a strongly overdriven detonation with a shock pressure typically about twice the steady value of 42. As the piston decelerates to its final velocity, the shock pressure begins to evolve towards the steady state value. For activation energies at and below 25, the shock pressure approaches the steady state value and a steady ZND detonation is obtained. For activation energies above 25, the detonation begins to exhibit oscillatory behavior. Slightly beyond the stability limit (e.g., $E = 26$), the shock pressure oscillation is quite regular and close to being sinusoidal with a well defined frequency (period = 12.7). As E is increased to 27, the oscillation deviates from the sinusoidal appearance and becomes nonlinear, although the frequency is unchanged. When the activation energy is increased further to 28, regular oscillatory pattern begins to break up and eventually a new periodic pattern appears near $t = 80$. Instead of the single mode

appearance for $E = 26$ and 27, the cycle now contains a lower maximum in addition to the largest one, with the overall period being almost doubled to 25.6. For even higher E of 30, the oscillation pattern becomes quite irregular and no repeatable cycle is captured within the time calculated.

The resulting temporal behavior of the detonation front indicates a period doubling type of bifurcation pattern which can be observed for a more general class of nonlinear dynamical system where the sequence of break-up would quickly lead to highly irregular behavior (Feigenbaum 1978, Guckenheimer and Holmes 1983). Figure 3.4 shows in more detail the break-up sequence for $E = 27$, 28, and 28.5 where the shock pressure oscillations are displayed after repeatable cycles have been obtained. For $E = 27$, the period of the oscillation is 12.7 which becomes doubled at $E = 28$, and tripled at $E = 28.5$. Higher order bifurcation sequence has not been obtained in the present numerical simulation due to the rapid approach to irregular behavior and the increasing difficulty to accurately capture the highly transient events. As irregular behavior is approached, the solution becomes highly sensitive to initial conditions and hence numerical noise would render the appearance of repeatable cycles irreproducible. Nevertheless, the results obtained have demonstrated the resemblance of the pulsating detonation to a broader class of nonlinear oscillators.

3.2.1 Dynamic Structure of the Pulsating Wave

Let us examine more closely the large amplitude oscillations during a periodic cycle by considering the structure of the one-dimensional detonation when repeatable cycles have been developed.

The detailed spatial profiles for $E = 28$ at different times is displayed in Fig. 3.5. The events cover the first half of the cycle as shown in Fig. 3.4 with the detonation front initially reaching a minimum pressure (at $t = 175$) and its subsequent acceleration to the maximum value, followed by a decay to a second (higher) minimum.

At the minimum state ($t = 175$), the shock pressure, temperature, and velocity are below the steady state values (cf. the steady ZND profiles on the right of the figure). The pressure behind the leading shock continuously decrease (in space) while the temperature rises as chemical reaction proceeds. When the reaction is complete (cf. the reaction rate curves also plotted in the figure) the profiles approach the CJ burnt gas values. At a later time level ($t = 178$), the detonation has begun to accelerate and the flow properties behind the shock increase accordingly. The pressure profile shows that there is a pressure build up behind the leading shock which is similar to that obtained for piston driven detonations (Fickett and Wood 1966). As a result, the maximum pressure is no longer at the shock front. The pressure build up is responsible for the acceleration of the detonation through compression waves that propagate towards the leading shock. In the third curve plotted, the detonation has almost reached its peak value with the shock pressure attaining close to twice the steady state value. The pressure behind the shock drops dramatically (in space) while the temperature rises sharply indicating very rapid chemical reaction immediately following the shock front. As the detonation decays in the subsequent curves, the shock pressure falls off with time. However, a region of relatively high pressure and velocity remains near the end of the reaction zone. The large pressure and velocity generated behind the shock during the peak value of the detonation produces large disturbances and therefore require a longer distance to equilibrate with the downstream flow.

It is interesting to note that during the acceleration of the detonation (from $t = 175$ to 178), the temperature behind the reaction zone continues to decrease. Moreover, the highest temperature in the reaction zone is only attained at $t = 184$ when the shock has begun to decay. These events indicate that there is a time lag for the flow conditions to be transmitted between the leading shock and its downstream elements. Since no heat loss is assumed in the present analysis, the large increase in temperature due to the fluctuation

in heat release remain visible downstream of the reaction zone, providing a "permanent" record of the oscillatory history.

Note also that while the shock pressure exhibits large fluctuations during the dynamical event, the pressure and velocity at the trailing end remain quite close to the mean burnt gas values. This effect has been made observable by having the piston moving at the steady burnt gas velocity, otherwise a nonsteady expansion fan would appear behind the detonation as the produce gas would decelerate to zero velocity at the left end boundary. The present results clearly indicate that the dominating events of the evolution of the pulsating detonation occur within a self-contained hydrodynamic structure. It seems that the far field boundary behind the detonation does not play a significant role in the problem. We will return to investigate this further later in the chapter.

The qualitative features of the particle velocity distributions (Fig. 3.5c) are quite similar to the corresponding pressure profiles. Since the velocity is measured relative to the piston, the downstream velocity approaches zero, i.e., it satisfies the piston boundary condition, which is at the burnt gas velocity for the steady state propagation. It is interesting to note that the trailing velocity is slightly larger than zero (i.e., higher than the piston velocity) when the detonation is at the lowest velocity (at $t = 175$). However, the velocity then decreases below zero (i.e., flow towards the piston surface) as the shock approaches the maximum state at $t = 181$. It is clear that a dynamic flow field exists in the detonation complex before reaching equilibrium downstream of the structure.

The gasdynamic interaction in the detonation complex can be more clearly illustrated by examining the distribution of Mach number (M) measured relative to the leading shock. In the profiles plotted in Fig. 3.5d, the Mach number in front of the shock represents the velocity of the shock wave measured in the laboratory frame which fluctuates with the instantaneous speed of the detonation front. Across the shock, the Mach number decreases

to a subsonic value and then rises to a value near 1 downstream of the structure. In the steady state solution, the Chapman-Jouguet condition dictates that the trailing end of the detonation must approach a sonic condition ($M = 1$) so that small flow perturbations from downstream are incapable of penetrating the detonation complex and hence isolating it from the downstream flow field. In the nonsteady propagation studied here, the trailing Mach number is subsonic when the detonation velocity is at its minimum ($t = 175$) and gradually increases to a supersonic value with the increase in detonation velocity ($t = 181$), before decreasing back to subsonic again. Thus, in the subsonic regime, the flow field behind the detonation would be able to influence the detonation until the trailing Mach number becomes supersonic.

In order to further investigate its relation to the steady state CJ solution, the time averaged flow quantities over a cycle is computed. It is found that the averaged shocked quantities (i.e., shock pressure, temperature, etc.) agree with the steady state ZND solution to within 2 percent. Moreover, the time averaged quantities at the end of the detonation complex, where the reactant mass fraction is depleted to 10^{-7}, also agree with the CJ burnt gas solution, and in particular, the relative Mach number recovers a value of one. Thus, although the wake of the pulsating structure traverses through both subsonic and supersonic regimes, the averaged flow at the trailing end of the complex satisfies the CJ sonic condition. These time averages have been computed for activation energies of 25.5, 26, 27, and 28, all having good agreement with the steady state solution.

3.2.2 Independence of Back Boundary

The nature of the nonsteady one-dimensional detonation is significantly determined by its relation with the back boundary condition. The fact that the time averaged pulsating detonation satisfies the CJ sonic condition suggests that the structure may indeed be independent of the flow field behind the detonation as in the steady state case. To

examine this, calculations have been carried out where the flow field behind the detonation complex (taken at $\alpha = 10^{-7}$) is "cut off" and replaced by (spatially) uniform quantities obtained at the beginning of the cut. This is equivalent to enforcing a "radiation condition" where flow perturbations originating from downstream of the detonation complex are removed, allowing only the perturbations generated within the complex. The numerical calculation is restarted from the full solution by enforcing this condition at all subsequent times. Figure 3.6 shows the resulting detonation for $E = 28$ and 27, where calculations are carried out for 2 and 4 cycles, respectively. The obtained detonations reproduce remarkably the full solutions and the shock pressure trace with time for $E = 27$ is indistinguishable from the original solution seen in Fig. 3.4. This confirms that the detonation complex is a self-contained system where the dynamic behavior is generated. It is important to note that the detonation complex defined here contains both the chemical reaction zone and the hydrodynamic equilibrium zone. For the parameters considered, the chemical reaction is essentially completed within a length of between 2 and 6 (when $\alpha = 0.05$) from the shock. Thermodynamic and hydrodynamic equilibrium, however, requires a longer length to be achieved. As already seen in Figs. 3.5a and 3.5c, as the detonation reaches a maximum velocity, the large flow disturbances generated within the complex requires a longer distance to equilibrate to the downstream value, even though the strong shock implies that high temperature and hence very rapid chemical reaction can be accomplished within a very short distance. In the present calculation, when the reactant mass fraction decreases to 10^{-7}, the zone length from the shock is approximately 10, the pressure and particle velocity both approach the steady state (or time averaged) values. Thus, the results indicate that the pulsating detonation can be characterized by a "hydrodynamic thickness" within which the mechanisms for sustaining the oscillatory detonation is contained.

For real cellular detonations, the boundary of the so-called "hydrodynamic thick-

ness" is where the energy associated with the transverse wave oscillation is assumed to be dissipated (Soloukhin 1969, Edwards et al. 1976). Experimentally, this thickness is estimated to be of the order of a few detonation cell lengths (Vasiliev et al. 1972, Edwards et al. 1976), although the chemical reactions are essentially completed within a fraction of a cell cycle. For the steady one-dimensional ZND detonation, the hydrodynamic thickness corresponds to the reaction zone length since there are no gasdynamic fluctuations. For the pulsating detonation, the hydrodynamic thickness is also greater than the reaction zone length. Therefore, it is not sufficient to require the termination of chemical reactions to define the self-contained detonation. A meaningful autonomous structure must include the thermodynamic and hydrodynamic equilibrium within it.

In summary, the structure of the pulsating detonation illustrated in the present study is qualitatively similar to that obtained by Fickett and Wood (1966).[1] However, with a piston overdriving the detonation, Fickett and Wood's solutions are open to interaction with the piston, since the flow field behind the detonation is everywhere subsonic. By removing the piston overdrive in the present study, it is now possible to clarify the autonomous nature of the detonation complex and its independence of the back boundary, even in the nonsteady case. This information is invaluable as well for understanding the propagation of real multi-dimensional detonations which are always nonsteady and where the existence of the sonic CJ plane is yet to be demonstrated. The present result suggests the existence of a CJ plane in the time-averaged sense.

[1]The oscillatory behavior obtained in the simulation is also closely related to the oscillations observed when a sphere or blunt body is fired through a combustible mixture at velocities close to the Chapman-Jouguet value (Alpert and Toong 1972; Lehr 1972). A detailed account of the experimental and theoretical treatment can be found in Toong (1983). This result has also been successfully simulated recently, see, for example, the work by Wilson and Sussman (1991).

3.3 Response of the Detonation to Perturbations—Failure

An important conclusion from the above analysis is that the pulsating detonation is not a stable wave propagation, but one that oscillates around the time-average steady state solution. To further explore the stability of the pulsating detonation and its ability to sustain perturbations, the response of the oscillatory wave to perturbations and the quenching process will be studied in this section.

To remove the piston support subsequent to the establishment of the self-oscillatory wave, the piston motion will be brought to stop shortly after the initial driving process. The initial motion of the driving piston is given as follows. At time zero, the piston is set to move at the particle velocity obtained behind the shock wave for the steady state detonation. This velocity will be maintained for 1.8 half-reaction times ($t_{1/2}$), which then decreases linearly to zero at $2t_{1/2}$. In the subsequent times, the piston will remain motionless to avoid any interference with the wave motion.

The parameters used are heat of reaction $Q = 50$, activation energy $E = 27$ and 26, and a constant specific heat ratio $\gamma = 1.2$.

3.3.1 Metastable State Following Failure

Figure 3.8 shows the shock pressure evolution with time of the resulting detonation wave and its failure for different amplitudes of density perturbations as sketched in Fig. 3.7. The activation energy used is $E = 27$. For the undisturbed detonation, Fig. 3.8 shows that the shock pressure oscillates with a well defined periodic pattern. The positive density perturbations applied (i.e., negative temperature perturbations for the same pressure) serve as a quenching process which breaks down the chemical reaction of the detonation. The wave form of the density perturbation is described by the positive portion of a sine wave. The amplitude of the perturbation is given with respect to the initial density in the quiescent

undisturbed mixture ahead of the wave (i.e., $\Delta\rho/\rho_0$). The wavelength is given by the period of the unperturbed detonation ($\tau = 12.7$) multiplied by the average (or CJ) detonation velocity ($D_{CJ} = 6.216$).

The perturbation is applied at $t = 46$, which is closed to the minimum pressure of the pulsating detonation. Due to the positive density, the perturbation has an initial effect of increasing the shock strength. However, the temperature deficit soon becomes dominant and the shock pressure starts to decrease. The decrease in shock strength can be understood in the following simple model. In the unperturbed detonation, the shock serves to compress the initial gas mixture to a high pressure and temperature. Subsequent to this compression, the temperature is high enough for chemical reaction to take place. As the mixture reacts, the burnt product increases in temperature and expands. The expansion of the product in turn acts like a piston to support the shock propagation. The velocity of the effective piston is given by the rate of increase in volume of the product gas and would be proportional to the rate of chemical reaction. As the detonation is perturbed, the temperature perturbation decreases the temperature behind the shock. Since the Arrhenius chemical reaction law dictates a high temperature sensitivity, the lower temperature would drastically decrease the reaction rate and hence the rate of expansion of the burnt particles. This then leads to a lower effective piston velocity to support the shock and its velocity will decrease. As the shock strength drops, the temperature behind the shock decreases further and for large enough temperature deficit, this would causes a perpetual effect to eventually weaken further the chemical reaction and decouple the detonation complex. As a whole, the application of the temperature deficit perturbation in the one-dimensional analysis can be likened to a thermal energy extraction from the initial mixture. For the actual multi-dimensional cellular detonation, an energy deficit is also imposed due to the absorption of the energy of the transverse shock waves upon collision with the walls. In both cases,

the effect is to drastically reduce the ability to sustain the fast chemical reaction that is necessary to support the detonation propagation.

By $t \sim 50$ (Fig. 3.8), the wave has passed over the perturbation. For a small perturbation (i.e., 10 percent), the shock decays to a pressure above 20 but is insufficient to decouple the detonation structure and it accelerates back to a detonation at $t \sim 60$. For larger density perturbations, the shock pressure is observed to decay to a value of between 10 and 15, which then stays at about a constant level before re-transition to detonation. For very large perturbations (i.e., 50 percent and higher), the shock pressure continues to decay slowly and re-transition is not observed for the time calculated.

Thus, after the detonation is quenched, Fig. 3.8 demonstrates that a metastable state exists where the shock pressure, and hence the shock velocity, remains approximately constant for some time before undergoing re-transition to detonation. For the conditions considered (i.e., $Q = 50, \gamma = 1.2$), the CJ detonation has a velocity (or Mach Number) of $M_D = 6.216$ and a shock pressure of $p_{sh} = 42.06$. The corresponding CJ deflagration solution, as can be calculated following Section 2.2.2, has a shock pressure of 12.1, shock velocity of 3.33, and flame velocity 3.08, corresponding to $0.53M_D$ and $0.496M_D$ respectively. The burnt gas properties for the CJ deflagration has $p_2 = 5.8, \rho_2 = 0.61$, and $T_2 = 9.5$. Thus, the shock pressures obtained in the quenched waves (Fig. 3.8) are close to the theoretical CJ deflagration solution as presented in Chapter 2. Moreover, in the nonsteady analysis, pressure jumps can be observed from time to time during the metastable propagation regime. These may in fact be the one-dimensional manifestation of the so-called hot-spots formations due to the localized excited chemical activities which can eventually cause re-transition to detonation. Also plotted in Fig. 3.8 is the solution for no heat input which is in effect from $t = 69.6$ after a 50 percent perturbation is applied to quenched the detonation. This calculation shows that without the heat release (i.e., no chemical reac-

tion), no pressure jumps are observed and the shock pressure decays to a lower level and at a faster rate that for the reactive solutions.

Let us now examine the flow profiles during the propagation of the resulting fast deflagration. Figure 3.9 displays the spatial profiles of pressure, temperature, velocity, and density at different times for 50 percent density perturbation. Also plotted with the temperature profiles are the reactant mass fraction distributions α to indicate the location of the reaction front. The first curve at $t = 47.8$ is obtained close to the initial application of perturbation, and a typical detonation wave profile is obtained. For this time, chemical reaction is rapidly completed behind the leading shock, which has pressure of about 42, and a CJ burnt gas pressure of about 21 is achieved. A so-called Taylor expansion fan then brings the particle velocity down to zero at the left boundary (i.e., $x = 0$) so that the pressure also decreases. At a subsequent time, ($t = 69.6$), the detonation is quenched, and the shock pressure, temperature, velocity and density all decrease to lower values. It can also be observed that the Taylor expansion wave has penetrated ahead of the reaction zone as the pressure drops continuously behind the shock to the reaction front (the location of the reaction front is indicated in Fig. 3.9b, where the mass reactant fraction is plotted with the temperature. The mass reactant fraction α is equal to 1 before reaction starts, and drops to zero when the reactants are consumed. The location where the rapid decrease in α indicates the location of the reaction front). Note that the the Taylor expansion wave has also decreased in strength as the pressure levels behind the shock are all lowered. By $t = 100$, an approximate shock-flame structure similar to the CJ deflagration model has emerged. The curves for $t = 110$ and later times show a leading shock followed by a relatively uniform region, and then a fast reaction zone that leads to a rapid decrease in pressure, velocity and density, while the temperature increases. The shock pressure obtained is approximately 14, slightly higher than the CJ deflagration solution, however, the solution is still transient and

localized pressure jumps are destroying the uniformity from time to time. The properties behind the wave (at $x \sim 300$ for curve $t = 110$) also approaches the Chapman-Jouguet condition where the pressure, temperature, velocity and density is practically equal to the CJ deflagration burnt gas solution that satisfies the sonic criterion. The flame velocity is very close to half the CJ detonation velocity, which propagates at a slightly lower speed than the leading shock. Because of this, the separation between the two increases slowly with time.

3.3.2 Mechanisms for Sustaining the CJ Deflagration Structure

Thus, the numerical simulations carried out have shown that when the detonation fails, the reaction zone separates from the leading shock so that the resulting complex is no longer a coupled system. By applying a lower ambient temperature, the Arrhenius reaction rate would drastically decrease where the reaction front can no longer support the shock at the detonation level. The rapid decay in shock pressure is thus due to the decrease in reaction rate. The Taylor expansion fan, however, would take a much longer time to penetrate into the wave complex to influence it during the initial failure.

On the other hand, the profiles shown in Fig. 3.9 indicate that the level of the shock pressure after the initial failure may depend on the Taylor expansion wave behind the initial detonation. This expansion wave initially supports a velocity equal to the CJ detonation burnt gas velocity ($u_{CJ} = 2.75$), which can also act as a piston to support the propagation of the leading shock at approximately half the CJ detonation velocity. To ensure that the propagation of the reaction front is not merely due to the effect of convection of the gas which could be supported by the Taylor expansion wave, the propagation velocity is further checked by evaluating the mass flux across the reaction front, which is given by:

$$\rho_1(\dot{R}_F - u_1) \times \Delta t = \rho_2(\dot{R}_F - u_2) \times \Delta t$$

The theoretical CJ deflagration solution yields a mass flux of 18.5, while the numerical simulation yields approximately 15.4 between time $t = 100$ and $t = 110$. Thus, the obtained reaction front indeed appears to propagate closely at the theoretical value. Furthermore, as the Taylor expansion wave decays with time (e.g., for $t > 100$), the shock pressure (and velocity) only decreases slowly. This indicates that chemical reaction is required for the propagation of the deflagration structure.

To illustrate the insensitivity of the flame velocity to the downstream flow field due to the residual Taylor expansion wave, the following steady state analysis has been performed. For a given shocked state (state 1), the flame velocity for different downstream conditions can be derived using the Hugoniot analysis (eqns. 2.4, 2.5, 2.6) to give:

$$\dot{R}_F = \frac{1}{u_2 - u_1}\left[\frac{1}{\gamma - 1}\left(\frac{p_2}{\rho_2} - \frac{p_1}{\rho_1}\right) + \frac{u_2^2 - u_1^2}{2} - \frac{Q}{\gamma}\right] \tag{3.16}$$

Consider a shock velocity (i.e., state 1) which is approximately fixed at the CJ deflagration value, and using the same heat release Q, the flame velocity can be computed for various downstream conditions, such as the pressure p_2. Table 3.1 illustrates the solution when the downstream pressure deviates from the theoretical CJ deflagration value. For the CJ deflagration solution, the downstream state falls at the CJ point on the Hugoniot curve as shown in Fig. 3.10. If the downstream pressure is higher than the theoretical value, the flame velocity remains very closed to the CJ deflagration solution of 3.07. Even when the downstream pressure is as large as 70 percent of the theoretical value, the flame propagation velocity is hardly changed. The decaying Taylor expansion wave would therefore not drastically alter the flame propagation velocity.

Thus, the heat release plays a key role in sustaining the propagation of the deflagration complex. Due to the lower shock temperature, the reaction rate for the CJ deflagration would be orders of magnitudes smaller than that for detonation so that the deflagration cannot depend on the induction type mechanism for its propagation. How-

Table 3.1: Insensitivity of the flame velocity to the downstream pressure

Pressure $\frac{p_2}{p_{CJ}}$	Flame velocity $\dot{R}_F$	Relative Mach No. $\frac{\dot{R}_F - u_2}{c_2}$	Burnt gas velocity u_2	Burnt gas sound speed c_2
1.0 (CJ)	3.0745	1.0 (sonic)	0	3.0748
1.05	3.0745	0.955	0.1232	3.0903
1.10	3.0736	0.912	0.2441	3.1017
1.20	3.0696	0.831	0.4738	3.1220
1.30	3.0628	0.755	0.6908	3.1397
1.40	3.0530	0.683	0.8987	3.1553
1.50	3.0396	0.612	1.1008	3.1691
1.70	2.9995	0.486	1.5036	3.0768

ever, the temperature gradient field which still exists even when the detonation fails will facilitate the propagation of the flame front. Without the temperature gradient, that is if the temperature is uniform behind the leading shock, the shock temperature would not be sufficient to cause ignition of the gas. In actual deflagrations, the effects of transport are present to further support the propagation of the reaction front. Although these are absent in the present model, the velocities of the flame and the shock still agree well with the theoretical values.

Moreover, the pressure jumps resulting from localized chemical excitation appears to provide important support for the propagation of the metastable structure. Figure 3.9 has indicated that there are occasional pressure buildups ahead of the main reaction front. In the quasi-steady shock-reaction structure, the competition between the effects of a decaying reaction front and the generation of localized perturbation in chemical reaction that exists behind the leading shock therefore constitutes the metastable structure. The preconditioned field behind the shock will play a key role in determining the growth of possible perturbation and the subsequent re-transition to detonation.

3.3.3 Natural Re-Transition to Detonation

The shock pressure evolution displayed in Fig. 3.8 has shown that there exists a range of perturbation amplitudes which will lead to failure of the detonation where the resulting deflagration would subsequently undergo re-transition to detonation. If the perturbation is too small, the shock pressure is still high enough to cause auto-ignition and the CJ deflagration state is not obtained. If the perturbation is too large, the localized pressure jumps produced are weak and the fast deflagration continues to decay slowly.

Figure 3.11 displays the profiles when a 30 percent density perturbation is applied to the detonation where natural re-transition is possible. In comparing Figs. 3.9 and 3.11, the pressure decay for the 30 percent perturbation is slower than that for the larger perturbation. At $t = 110$, large pressure jumps are already observable in the profile, which eventually lead to re-transition to detonation. The reactant mass fraction α in Fig. 3.11b shows that as re-transition occurs, reactants are consumed (as α decreases to zero) at several locations in the region between the leading shock and the flame front. These localized chemical activities are thus a key mechanism for the natural re-transition to detonation, as is observed in the previous experimental studies of Oppenheim (Urtiew and Oppenheim 1965, 1966, 1967, 1968; Meyer and Oppenheim 1971).

However, for a large perturbation (50 percent), the magnitudes of the localized pressure rise become smaller with time. After $t = 160$, Fig. 3.8 shows that the shock pressure jumps become negligible and re-transition is not achieved. Note that for the 50 percent amplitude perturbation, the disappearance of the pressure jumps coincides with the time when the shock pressure just decreases below the CJ deflagration value of $p_{sh} = 12$ (at $t = 160$). Similar result is also observed for perturbations larger than 50 percent. This suggests that when the deflagration has decayed below the CJ deflagration value (i.e., the maximum velocity deflagration), natural re-transition is less likely, if not impossible. This

again reinforces the metastable nature of the CJ deflagration state as a regime just prior to the transition to detonation.

3.3.4 Effect of Activation Energy

The activation energy is a key parameter that governs the stability of the detonation wave. To understand the influence of activation energy on the ability of the detonation to sustain perturbations, similar calculations have been repeated when the activation energy is decreased to 26. Figure 3.12 displays the evolution of the shock pressure when the detonation is perturbed with perturbation amplitudes ranging from 50 to 80 percent. The unperturbed detonation is a slightly more stable detonation as it fluctuates with a smaller amplitude than that obtained for $E = 27$. To minimize the difference between the flow structures for the two cases studied, the initial point of application of the perturbation is chosen at approximately the same time and the same shock pressure as those for $E = 27$. Comparing Figs. 3.12 and 3.8, it can be seen that by decreasing the activation energy, a larger perturbation is required to induce failure, furthermore, re-transition can be accomplished even for a larger amplitude. For 50 percent and larger perturbations, Fig. 3.8 showed that the resulting wave remains as a fast deflagration for $E = 27$, but this is not so when $E = 26$, where re-transition is possible even for an 80 percent perturbation. Since the Arrhenius law dictates that the reaction rate for high activation energy mixtures is more temperature sensitive than for low activation energy, when E is high, a small amplitude deficit can have a large effect in decreasing the reactivity behind the shock to cause decoupling of the detonation structure.

3.4 Summary

The numerical simulation carried out have shown that the one-dimensional detonation is a self-organized structure that manifests as a longitudinal oscillatory wave. The

resulting oscillatory pattern depends strongly on the activation energy of the gas. For the set of parameters studied, the one-dimensional detonation evolves into a steady ZND structure for activation energy at and below 25. As E increases from this stability limit, a regular periodic structure is obtained. When E is increased further, the periodic pattern is seen to break up that follows a period-doubling type of sequence. For very high activation energies, the oscillation pattern becomes quite irregular.

The pulsating detonation is found to agree with the steady Chapman-Jouguet solution when averaged over a cycle of the pulsation. In particular, the time averaged trailing flow satisfies the CJ sonic condition. The computations also indicated that the structure is autonomous in that it is quite independent of the far rearward boundary condition. The self-contained structure consists of the chemical reaction zone and a gasdynamic equilibrium region characterized by a hydrodynamic thickness within which chemical reaction terminates and thermodynamic and hydrodynamic equilibrium has been attained.

The stability of the pulsating wave to density or temperature perturbations and its subsequent failure is analyzed. By decreasing the chemical reactivity through the decrease in initial temperature, the fast reaction necessary for supporting the propagation of the detonation structure breaks down. The self-oscillatory coupling between the shock and the chemical reaction is destroyed together with a decrease in wave velocity. The results indicate that the properties of the obtained quasi-steady regime agree quite well with the CJ deflagration solution proposed in Chapter 2. The fast deflagration then propagates in a metastable manner for some time before undergoing re-transition to detonation. The re-transition process appears to be facilitated by the occurrence of localized random pressure rise in the wave structure.

The one-dimensional pulsating detonation is thus shown to be a self-organized structure and the transition process can be considered as the formation of an oscillatory

structure rather than the steady ZND detonation. Furthermore, the oscillatory behavior and the break-up sequence exhibited by the pulsating wave indicate that the detonation is analogous to classical oscillators. In order to further understand the mechanisms for sustaining and establishment of the pulsating structure, it would be of great value to develop an oscillator model to describe the detonation.

Chapter 4

Transition from CJ Deflagration to Detonation

In the preceding chapters, the quasi-steady regime just prior to the onset of detonation has been analyzed. The properties of the detonation wave is also examined and it is shown that the one-dimensional detonation is inherently oscillatory for large activation energies. In this chapter, the transition of the quasi-steady maximum velocity deflagration to the nonsteady detonation will be examined. As opposed to the initiation of detonation with a piston, which is an externally driven event and is strongly dependent on the piston condition, the present study will concentrate on the transition process which is the natural development of the self-sustained structure. Since the final obtained detonation is an oscillatory entity, period perturbations will be used to stimulate transition by helping to regenerate the detonation structure.

The fast deflagration complex as obtained in Section 3.3 will be used as the initial condition for analyzing the transition process, where the left end boundary consists of a closed end non-moving piston. The gas mixture properties will also be identical to those described in that section. The deflagration chosen for the initial condition will be the ones that remain as fast deflagrations (i.e., no natural re-transition) unless otherwise stimulated by perturbations so that any subsequent transition is due purely to external excitations on the structure. For this reason, the deflagrations generated initially with large density

perturbations will be used here. The sequence of failing the established detonation with a 50 percent density perturbation for $E = 27$ is described in Fig. 3.8 and with an 80 percent perturbation for $E = 26$ is displayed in Fig. 3.12. To stimulate re-transition, the deflagration complex will be systematically perturbed using a wave train of flow disturbance of different frequencies.

The governing equations used in the study are again the one-dimensional reactive Euler equations written in the Lagrangian form and the numerical method for solving them is presented in Chapter 3.

4.1 Periodic Flow Perturbation to Induce Transition

The flow disturbance consists of a stationary wave train of sinusoidal density perturbation, but constant pressure, of fixed length placed just in front of the leading shock at a specified time $t = t_0$. The wavelength Λ of the flow perturbation is given by:

$$\Lambda = \frac{D_{CJ}}{2}\tau_p \tag{4.1}$$

where D_{CJ} is the steady CJ detonation velocity, and τ_p is the period of the applied excitation which can be scaled with the unperturbed pulsating detonation period τ. Since the fast deflagration propagates at about $D_{CJ}/2$, the spatial wavelength of the imposed perturbation would be approximately equal to that for the unperturbed pulsating detonation if $\tau_p = \tau$. The period of the perturbation will be varied to generate perturbations of different wavelengths. The total length of the perturbation is fixed at four wavelengths that have period τ:

$$l = 4\frac{D_{CJ}}{2}\tau \tag{4.2}$$

The perturbation amplitudes of $\Delta\rho/\rho_0 = 0.2$ and 0.4 of the original density will be studied. In the present work, two activation energies ($E = 27$ and 26) will be examined. For $E = 27$,

the resulting detonation would be a large amplitude pulsating detonation with a single dominant frequency. As E decreases to 26, the detonation would be more stable with a smaller amplitude oscillation.

4.2 Effect of Perturbation Frequency on Re-Transition

We will first examine the re-transition process for $E = 27$ when the period perturbations are applied at time $t_0 = 100$. Figure 4.1 displays the pressure, density, and temperature profiles for $E = 27$ at $t = 100$ when the flow perturbation with an amplitude of 20 percent of the initial density is applied.

The shock pressure subsequent to the application of the periodic perturbation is displayed in Fig. 4.2 where the period of the perturbation varies from $\tau_p = 0.635$ to 25.4. As the shock propagates into the sinusoidal perturbation, the shock pressure exhibits oscillations which persist until the end of the perturbation near $t = 150$ (Fig. 4.2). Due to the overplotting of the solutions for various disturbance frequencies, the detailed fluctuation in pressure cannot be distinguished from the figure. Nevertheless, because of the relatively low amplitude of the perturbations, their growth has not been fed back to the shock so that the shock pressure does not rise until the wave has propagated pass the disturbance.

The application of periodic flow perturbations does appear to be able to stimulate deflagration to detonation transition. The re-transition process consists of abrupt sharp rise in the shock pressure to values of about twice the CJ shock pressure ($p_{CJ} = 42$). The strong detonation then decays gradually towards the CJ value while oscillations begin to grow. For the time calculated, the resulting detonations have not established the oscillatory pattern as observed in the unperturbed detonation yet. However, the solution for $\tau_p = 3.81$ does appear to evolve towards the natural detonation period of 12.7. The pulsating detonation, therefore, seems to have the capability to select the final frequency to excite the system. In

contrast to the pressure spikes or hot spots as seen in the natural transition in Fig. 3.8, which represents the selection from a wide spectrum of random flow perturbation frequencies for amplification, the application of well defined frequencies seems to bring out the frequency dependence nature of the transition process, as is so common in many nonlinear oscillators.

For perturbations with periods around 3, Fig. 4.2 indicates that the transition process takes place within the shortest time. For periods larger than 8 and less than 2, transition is much slower. For $\tau_p = 25.4, 0.635$, and 0.127, transition is not observed within the times studied, and it is not likely to occur in the latter two cases since the shock pressures are found to remain very close to that corresponding to the fast deflagration.

4.2.1 Frequency Selectivity of Perturbation Growth

The frequency selective process of the growth of the perturbations can best be illustrated in the spatial profiles of temperature where the spatial distribution and the history of the gas particles are represented in the Lagrangian (i.e., particle fixed) spatial coordinate ξ as the wave propagates over the perturbation (Fig. 4.3). Four perturbation periods, $\tau_p = 1.27, 3.175, 12.7$, and 25.4, are plotted in Figs. 4.3a-d. At $t = 100$ when the perturbation is imposed, the figure shows the sinusoidal temperature perturbation ahead of the leading shock, which is represented by the temperature jump at $\xi \sim 510$. As the shock propagates into the perturbation, the temperature of the particles rises according to the same Lagrangian wavelength of the perturbation. In other words, the temperature perturbation is convected downstream of the shock. Since the gas particles are compressed behind the shock, the actual wavelength of the temperature distribution behind the shock would be smaller than that ahead of the shock. The compression of the spatial variation is given directly by the density ratio across the shock.

For very small periods, the amplitude of the temperature perturbation is seen to decay behind the shock ($\tau_p = 1.27$, Fig. 4.3a). As the period decreases these diminishing

disturbances therefore have a negligible effect on the deflagration complex and transition would require a much longer time to accomplish. For $\tau_p = 3.175$, Fig. 4.3b shows that the perturbation grows in amplitude behind the shock and at $t = 140$, the temperature perturbation has increased significantly for a large amount of gas ($\xi = 510$ to 560). The increase in temperature would drastically accelerate chemical reaction to result in transition to detonation. For this perturbation period, re-transition is observed within the shortest time. As the period is increased to 12.7, the perturbation amplitude is also capable of growing behind the leading shock. However, the larger wavelength here leads to a larger separation between the temperature peaks and confines the temperature increase to a smaller amount of gas than that for $\tau_p = 3.175$. When the period is increased further to 25.4 (Fig. 4.3d), the growth rate is drastically reduced. Hence, the quasi-steady regime sets up a flow field behind the leading shock where the growth rate of the perturbation amplitude is frequency selective.

The distributions of pressure and density in physical (Eulerian) space x are shown in Figs. 4.4 to 4.6 for $\tau_p = 1.27, 3.175$, and 12.7 respectively. In these figures, the pressure and density profiles are plotted for three times as the wave propagates into the sinusoidal perturbation. Since the pressure is assumed constant in the perturbation field, the disturbance ahead of the leading shock is only observable in the density profile. The effect of compression of the perturbation wavelength by the shock can be seen in the density distributions at $t = 120$ and 140 in all the figures. For a period $\tau_p = 1.27$, the pressure and density profiles continue to decay to lower values. For $\tau_p = 3.175$, the density perturbations grow behind the leading shock (Fig. 4.5b). Note also that as the disturbances react (at $t = 140, x \sim 620$), the expansion of the burnt gas causes the wavelength of the disturbance to increase accordingly. The induced reactions are accompanied with a region of higher pressure which propagates towards the leading shock (Fig. 4.5a, $t = 140$). These pressure

waves will feed back to the leading shock to help amplify it and accelerate the transition process. Similar events can be observed in Fig. 4.6 for $\tau_p = 12.7$, although the region of induced reaction and pressure increase is not as severe as for $\tau_p = 3.175$.

Note that as the wavelength of the perturbation decreases, and therefore the spatial gradient of the flow perturbation increases, the time for transition to take place does not decrease indefinitely. Indeed, there is an optimal perturbation period near $\tau_p = 3.175$ that favors re-transition the most. The existence of an optimal period for transition to detonation is closely related to the the critical temperature gradient necessary for the development of detonation first investigated by Zel'dovich et al. (1970) and later by Zel'dovich (1980) and also by Yoshikawa (1980). In their study, Zel'dovich et al. (1970) examined the formation of detonation waves in a non-uniformly preheated gas. They considered a finite length of gas in an initially quiescent container with an adiabatic wall. The initial temperature distribution is assumed such that the temperature decreases linearly from a fixed high temperature at the wall with a prescribed gradient to the ambient level. The higher temperature near the wall would increase the rate of chemical reaction and the expansion of the burnt gas would produce a shock wave. The flow field for different initial temperature gradients were analyzed and they demonstrated that there exists a range of initial temperature gradient which could facilitate the amplification of the shock to detonation. Since the rate of chemical reaction is a strong function of temperature, if the temperature gradient is too steep so that the reaction proceeds in the neighborhood of the hot wall only, then the shock formed would rapidly separate from the reaction zone and the shock cannot amplify and transition to detonation does not take place. On the other hand, if the temperature distribution is nearly uniform, the reaction proceeds at about the same rate throughout the entire space and the condition of constant volume thermal explosion arises. If the temperature gradient is intermediate between the two extremes, then the shock wave

generated can, in turn, induce intensive reaction to produce a closely coupled system of shock-reaction complex leading to the development of a detonation wave. In the present study, the wavelength of the imposed perturbation can be considered as having an effective prescribed gradient in the shock processed gas. Hence, the existence of an optimal perturbation wavelength to induce transition to detonation is also expected. Moreover, the flow condition considered in the present study is far more relevant to the transition problem. The frequency sensitive amplification of flow perturbations observed here also appears to be connected to the random generation of "hot spots" observed in previous transition experiments, which would correspond to the competition for amplification of a wide frequency spectrum of flow perturbations.

The above calculation shows that the optimal period for re-transition to take place is of the order of the reaction time for the steady detonation solution (recall that the time units used are the half-reaction time calculated for the steady ZND detonation, thus the reaction time is of the order of $2t_{1/2}$). In the natural detonation, the characteristic time for chemical reaction to take place is proportional to the steady value of half-reaction time $t_{1/2}$. This is the time required for rapid chemical reaction to occur in order to maintain the crucial interaction between the leading shock and the chemical reaction so that they propagate in a closely coupled manner. In order to have transition to detonation, the perturbation must also promote the close coupling between the shock and the chemical reaction that grows with the temperature disturbance. Hence, the perturbation with a period of the order of the detonation reaction time will best facilitate the coupling between the two elements and promote transition. The reaction (or induction) time of the detonation wave is therefore a key parameter that controls the transition process.

The frequency selective amplification of flow nonuniformities has been recognized in other combustion processes, one of which is the chemical-acoustic amplification in a

constant volume gas. The behavior of small amplitude acoustic amplification in a constant volume reacting gas has been analyzed by Riley (1984) and the frequency selectivity of the amplification rates has been established. Using a linearized analysis, the period of the fastest growing acoustic perturbation $\tau_{p_{max}}$ can be computed. By curve-fitting the numerical results, an empirical expression was obtained (Riley 1984) which also indicates that the fastest growing perturbation has a period proportional to the chemical reaction time, and hence the induction time, of the gas.

In a more related context, the works of Majda and Rosales (1987) and Almgren et al. (1990) have studied the high frequency wave interaction in chemically reacting gases during the induction period. Using asymptotic techniques, they examined the effects of high frequency waves on the acceleration of the burning rate that is related to the generation of "hot spots" due to the presence of nonuniformities in the medium. These analyses have demonstrated several results that are of direct relation to the present work. First, it was shown that any spatial inhomogeneity in the temperature will enhance temperature growth so that the gas can explode in a time earlier than the homogeneous explosion time as predicted by the induction mechanism. Second, high frequency simple waves will always contribute to additional temperature rise of the mean field than when only low frequency waves are present. The high frequency temperature waves studied which are convected with the gas particles are similar to the temperature perturbations examined in this chapter. These so-called "entropy wave" due to the particle-fixed nature (as opposed to the acoustic pressure waves) are demonstrated mathematically to interact with the mean flow to enhance combustion. Their findings seem to support the notion of inducing transition to take place by periodic perturbations. However, the frequency selectivity of the growth rate has not been explored in their studies which is also confined to small amplitudes.

4.3 Effect of Time of Application of Perturbation

To examine the effect of the time of application of perturbation, the computational study is repeated when the flow perturbation is applied at a later time at $t_0 = 125.5$. The profiles for the deflagration complex at this moment are shown in Fig. 4.7 which are very similar to those obtained at $t_0 = 100$ in Fig. 4.1, although the separation between the leading shock and the reaction zone is increased. Moreover, since the deflagration complex considered is a continuously decaying wave, its properties (i.e., pressure, temperature, etc.) would decrease to a lower level at $t_0 = 125.5$ so that transition is expected to require a longer time to accomplish.

The shock pressure evolution subsequent to the application of the flow perturbation at $t_0 = 125.5$ is shown in Fig. 4.8. The times for transition to take place (t^*) can be seen to be larger than those where the flow perturbations are applied at an earlier time. Nevertheless, the optimal perturbation period to induce transition remains around $\tau_p \sim 3$, while a slight deviation from this value would drastically change the time for transition to take place. Figure 4.9 plots the time required for transition to occur versus different periods of perturbation applied, where the time required for re-transition t^* is defined to be the time when the leading shock has reached the steady-state detonation pressure (i.e., $p_{sh} = 42$) minus the initial time of application of the perturbation t_0. The figure illustrates clearly the existence of an optimal frequency (or period) for transition to occur.

4.4 Effect of Perturbation Amplitude

The amplitude of the sinusoidal flow perturbation $\Delta\rho/\rho_0$ has so far been restricted to 20 percent of the initial density. In this section, the re-transition process is examined for a larger perturbation amplitude of 40 percent of the initial density.

The shock pressure evolution due to the stimulation of the larger amplitude per-

turbation for $E = 27$ is shown in Fig. 4.10. Perturbation period of $\tau_p = 1.016$ to 12.7 have been calculated. For these perturbations, re-transition is found to be facilitated and requires much less time than when 20 percent perturbations were used. Indeed, the shock pressure traces in Fig. 4.10 show that the perturbations grow after a short delay upon the initial application of the perturbation. Unlike the smaller amplitude perturbations studied above where the shock remains near a relatively low pressure of 14 before undergoing a rather abrupt jump, the shock pressure here grows gradually to values around the CJ detonation shock pressure of 42. Superimposing on the shock pressure rise are the imposed fluctuations due to the external source, which have undergone rapid growth to larger amplitudes. Subsequent to the termination of the externally applied perturbations, the pulsating wave rapidly evolves into one with frequency and amplitude very close to the unperturbed detonation. The rapid adjustment of the detonation once the imposed oscillation has terminated can be clearly seen for $\tau_p = 1.905$, as the shock has propagated passed the high frequency perturbation (at $t \simeq 130$), the period of the detonation pulsation is quickly increased to its natural value of 12.7.

Note that the re-transition observed in Fig. 4.10 is not accompanied by abrupt shock pressure jumps which usually lead to overpressures near twice the CJ shock pressure for the smaller perturbations and for natural transitions. Except for $\tau_p = 1.016$, where the applied perturbation appears to have little effect on the wave, and hence when re-transition does occur, the effect of the applied perturbation would be small so that it resembles the natural re-transition due to a wide spectrum of perturbation frequencies. The re-transition for this extremely small period occurs after a much longer time and is accompanied with an abrupt pressure jump.

The pressure trace for $\tau_p = 1.905$ shown in Fig. 4.10 is found to have the fastest amplification to detonation. Although the shock pressure does rise gradually for $\tau_p = 12.7$

to the detonation value, its growth rate is clearly not as rapid. The frequency selective amplification of the flow perturbation within the wave complex for the large amplitude perturbation is shown in Fig. 4.11. As in Fig. 4.3, the temperature profiles for four different perturbation periods, and at different times, are plotted with the Lagrangian spatial coordinate ξ. Again, perturbations of very small period ($\tau_p = 1.016$) appears to decay within the wave complex. Thus, although the gradient generated by the large frequency perturbation is large, the perturbation cannot grow. For period $\tau_p = 1.905$, which is closed to the optimal value to induce re-transition, the flow disturbances appear to grow rapidly. At time $t = 120$, the temperature perturbations near $\xi = 520$ to 580 has already increase to the CJ burnt gas temperature of 12. As τ_p is increased, the amplification rate is shown to be reduced (Figs. 4.11c-d).

The effects of perturbation magnitudes on the time of re-transition is summarized in Fig. 4.12, where the time required for re-transition is plotted for different periods of perturbation for the two amplitudes studied. Since the shock pressure fluctuates widely during the transition process of the larger amplitude perturbations, the time required for re-transition is estimated from a local time-averaged pressure (to filter out the oscillatory components) which has attained the steady detonation pressure of 42. The figure indicates that the qualitative trend of the frequency selectivity for the two amplitudes are quite similar, with the larger amplitude perturbation requiring consistently less time for re-transition to take place. The optimal perturbation period to facilitate re-transition is again of the order of the reaction time, and is obtained to be near 1.6 for the 40 percent amplitude. This is about half the value obtained for the smaller amplitude case. Since the reaction rate is highly temperature sensitive, the larger temperature perturbation can influence the chemical reaction rate more rapidly, and with a shorter wavelength perturbation the reaction rate can increase shortly after as the gas particle passes the leading shock. Thus, the

larger amplitude temperature perturbation with short wavelength (or period) will promote amplification of the disturbance and hence facilitates transition. Consequently, the optimal wavelength (or period) to induce transition for the large amplitude perturbation is expected to be smaller. However, it should be noted that if the amplitude is too large, an abrupt shock pressure can result which can lead to transition regardless of the frequency of the perturbation. This would not be a natural development process but an externally driven one. It is the small amplitude perturbation that will bring out the intrinsic frequency selectivity of the transition process.

4.5 Effect of Activation Energy

The activation energy is known to play a key role in determining the nonsteady response of the detonation wave. It is therefore necessary to investigate the effect of different activation energies on the transition process, which have thus far limited to the case for $E = 27$. The computations are repeated for $E = 26$ which would correspond to a more stable pulsating detonation. Figure 4.13 shows the shock pressure evolution of the re-transition process when the wave is originally failed using a large density perturbation (80 percent, see Fig. 3.12). As already pointed out in Fig. 3.12, the more stable wave is capable of achieving natural re-transition even when a larger perturbation is applied (compared to that for $E = 27$) to induce failure. Fig. 4.13 shows that natural re-transition is attained near $t = 200$.

Artificially applied perturbations with 20 percent amplitude and different periods were calculated. Similar to the events observed in Fig. 4.2, Fig. 4.13 shows that transition can be stimulated at a much faster rate than when no flow perturbation is applied. Comparing Fig. 4.13 with 4.2, it appears that the shock pressure requires less time to rise when the activation energy is decreased. Chemical reactions with low activation energies

are sometimes referred to as fast kinetics as reaction is less temperature sensitive so that it will proceed more uniformly at different temperatures. Thus, for lower values of E, after the mixture is processed by the leading shock, chemical reaction proceeds at a more uniform rate and the feedback of the amplification of the perturbation can be felt at an earlier time. On the other hand, if E is high, the chemical reaction rate is more temperature sensitive. Reactivity will initially be very slow, only as the temperature begins to build up will reaction abruptly accelerate. Thus, for high E, a longer time is required to feedback the information regarding the growth of the perturbation to the shock.

Due to the relatively small amplitude of the applied perturbation, as transition occurs, abrupt shock pressure rise is again observed while oscillatory patterns begin to develop with the period of oscillation approaching that of the natural unperturbed detonation.

The time for re-transition for different perturbation periods is plotted in Fig. 4.14 for both $E = 27$ and 26. The faster re-transition for the lower activation energy is again apparent, indicating that as the stability boundary is approached (i.e., for a more stable wave with low E) transition is accomplished within less time. The minimum re-transition time calculated for $E = 26$ is about half that for $E = 27$. For τ_p larger than about 3, the time for re-transition for $E = 26$ is typically about 3 detonation periods (τ). Since the detonation period τ remains almost identical ($\tau \simeq 12.7$) for both activation energies, transition takes place within a shorter time for the lower value of E.

Furthermore, Fig. 4.14 indicates that the period that will induce transition fastest is quite similar for the two activation energies calculated, and has value close to $\tau_p = 3$, which is of the order of the chemical reaction time. As the period decreases from this value, the time for re-transition increases drastically. However, the results for $E = 26$ in Fig. 4.14 show that perturbations with periods larger than the optimal value have less influence on the rapidity of re-transition as t^* does not increase as drastically as for $E = 27$ when

the perturbation period increases. Since the temperature sensitivity of the reaction rate is lower for small activation energies, it is expected that there is less sensitivity toward different wavelengths of the perturbation which essentially provide a variety of spatial temperature disturbances behind the shock to accelerate chemical reactions.

4.6 Summary

The one-dimensional analysis carried out illustrates that the flow condition set up just prior to the transition to detonation provides a preconditioned environment for which a frequency selective process for perturbation amplification takes place. The calculations showed that there exists an optimal perturbation frequency (or period) that can induce re-transition within the shortest time. The optimal period appears to be of the order of the reaction time of the detonation wave itself. This is the characteristic time required for the close coupling between the leading shock and the fast reaction zone in the integral detonation structure and hence should also be the time scale for controlling the coupling required for the formation of the detonation itself. For perturbations with periods close to the optimal value, the perturbation amplitudes are observed to grow rapidly behind the shock which would generate a region of high pressure to amplify the leading shock further. The transition process also appears to be highly frequency selective since the newly formed detonation can adjust rapidly from the imposed frequency to the natural detonation frequency once the perturbation terminates.

The results therefore indicate that the transition from deflagration to detonation can indeed be considered as the formation of a self-organized system. The oscillatory character of detonation observed in Chapter 3 have indicated its similarity to oscillators. The existence of an optimal frequency to induce transition to detonation further supports the possibility to treat the transition process as the excitation of the oscillator, which would

be strongly dependent on the characteristic frequency of the final oscillator. This aspect has not been fully recognized in previous research which has thus far treated the transition as mainly a process of attaining the required shock strength for auto-ignition to take place. The oscillatory nature of detonation points out that its propagation and its formation should be considered as dynamic processes which may depend on the response of the final system and the mechanisms that govern its intrinsic frequency. In order to further understand the basic mechanisms for sustaining and development of detonations, it would be of great value to formally establish the analogy between the pulsating wave with classical oscillators.

Chapter 5

Experimental Studies of Transition

5.1 Introduction

The one-dimensional investigation carried out in the previous chapter have indicated that the transition phenomenon can be described as the selective amplification of perturbations which depends on the frequency. While the random generation of localized explosion centers previously observed between the leading shock and the reaction zone in actual transition experiments (Urtiew and Oppenheim 1965) may have indicated similar mechanisms for a spectrum of random frequencies, the frequency selective character of the transition process have not been explored. An experimental investigation has therefore been carried out to support the computational study in order to further examine the frequency sensitivity of the transition process.

In this chapter, we will investigate experimentally the transition from high speed deflagration to detonation. It should be emphasized that the present study will concentrate on the onset of detonation once the maximum velocity deflagration (i.e., the quasi-steady regime) is attained. The initial condition used for the transition experiments will be obtained by damping out the transverse waves of the detonation using acoustic absorbing materials at the channel wall to general an approximate one-dimensional shock-flame com-

plex.

Because real detonations are inherently three-dimensional, there will be some difficulties in performing experiments identical to the conditions of the idealized one-dimensional theoretical model. The oscillatory nature of the detonation would manifest itself as a pattern of transverse shocks or pressure waves. In general, the behavior of the detonation and its failure can also be functions of the tube size. Furthermore, it would be difficult to generate relatively simple one-dimensional longitudinal waves to perturb the high speed deflagration complex which would, in turn, undergo transition to a multi-dimensional cellular detonation rather than a one-dimensional entity.

In view of these differences, the present investigation will follow a similar concept, but using a different technique to carry out the study. The experiments of Dupré et al. (1988) have shown that when the transverse pressure waves of a detonation are damped, the detonation will fail. To induce re-transition, artificial transverse pressure waves will be applied to the decoupled shock-deflagration structure to simulate the re-establishment of the natural transverse wave pattern. The artificial transverse pressure waves are generated by placing periodic obstacles along the channel walls where the obstacle spacings are varied to change the frequency of the transverse perturbations. However, no attempt has been made in the present study to vary the amplitude of the pressure perturbation by changing the obstacle height.

5.2 Experimental Details

The experiments are performed in a rectangular detonation tube of approximately 140 cm in length with a cross section of 2.8 x 1.6 cm. Two large glass windows extending over the entire length of the detonation tube are mounted on the side walls to facilitate flow visualization. The tube consists of three sections: the ignition section where a CJ

detonation is formed, followed by a damping section to remove the transverse waves to obtain a fast deflagration, and the obstacle-filled test section to perturb the deflagration to stimulate re-transition to detonation. The beginning of the damping section is located approximately 40 cm from the ignition source. The length of the damping section in the present experiments is 12 cm. The obstacle section has a length of 30 cm. The initiation of the detonation is achieved using a powerful spark discharge through a gap at the tip of an igniter rod. The electrical energy is stored in a 100μf capacitor charged to 4 kV using a high voltage supply. The energy release in the discharge triggers direct initiation of detonation in the ignition section. The acoustic absorbing walls of the damping section are constructed with layers of wire screen (nine layers of 1- x 1 mm mesh) to simulate a porous medium. The transverse pressure perturbations in the transition section are generated by periodically spaced obstacles on the walls. The obstacles are made of small sections of round solid rods of 3 mm diameter, and the spacings of the obstacles are varied to change the perturbation frequency. A sketch of the damping and obstacle sections is shown in Fig. 5.1.

The phenomenon of transition to detonation is observed using laser stroboscopic Schlieren photography as well as streak Schlieren photography. The laser pulses for the framing photographs are generated at 18.6 μsec between frames using a ruby laser. The streak photographs are taken with a Cordin 330 camera using a xenon flash tube as the light source. Figure 5.2 displays the schematic of the experimental setup, which is similar for the two camera systems, showing the double-pass Schlieren system and the triggering system used in the study. For streak photography the image is taken along the centerline of the channel. The field of view for photographing the transition process covers about 20 cm of the obstacle-filled test section and also the end of the damping section so that the initial structure of the deflagration prior to re-transition can be confirmed. As a further diagnostic, photodiodes are employed to check the velocity of the deflagration before being

perturbed by the obstacles as well as at the end of the obstacle section (beyond the field of view for photography) to monitor the resulting detonation velocity.

5.3 Experimental Results and Discussions

In the present study, three different mixtures were used: stoichiometric oxy-acetylene with 75 percent argon dilution, stoichiometric propane-oxygen, and stoichiometric methane-oxygen. These represent typical mixtures that exhibit, respectively, regular-, irregular, and highly irregular detonation cellular patterns. The cell size of the combustible mixtures represents the natural oscillatory wavelength of the detonation and can be controlled using the initial pressure for a given mixture. For the first two mixtures used, the cell size is approximately equal for the same initial pressure, and provides a comparison of the effects of cell regularity on the transition process.

5.3.1 Transition Induced by Transverse Pressure Waves

The perturbation of the quasi-steady regime using periodic wall obstacles will be examined using the high speed Schlieren framing photographs. Figure 5.3 shows the framing photographs as the quasi-steady shock-reaction complex propagates through the section with obstacles (obstacle spacing equal to the channel height, 28 mm). The mixture used for this figure is stoichiometric acetylene-oxygen with 75 percent argon dilution initially at 100 Torr. In the first frame, the approximately one-dimensional structure of the decoupled detonation can be observed. Between the leading shock and the reaction zone, a region of relatively uniform state can be seen to separate the two fronts. As the wave complex propagates to the right, the separation distance increases slowly. This shock-reaction zone complex serves as the initial condition for re-transition to occur when it is stimulated by transverse pressure perturbations. In the subsequent frames, the leading shock interacts with the wall obstacles, reflected transverse pressure waves are generated and propagate

away from the obstacles as a pair of circular fronts (e.g., third and fifth frames). The forward propagating fronts of these reflected waves intersect with the leading shock while the rearward portion propagates into the reaction zone. These events are repeated as the leading shock interacts with a new pair of wall obstacles. At the same time, the reaction zone becomes more turbulent as it enters the obstacle section and interacts with the transverse pressure waves. The transverse pressure perturbations can increase the rate of burning by the production of vorticity through two mechanisms. The three-shock Mach interaction of the transverse pressure waves with the leading shock produces shear layers in the unburned mixture ahead of the turbulent flame brush. Also the pressure gradient from the transverse pressure perturbations interacts with the density gradient in the flame zone and generates vorticity through the baroclinic mechanism ($\nabla p \times \nabla 1/\rho$). Note that these mechanisms are to be distinguished from the shear flow turbulence generated by the wall roughness and obstacles, as pointed out in the introduction. The increase in burning rate of the mixture will then generate pressure waves of its own. If the self-generation of the pressure waves is coherent with the induced perturbation, then coupling is facilitated and transition to detonation occurs. The conditions for coherence are a function of the sensitivity of the mixture (i.e., initial pressure) as well as the frequency of the induced perturbation. For the initial pressure tested in Fig. 5.3 coherence is not achieved and the deflagration complex remains unaccelerated with the leading shock and reaction zone propagating at constant velocities. Since the reaction zone propagates at a slightly lower velocity than the leading shock, the relatively uniform region separating the shock and the reaction zone grows continuously.

When the initial pressure is increased to above 130 Torr, the deflagration complex is observed to undergo re-transition to detonation. Figure 5.4 displays the time sequence of framing photographs of the transition process for the mixture at an initial pressure of

140 Torr. The initial interaction of the leading shock with the obstacles is very similar to that illustrated in Fig. 5.3, however, the interaction of the transverse pressure waves with the mixture behind the leading shock results in the intensification of reaction as indicated by the progressively smaller separation between the leading shock and the reaction zone. The relative position of the reaction zone from the shock is much closer than that observed in Fig. 5.3 for the same time. The stronger interaction of the pressure waves with the fast deflagration also results in a more turbulent structure behind the leading shock. The resulting region of intense chemical reaction in the otherwise uniform field of separation immediately behind the shock is very similar to that obtained in the one-dimensional computational studies. At the 10th frame transition is observed to occur as the reaction zone is confined to a thin region attached to the leading shock. In the last two frames, a detonation is generated which propagates at about the CJ detonation velocity of the mixture.

5.3.2 The Effect of Initial Pressure

The effect of initial pressure on transition can be further demonstrated in the streak photographs shown in Fig. 5.5. The orientations of the time and distance axes are indicated in the figure. The thin vertical dark line on the left of each streak photograph marks the beginning of the obstacle section. In the photographs, the trajectories of the leading shock and flame front can be clearly identified and they propagate at quite constant velocities (i.e., slopes of the trajectories) as they exit from the damping section. For an initial pressure of 100 Torr (Fig. 5.5a), as the deflagration enters the obstacle region, the reflections of the leading shock at the obstacles generate a series of transverse pressure waves propagating away from the locations of reflection (at the obstacles). The forward and backward propagating waves form a thick band of V-shaped trajectories near each obstacle. The average velocity of the structure remains fairly constant throughout the distance traveled and transition to detonation is not observed. As the initial pressure is

increased to 135 Torr (Fig. 5.5b) the initial deflagration appears very similar to the previous case for 100 Torr. However, as time progresses, the reaction zone becomes more intensified and extends much closer to the shock trajectory. A thick dark region then appears which covers a wide length behind the leading shock indicating the formation of an intensified chemical reaction zone that forms a V-shaped trajectory on the streak photograph. The forward traveling front rapidly overtakes the leading shock and cause an abrupt change in slope of the shock trajectory.

A series of tests were performed systematically for each of the three mixtures at different pressures. The initial pressure tested for stoichiometric acetylene-oxygen with 75 percent argon ranges from 100 to 160 Torr, for stoichiometric propane-oxygen the initial pressure tested ranges from 28 to 46 Torr, and for stoichiometric methane-oxygen the pressure tested ranges from 60 to 160 Torr. The results clearly indicate that high initial pressure (i.e., high mixture sensitivity) favors transition, as would be expected.

5.3.3 Effect of Obstacle Spacing

To examine the effect of obstacle spacing or frequency of the transverse pressure perturbation on re-transition to detonation, the experiments are performed for obstacle spacing of 10, 20, and 28 mm, corresponding to spacing over channel height ratio (s/D) of 0.36, 0.71, and 1. To further compare the results for no pressure perturbations, the experiments are repeated when the obstacles are removed, that is, when the quasi-steady regime propagates into a smooth channel. Figure 5.6 shows a series of streak photographs for the C_2H_2–O_2–Ar mixture for different obstacle spacings. Figures 5.6a-c are obtained at approximately the same initial pressure near 125 Torr. By comparing Fig. 5.6a and 5.6b, it can be seen that the frequency of the generated reflected waves for s = 10 mm is doubled over that for s = 20 mm due to the decrease in obstacle spacing. Although there are more obstacles to perturb the deflagration for s = 10 mm, the mixture remains

as a steady deflagration with a propagation velocity of about 790 m/s. When the obstacle spacing is increased to 20 mm, transition is observed (Fig. 5.6b). The figure shows that, amongst the different spacings tested, the obstacle spacing of 20 mm is the most favorable for transition to occur. When no obstacles are present, no transition was observed for the mixture at the pressures tested. Figure 5.6d illustrates the shock-flame structure of the fast deflagration with the leading shock and flame front having quite constant velocities (or slopes) in the streak photograph obtained at the maximum test pressure. The thick dark trajectory behind the shock indicates that it is indeed an active flame propagating in the channel.

Figure 5.7 displays a similar set of streak photographs for the propane-oxygen mixture with different obstacle sections used. These photographs are taken at approximately the same initial pressure of 35 Torr. Again, by comparing Figs. 5.7a and 5.7b, which have obstacle spacings of 10 mm and 20 mm, respectively, it appears that although there are more obstacles to perturb the deflagration, the rapidity of transition is decreased for $s = 10$ mm as transition appears to take place at the end of the field of view. When the obstacles are removed, Fig. 5.7c shows that transition is not achieved. However, the flame is seen to accelerate to about the same velocity as the shock as indicated by the almost parallel trajectories of the two fronts. A closer examination of the streak photograph reveals the acceleration of localized chemical reaction zones that catch up with the shock front, as indicated by the fine dark trajectories in the thin reaction zone that joint with the shock trajectory from time to time. These localized activities are analogous to the local intensified reaction regions and pressure jumps obtained in the one-dimensional computation of the quasi-steady structure in Chapters 3 and 4. The shock-flame complex is indeed a quasi-steady CJ deflagration as discussed where the localized enhancement of reaction may lead to natural re-transition to detonation, which would be quite possible to occur given sufficient

distance. When the initial pressure is increased to 44 Torr, transition is achieved within the test section, although the transition distance is drastically increased when there are no obstacles.

In comparing the transition processes for $2C_2H_2 + 5O_2 + 75\%Ar$ and $C_3H_8 + 5O_2$ in Figs. 5.6 and 5.7, it appears that the transition process for the argon-diluted mixture (a mixture that has regular detonation cell structure) is accompanied with a rather abrupt change in slope of the leading shock trajectory. For propane-oxygen (a mixture with irregular cell structure), instead of a sharply defined onset, the transition is accomplished over several "steps," as the shock trajectory experiences a series of more gradual accelerations.

The minimum initial pressures above which transition is observed for the three mixtures tested and for different obstacle spacings are tabulated in Table 5.1. The minimum pressure required for transition to occur in the available tube length for the configurations tested is lowest (i.e., lowest sensitivity) for obstacle spacing of 20 mm, indicating that an optimal spacing for transition for the present experiment lies near $s/D = 0.71$ (i.e., of order 1). In all of the conditions tested, the generation of transverse pressure waves with obstacles always leads to transition at a lower initial pressure than the smooth wall case. This clearly demonstrates the influence of transverse pressure perturbation in the formation of detonation.

Table 5.1: Minimum initial pressure above which transition is observed

Mixture	Minimum pressure for transition, Torr			
	Obstacle spacing, mm			
	10	20	28	No obstacle
$2C_2H_2 + 5O_2 + 75\%Ar$	125	110	130	—
$C_3H_8 + 5O_2$	40	34	34	44
$CH_4 + 2O_2$	100	60	65	125

The above results are summarized in Fig. 5.8 which plots the transition distance

for the various cases. The transition distance L^* is estimated from the streak photographs where the location of transition is calculated from the intersection of the initial and final slopes of the wave trajectories. In the figure, L^* is plotted against the mixture sensitivity as characterized by the cell size λ, both being normalized with respect to the channel height D. Several aspects can be observed from the figure. First, it shows that the transition distance is strongly dependent on the mixture sensitivity. As the cell size increases (or equivalently, decreasing the initial pressure), the transition distance increases. Secondly, the results show that above a certain sensitivity (e.g., about $\lambda/D < 0.16$, for $2C_2H_2 + 5O_2 + 75\%Ar$ with $s = 10$ mm) transition occurs consistently after about one channel height ($L^*/D \sim 1$). This distance seems to be the minimal distance for onset to take place. However, there appears to be no correlation between the transition with λ/D as it is clearly dependent on other factors, such as obstacle spacing and the detonation cell regularity of the mixture. Furthermore, the transition distance is influenced by the obstacle spacing, which corresponds to the frequency of the transverse wave perturbation. Thirdly, the transition distance for the obstacle spacing of 20 mm ($s/D = 0.71$) is consistently lower than for the other obstacle spacings tested and when no obstacles are used. This again indicates that there is an optimal transverse perturbation frequency for transition to occur. Another important feature noted is that for the same transition distance, the cell size for the propane-oxygen and methane-oxygen mixtures (Figs. 5.8b and 5.8c) is generally an order of magnitude higher than that for the argon-diluted acetylene-oxygen mixture (Fig. 5.8a). Propane-oxygen and methane-oxygen are known to have much more irregular cell structure than the argon-diluted mixture. It indicates that transition is greatly influenced by the regularity of the detonation cell pattern of the mixture.

5.3.4 Relation of Cell Regularity with Detonation Instability

Two of the main parameters for characterizing detonation waves are the cell size and the regularity of the cell pattern. The relationship between cell size and the sensitivity of the combustible mixture is well established. For a mixture with given chemical composition, a smaller cell size implies a shorter chemical reaction time and hence higher sensitivity. Thus, high initial pressures would promote rapid chemical reaction to facilitate transition from deflagration to detonation, as demonstrated by the present experimental results. On the other hand, the relations of the regularity of the detonation cell pattern with the detonation characteristics are not so clearly understood.

Experimental observations of detonation cell structure have indicated that irregular cell patterns are associated with frequent local failure and re-initiation in the gas mixture. It appears that cell irregularity is due to the ease of local failure, while the detonation propagation is sustained through local re-initiation. Complete failure of the detonation propagation is brought about by the inability to achieve local re-initiations (Lee 1993). For detonations with regular cell structure, the oscillatory pattern is quite "stable" and the cell pattern is maintained. This is in fact supported by the existence of galloping waves which are more readily observed in irregular systems than in regular ones. For the highly argon-diluted mixtures, the galloping mode (i.e., failure and re-initiation) is very difficult, if not impossible, to observe as demonstrated in the near limit detonation study of Dupré et al. (1990).

The relationship between cell regularity and activation energy was first pointed out by Ul'yanitski (1981) who observed that mixtures with low activation energies have more regular cell structures. This is in accord with the temperature sensitivity of the chemical reaction time which depends on the value of E. The higher temperature sensitivity for high E implies a more non-uniform reaction process as chemical reaction is initially quite slow

but awaits the temperature to build up before quickly accelerating the chemical reaction. As discussed in Chapter 3 for the one-dimensional detonation, low activation energies are associated with regular oscillatory patterns while high activation energies would correspond to more irregular patterns. The theoretical analyses of Erpenback (1962, 1964) and Lee and Stewart (1990) have also shown that high activation energy is associated with a wide spectrum of unstable frequencies and hence a more complex oscillatory pattern. Thus, high activation energy seems to be associated with irregular detonation cell structure whereas low activation energy would be associated with regular cell structure.

Shepherd et al. (1987) later demonstrated that activation energy may not be an appropriate parameter and the complete characterization of cell regularity has not been achieved to date. Nevertheless, the connection between the stability of the detonation and the regularity of the cell pattern is clear. Mixtures with regular cell pattern would correspond to stable detonations. These mixtures would be more capable of sustaining detonation propagation and require less time to undergo transition from deflagration to detonation. Mixtures with irregular cell structure would correspond to unstable detonations which are easier to fail. Moreover, irregularity is related to a wider spectrum of unstable frequencies which would imply the requirement to establish different kinds of conditions in order for transition to occur. Thus a longer time would be needed to accomplish re-transition in irregular mixtures. These properties are supported by the results in Chapters 3 and 4.

On the other hand, the results from Fig. 5.8 have shown that for the highly argon diluted mixture (a regular cell mixture), a value of λ/D of the order of 0.1 is needed for transition to occur, whereas for the irregular mixtures of propane-oxygen and methane-oxygen, transition can occur with a λ/D of order 1. Thus, it appears that irregular cell mixtures can achieve re-transition under a less sensitive condition (larger cell size). This can

be attributed to the fact that irregular cell structure is associated with the ability to amplify perturbations of a wide spectrum of frequencies. However, as pointed out recently by Lee (1993), the mechanisms responsible for the failure of detonation are different for regular and irregular cell mixtures. Consequently, one may not be able to use the same parameter (i.e., cell size) to measure the ability to sustain and re-initiate detonation propagation.

It can be remarked that the relationship of cell regularity and its characterization of detonation has not been fully understood and requires further studies.

5.4 Concluding Remarks

In the present experimental investigation, the results show that transverse pressure waves play an important role in the transition from deflagration to detonation. There is a strong indication that there is an optimal obstacle spacing, or alternatively an optimal transverse wave frequency, that facilitates transition the most. The optimal obstacle spacing obtained for the present experimental condition is of the order of the tube dimension (wall spacing). This seems to be consistent with near limit detonations in tubes since the intrinsic frequency for excitation will be related to the fundamental acoustic mode oscillation in the tube. While the acoustic interaction of detonation with the channel is absent in the one-dimensional model, the experimental results do support the existence of an optimal perturbation frequency as predicted by the one-dimensional simulation. This suggests that the transition phenomenon is one of resonance coupling between the gasdynamic processes and the chemical reactions that drive the pressure oscillation.

The results also show that sensitivity with respect to transition is strongly affected by the mixture's cell regularity. However, a complete understanding of the relations of cell regularity with the ability to sustain detonation propagation and to achieve transition requires further studies. Nevertheless, since cell regularity is related to the ease in which

pressure perturbations can be amplified, the results therefore reinforce the notion that the formation of a detonation is a consequence of generating a self-organizing structure from the gasdynamic and chemical processes. Thus, the experimental results for transition further support the need to construct a model in order to understand the self-organizing nature of detonations.

Chapter 6

Pulsating Detonation as an Oscillator

In Chapter 3, the oscillatory characteristics of the one-dimensional detonation and the period doubling type break-up sequence as the activation energy increases have indicated its similarity with many nonlinear oscillators. The apparent existence of optimal frequency to stimulate transition observed in Chapters 4 and 5 indicates further that the formation of detonation is the excitation of a self-organized oscillatory system. These results point out the possibility to model the pulsating detonation as an oscillator which would provide insight for understanding the mechanisms responsible for developing and sustaining the oscillatory behavior.

Yet, the remarkable resemblance of the pulsating detonation with classical nonlinear oscillators has not been fully realized and discussed in previous literature. This chapter will hence attempt to establish more clearly the analogy of the one-dimensional detonation with classical nonlinear oscillators by formally deriving an analogous oscillator equation to describe the one-dimensional pulsating detonation.

It should, however, be noted that the purpose here is not to develop an alternate formulation to solve the pulsating detonation problem, but to provide a framework to interpret the results obtained by direct numerical integration of the governing equations of gasdynamics.

We will first discuss some of the simple oscillator concepts that may be useful in understanding the instabilities of the pulsating detonation. We then return to the governing equations to formulate a nonlinear oscillator model.

6.1 Instabilities in Simple Oscillators

The question regarding why detonations behave in a nonsteady manner has been studied for a long time. The small perturbation analyses of Erpenbeck (1962, 1964) had demonstrated that for high enough activation energies, the one-dimensional ZND structure is unstable to small perturbations. However, the physical mechanisms that lead to instability are not clear from these studies. Neither can these analyses describe the behavior of the detonation subsequent to the initial instability. It is also unclear why the unsteady detonation should propagate in an oscillatory manner (i.e., rather than simply grow or decay exponentially, which could be another form of instability).

To provide the proper perspective to examine the obtained numerical results, it is useful to review some of the basic concepts of instability and oscillatory behavior in the general sense. We will consider i) static versus dynamic instabilities in an oscillator, ii) instability causing elements—such as negative spring constant, negative damping, and time lag, and, iii) to revisit the Rayleigh criterion of combustion instability for unsteady heat input to illustrate the possible role of phase relations in an oscillating system, and finally, iv) to provide some simple examples of nonlinear oscillators and their characteristic behavior. These basic concepts are, of course, the most simplified version of real systems, nevertheless, they may provide a guide for a meaningful interpretation of the numerical detonation results.

Consider a simple oscillator that can be described by the second order equation:

$$\frac{d^2x}{dt^2} + 2b\frac{dx}{dt} + kx = 0 \tag{6.1}$$

This may represent a mechanical oscillator with unit mass, spring constant k, and damping coefficient $2b$. Confining the discussion first to linear theory (i.e., for small x with constant b and k), the response of the oscillator can be readily obtained as follows:

$$x(t) = Ae^{(-b+\sqrt{b^2-k})t} + Be^{(-b-\sqrt{b^2-k})t} \tag{6.2}$$

From this solution, the instability can be classified into two categories:[1]

1. $k < 0$ (i.e., a negative spring constant). This instability leads to exponential growth of the solution $x(t)$, but no oscillatory behavior is obtained. This is therefore labeled as static instability.

2. $b < 0$ and $k > b^2$ (i.e., negative damping). This instability is oscillatory with exponential growing amplitude. Because the behavior of this instability is dynamic, it has been termed dynamic instability.

Static instabilities can be inferred from viewing the transient evolution of the system as a sequence of (quasi-) steady states. Hence steady-state consideration is enough to define the instability. In the prediction of dynamic instability, on the other hand, parameters such as inertance and capacitance must be included since they play an essential role in determining the transient response of the system to disturbances. These parameters are not part of the information needed to describe the steady-state system. Hence knowledge of steady-state characteristics alone are not sufficient for prediction of dynamic instability, and additional information about quantities such as zone length and system volume (associated with the inertance and storage capacity, respectively), etc., must also be included.

Many unstable oscillatory fluid dynamic and combustion systems have been found to be associated with dynamic instabilities and elements of "negative damping" can be

[1]The distinction between the two types of instability appears to have been first recognized by Maxwell (1868)

identified (Greitzer 1981). For detonations, the linear stability theories of Erpenbeck (1962, 1964) and Lee and Stewart (1990) have demonstrated that the instability is associated with a spectrum of unstable frequencies. The existence of these unstable frequencies implies that the instability of detonation is dynamic and oscillatory behavior can be expected near the stability boundary. The description of the dynamic behavior of the detonation must also involve a dynamic parameter, the hydrodynamic thickness, which, as pointed out in Section 3.2.2 is quite different from the steady-state chemical reaction zone thickness.

6.1.1 Role of Phase Relation

In many simple oscillators where the behavior is dynamic but yet there may be no damping elements in the systems. One way negative damping may arise is through the concept of time lag (or delay). For example, consider a simple spring oscillator with unit mass and unit spring constant:

$$\frac{d^2x}{dt^2} + \underbrace{x(t)}_{\text{function of } t} = 0 \tag{6.3}$$

Now, if the action of the restoring force has a time delay of t_l, then

$$\frac{d^2x}{dt^2} + \underbrace{x(t-t_l)}_{\text{function of } t-t_l} = 0 \tag{6.4}$$

Expanding the restoring force in a Taylor series in powers of t_l, and retaining only the first term, we get:

$$\frac{d^2x}{dt^2} \underbrace{-t_l\frac{dx}{dt}}_{\text{negative damping}} + x = 0 \tag{6.5}$$

This is the equation for a system with negative damping, in other words, a system that will exhibit oscillatory (or dynamic) instability.

Through the concept of time delayed action, it is possible to understand why an induction-type detonation is dynamically unstable. The induction process behind the shock

front of a detonation is essentially a time delay before rapid combustion occurs. A second delayed action takes place for the effect of products expansion to be propagated back to the shock to maintain its propagation.

The concept of time delay is an indication that the "phase" of action can place an important role in dynamic instabilities. The most simple and illustrative example is perhaps the original one by Lord Rayleigh (Rayleigh 1878), who established the Rayleigh criterion stating that: "If heat be given to the air at the moment of greatest condensation, or taken from it at the moment of greatest rarefaction, the vibration is encouraged." In other words, the criterion for the maintenance of oscillations by an unsteady heat input is that the heat input is "in phase" with the pressure rise.

The Rayleigh criterion can be demonstrated using the simplified Helmholtz oscillator derived in Appendix B. Consider the unsteady heat input to a plenum (volume) that experiences pressure fluctuation. The fluid under consideration is assumed to be a perfect gas, and the inertial and flow storage are lumped into two elements, with the mass under flow oscillation given by that in the inlet duct ρAL (see Appendix B), and the storage being due to the compressibility in the plenum of volume V. For a small heat release rate $\dot{Q}$ which is proportional to the pressure fluctuation P in the oscillator,

$$\dot{Q} = \phi P$$

where ϕ describes the phase relationship between $\dot{Q}$ and P, an equation for the pressure fluctuation P is found to be

$$\frac{d^2P}{dt^2} - \frac{\gamma - 1}{V}\phi\frac{dP}{dt} + \frac{c^2A}{LV}P = 0 \tag{6.6}$$

which is an oscillator equation with a damping coefficient proportional to the phase of the heat input rate with respect to the pressure. For $\phi > 0$, $\dot{Q}$ is in phase with the pressure fluctuation and dynamic instability is most favored. If $\phi < 0$, $\dot{Q}$ is 180° out of phase with

the pressure oscillation, the system is positively damped and no oscillation will result. This describes the phase relationship as stated by the Rayleigh criterion.

Note also that the "spring constant" of (6.6) is proportional to square of the sound speed of the gas inside the system. The compressibility of the gas therefore corresponds to the compressibility of the spring in an analogous mechanical oscillator.

6.1.2 Simple Nonlinear Oscillators

For systems that exhibit finite amplitude "limit cycle" oscillatory behavior, it will be necessary to consider the effects of nonlinearity associated with them. The second order equation in (6.1) illustrates a simple linear oscillator during the initial growth of the instability and will not be sufficient to describe real nonlinear systems. In general, the system mass m, spring constant k, and damping coefficient b, are not constant. Indeed, the spring restoring force kx and the damping term $-2bdx/dt$ are general functions of time. However, by making some slight modifications to the linearized equation, the characteristics of nonlinear "limit cycle" type oscillators can be obtained.

For a mechanical autonomous system with mass m, the standard nonlinear oscillator equation can be written in the form of

$$m\ddot{x} + kx = \mu f(x, \dot{x}) \tag{6.7}$$

where μ is in general a small positive parameter. The term on the left hand side of equation (6.7) has their usual meaning of inertia force ($m\ddot{x}$) and spring or restoring force (kx). The linear natural frequency of the system is $\omega_0 = \sqrt{k/m}$. The right hand term (μf) refers to a self-excited driving force since $f(x, \dot{x})$ is not an explicit function of time. As examples, for $\mu f = -2b\dot{x}$, the simple damping term of (6.1) in classical system is recovered. For $\mu > 0$, μf can provide a negative damping that is responsible for a self-excited oscillation of the system. For $f = (1 - \alpha\dot{x}^2)\dot{x}$, α being a small positive parameter, equation (6.7) would

describe a Rayleigh or van der Pol oscillator, a common nonlinear oscillator studied.

Nonlinearity can also be manifested through the addition of a nonlinear spring force. For instance, the simple structure of the Duffing's equation has embedded in it the necessary ingredients through which the transformation of the oscillatory patterns by period doubling and tripling can be manifested. Duffing's equation can be written as:

$$\ddot{x} + \beta\dot{x} + \sigma^2 x + \delta x^3 = \alpha \cos \omega t \tag{6.8}$$

($\beta, \sigma, \delta, \alpha$, and ω are constants) which describes the nonlinear interaction between the cubic restoring force (δx^3) and the periodic driving force (see Fig. 6.1). Due to the explicit time dependence of the external driving force, the Duffing oscillator is not autonomous. However, replacing the external forcing term with a self-excited force retains the general transformation features of the Duffing equation.

The above given examples of oscillators, although oversimplified, can provide the proper perspective to understand the oscillatory behavior of detonations. To achieve this, it will be necessary to express the governing equations in a particular convenient form and to lump some of the flow parameters into definite elements in order to overcome the overwhelming information generated from the continuum description.

6.2 Nonlinear Oscillator Model for Detonation

The analogy of the one-dimensional structure to classical nonlinear oscillators will now be formally demonstrated. In this section, an equation that has the fundamental properties of a nonlinear oscillator will be derived from the basic conservation laws of gas dynamics. The analysis will be based on the conservation of energy since the "driving force" for the pulsating detonation is provided by the chemical energy release. This equation will be derived from the integral form of the conservation equation so that the flow variables can be lumped into more meaningful components of an analogous system. The key elements

that constitute the oscillator will be identified and compared with those for a mechanical nonlinear oscillator to illustrate the analogy.

6.2.1 Theoretical Model

Consider a control volume that moves with the detonation complex. The system begins at the leading shock front and is bounded by a rear boundary shown in Fig. 6.2. The rear boundary is taken to be some constant distance l_h from the shock front where equilibrium CJ condition is assumed to prevail. Physically, such a rear boundary corresponds to the hydrodynamic thickness. In the present model, knowledge of the exact hydrodynamic thickness is not necessary. It is sufficient to assume that such a rear boundary exists. In general, an unsteady flow region follows behind the hydrodynamic thickness or the rear boundary. However, one can assume that a uniform flow created by a piston moving at the equilibrium CJ particle velocity follows the rear boundary, as will be the case in the numerical simulation carried out. This assumption again does not alter the main result, but simplifies the formulation of the analogous oscillator equation.

Since the numerical results in Section 3.2.1 have shown that the time-averaged shock velocity agrees with the steady state Chapman-Jouguet value, the instantaneous shock front location $x_s(t)$ is assumed to be composed of a time-averaged part and a fluctuating displacement $F(t)$ from this mean trajectory:

$$x_s(t) = D_{CJ}t + F(t) \tag{6.9}$$

and the shock velocity

$$\dot{x_s}(t) = D(t) = D_{CJ} + \dot{F}(t) \tag{6.10}$$

where D_{CJ} is the CJ detonation velocity which equals to the mean speed of the oscillatory detonation over the period τ, i.e.,

$$D_{CJ} = \frac{1}{\tau}\int_0^\tau D(t)dt \tag{6.11}$$

Thus, the shock front displacement $F(t)$ satisfies

$$\frac{1}{\tau}\int_0^{\tau} F(t)dt = 0 \tag{6.12}$$

from (6.10). The fluctuation of the shock trajectory $F(t)$ is chosen as the dependent variable in the oscillator equation to be formulated.

Using the control volume that follows the instantaneous motion of the shock front, the reactive Euler equation (eqns. 3.1-3.3) can be cast in the integral form. The conservation of mass, momentum, and energy can respectively be rewritten as:

$$\frac{d}{dt}\int_0^{l_h} \rho dx + \rho_{CJ}(D - u_{CJ}) - \rho_0 D = 0 \tag{6.13}$$

$$\frac{d}{dt}\int_0^{l_h} \rho(D-u)dx + \rho_{CJ}(D-u_{CJ})^2 - \rho_0 D^2 = -p_{CJ} + p_0 + \int_0^{l_h} \rho\frac{dD}{dt}dx \tag{6.14}$$

$$\frac{d}{dt}\int_0^{l_h} \rho\left[e_i + \frac{(D-u)^2}{2}\right]dx + \rho_{CJ}(D-u_{CJ})\left[e_{CJ} + \frac{(D-u)^2}{2} + \frac{p_{CJ}}{\rho_{CJ}}\right]$$
$$-\rho_0 D\left(e_i + \frac{D^2}{2} + \frac{p_0}{\rho_0}\right) = Q\int_0^{l_h} \rho w dx + \int_0^{l_h} \rho\frac{dD}{dt}(D-u)dx \tag{6.15}$$

These equations are expressed in their dimensional form and the velocities are measured in the absolute laboratory frame. Here, e_i is the internal energy, subscript 0 refers to the initial unperturbed state, and subscript CJ denotes the CJ equilibrium (downstream) state. The last integral term on the right hand side of equation (6.14) represents the pseudo-force term for the moving control volume. The first term on the right hand side of equation (6.15) denotes the rate of the chemical energy release, while the second term denotes the rate of work done by the pseudo-force. Using the continuity and momentum equations (6.13, 6.14), the energy equation (6.15) can be manipulated to the following form

$$\frac{d}{dt}\int_0^{l_h} \rho e dx + \rho_{CJ}e_{CJ}(D-u_{CJ}) - \rho_0 e_0 D - p_{CJ}u_{CJ} = Q\int_0^{l_h} \rho w dx \tag{6.16}$$

where e is, again, the total energy term defined to be the sum of the internal and kinetic energy, i.e., $e = e_i + u^2/2$.

For a steady ZND detonation where $D(t) = D_{CJ}$, the unsteady integral term drops and (6.16) reduces to

$$\rho_{CJ}e_{CJ}(D_{CJ} - u_{CJ}) - \rho_0 e_0 D - p_{CJ}u_{CJ} = Q\int_0^{l_h} \rho^0 w^0 dx \tag{6.17}$$

where superscript 0 refers to the steady ZND wave. The integral term in the above equation is obtained from the conservation of reactant mass to be

$$\int_0^{l_h} \rho^0 w^0 dx = \rho_0 D_{CJ} \tag{6.18}$$

which simply states that the rate of reactant depletion inside the control volume is equal to the unburned mass flux entering the control volume for the steady ZND wave. Subtracting the steady state equation (6.17) from equation (6.16), one obtains

$$\frac{d}{dt}\int_0^{l_h} \rho e dx + \rho_{CJ}e_{CJ}\dot{F} = Q\int_0^{l_h} \rho w dx - Q\rho_0 D_{CJ} \tag{6.19}$$

where the term $\rho_0 e_0 \dot{F}$ has been neglected since $\rho_0 e_0/\rho_{CJ}e_{CJ}$ is of the order of $1/M_{CJ}^2 << 1$ (M_{CJ} is the CJ detonation Mach number).

Two nondimensional volume-averaged quantities, the reaction rate W and the energy I, will be defined for the system under consideration:

$$W = \int_0^1 \frac{\rho w}{\rho_0 D_{CJ} l_h^{-1}} d\xi \tag{6.20}$$

$$I = \int_0^1 \frac{\rho e}{\rho_0 D^2/2} d\xi \tag{6.21}$$

where $\xi = x/l_h$. Defining $W_1 = W - 1$ to be the fluctuation of the dimensionless mean rate of the reactant depletion and $\dot{I}$:

$$\begin{aligned} \dot{I} = \frac{d}{dt}(I - I^0) &= \frac{d}{dt}\left(\int_0^1 \frac{\rho e}{\rho_0 D^2/2} d\xi - \int_0^1 \frac{\rho^0 e^0}{\rho_0 D_{CJ}^2/2} d\xi\right) \\ &= \frac{d}{dt}\int_0^1 \frac{\rho e}{\rho_0 D^2/2} d\xi \end{aligned} \tag{6.22}$$

as the rate of fluctuation of the dimensionless mean internal-kinetic energy inside the control volume, the energy equation (6.19) can be reduced to

$$l_h I\ddot{F} + \frac{\rho_{CJ} e_{CJ}}{\rho_0 D}\dot{F} + \frac{l_h D}{2}\dot{I} = \frac{D_{CJ} Q}{D} W_1 \tag{6.23}$$

where the $(\dot{})$ convention denotes time derivative. Thus, equation (6.23) states a balance relation of the rate of energy fluctuation for the control volume. The first term on the left hand side denotes the energy fluctuation rate associated with the shock velocity oscillation. The second term corresponds to the unsteady exit condition at the rear boundary. The third term represents the rate of the energy fluctuation within the control volume itself, and the term on the right hand side denotes the fluctuation of the chemical energy release rate inside the control volume. Note that equation (6.23) has the form of a second order nonlinear differential equation in terms of the variable F similar to that describing a mechanical oscillator.

6.2.2 Analogy to Nonlinear Mechanical Oscillators

Equation (6.23) is in essence the energy conservation equation recast in a form to model the mathematical behavior of a nonlinear oscillator. The remaining task here is to identify the elements that constitute an analogous oscillator.

In examining the results from the numerical simulation of the fully developed pulsating detonation, it appears that the oscillatory characteristics can best be described by:

1. The fluctuation of the volume-averaged reaction rate has the same frequency as the shock velocity fluctuation with a small phase shift due to the ignition delay. Thus, W_1 can be expressed in the form of

$$W_1 = g(F, \dot{F})\dot{F} + \mu h(F) \tag{6.24}$$

where μ is a small parameter and $h^0(F) = 0$.

2. The rate of fluctuation of the volume-averaged total energy is in phase with the fluctuation of the shock trajectory, because the variation of the shock front displacement (F) from the mean trajectory represents the temporal change of the system potential energy. Hence $D\dot{I}$ in equation (6.23) would be proportional to F, and has the form of

$$D\dot{I} = s(F, \dot{F})F \tag{6.25}$$

Its Taylor expansion with respect to the steady ZND state can be expressed as

$$\begin{aligned} D\dot{I} &= F\sum_{n=0}^{\infty}\sum_{m=0}^{n}\frac{1}{n!}C(n,m)\left[\frac{\partial^n s(F,\dot{F})}{\partial x_s^{n-m}\partial \dot{x}_s^m}\right]^0 F^{n-m}\dot{F}^m \\ &= b_0 F + \sum_{n=1}^{\infty}\sum_{m=0}^{n} b_n^m F^{n-m+1}\dot{F}^m \end{aligned} \tag{6.26}$$

where

$$b_0 = \frac{8\pi^2 I^0}{\tau_0^2} \tag{6.27}$$

with τ_0 being the period obtained from the linearized limit. The period τ should scale with the hydrodynamic thickness (i.e., $l_h \sim D_{CJ}\tau$). Hence, the coefficient b_0 in equation (6.26) is proportional to D_{CJ}^2, i.e., to c_{CJ}^2 (the CJ equilibrium sound speed). Therefore, the coefficient b_0 exhibits the acoustic compressibility of the system inside the control volume similar to that obtained in equation (6.6).

Based on the above considerations, equation (6.23) can now be expressed in a more analogous form of a nonlinear oscillator:

$$l_h I\ddot{F} + \frac{4\pi^2}{\tau_0^2}l_h I^0 F + \frac{l_h}{2}\sum_{n=1}^{\infty}\sum_{m=0}^{n} b_n^m F^{n-m+1}\dot{F}^m = \mu f(F,\dot{F}) \tag{6.28}$$

where

$$\mu f(F,\dot{F}) = \frac{1}{D}\left(QD_{CJ}W_1 - \frac{\rho_{CJ}}{\rho_0}e_{CJ}\dot{F}\right) \tag{6.29}$$

denotes the net energy input to the system, i.e., the difference between the unsteady part of the chemical energy release and the energy fluxed out of the system. Comparing equation (6.28) with those for a mechanical oscillator, i.e. (6.7, 6.8), one notes that the pulsating detonation can be modeled as a self-organized nonlinear oscillator. The energy $l_h I$ stored in the system, the system compressibility embedded in the term $\dot{I}$ and the net energy input μf correspond, respectively, to the mass, spring, and damper elements in a mechanical oscillator. These are the key components responsible for the mechanism of self-sustained nonlinear oscillatory detonation and the transformation of temporal patterns via period doubling and tripling in the first bifurcation steps. The linear natural frequency for the detonation system is given by $\omega_0 = 2\pi/\tau_0$.

6.2.3 Numerical Verification of the Oscillator Model

The oscillator model derived for the pulsating detonation is verified by numerically computing the various terms in the oscillator equation. The numerical solutions are calculated using the method described in Chapter 3 after which the various terms in the oscillator equation are evaluated. The solutions considered are confined to the fully developed detonations that have established repeatable cyclic oscillations. To eliminate the nonsteady expansion flow field that exists between the wake of the detonation and the back boundary, the detonation is supported by a piston which propagates at the steady CJ burnt gas velocity. The parameters used for the calculations are again those used in Chapters 3 and 4, where $Q = 50$, $\gamma = 1.2$, while the activation energy will be varied.

The hydrodynamic thickness required to define the detonation structure is obtained by examining the spatial profiles of the pulsating structure. The particle velocity profile for $E = 27$ with period $\tau = 12.7$ is displayed in Fig. 6.3. As the particle velocity is approaching the steady burnt gas velocity u_{CJ} at $x = 405$, an inert acoustic disturbance is created by the mismatch of the sonic choking condition and running away from the deto-

nation wave system into the far field. Its amplitude does not attenuate since there are no physical diffusion terms in the governing equations. This disturbance is in reality dissipated and its amplitude maintenance in the far field has never been observed. Thus, in the following analysis the hydrodynamic thickness l_h is chosen ahead of, but close to, this disturbance origin, i.e., $l_h = 20$, that gives a small velocity deviation of $|u - u_{CJ}|/u_{CJ} = 0.03$. The solution of the oscillator equation (6.23) with the chosen l_h agrees well with the full direct numerical solution (see Fig. 6.4).

The terms in (6.23) and (6.28) are obtained from the numerical values of the flow variables and their derivatives. $E = 27$ is chosen as the first example because the onset of a period doubling from the limit cycle of $\tau = 12.7$ occurs at this activation energy (see the phase portrait of $W_1 - D_1$ in Fig. 6.5 where $D_1 = \dot{F}/D_{CJ}$) and the nonlinearity is well developed. The evolution of the four terms in (6.23) over 2τ is displayed in Fig. 6.6. The two terms associated with $\dot{F}$ and W_1 are evaluated directly from the flow variables, while the other two terms concerning $\ddot{F}$ and $\dot{I}$ are calculated from the flow variables and their derivatives. Although the derivatives are locally oscillatory as the numerical data are insufficiently smooth, the frequency and the phase of the pulsating detonation are not influenced.

Except for the small phase shift, the main part of the fluctuation of the chemical energy release rate (i.e., the W_1 term) varies in phase with the energy out-flux fluctuation (i.e., the term $\dot{F}$). Moreover, this value of the phase shift is of the order of $2t_{1/2}$, or about the induction delay, as is expected. This verifies the first statement (i.e., eqn. 6.24) that the fluctuation of the chemical energy release rate has the same frequency as that of the shock velocity fluctuation with a small phase shift, since the energy out-flux fluctuation is proportional to the shock velocity fluctuation. Figure 6.7 illustrates that the rate of the fluctuation of the total energy (i.e., the $\dot{I}$ term) is in phase with the fluctuation of the

shock trajectory (i.e., F) in spite of the large nonlinearity obtained in the present example. This agreement can also be seen in Fig. 6.6 where the stationary points of the $\dot{I}$ term corresponds to the maxima and minima of the term $\dot{F}$. Therefore, the second statement (i.e., eqn. 6.25) is also verified. Note the close symmetry between the $\dot{I}$ and the $\ddot{F}$ terms with the same transient magnitudes but opposite signs, which is a clear indication of the sign change between the analogous $m\ddot{x}$ and kx terms in a mechanical system.[2] However, unlike the restoring force and the inertia term in the linear mass-spring oscillation system, the symmetry of the two terms with respect to the time abscissa is broken due to the nonlinearity and their sum equals the value of the net energy input $\mu f(F, \dot{F})$, displayed in Fig. 6.8. μf can be regarded as a damping with an alternating value which is of one order less than the restoring force caused by the term $\dot{I}$. This indicates that the damping coefficient μ is indeed small and that the comparatively large restoring force plays a significant role in the dynamic instability of the oscillatory behavior.

To verify the linear acoustic compressibility coefficient of (6.27) in the restoring force term with $\dot{I}$, we consider the case of $E = 25.5$ since it is closer to the neutral boundary (i.e., $E = 25$) below which the steady ZND wave is recovered. The periodic pattern for $E = 25.5$ is a limit cycle (its period $\tau = 12.7$) just bifurcated from the steady ZND state and therefore weakly nonlinear (see Fig. 6.9). The evolution of the four terms in (6.23) over two periods is shown in Fig. 6.10 which indicates the same features as in those in Fig. 6.6. Figure 6.11 clearly demonstrates that the $\dot{I}$ term of (6.23) is well in agreement with the linear compressibility term F of (6.28) for the weakly nonlinear oscillatory detonation. Thus expression (6.27) for b_0 is justified. Adding a cubic power of F improves the agreement.

[2]For a linear mechanical response $x = x_0 \sin \omega t, m\ddot{x} = -mx_0\omega^2 \sin \omega t, kx = kx_0 \sin \omega t$, hence a sign change occurs between the inertia and the restoring force terms.

6.2.4 Mechanisms for Sustaining the Oscillations

The analogy to nonlinear mechanical oscillator indicates that the net energy input and the fluctuation rate of the internal-kinetic energy inside the system which correspond, respectively, to an alternating damping and a restoring force, are the key components of the self-sustained pulsating detonations. The self-excited driving force is initiated by a negative damping, i.e., the unsteady part of the chemical energy release is greater than the energy out-flux fluctuation at first. Thus, the system gains the energy to increase the fluctuation amplitude. However, without the restoring force the fluctuation of the system can only undergo a monotonic increase. With sufficient restoring force the system is able to behave in an oscillatory manner, but the fluctuation amplitude would continuously grow if the damping remains negative. Thus, an alternating damping, i.e., an alternating net energy input whose integral over the oscillatory cycles equals zero, is required to maintain the oscillatory detonation with repeated cycles.

The alternating net energy input is a result of the coupling between the unsteady part of the chemical energy release (i.e., $\dot{Q}_1 = \rho_0 D_{CJ} Q W_1$) and the shock velocity fluctuation (i.e., $D_1 = \dot{F}/D_{CJ}$), since D_1 is proportional to the energy out-flux fluctuation. Note that $\dot{Q}_1$ has the same frequency as D_1 by a small phase lag associated with the ignition delay. Thus, the coupling is almost resonant.

According to the Rayleigh criterion for instabilities associated with unsteady heat inputs (Rayleigh 1878), resonant oscillation can result when the unsteady heat release is in phase with the pressure oscillation. If the pressure oscillation for the oscillatory detonation is characterized by the shock velocity perturbation D_1, the Rayleigh resonant criterion requires $\dot{Q}_1$ fully in phase with D_1 so that $\dot{Q}_1 D_1 \geq 0$ holds over the entire period and that the temporal evolution of $\dot{Q}_1 D_1$ is located above the time abscissa. This is not the case in the present result. In fact, the temporal evolution of $\dot{Q}_1 D_1$ has a small negative part below

the time abscissa because of the phase lag between the two (see Fig. 6.12). The detonation for $E = 28$ displayed in the figure is a fully developed quasi-periodic oscillation by period doubling. Note that the integral of the product of $\dot{Q}_1$ and D_1 over a cycle would still be greater than zero. Thus, a generalized resonance coupling criterion can be expressed as

$$J = \frac{1}{\tau} \int_0^\tau \dot{Q}_1 D_1 dt > 0 \tag{6.30}$$

where J has units of $jm^{-2}s^{-1}$, and $\tau J > 0$ refers to the net excess energy (over the steady ZND value) needed for the maintenance of a one-dimensional oscillatory detonation. This energy concept can be clearly elucidated by the nonlinear oscillator model described by (6.23). The product of the self-excited "driving force" (i.e., the term $\rho_0 D_{CJ} Q W_1 / D$ on the right hand side of (6.23)) and the "velocity" of the dependent variable (i.e., $\dot{F}$) denotes the "power" input to the system. The integral of this power over a cycle provides the self-excited energy required for the oscillating motion of the shock front. Thus, from the energy point of view, the criterion (6.30) describes a basic mechanism of the shock perturbation by the resonance-excited chemical energy release for the self-sustained pulsating detonations.

It is also implied in (6.30) that the response of the nonlinear restoring force to the driving force provides a mechanism for transition of the instability patterns. The restoring force, i.e., the rate of the fluctuation of the total system energy, is in phase with the fluctuation of the shock trajectory (F) by equation (6.25), whereas $dJ \sim \dot{Q}_1 dF$ from (6.30). Thus, expression (6.30) states the integral relation between $\dot{Q}_1$ and F over a cycle as well. The value of J remains constant as the detonation propagates with a fixed oscillatory structure. When J increases from zero to some threshold, it describes the variety of instability patterns ranging from the steady ZND state ($E = 25$), regularly periodic motion ($E = 25.5$), onset of the first period doubling ($E = 27$), quasi-periodic motion (e.g., $E = 28$) to strong irregular motion (see Fig. 6.13). Although it must be further studied how the threshold value of J behaves for the highly irregular motion, it is conclusive that the higher level the

detonation instability pattern, the more energy is required to maintain the propagation of its oscillatory wave.

6.3 Transition as the Excitation of the Oscillator

The formation of the pulsating detonation and its relation to the excitation of an oscillator will be discussed in the following sections. The qualitative influence of nonlinearity on the excitation process will be briefly examined to point out the differences from linear oscillators.

6.3.1 Frequency Selectivity for Transition

In analyzing the transition from the quasi-steady regime to the pulsating detonation in Chapter 4, the frequency selectivity for amplification of flow perturbations is recognized. In general, the intrinsic frequency for a gaseous system is related to the acoustic frequency, which should agree with the natural detonation frequency when the detonation is established. The relation of the acoustic compressibility with the natural frequency of the detonation oscillator has already been illustrated in Section 6.2.2. In reactive flows, the work of Riley (1984) on constant volume chemical-acoustic interaction suggests that the acoustic time scales of the order of the chemical reaction time could most efficiently promote amplification of acoustic perturbations. There is thus a clear connection between the establishment of the pulsating detonation with the excitation of an equivalent oscillator.

However, the transition from deflagration to detonation represents a distinct change in the propagation mechanism of the combustion wave. In the initial state, the quasi-steady regime is quite different from the final detonation since it is not a coupled system of shock and reaction complex. The thermodynamic and flow properties (e.g., shock velocity and temperature) are also much lower than the final detonation values. Therefore, the chemical and gasdynamic time scales as well as the equations describing the initial system will be

quite different from the final ones. The intrinsic frequency would then be variable during the highly transient transition process. Nonetheless, the characteristic time scale of a detonation is one that is necessary to accomplish rapid chemical reaction after a gas particle has been compressed by the leading shock. To achieve this, the reaction time must be of the order of the reaction time of the detonation, which is represented by its half reaction time $t_{1/2}$. This is therefore the intrinsic time scale of the coupling required for detonative propagation. Thus, perturbations with periods of the order of $t_{1/2}$ are expected to promote transition to detonation. This is indeed the case as shown in Chapter 4.

When the initial development of rapid chemical reaction is achieved, the detonation level of pressure and other flow properties are approached and the shock-reaction coupling is attained. The intrinsic frequency selectivity of the pulsating detonation then takes over and provides the adjustment or evolution to the final natural frequency.

6.3.2 Excitations in Nonlinear Oscillator

From linear oscillator theory, the frequency of perturbations that can best promote excitation of the oscillator is of course the natural frequency of the oscillator. While the numerical results in Chapter 4 does seem to indicate that the optimal period is within the order of the natural period of the final detonation ($\tau_0 = 12.7$), it is not conclusive that it is due to the effect of linear resonance. Indeed, the nonlinearity associated with the pulsating detonation solution can intensify rapidly as the activation energy increases beyond the neutral stability limit. Hence, the effect of nonlinearity may play an important role in the frequency selectivity for the excitation of the nonlinear oscillator.

An important additional consequence of nonlinearity is the facility for interaction among perturbations of different frequencies and the generation of new frequency components. For a nonlinear oscillator under an external excitation, resonance may occur at frequencies other than the natural frequency of the free (i.e., unforced) oscillator. To illus-

trate this, let us return to the Duffing's equation (6.8) which has a cubic nonlinear restoring force term. For small amplitude oscillations, the oscillator is approximately linear and an excitation frequency ω equal to the natural frequency σ would lead to resonant excitation. For finite amplitude oscillations, the nonlinear system described by Duffing's equation can be excited (i.e., can have a relatively large amplitude response) under three different conditions (Nayfeh and Mook 1979):

1. Primary resonance: the system is excited when the forcing frequency of the free oscillator is close to the natural frequency ($\omega = \sigma$),

2. One-third subharmonic resonance: the system is excited when the forcing frequency is one-third the natural frequency ($\omega = 1/3\sigma$), and

3. Superharmonic resonance of order 3: the system is excited when the forcing frequency is three times the natural frequency ($\omega = 3\sigma$),

where the response of the nonlinear system is, in general, a function of the forcing term as well as the initial condition. Nonlinearity can therefore have a significant influence on the frequency sensitivity for exciting the oscillatory system.

Since real systems (such as the pulsating detonation under consideration) will generally have finite amplitude fluctuations and hence nonlinear interactions among different frequencies will alter the frequency selectivity for excitation of the system, the ability to select and amplify disturbances and to excite the final system is common. It therefore appears that the present proposed oscillator model may provide a useful framework to examine the dynamic behavior of detonation waves.

The establishment of the oscillator concept for detonation propagation indicates that the transition process can be considered as the formation of an oscillatory structure rather than the steady ZND detonation. The results obtained in the present work strongly

support the need to examine the propagation and formation of the detonation as one that is analogous to the response of a nonlinear oscillator.

Chapter 7

Conclusions

The transition from high speed deflagration to detonation has been studied theoretically and experimentally in this thesis. The present investigation was motivated by the need to better understand the detailed events during the final phase of deflagration to detonation transition. The ability to obtain a maximum velocity deflagration which is the quasi-steady regime quite universally observed just prior to transition to detonation has provided an excellent opportunity to achieve our objective. This has permitted the study to be focused on the physical processes that occur during the final onset of detonation.

To define clearly the initial condition for onset to occur, an analytical study has been carried out to examine the quasi-steady regime that occurs just prior to onset. This high speed deflagration can be obtained by damping out the transverse waves of an established detonation. Previous experimental observations have indicated that its structure can be represented by a one-dimensional shock-reaction front complex. A theoretical model has been developed and the velocity of propagation of the quasi-steady one-dimensional complex has been derived. It is found that both the leading shock and the deflagration front propagate at about half the detonation velocity of the mixture, with the shock wave traveling at a slightly higher velocity than the reaction front. The deflagration propagation is not due to an induction type process since it slowly separates from the leading shock. The propagation velocity of the quasi-steady structure is found to be governed by energetics and

quite insensitive to the detailed flow structure. This has great implications for the prediction of propagation velocities for high speed deflagrations, which can have a highly complex flow structure and are difficult to predict. Comparisons of the theoretical propagation velocity with that of the high speed deflagration experimentally obtained by damping out the transverse waves of a detonation, and with the highly turbulent high speed deflagrations in the choking regime showed good agreement and demonstrated that these maximum velocity deflagrations obtained before transition to detonation are indeed Chapman-Jouguet deflagrations which can be readily observed in experiments.

Previous experimental and theoretical observations have shown that real detonations are inherently oscillatory and thus it may be necessary to examine the transition process from the point of view of the formation of a self-sustained system. The final product of the transition process, that is the detonation itself, is therefore analyzed to help understand how the nonsteady behavior may affect the transition process. A one-dimensional computational analysis has been carried out using the Lagrangian form of the reactive Euler equations. In order to examine non-overdriven detonations, which are more useful than overdriven ones for understanding real detonations, the piston support is limited to velocities no more than the burnt gas velocity of the steady CJ detonation wave. The nonsteady one-dimensional detonation is manifested as a longitudinal pulsating wave. In spite of the oscillatory behavior, the time-averaged properties of the pulsating detonation is found to agree well with the steady Chapman-Jouguet detonation solution for the range of activation energies studied. Moreover, the wake of the detonation also satisfies the sonic condition over a cycle. This indicates strongly that the oscillatory detonation is quite independent of the far rearward boundary condition as it is for the steady CJ wave. Numerical "radiation conditions" are implemented to confirm this.

The characteristics of the oscillatory patterns of the pulsating detonation is ex-

amined by varying the activation energy. It is observed that when the activation energy is below the neutral stability limit, a steady ZND detonation is obtained. When the activation energy is slightly above the neutral stability limit, regular oscillatory solution occurs. As the activation energy is increased, the periodic pattern breaks up in a period doubling type sequence. As the activation energy is increased further, the periodic pattern becomes quite irregular and repeatable cycles were not obtained within the time of computation. The break-up sequence of the periodic pattern appears to be similar to those observed in many nonlinear oscillator systems. The stability of the pulsating detonation when perturbed with a density (or temperature) disturbance has also been analyzed. Due to the high temperature sensitivity of the reaction rate dictated by the Arrhenius law, the imposed temperature deficit can result in a rapid decoupling of the fast reaction zone from the leading shock. The failed wave then evolves into a quasi-steady high speed deflagration structure quite similar to that studied in Chapter 2. This metastable structure also propagates at about half the CJ detonation velocity. Localized pressure build-ups are observed in the deflagration complex which are similar to the so-called "hot-spots" observed in previous experiments and can lead to re-transition to detonation. The numerical results showed that the high temperature sensitivity associated with high activation energy will result in decoupling of the detonation wave for a smaller amplitude temperature disturbance, and requires a longer time to undergo re-transition to detonation, whereas low activation energy gas can sustain larger amplitude disturbances before failure and is capable of re-transition to detonation within a shorter time.

The high speed deflagration resulting from failing the pulsating detonation is then used as the initial condition to examine the onset of detonation using the computational analysis. Since the final detonation is a self-organized oscillatory structure, periodic perturbations are placed ahead of the wave to stimulate the re-generation of the detonation

structure. The periodic wave train of temperature perturbations used is observed to convect with the gas particles after being processed by the leading shock. The temperature peaks in the disturbance can grow rapidly as they convect behind the shock. The amplification of the temperature level and the acceleration of the chemical reaction then generate regions of high pressure which would propagate towards the leading shock to increase the shock strength and further intensifies the chemical activities. The effect of different periods or frequencies of the perturbations were investigated and it is observed that the amplification of the perturbations and the subsequent acceleration of the transition process is quite frequency dependent. Re-transition was found to be most rapid when the period of the perturbation is of the order of the chemical reaction time of the detonation wave. When the amplitude of the temperature perturbation is increased, the numerical results show that the disturbances grow at a faster rate and re-transition is accomplished within a shorter time. The observed rapid re-adjustment of the oscillation period to the natural detonation period once the perturbation has terminated demonstrated the strong frequency selective nature of the formation of the self-oscillatory detonation. The optimal perturbation period that can stimulate re-transition within the shortest time for the larger amplitude perturbations is also of the order of the chemical reaction time. Furthermore, the rapidity of the transition process is found to be a strong function of the activation energy. For mixtures with a low activation energy, and hence a more stable detonation wave, transition is observed to occur within a shorter time than that for a higher activation energy. However, the optimal period obtained for both cases are quite similar. The frequency selective character of the transition process has demonstrated the importance of viewing transition as the establishment of a self-organized system and the process may be quite analogous to the excitation of an oscillator.

An experimental investigation has been carried out to further examine the onset

of detonation from the quasi-steady regime, which is obtained by damping out the transverse waves of an established detonation. Since the oscillatory structure of real detonations is manifested as an organized pattern of transverse pressure waves, the experiments are performed by stimulating the transition process using artificially generated transverse pressure waves. Periodic wall obstacles are placed along the channel to interact with the fast deflagration complex and the transverse pressure waves generated are observed to promote re-transition to detonation. The distance required for transition has been measured for different obstacle spacings (and hence frequency) and the results indicate the existence of an optimal spacing to facilitate transition. The optimal spacing obtained for the present configuration is of the order of the channel height which may be related to the acoustic interaction of the detonation with the tube as has been previously observed in near limit detonations. The frequency sensitive nature of the experimentally observed transition process again supports the notion that the establishment of detonation is analogous to the excitation of an oscillatory system. It is also observed that the regularity of the detonation cell pattern of the mixture plays a significant role in the transition process. Since cell regularity is directly related to the oscillatory characteristics of the detonation as well as to the ability to amplify perturbations of different frequencies, the results further indicate that the transition process is a strong function of the final oscillatory structure. However, the relationship of cell regularity with the formation and self-sustaining propagation of detonation is still not fully understood. Indeed, it is still not possible to characterize cell regularity with physical parameters. The success of establishing such characterization would provide the crucial information for future analytical treatment and would thus greatly facilitate the understanding of the mechanisms responsible for the complex oscillatory behavior of detonation waves.

The oscillatory characteristics of the pulsating detonation, the period doubling

type break-up sequence of the oscillation pattern, and the frequency selective character of the transition process all indicate that the pulsating detonation can be modeled as a nonlinear oscillator. By reformulating the energy equation in the integral form, which should contain all the energy sources that lead to the unsteady interaction necessary in the solution, a second order differential equation was obtained for the one-dimensional pulsating detonation which has the characteristics of a nonlinear mechanical oscillator. The equivalent "mass" is given by the total energy in the detonation complex, the "spring force" is associated with the rate of change of this energy, while the "damping" or "driving" force is provided by the chemical energy input minus the energy flux out of the control volume. The terms in the model equation are verified using the numerical data from direct numerical simulations of the regular oscillatory detonation. The solutions very close to the neutral stability limit are shown to agree with the linear limit of the equivalent oscillator model. However, the derivation of the explicit expression for the restoring force term and its rapid deviation from linear behavior will require further work. Nevertheless, the proposed oscillation model does seem to provide a useful framework to interpret the numerical results of the pulsating detonation and supports the notion that the transition process is analogous to the excitation of a self-excited oscillatory system. Further analytical verification of the equivalent oscillator model should concentrate on deriving the full relationships between the equivalent oscillator component terms from the governing equations. A useful approach would be to utilize the information from the linearized description of the detonation solution as obtained by Lee and Stewart (1990). The linearized analysis should provide a tool to calculate explicitly all the terms related to the oscillator equation near the stability limit, as well as a basis from which nonlinear analyses can be derived. The establishment of a full analytical nonlinear oscillator model for detonation should greatly facilitate the understanding of the mechanisms for developing and maintaining the oscillatory structure

of the detonation wave.

The present thesis has provided a clear quantitative description of the physical processes during the onset of detonation. The oscillatory properties of the resulting detonation has been recognized as a significant feature for which the transition process must achieved. This aspect has not been fully realized in previous studies on transition which had mainly concentrated on the generation of strong enough local explosion centers or shock strength for auto-ignition to occur. The present results serve to emphasize the need to understand detonation from the point of view as a self-organized system. Indeed, the formation, steady propagation, and failure of detonation waves are all related to the self-excited nature of the oscillatory structure, and a unified understand of detonative combustion must address the dynamic oscillatory nature of the wave.

Contributions to Original Knowledge

The theoretical and experimental studies carried out in the present research has contributed to the understanding of high speed deflagrations and the transition from deflagration to detonation by:

1. providing a quantitative description of the high speed deflagration observed just prior to the onset of detonation. This quasi-steady regime is quite universally observed in many transition and detonation initiation experiments. The present work has also elucidated on the nature of this maximum velocity deflagration—it is in fact a Chapman-Jouguet deflagration where the propagation velocity is governed by energetics rather than the detailed flow structure. This has great implications for the prediction of propagation velocities for high speed deflagrations which are in general highly turbulent and difficult to predict. The agreement between the predicted CJ deflagration velocities with the velocities of the highly turbulent deflagrations in the choking regime confirms the existence of CJ deflagrations, which had been previously believed to be quite difficult to observe in experiments.

2. analyzing in detail the oscillatory characteristics of the one-dimensional pulsating detonation. While the oscillatory behavior of detonations is not new, the relationship between the pulsating structure and the steady Chapman-Jouguet solution, and the existence of a time-averaged CJ plane are, to the author's opinion, brought out clearly for the first time. The identification of the period doubling type break-up sequence as the activation energy gradually increases beyond the neutral stability limit also

demonstrates the similarity of pulsating detonation to a more general class of nonlinear oscillators. The results point out the importance of viewing detonation as a self-organized structure.

3. elucidating on the physical processes of transition to detonation by focusing on the final phase of onset of detonation. This is made possible in the present studies by using the quasi-steady regime, which is a maximum velocity deflagration, as the initial condition for transition to occur. In previous studies, the occurrence of the initial flame acceleration phase would lead to a highly random flow structure prior to the onset of detonation and would often render the detailed study of the final phase difficult. The computational and experimental studies carried out have shown that the essential mechanism responsible for transition is the preferential amplification of perturbations of certain resonant modes that can result in the formation of the self-organized structure of the detonation wave.

4. developing an equivalent oscillator model to describe the propagation of the pulsating detonation. The establishment of the oscillator model can greatly assist the understanding of the mechanisms responsible for the oscillatory propagation and the formation of the detonation, and thus will facilitate a unified description of the birth and life of detonations.

The results have indicated the importance to examine detonations from the point of view of an organized oscillatory system rather than the classical view of one with a critical shock strength necessary for auto-ignition to take place.

List of References

1. Abouseif, G. E. and Toong, T. Y. (1982). "Theory of Unstable One-Dimensional Detonations," *Combustion and Flame*, Vol. 45, pp. 67-94.

2. Almgren, R., Majda, A., and Rosales, R. R. (1990). "Rapid Initiation in Condensed Phases through Resonant Nonlinear Acoustics," *Physics of Fluids A*, Vol. 2, No. 6, June, pp. 1014-1029.

3. Alpert, R. L. and Toong, T. Y. (1972). "Periodicity in Exothermic Hypersonic Flows about Blunt Projectiles," *Astronautica Acta*, Vol. 17, pp. 539-560.

4. Bach, G. G., Knystautas, R., and Lee, J. H. (1969). "Direct Initiation of Spherical Detonations in Gaseous Explosives," *12th Symposium (International) on Combustion*, The Combustion Institute, Pittsburgh, PA, p. 853.

5. Bach, G. G., Knystautas, R., and Lee, J. H. (1971). "Initiation Criteria for Diverging Gaseous Detonations," *13th Symposium (International) on Combustion*, The Combustion Institute, Pittsburgh, PA, pp. 1097-1110.

6. Book, D. L., Boris, J. P., and Hain, K. (1975). "Flux-Corrected Transport II. Generalizations of the Method," *Journal of Computational Physics*, Vol. 18, pp. 248-283.

7. Boris, J. P. and Book, D. L. (1973). "Flux-Corrected Transport. I. SHASTA, A Fluid Transport Algorithm That Works," *Journal of Computational Physics*, Vol. 11, pp. 38-69.

8. Boris, J. P. and Book, D. L. (1976). "Flux-Corrected Transport. III. Minimal-Error FCT Algorithms," *Journal of Computational Physics*, Vol. 20, pp. 397-431.

9. Bourlioux, A., Majda, A., and Roythurd, V. (1991). "Theoretical and Numerical Structure for Unstable One-Dimensional Detonations," *SIAM Journal of Applied Mathematics*, Vol. 51, pp. 303-343.

10. Bourlioux, A. and Majda, A. (1992). "Theoretical and Numerical Structure for Unstable Two-dimensional Detonations," *Combustion and Flame*, Vol. 90, No. 3, September, pp. 211-229.

11. Chu, B. T. (1955). "Pressure Waves Generated by Addition of Heat in a Gaseous Medium," NACA Technical Note 3411.

12. Clarke, J. F. (1978). "Small Amplitude Gasdynamic Disturbances in an Exploding Atmosphere," *Journal of Fluid Mechanics*, Vol. 89, Part 2, pp. 343-355.

13. Clarke, J. F. (1979). "On the Evolution of Compression Pulses in an Exploding Atmosphere: Initial Behavior," *Journal of Fluid Mechanics*, Vol. 94, Part 1, pp. 195-208.

14. Clarke, J. F., Kassoy, D. R., and Riley, N. (1986). "On the Direct Initiation of a Plane Detonation," *Proceedings of the Royal Society of London, Series A*, 408, pp. 129-148.

15. Clarke, J. F., Kassoy, D. R., Meharzi, N. E., Riley, N., and Vasantha, R. (1990). "On the Evolution of Plane Detonations," *Proceedings of the Royal Society of London, Series A*, 429, pp. 259-283.

16. Döring, W. (1943). "Über den Detonationsvorgang in Gasen," *Ann. Phys.*, Vol. 43, pp. 421-436, 1943, also W. Döing and G. Burkhardt, "Contribution to the Theory of Detonation," *Wright-Patterson Air Force Base Tech. Rep.* F-TS-1227-IA (GDAM A9-T-46), Dayton, Ohio, 1949.

17. Dupré, G., Peraldi, O., Lee, J. H., Knystautas, R. (1988). "Propagation of Detonation Waves in an Acoustic Absorbing Walled Tube," *Progress in Astronautics and Aeronautics*, Vol. 114, pp. 248-263.

18. Dupré, G., Joannon, J., Knystautas, R., and Lee, J. (1990). "Unstable Detonations in the Near-Limit Regime in Tube", *23rd Symposium (International) on Combustion*, The Combustion Institute, pp. 1813-1820.

19. Edwards, D. H., Jones, A. T., and Phillips, D. E. (1976). "The Location of the Chapman-Jouguet Surface in a Multiheaded Detonation Wave," *Journal of Physics D: Applied Physics*, Vol. 9, pp. 1331-1342.

20. Edwards, D. H., Hooper, G., Morgan, J. M., and Thomas, G. O. (1978). "The Quasi-Steady Regime in Critically Initiated Detonation Waves," *Journal of Physics D: Applied Physics*, Vol. 11, No. 15, October, pp. 2103-2217.

21. Edwards, D. H., Thomas, G. O., and Nettleton, M. A. (1979). "The Diffraction of a Planar Detonation Wave at an Abrupt Area Change," *Journal of Fluid Mechanics*, Vol. 95, Part 1, pp. 79-96.

22. Erpenbeck, J. J. (1962). "Stability of Steady-state Equilibrium Detonations," *Physics of Fluids*, Vol. 5, pp. 604-614.

23. Erpenbeck, J. J. (1964). "Stability of Idealized one-reaction Detonations," *Physics of Fluids*, Vol. 7, pp. 684-696.

24. Feigenbaum, M. J. (1978). "Quantitative Universality for a Class of Nonlinear Transformations," *Journal of Statistical Physics*, Vol. 19, pp. 25-52.

25. Fickett, W. and Wood, W. W. (1966). "Flow Calculation for Pulsating One-Dimensional Detonation," *Physics of Fluids*, Vol. 9, pp. 903-916.

26. Fickett, W., Jacobson, J. D., and Schott, G. L. (1972). "Calculated Pulsating One-Dimensional Detonations with Induction-zone Kinetics," *AIAA Journal*, Vol. 10, pp. 514-516.

27. Fujiwara, T. and Reddy, K. V. (1989). "Propagation Mechanism of Detonation–Three Dimensional Phenomenon", *Memoirs of the Faculty of Engineering*, Nagoya University, Vol. 41, No. 1.

28. Greitzer, E. M. (1981) "The Stability of Pumping Systems – The 1980 Freeman Scholar Lecture," *Journal of Fluids Engineering*, Vol. 103, pp. 193-242.

29. Guckenheimer, J., Holmes, P.(1983). *Nonlinear Oscillators, Dynamical Systems, and Bifurcations of Vector Fields*, Applied Mathematical Sciences, Vol. 42, Springer-Verlag, New York.

30. Hung, C. M. and MacCormack, R. W. (1976). "Numerical Solutions of Supersonic and Hyperbolic Laminar Compression Corner Flows," *AIAA Journal*, Vol. 14, p. 475.

31. Jackson, T. L., Kapila, A. K., and Stewart, D. S. (1989). "Evolution of a Reaction Center in an Explosive Material," *SIAM Journal of Applied Mathematics*, Vol. 49, No. 2, pp. 432-458.

32. Kuhl, A. L., Kamel, M. M., and Oppenheim, A. K. (1973). "Pressure Waves Generated by Steady Flames," *14th Symposium (International) on Combustion*, pp. 1201-1215, The Combustion Institute, Pittsburgh, PA.

33. Kurylo, J. Dwyer, H. A., and Oppenheim, A. K. (1979). "Numerical Analysis of Flow-Fields Generated by Accelerating Flames," *AIAA Journal*, Vol. 98, No. 3, p. 302.

34. Knystautas, R., Lee, J. H. S., Peraldi, O., and Chan, C. K. (1986). "Transmission of a Flame from a Rough to a Smooth-Walled Tube," *Progress in Astronautics and Aeronautics*, Vol. 106, pp. 37-52.

35. Laderman, A. J. and Oppenheim, A. K. (1961). "Initial Flame Acceleration in an Explosive Gas," *Proceedings of the Royal Society of London, Series A*, Vol. 268, pp. 153-180.

36. Laffite, P. (1928). *Compter Rendus Hebdomadaires des Seances de l'Academie des Sciences*, Vol. 186, p. 95.

37. Lee, H. I. and Stewart, D. S. (1990). "Calculation of Linear Detonation Instability: One-Dimensional Instability of Plane Detonation," *Journal of Fluid Mechanics*, Vol. 216, pp. 103-132.

38. Lee, J. H. S. (1977). "Initiation of Gaseous Detonations," *Annual Review of Physical Chemistry*, Vol. 28, pp. 75-104.

39. Lee, J. H. S. (1986). "The Propagation of Turbulent Flames and Detonations In Tubes," Rentzepis, P. M. and Capellos, C. (Eds.). *Advances in Chemical Reaction Dynamics*, pp. 346-378.

40. Lee, J. H. (1991). "Dynamic Structure of Gaseous Detonation," in *Dynamic Structure of Detonation in Gaseous and Dispersed Media*, Ed. A. A. Borissov, pp. 27-50, Kluwer Academic Publishers.

41. Lee, J. H. (1993). "On the Critical Diameter Problem," to appear in special volume in the *Combustion Science and Technology Series* in honor of Anthony K. Oppenheim, Gordon and Breach.

42. Lee, J. H., Soloukhin, R. I., and Oppenheim, A. K. (1969). "Current Views on Gaseous Detonation," *Astronautica Acta*, Vol. 14, Pergamon Press, pp. 565-584.

43. Lee, J. H. and Ramamurthi, K. (1976). "On the Concept of the Critical Size of a Detonation Kernel," *Combustion and Flame*, Vol. 27, p. 331.

44. Lee, J. H., Knystautas, R., and Yoshikawa, N. (1978). "Photochemical Initiation of Gaseous Detonations," *Acta Astronautica*, Vol. 5, No. 11, November, pp. 971-982.

45. Lee, J. H. S. and Moen, I. O. (1980). "The Mechanism of Transition from Deflagration to Detonation in Vapor Cloud Explosions," *Prog. Energy Combust. Sci.*, Vol. 6, pp. 359-389.

46. Lee, J. H., Knystautas, Freiman, A. (1984). "High Speed Turbulent Deflagrations and Transition to Detonation in H2-Air Mixtures," *Combustion and Flame*, Vol. 56, pp. 227-239.

47. Lee, J. H., Knystautas, R., Chan, C. K. (1985). "Turbulent Flame Propagation in Obstacle- Filled Tubes," *20th Symp. (Intl.) on Combustion*, The Combustion Institute, pp. 1663-1672.

48. Lehr, H. F. (1972). "Experiments on Shock-Induced Combustion," *Astronautica Acta*, Vol. 17, pp. 589-596.

49. MacCormack, R. W. (1972). "Numerical Solution of the Interaction of a Shock Wave with a Laminar Boundary Layer," *Lecture Notes in Physics*, Springer-Verlag, Vol. 8, p. 151.

50. Majda, A. and Rosales, R. R. (1987). "Nonlinear Mean Field-High Frequency Wave Interactions in the Induction Zone," *SIAM Journal of Applied Mathematics*, Vol. 47, No. 5, October, pp. 1017-1039.

51. Maxwell, J. C. (1868). "On Governors," *Proceedings of the Royal Society of London*, No. 100, reprinted in *Collected Works*, Vol. II, Dover Publications, New York 1965,, pp. 104-120.

52. Meyer, J. W., Urtiew, P. A. and Oppenheim, A. K. (1970). "On the Inadequacy of Gasdynamic Processes for Triggering the Transition to Detonation," *Combustion and Flame*, Vol. 14, No. 1, February, pp. 13-20.

53. Meyer, J. W. and Oppenheim, A. K. (1971). "On the Shock-Induced Ignition of Explosives Gases," *13th Symposium (International) on Combustion*, The Combustion Institute, Pittsburg, PA, pp. 1153-1164.

54. Moen, I. O., Funk, J. W., Ward, S. A., Rude, G. M., and Thibault, P. A. (1984). "Detonation Length Scales for Fuel-Air Explosives," *Progress in Astronautics and Aeronautics*, Vol. 94, pp. 55-79.

55. Nayfeh, A. H. and Mook D. T. (1979). *Nonlinear Oscillations*, John Wiley and Sons, New York.

56. Oppenheim, A. K. (1953). "Gasdynamic Analysis of the Development of Gaseous Detonation and its Hydraulic Analogy," *Fourth Symp. (Intl.) on Combustion*, Baltimore, pp. 471-480.

57. Oran, E. and Boris, J. P. (1987). *Numerical Simulation of Reactive Flow*, Elseview, New York.

58. Peraldi, O., Knystautas, R., Lee, J. H. (1986). "Criteria For Transition to Detonation in Tubes," *21st Symp. (Intl.) on Combustion*, The Combustion Institute, pp. 1629-1637.

59. Reynolds, Wm. C. (1987). STANJAN Chemical Equilibrium Solver, Version 3.93 on IBM-PC, Department of Mechanical Engineering, Stanford University.

60. Rayleigh, Lord (1878). "The Explanation of Certain Acoustical Phenomena," Friday Evening Lecture at the Royal Institute, March 15. See also *The Theory of Sound*, Dover Publications, New York 1945, Vol. II, pp. 226-230.

61. Reddy, K. V., Fujiwara, T. and Lee, J. H. (1988). "Role of Transverse Waves in a Detonation Wave – A study based on Propagation in a Porous Wall Chamber," *Memoirs of Faculty of Engineering*, Nagoya University, Vol. 40, No. 1.

62. Riley, M. E. (1984). "Frequency Selectivity of Chemi-Acoustic Amplification in a Constant Volume Gas," Sandia Report SAND84-0764, June, Sandia National Laboratories.

63. Shchelkin, K. I. (1940). *Soviet Physics Journal of Experimental and Technical Physics*, Vol. 10, p. 823.

64. Shchelkin, K. I., Troshin, Ya. K. (1964). "Gasdynamics of Combustion," Izdatel'stvo Akademii Nauk USSR, Moscow. English translation in NASA TT F-231.

65. Shephard, J. E., Moen, I. O., Murray, S. B., and Thibault, P. A. (1987). "Analyses of the Cellular Structure of Detonations," in *21st Symposium (International) on Combustion*, The Combustion Institute, Pittsburg, PA, pp. 1649-1658.

66. Shephard, J. E. and Lee, J. H. S. (1992). "On the Transition from Deflagration to Detonation," in *Major Research Topics in Combustion*, ICASE/NASA LaRC Series, Edited by Hussaini M. Y., Kumar A., Voigt R. G., pp. 439-487, Springer-Verlag, New York.

67. Singh, G. and Clarke, J. F. (1992). "Transient Phenomena in the Initiation of a Mechanically Driven Plane Detonation,", *Proceedings of the Royal Society of London, Series A*, Vol, 438, pp. 23-46.

68. Soloukhin, R. I. (1969). "Nonstationary Phenomena in Gaseous Detonation," *12th Symposium (International) on Combustion*, The Combustion Institute, Pittsburgh, PA, pp. 799-807.

69. Taki, S. and Fujiwara, T. (1978). "Numerical Analysis of Two-Dimensional nonsteady Detonations," *AIAA Journal*, Vol. 16, No. 1, January.

70. Taki, S. and Fujiwara, T. (1981). "Numerical Simulations of Triple Shock Behavior of Gaseous Detonation," *18th Symposium (International) on Combustion*, The Combustion Institute, Pittsburg, PA, p. 1671.

71. Taki, S. and Fujiwara, T. (1984). "Numerical Simulations on the Establishment of Gaseous Detonation," *Progress in Astronautics and Aeronautics*, Vol. 94, pp. 186-200.

72. Taylor, G. I. and Tankin, R. S. (1958). "Gasdynamical Aspects of Detonation," in *Fundamentals of Gas Dynamics, High Speed Aerodynamics and Propulsion*, Vol. III, Howard W. Emmons (Editor), Chapter 3, pp. 634, 635, 637, 647, Princeton University Press, Princeton, NJ.

73. Teodorczyk, A. (1989). Unpublished schlieren photographs on the damping of transverse waves of detonations, McGill University.

74. Toong, T. Y. (1983). *Combustion Dynamics: The Dynamics of Chemically Reacting Fluids*, pp. 234-245, McGraw Hill, NY.

75. Ul'yanitski, V. Yu. (1981). *Frz. Goreniya Vzrya*, Vol. 17, Part 2, pp. 127-133.

76. Urtiew, P. A. and Oppenheim, A. K. (1965). "Onset of Detonation," *Combustion and Flame*, Vol. 9, No. 4, December, pp. 405-407.

77. Urtiew, P. A. and Oppenheim, A. K. (1966). "Experimental Observations of the Transition to Detonation in an Explosive Gas," *Proceedings of the Royal Society of London, Series A*, Vol. 295, No. 1440, November, pp. 13-28.

78. Urtiew, P. A. and Oppenheim, A. K. (1967). "Detonative Ignition Induced by Shock Merging," *11th Symposium (International) on Combustion*, The Combustion Institute, Pittsburgh, PA, pp. 665-670.

79. Urtiew, P. A. and Oppenheim, A. K. (1968). "Transverse Flame-Shock Interactions in an Explosive Gas," *Proceedings of the Royal Society of London, Series A*, Vol. 304, No. 1478, April, pp. 379-385.

80. Vasiliev, A. A., Gavrilenko, T. P., and Topchian, M. E. (1972). "On the Chapman-Jouguet Surface in Multi-headed Gaseous Detonations," *Astronautics Acta*, Vol. 17, pp. 499-500.

81. von Neumann, J. (1942). "Theory of Detonation Waves," *Off. Sci. Res. Dev. Rep. 549, Ballist. Res. Lab. File No.* X-122, Aberdeen Proving Ground, Md.

82. Wagner, H. Gg. (1981). "Some Experiments about Flame Acceleration," *Proc. of the Intl. Specialist Conf. on Fuel-Air Explosions*, U. of Waterloo Press, pp. 77-99.

83. Wilson, G. I. and Sussman, Myles (1991). "Computations of Oscillating Shock-Induced Combustion Observed in Ballistic-Range Experiments," presented at Fourth International Symposium on Numerical Combustion, Dec. 2-4, 1991, St. Petersburg Beach, Florida.

84. Yoshikawa, N. (1980). "Coherent Shock Wave Amplification in Photochemical Initiation of Gaseous Detonations," Ph.D thesis, McGill University.

85. Zel'dovich, Ya. B. (1940). "K Teorii Rasprostranenia Detonatsii v Gasoobraznykh Sistemakh," *Zh. Exsp. Teor. Fiz.*, Vol. 10, pp. 542-568, 1940; translated in *NACA Tech. Mem. 1261*, 1950; also "Theory of Combustion and Detonation in Gases," *Wright-Patterson Air Force Base Tech. Rep.*, F-TS-1226-IA (GDAM A9-T-45), Dayton, Ohio, 1949.

86. Zel'dovich, Ya. B. (1980). "Regime Classification of an Exothermic Reaction with Nonuniform Initial Conditions," *Combustion and Flame*, Vol. 39, No. 2, pp. 211-214.

87. Zel'dovich, Ya. B., Librovich, V. B., Makhviladze, G. M., and Sivashinsky, G. I. (1970). "On the Development of Detonation in a Non-Uniformly Preheated Gas," *Astronautica Acta*, Vol. 15, No. 5, pp. 313-321.

Appendix A

Numerical Methods

The numerical method used to solve the set of time dependent governing equations is a second order MacCormack explicit finite difference algorithm (MacCormack 1976, Hung and MacCormack 1976) combined with the Boris-Book flux-corrected transport (FCT) scheme (Boris and Book 1973, Book and Boris 1975, Boris and Book 1976). The present computational code is based on the work of Yoshikawa (1980) and Moen et al. (1984). The basic algorithm used is identical to that used by Moen et al. (1984), and has been further tested and compared with the previous results of Fickett and Wood (1966) and Bourlioux et al. (1991). The code has been adapted for the different boundary and initial conditions under consideration in the present work.

The nondimensional governing equations in Lagrangian form obtained in Chapter 3 can be expressed in the following flux form:

$$\frac{\partial F}{\partial t} + \frac{\partial G}{\partial \xi} = S \tag{A.1}$$

where

$$F = \begin{pmatrix} v \\ u \\ e \\ \alpha \end{pmatrix}, \quad G = \begin{pmatrix} -u \\ p/\gamma \\ pu/\gamma \\ 0 \end{pmatrix}, \quad S = \begin{pmatrix} 0 \\ -a_p \\ -\frac{Q}{\gamma}\dot{\alpha} - a_p u \\ -k\alpha e^{-E/T} \end{pmatrix} \tag{A.2}$$

The procedure for solving this equation is given below.

MacCormack Predictor-Corrector Algorithm

The MacCormack scheme is a two-step predictor-corrector algorithm with non-centered spatial differences. In the predictor step, the forward spatial difference is calculated as follows:

$$\tilde{F}^{n+1}_{m,1} = F^n_m - \frac{\Delta t}{\Delta \xi}(G^n_{m+1} - G^n_m) + S^n_m \Delta t \tag{A.3}$$

where m denotes the spatial location $m\Delta\xi$, and n represents the n^{th} time level. The predicted value of $\tilde{F}^{n+1}_{m,1}$ is then corrected in the second (corrector) step using the backward spatial difference:

$$\tilde{F}^{n+1}_{m,2} = \frac{1}{2}[F^n_m + \tilde{F}^{n+1}_{m,1} - \frac{\Delta t}{\Delta \xi}(\tilde{G}^{n+1}_{m,1} - \tilde{G}^{n+1}_{m-1,1}) + \tilde{S}^{n+1}_{m,1}\Delta t] \tag{A.4}$$

where $\tilde{G}^{n+1}_{m,1}$ and $\tilde{S}^{n+1}_{m,1}$ have been obtained from the predicted value $\tilde{F}^{n+1}_{m,1}$.

Flux Corrected Transport Scheme

The Boris-Book FCT antidiffusion scheme is then applied to the conservation equations to improve the accuracy of the solution near shock waves. The scheme is carried out in the following procedure:

i) Diffuse the solution

$$\bar{F}^{n+1}_m = \tilde{F}^{n+1}_{m,2} + \eta_{m+1/2}(F^n_{m+1} - F^n_m) - \eta_{m-1/2}(F^n_m - F^n_{m-1}) \tag{A.5}$$

$$\Delta_{m+1/2} = \bar{F}^{n+1}_{m+1} - \bar{F}^{n+1}_m \tag{A.6}$$

$$\phi_{m+1/2} = \eta_{m+1/2} \cdot \Delta_{m+1/2} \tag{A.7}$$

ii) Limit the anti-diffusion fluxes

$$\kappa_{m+1/2} = \operatorname{sgn}\Delta_{m+1/2} \max\{0, \min[\Delta_{m-1/2}\operatorname{sgn}\Delta_{m+1/2}, |\phi_{m+1/2}|, \Delta_{m+3/2}\operatorname{sgn}\Delta_{m+1/2}]\} \tag{A.8}$$

iii) Antidiffusion step

$$F_m^{n+1} = \bar{F}_m^{n+1} - \kappa_{m+1/2} + \kappa_{m-1/2} \tag{A.9}$$

where $\eta_{m\pm1/2}$ is the diffusion-antidiffusion coefficient given by:

$$\eta_{m\pm1/2} = \begin{cases} \frac{1}{12}\left(\left|\frac{u^n_{m\pm1}}{c^n_{m\pm1}}\right| + \left|\frac{u^n_m}{c^n_m}\right|\right) & \eta_{m\pm1/2} \le \frac{1}{6} \\ \frac{1}{6} & \eta_{m\pm1/2} > \frac{1}{6} \end{cases} \tag{A.10}$$

with c being the local nondimensional sound speed. The solution F_m^{n+1} at the next time level is thus given by equation (A.9).

Resolution used

In the present analysis, the grid size $\Delta\xi$ is chosen such that there are 50 numerical cells in the half reaction zone for the steady ZND detonation profile. Preliminary calculations have also been carried out using 20 and 70 numerical cells in the half reaction zone for a relatively high activation energy of 28. It was found that all three resolutions can reproduce the same qualitative results, that is a pulsating detonation with the same frequency and amplitude. Detail quantitative features during the initial formation of detonation do differ slightly with 20 numerical cells, but the final oscillatory solution is not affected. The solutions for 50 and 70 cells showed good agreement indicating that the former is sufficient for describing the oscillatory detonation phenomena. Higher activation energies were also tested (up to $E = 50$) and it was found that the low resolution used (20 cells) may not be sufficient for capturing the high frequency pressure fluctuations prior to the formation of detonation. The resolution of 50 numerical cells is thus chosen in the present simulation to ensure the ability to capture the spectrum of flow fluctuations for the study of deflagration to detonation transition.

The time step Δt is obtained for a Courant number of 0.5.

Appendix B

Derivation of the Helmholtz Oscillator

The Rayleigh criterion will be demonstrated in the following simplified analysis. Consider the unsteady heat input to a volume (plenum) that experiences pressure fluctuation. For simplicity, the fluid under consideration is assumed to be a perfect gas; the inertial and flow storage will be lumped into two elements—inlet duct and plenum volume, and small flow perturbations are considered only (see Fig. B.1). Note that this simple model is commonly referred to as a Helmholtz oscillator.

In the inlet tube, the mass and the mass flow rate are given by:

$$\text{Mass in tube :} \quad m = \rho A L$$

$$\text{Mass flow rate :} \quad \dot{m} = \rho A u$$

where ρ, u are the density and velocity of the incoming fluid, and A, L are the area and length of the inlet duct. The inertial force in the inlet tube is:

$$m\frac{du}{dt} = (\rho A L)\frac{1}{\rho A}\frac{d\dot{m}}{dt} = L\frac{d\dot{m}}{dt} \tag{B.1}$$

The pressure force exerted on the tube is $A(p_0 - p_1)$, where p_0 and p_1 are, respectively, the constant ambient pressure outside the system and the instantaneous pressure inside the

plenum which is assumed to be uniform. The momentum balance across the tube is:

$$A(p_0 - p_1) = L\frac{d\dot{m}}{dt} \tag{B.2}$$

Writing the thermodynamic first law for the plenum:

$$\frac{dE}{dt} = \dot{Q} + h_{in}\dot{m}_{in}$$

where E is the internal energy inside the control volume, $\dot{Q}$ is the heat release rate, $h_{in}\dot{m}_{in}$ is the enthalpy flux entering the system. For small changes,

$$\frac{dE}{dt} = \dot{Q}' + \overbrace{h'_{in}\bar{\dot{m}}_{in}}^{\to 0} + \bar{h}_{in}\overbrace{\dot{m}'_{in}}^{=\dot{m}_{in}}$$

Here, the $(\bar{})$ denotes the time-mean quantity and $(\,)'$ denotes the perturbation component. The internal energy of the system for a perfect gas is given by

$$E = \rho V C_v T_1 = \frac{V}{\gamma - 1}p_1.$$

Thus, the First Law can be expressed as:

$$\frac{V}{\gamma - 1}\frac{dp_1}{dt} = \dot{Q}' + C_p T_1 \dot{m}_{in}$$

Upon relating $C_p T_1$ to the sound speed c, $\dot{m}_{in}$ becomes:

$$\dot{m}_{in} = \frac{V}{c^2}\frac{dp_1}{dt} - \frac{\dot{Q}'}{C_p T_1} \tag{B.3}$$

Let the heat input $\dot{Q}'$ be described by:

$$\dot{Q}' = \phi P$$

where P is defined to be the $p_1 - p_0$ and ϕ is a constant. For $\phi > 0$, the unsteady heat input is in phase with the pressure fluctuation. For $\phi < 0$, they are 180° out of phase. Upon substituting the expression for $\dot{Q}'$ and the First Law into equation (B.1), an oscillator equation is obtained:

$$\frac{d^2P}{dt^2} - \frac{\gamma - 1}{V}\phi\frac{dP}{dt} + \frac{c^2 A}{LV}P = 0 \tag{B.4}$$

For this equation, ϕ plays the role of the damping coefficient of the oscillatory system. Thus, for $\dot{Q}$ and the pressure to be "in phase" (i.e., $\phi > 0$), the dynamic instability is most favored. If $\dot{Q}$ is "out of phase" with the pressure rise ($\phi < 0$), the system is damped and no oscillation will result. This demonstrates the role of phase relation as stated by the Rayleigh criterion.

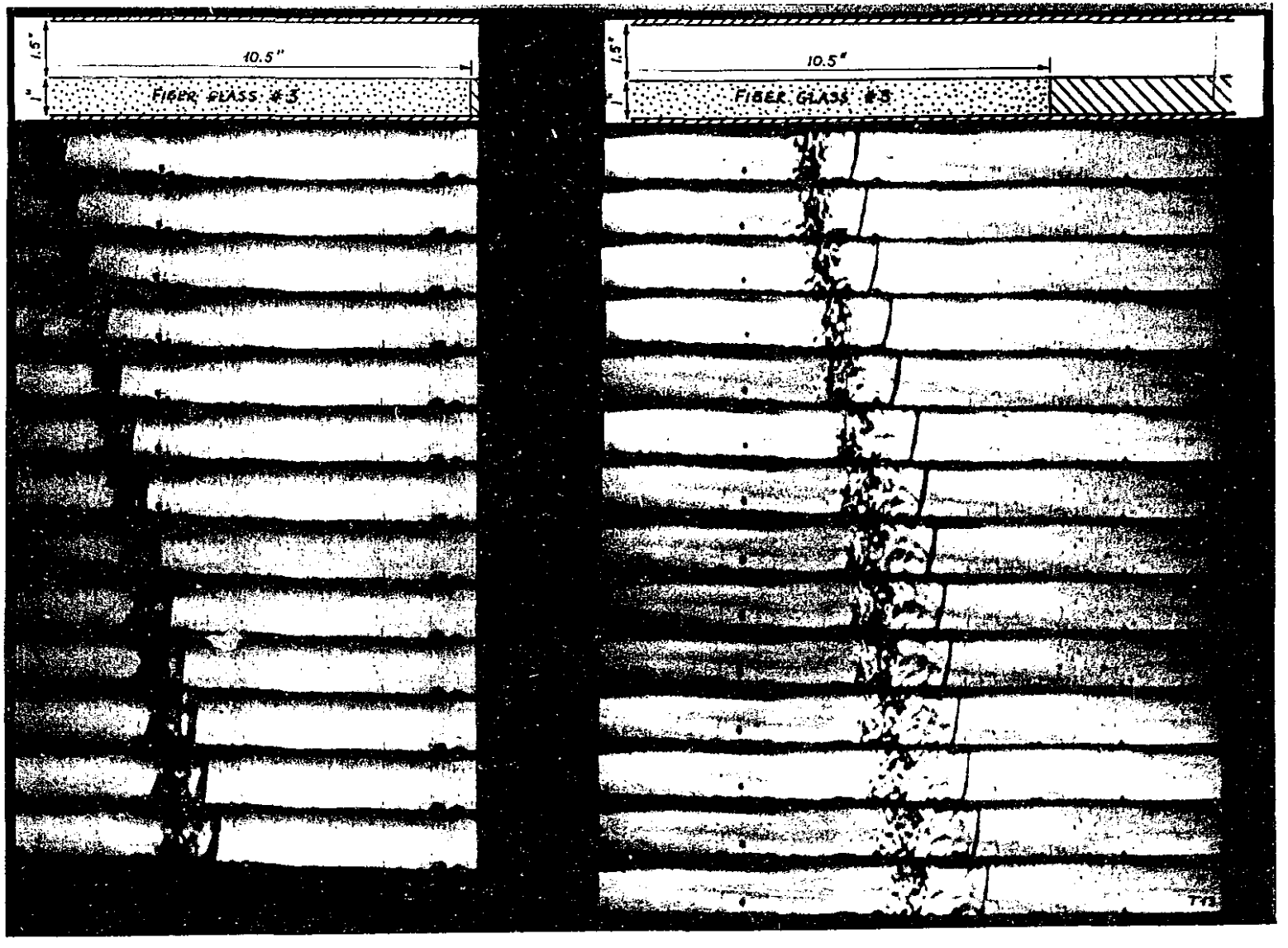

Figure 2.1: Time sequence of Schlieren photographs of the damping of transverse waves of an established detonation by an acoustically absorbing wall. Stoichiometric $H_2 - O_2$ mixture at 120 Torr, channel height is 65 mm, width is 65 mm, the time interval between frames is approximately 3.3 μsec.

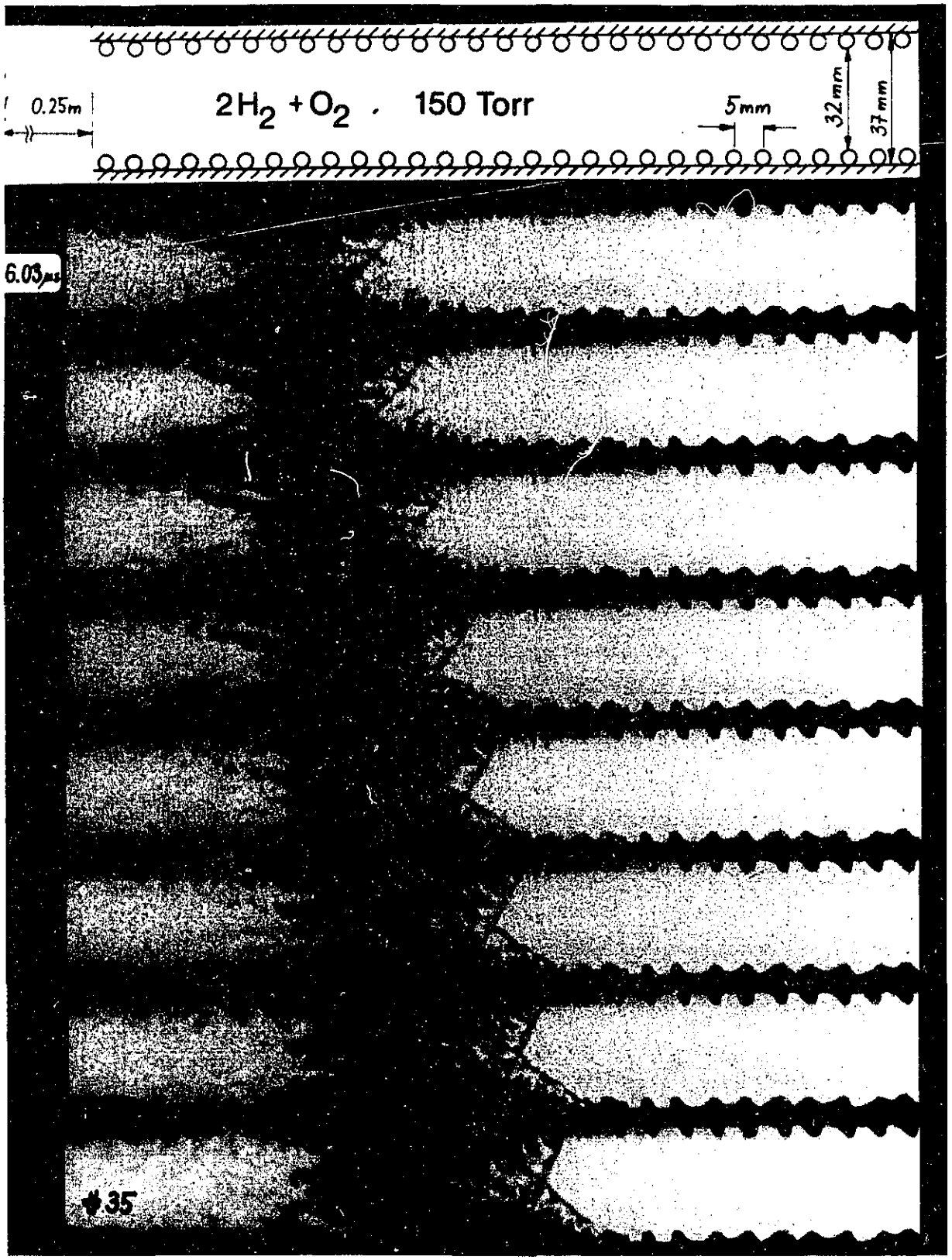

Figure 2.2: Time sequence of Schlieren photographs illustrating the complex structure of the propagation of a turbulent high speed deflagration in a rough channel. Stoichiometric $H_2 - O_2$ mixture at 150 Torr.

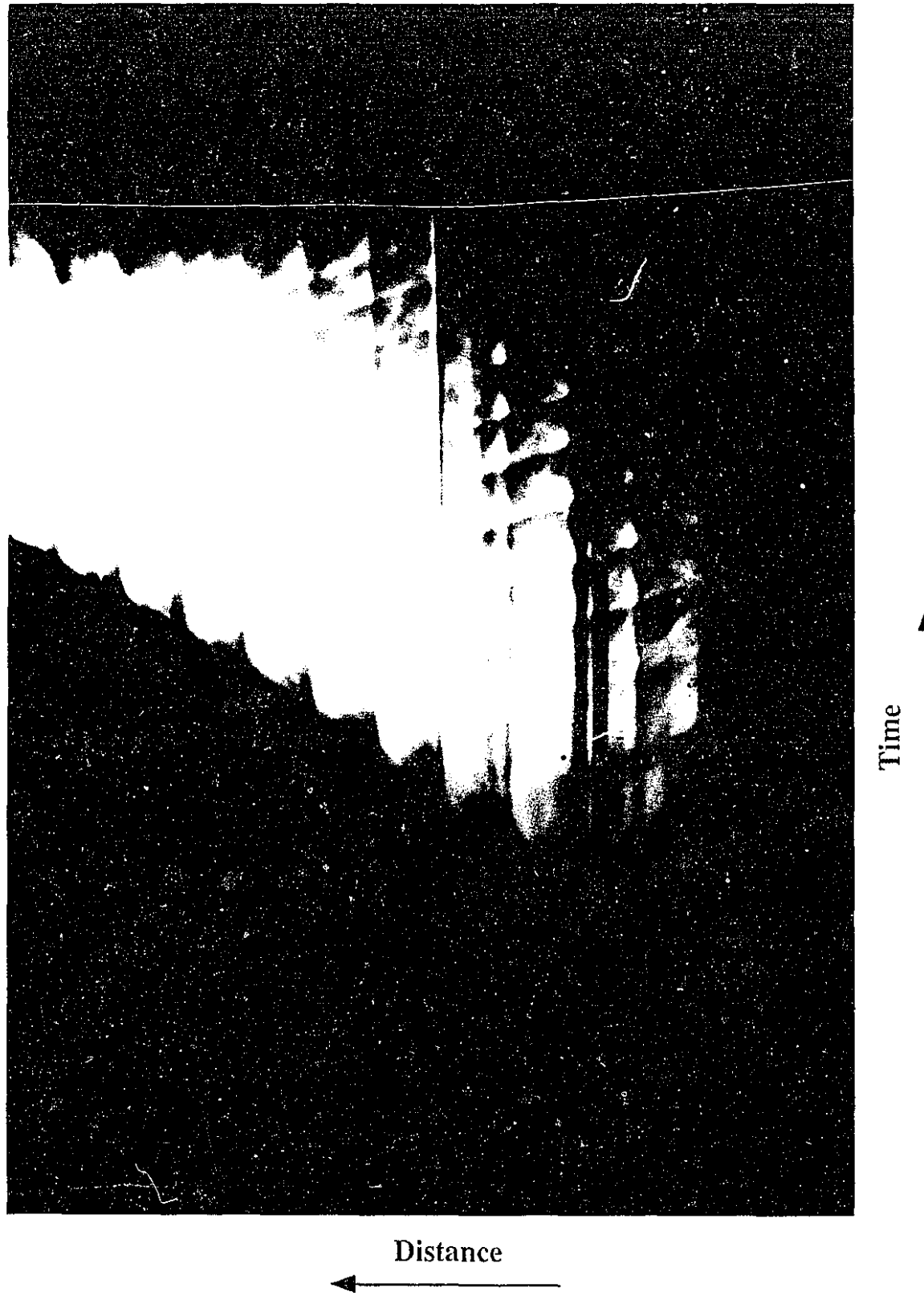

Figure 2.3: Streak photograph of the acceleration to the steady state choking regime for a flame in CH_4–air mixture in a 4 cm diameter tube with orifice plate obstacles spaced 10 cm apart. From Wagner (1981).

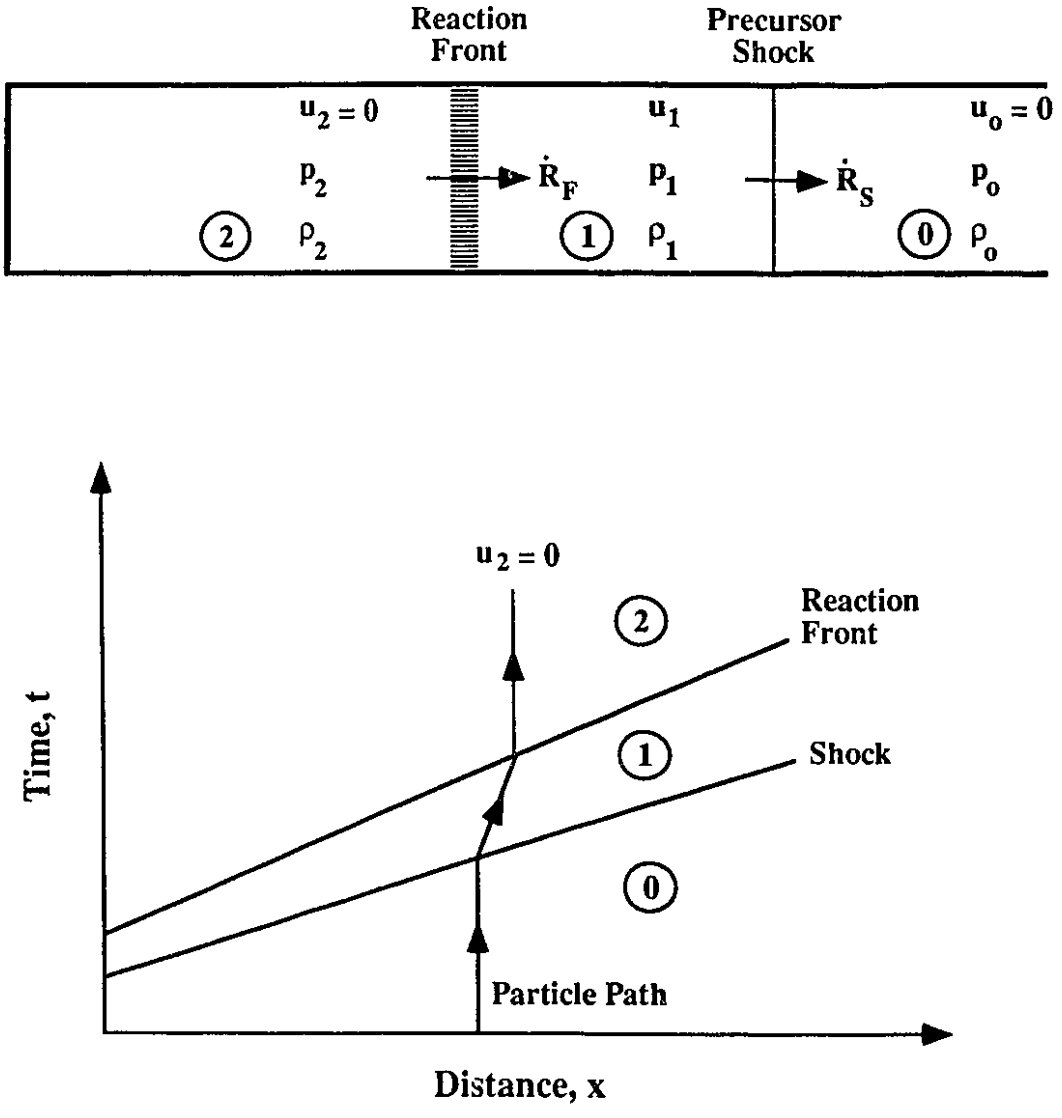

Figure 2.4: Schematic of one-dimensional deflagration model.

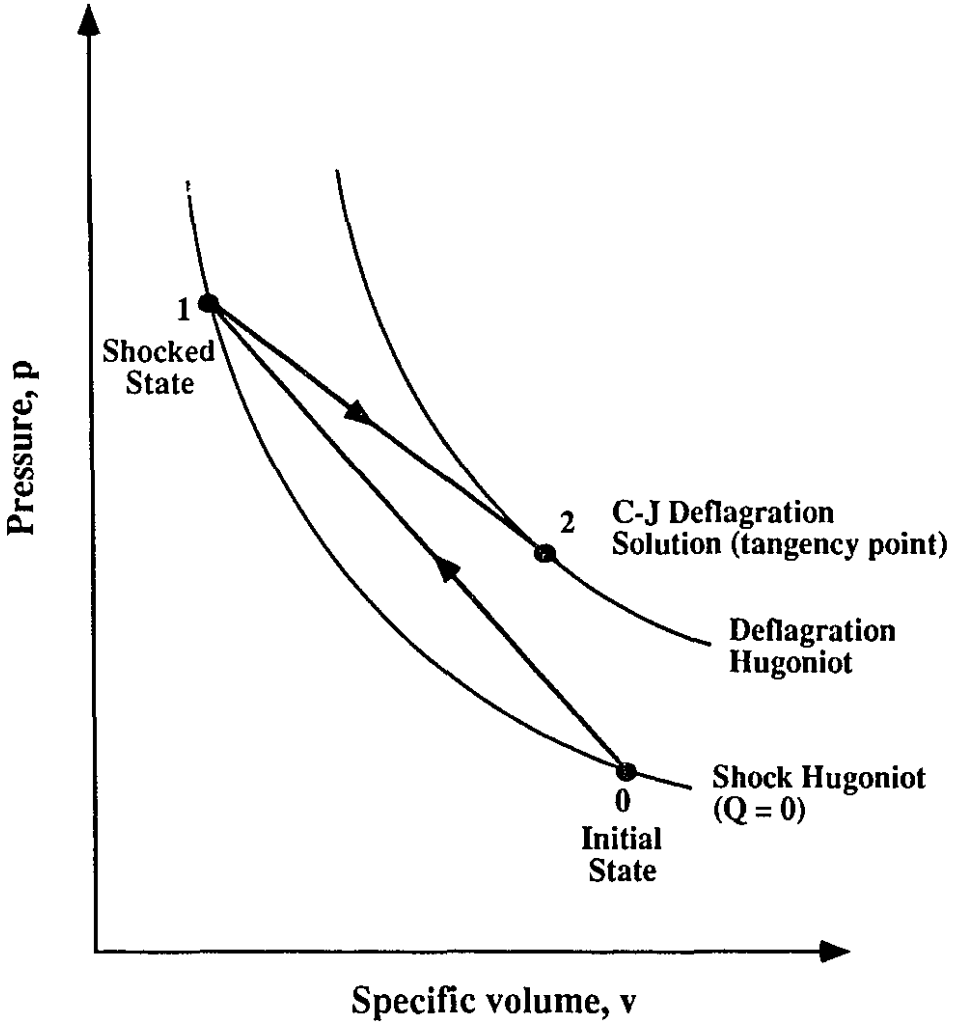

Figure 2.5: Graphical solution of the shock/reaction-zone complex using

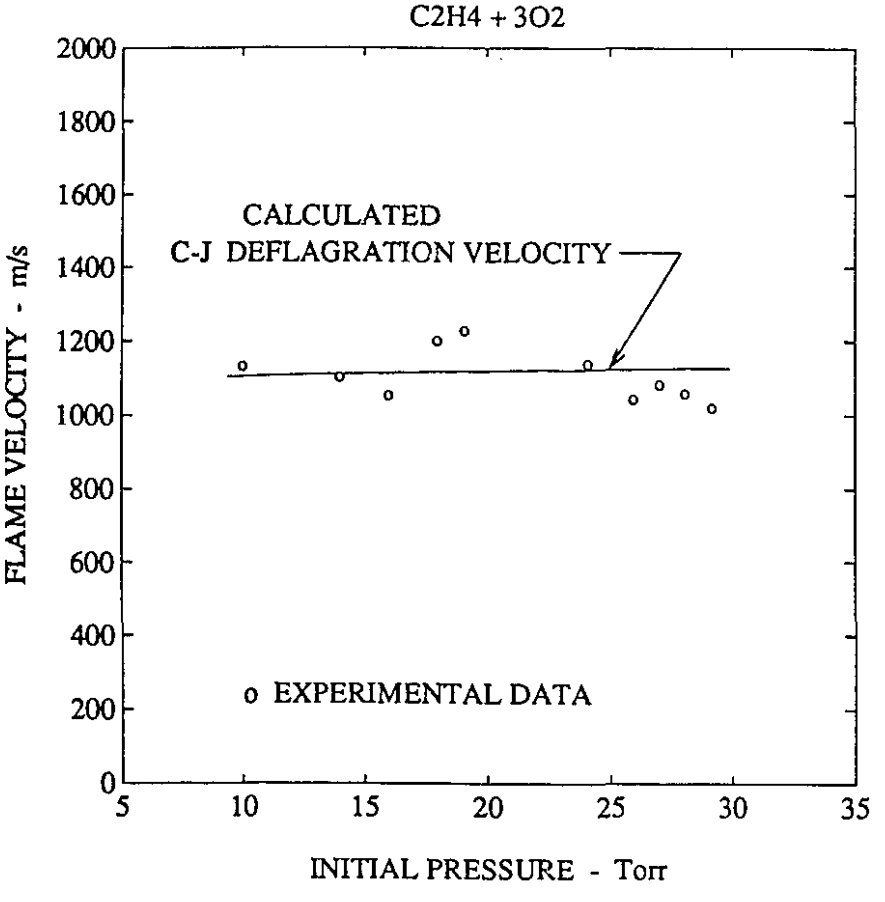

Figure 2.6: Comparison of theoretical CJ deflagration velocity with the approximate one-dimensional deflagration velocity from Dupré's experiment (1988). Stoichiometric ethylene-oxygen mixture at initial temperature of 298K.

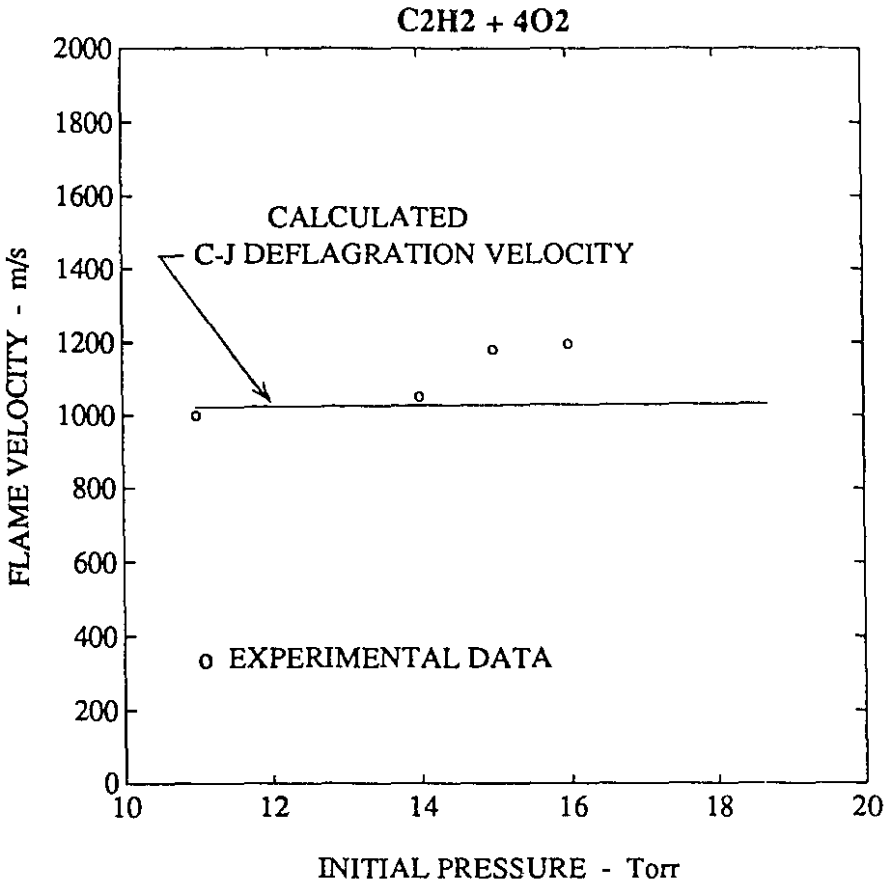

Figure 2.7: Comparison of theoretical CJ deflagration velocity with the approximate one-dimensional deflagration velocity from Dupré's experiment (1988). Stoichiometric acetylene-oxygen mixture at initial temperature of 298K.

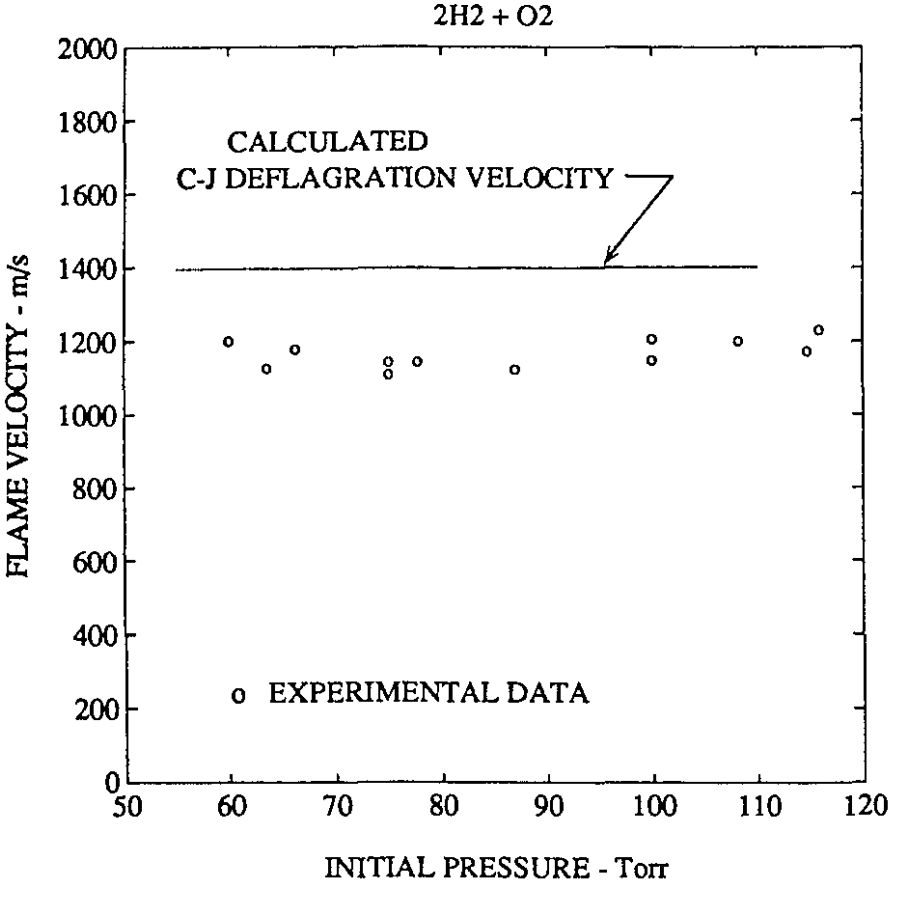

Figure 2.8: Comparison of theoretical CJ deflagration velocity with the approximate one-dimensional deflagration velocity from Dupré's experiment (1988). Stoichiometric hydrogen-oxygen mixture at initial temperature of 298K.

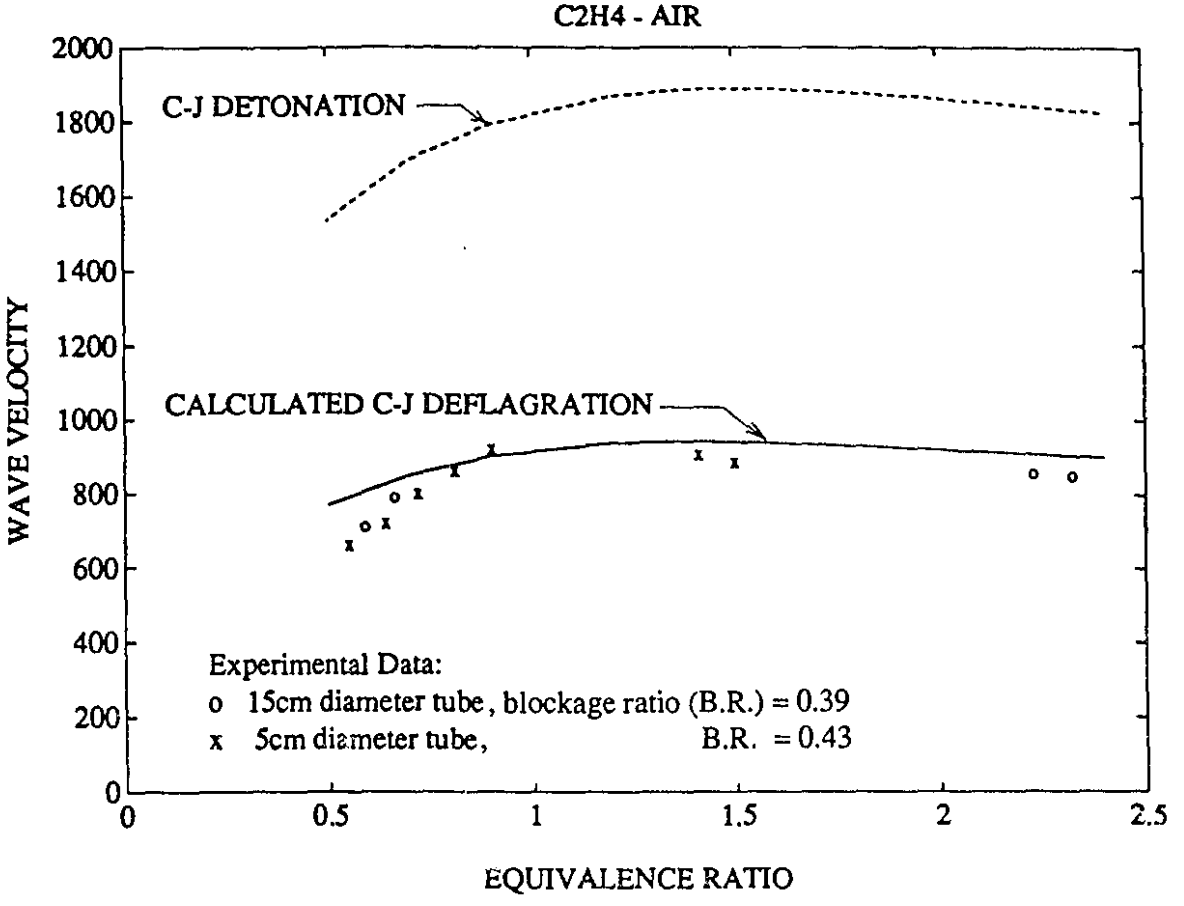

Figure 2.9: Comparison of theoretical CJ deflagration velocity with the turbulent high speed deflagration terminal velocity in rough tubes (Lee 1986), plotted against chemical concentration. Ethylene-air mixture initially at 1 atm. and 298K. The corresponding CJ detonation velocity is also shown for reference.

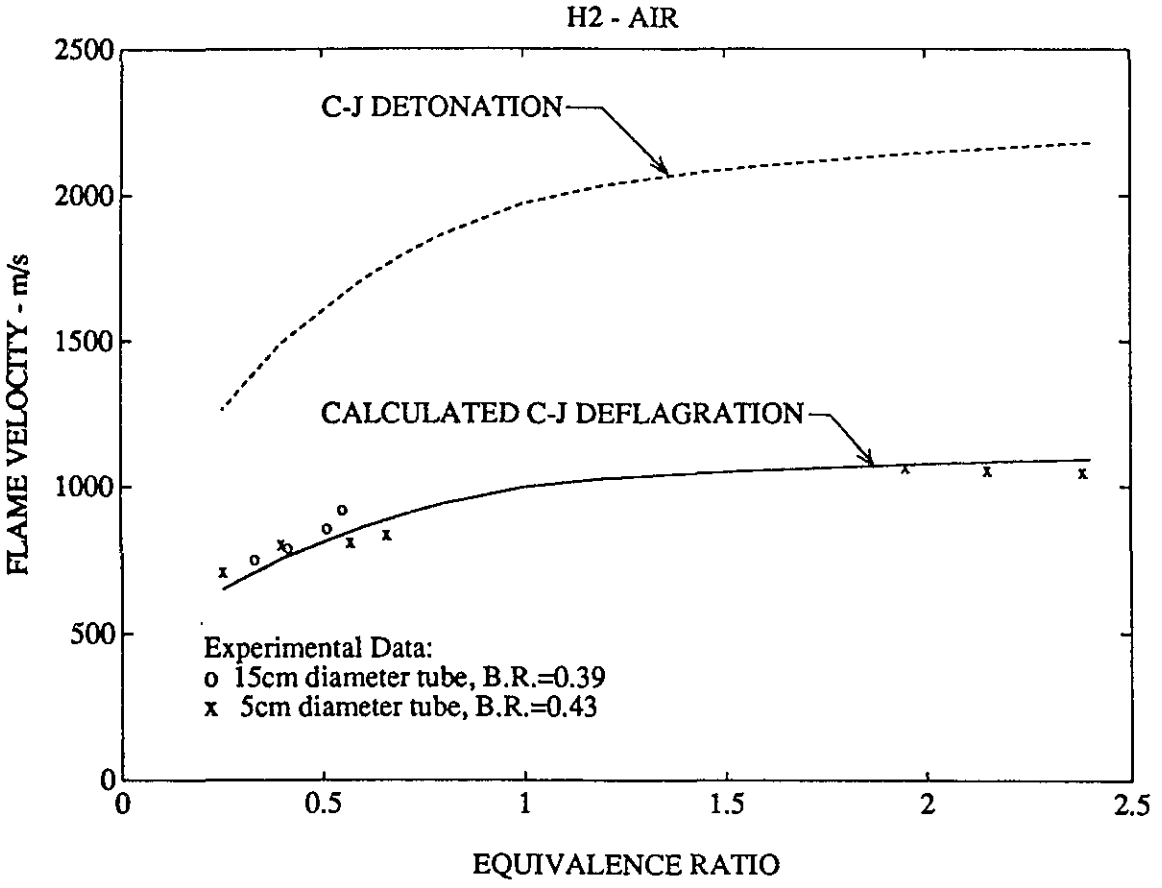

Figure 2.10: Comparison of theoretical CJ deflagration velocity with the turbulent high speed deflagration terminal velocity in rough tubes (Lee 1986). Hydrogen-air mixture initially at 1 atm. and 298K.

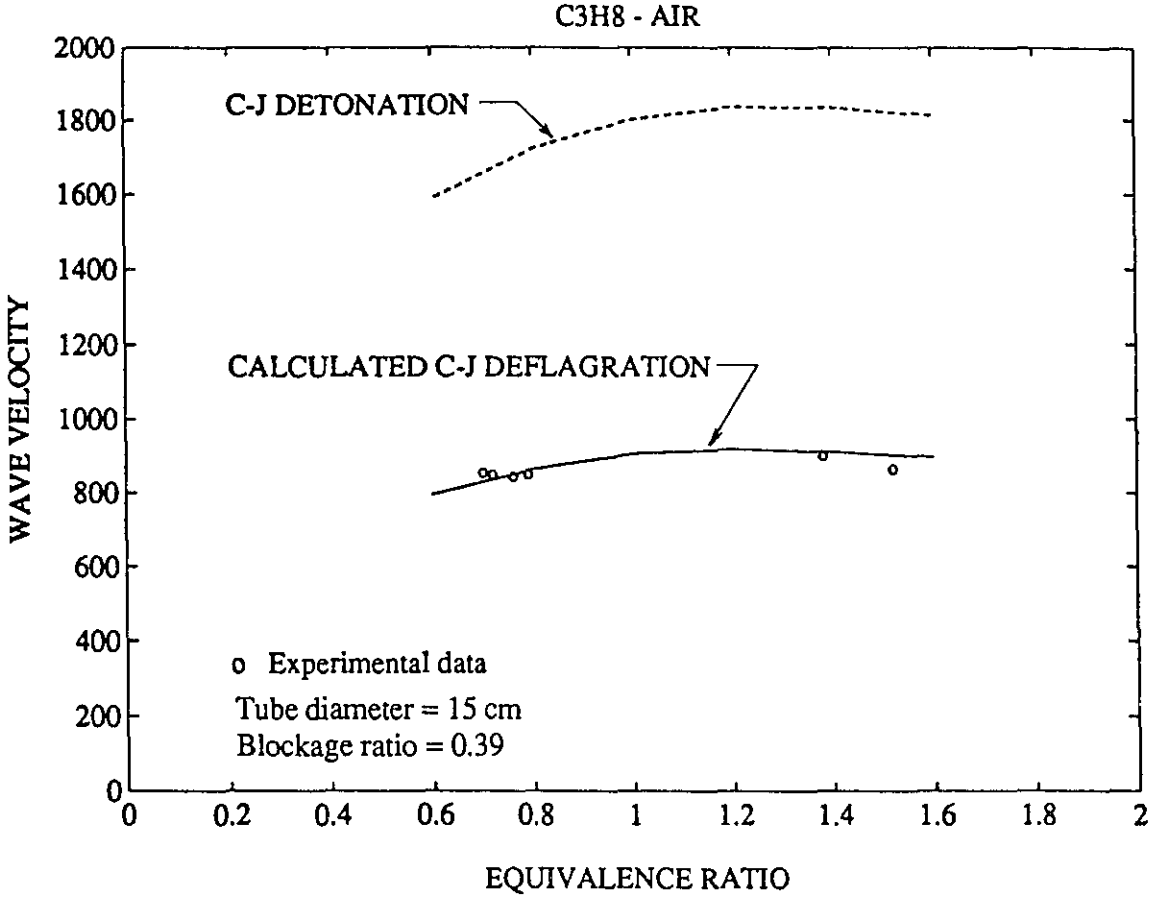

Figure 2.11: Comparison of theoretical CJ deflagration velocity with the turbulent high speed deflagration terminal velocity in rough tubes (Lee 1986). Propane-air mixture initially at 1 atm. and 298K.

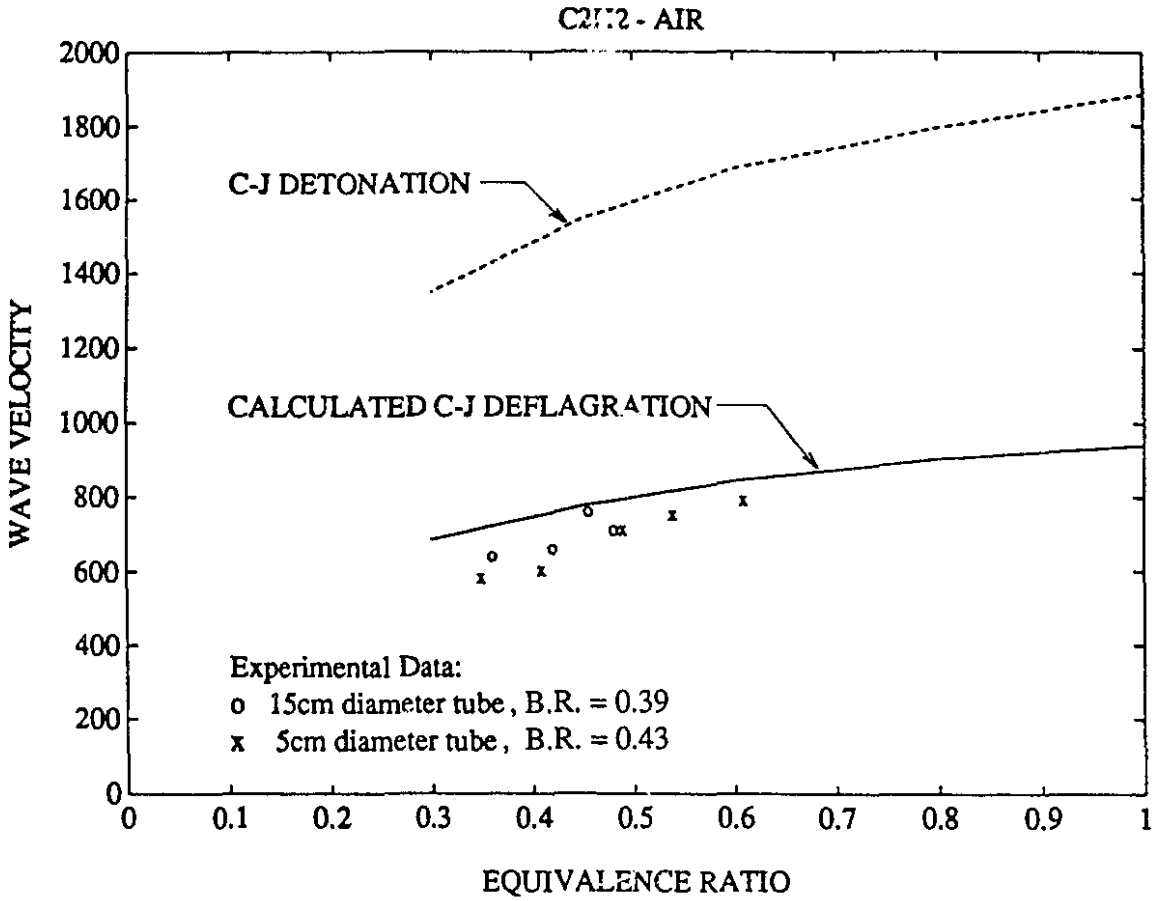

Figure 2.12: Comparison of theoretical CJ deflagration velocity with the turbulent high speed deflagration terminal velocity in rough tubes (Lee 1986). Acetylene-air mixture initially at 1 atm. and 298K.

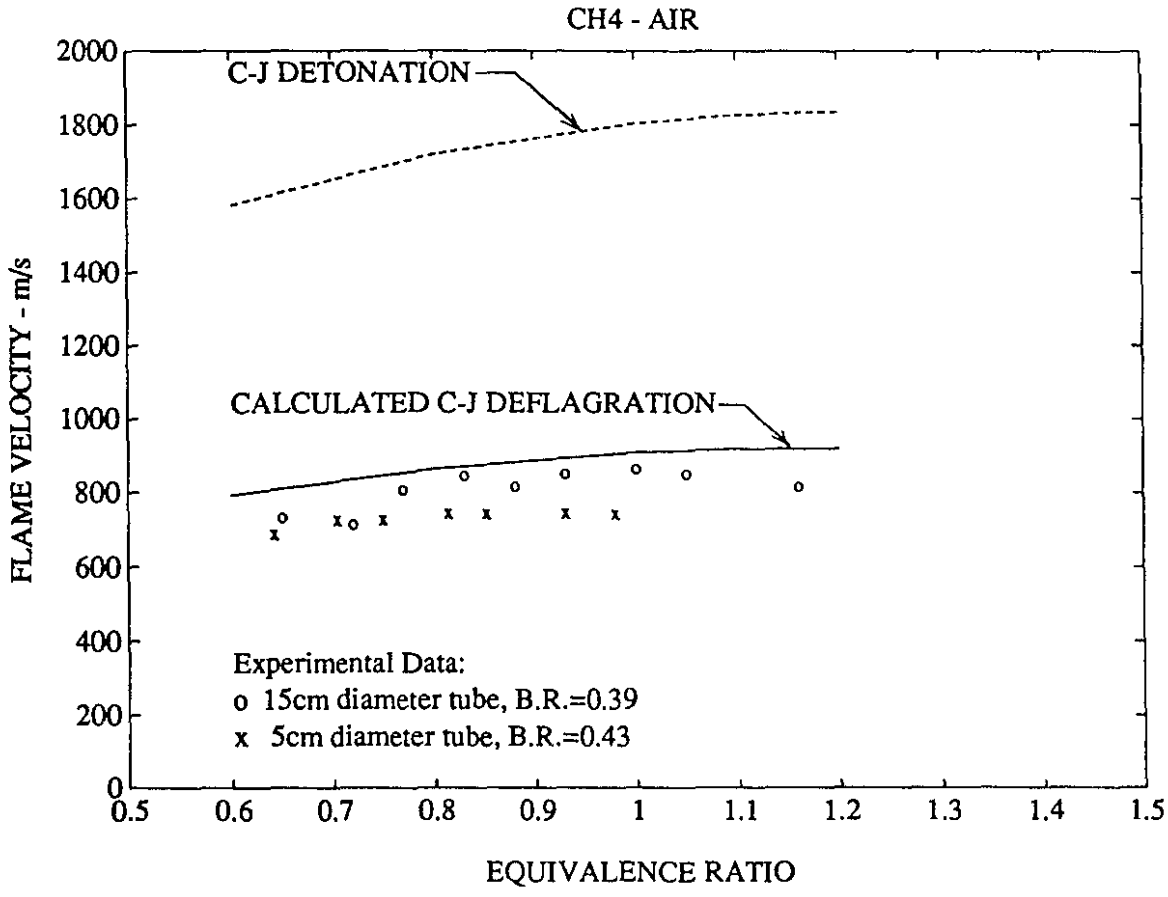

Figure 2.13: Comparison of theoretical CJ deflagration velocity with the turbulent high speed deflagration terminal velocity in rough tubes (Lee 1986). Methane-air mixture initially at 1 atm. and 298K.

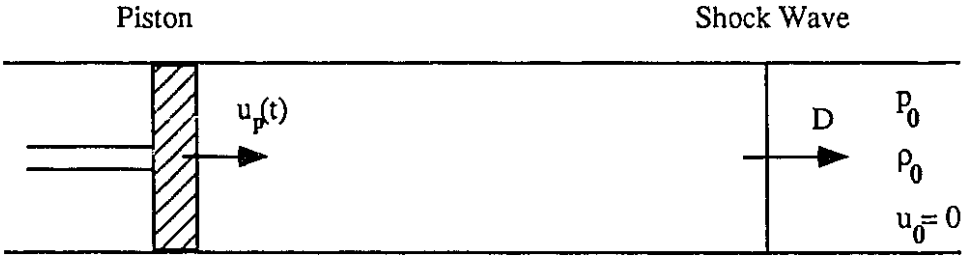

Figure 3.1: Schematic of the piston generated detonation.

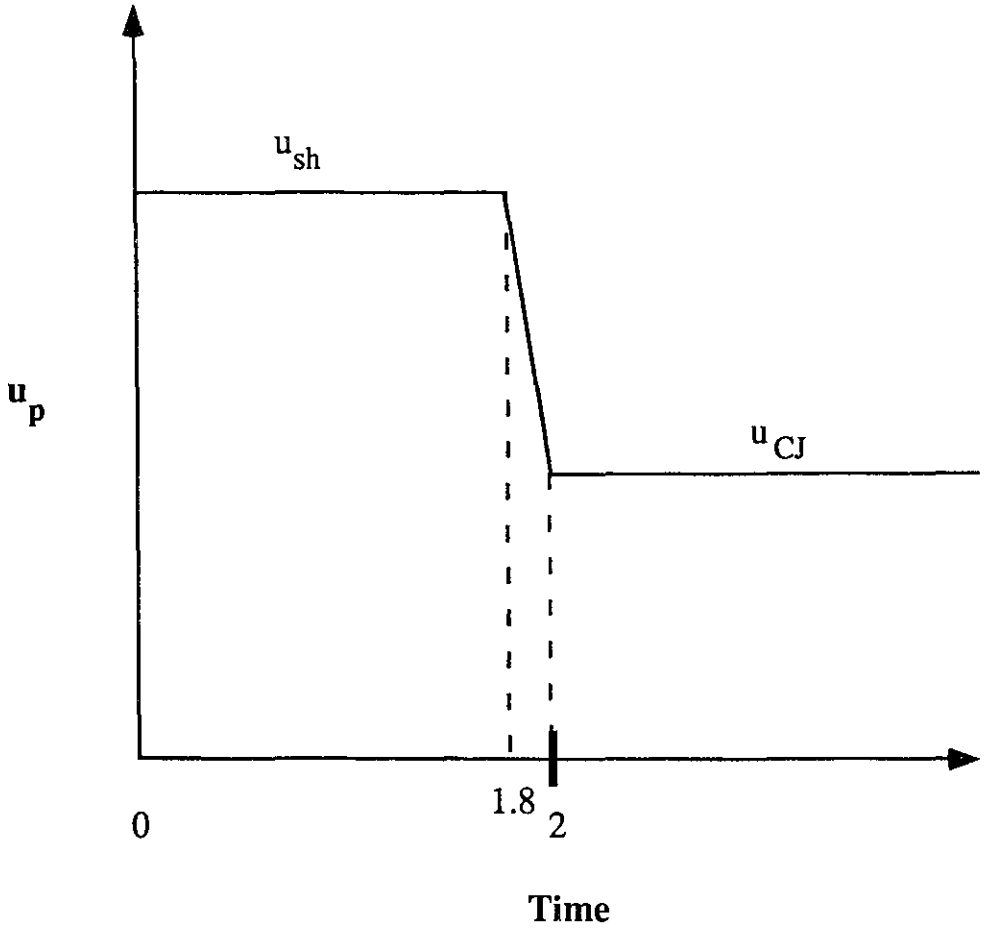

Figure 3.2: Initial piston velocity for initiating the one-dimensional detonation.

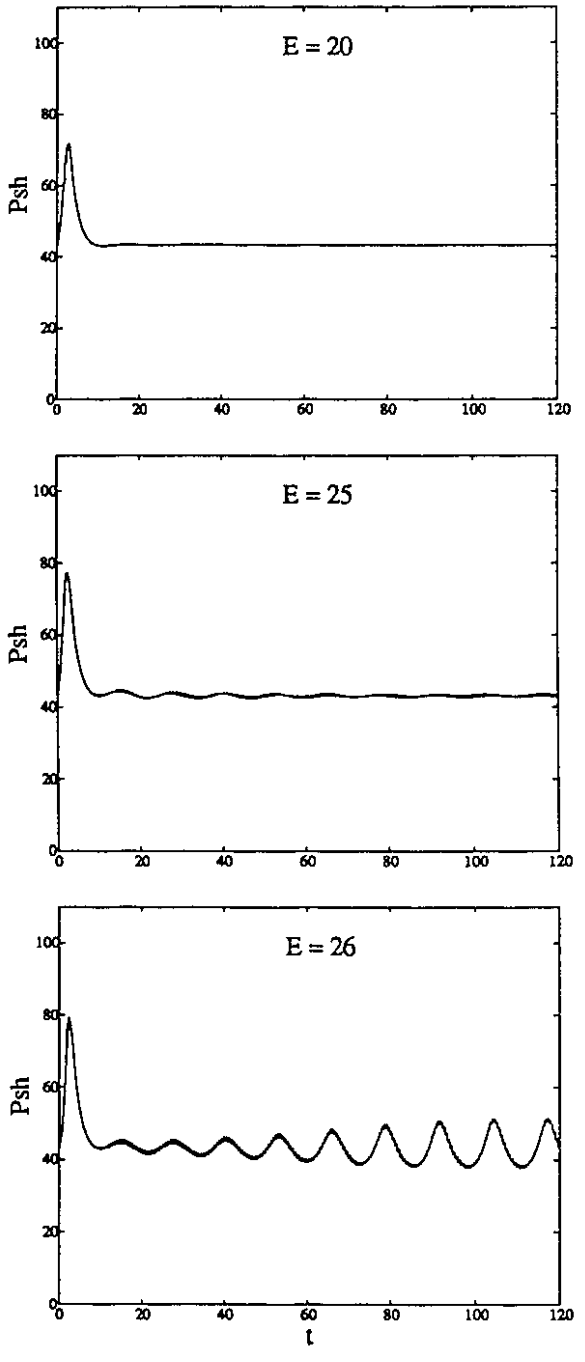

Figure 3.3: The oscillatory shock pressure pattern of the pulsating detonation for different activation energies.

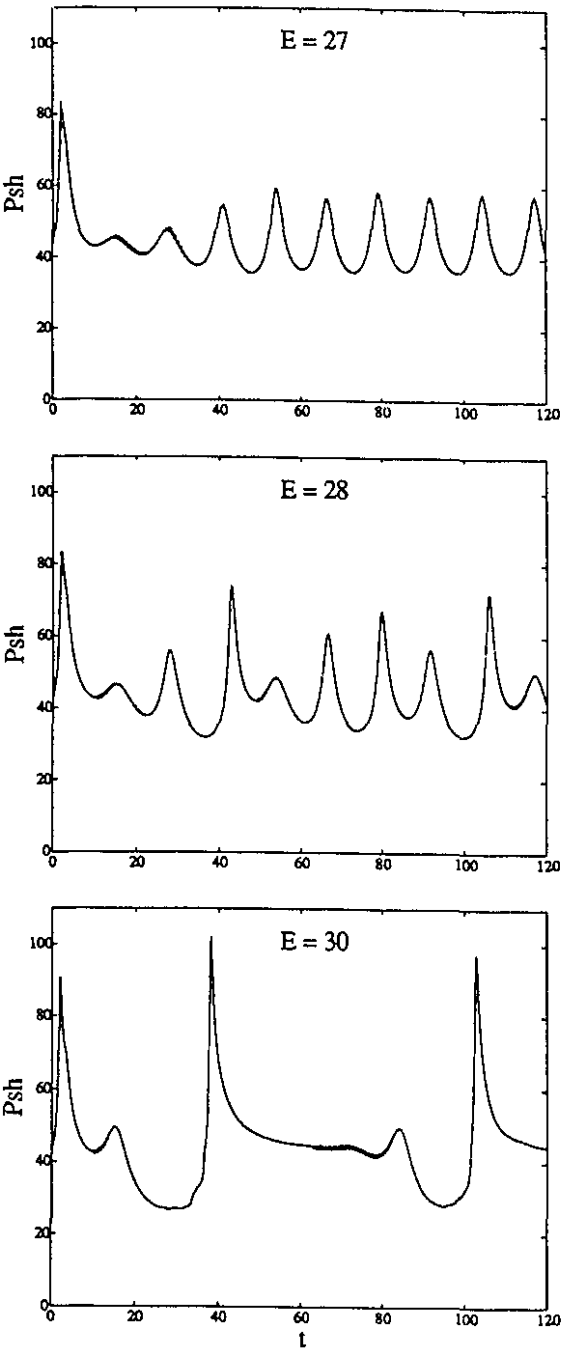

Figure 3.3 (cont'd)

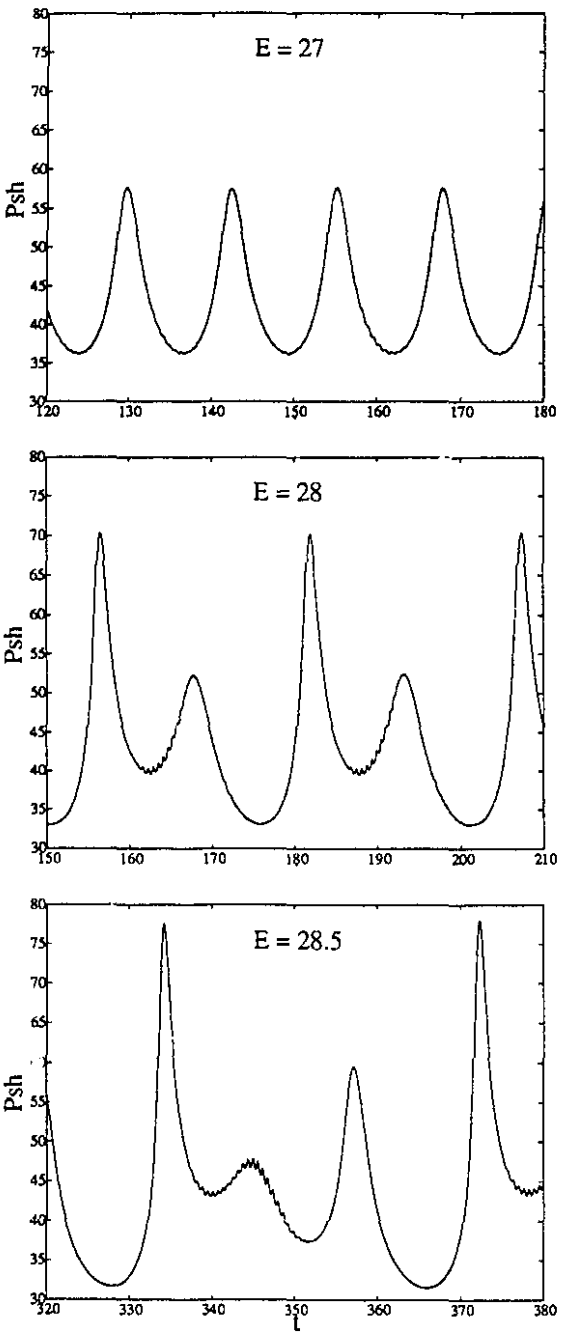

Figure 3.4: The bifurcation of the shock pressure pattern of the pulsating as E increases from 27 to 28.5.

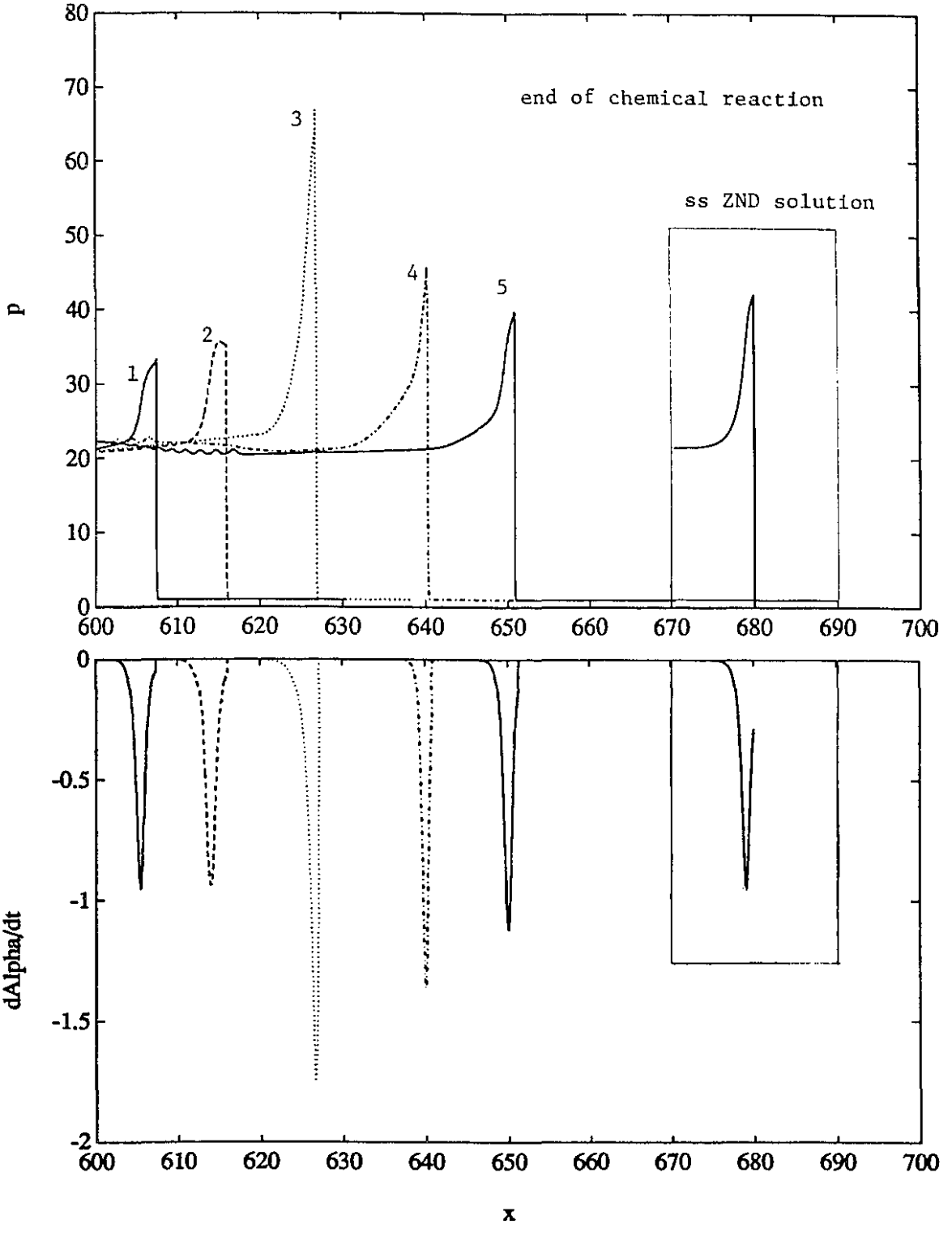

Figure 3.5: Spatial profiles of the pulsating detonation at different times for $E = 28, Q = 50, \gamma = 1.2$. Curves 1 to 5 refers to t = 175, 178, 181, 184, and 187, respectively. The distribution shown on the far right is the corresponding steady-state ZND solution. (a) Pressure.

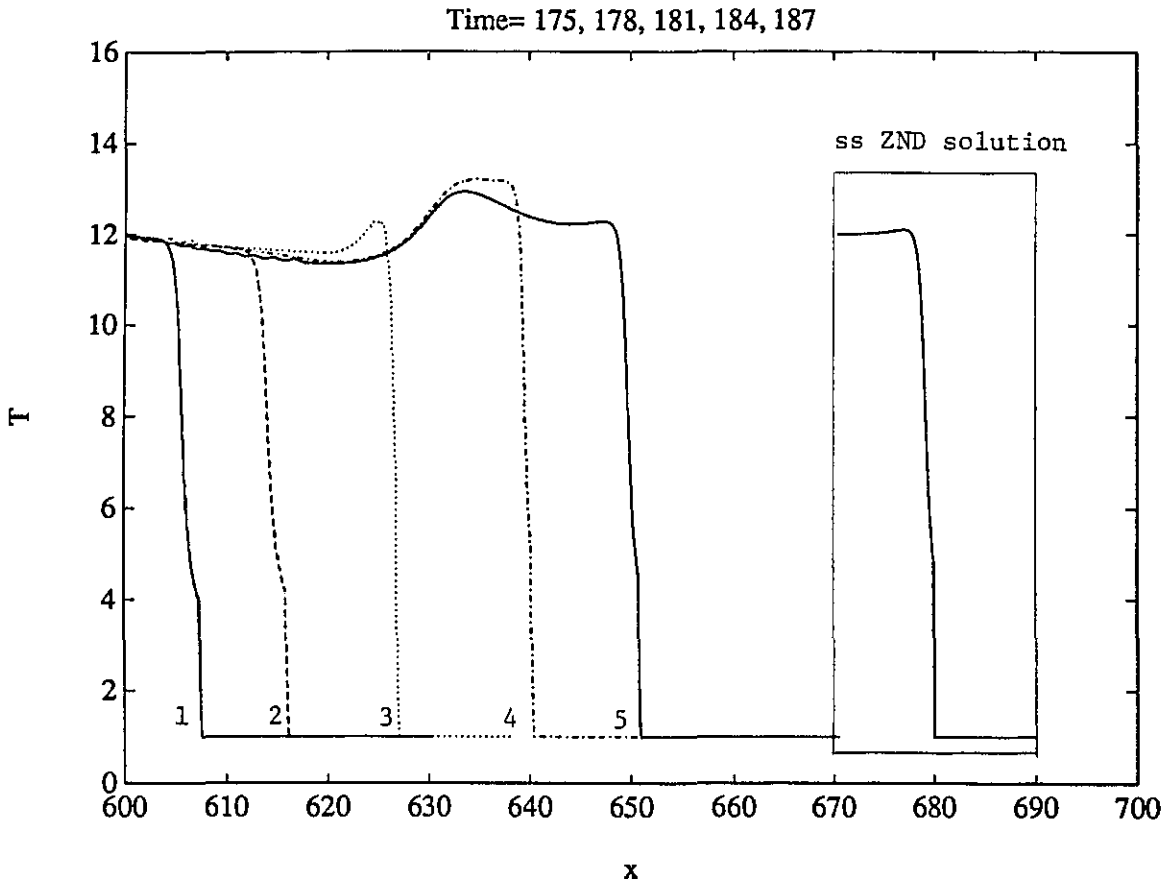

Figure 3.5: (b) Temperature.

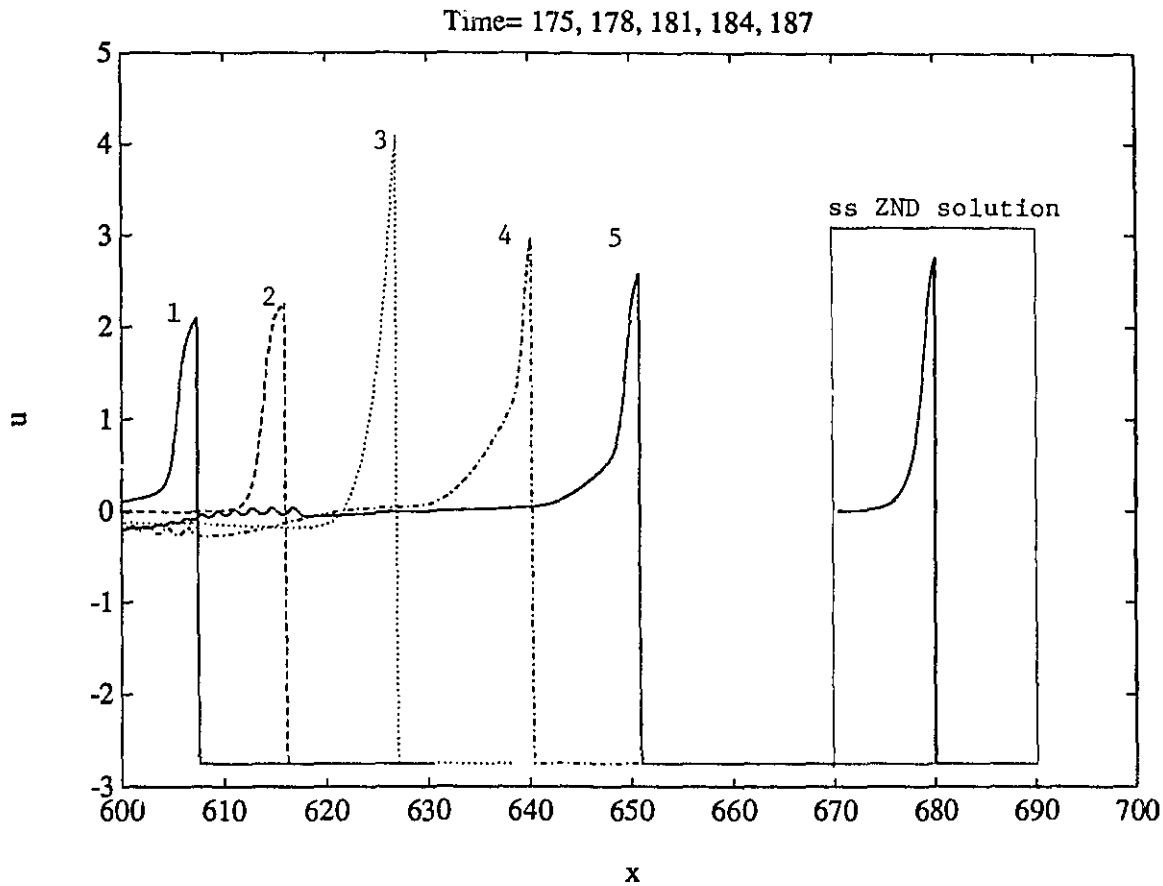

Figure 3.5: (c) Particle velocity.

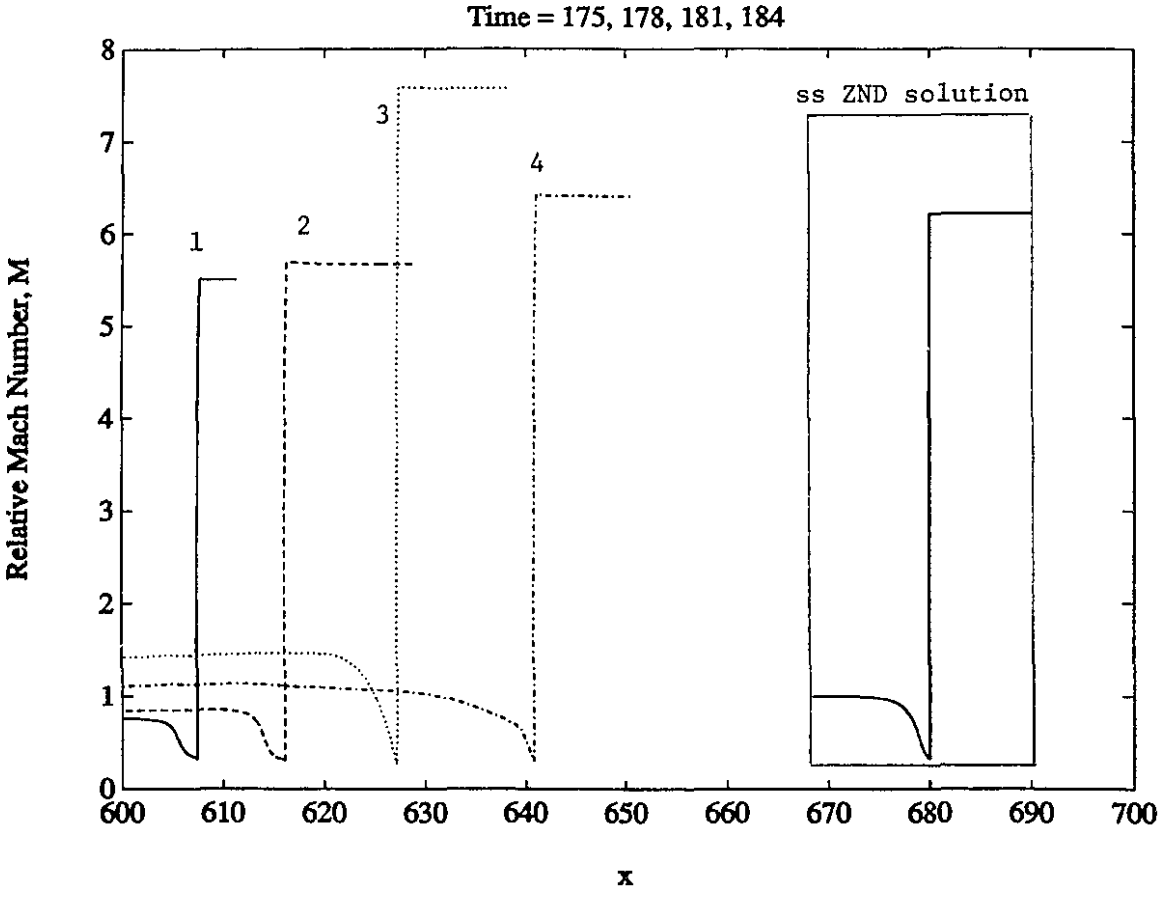

Figure 3.5: (d) Relative Mach number.

(a)

(b)

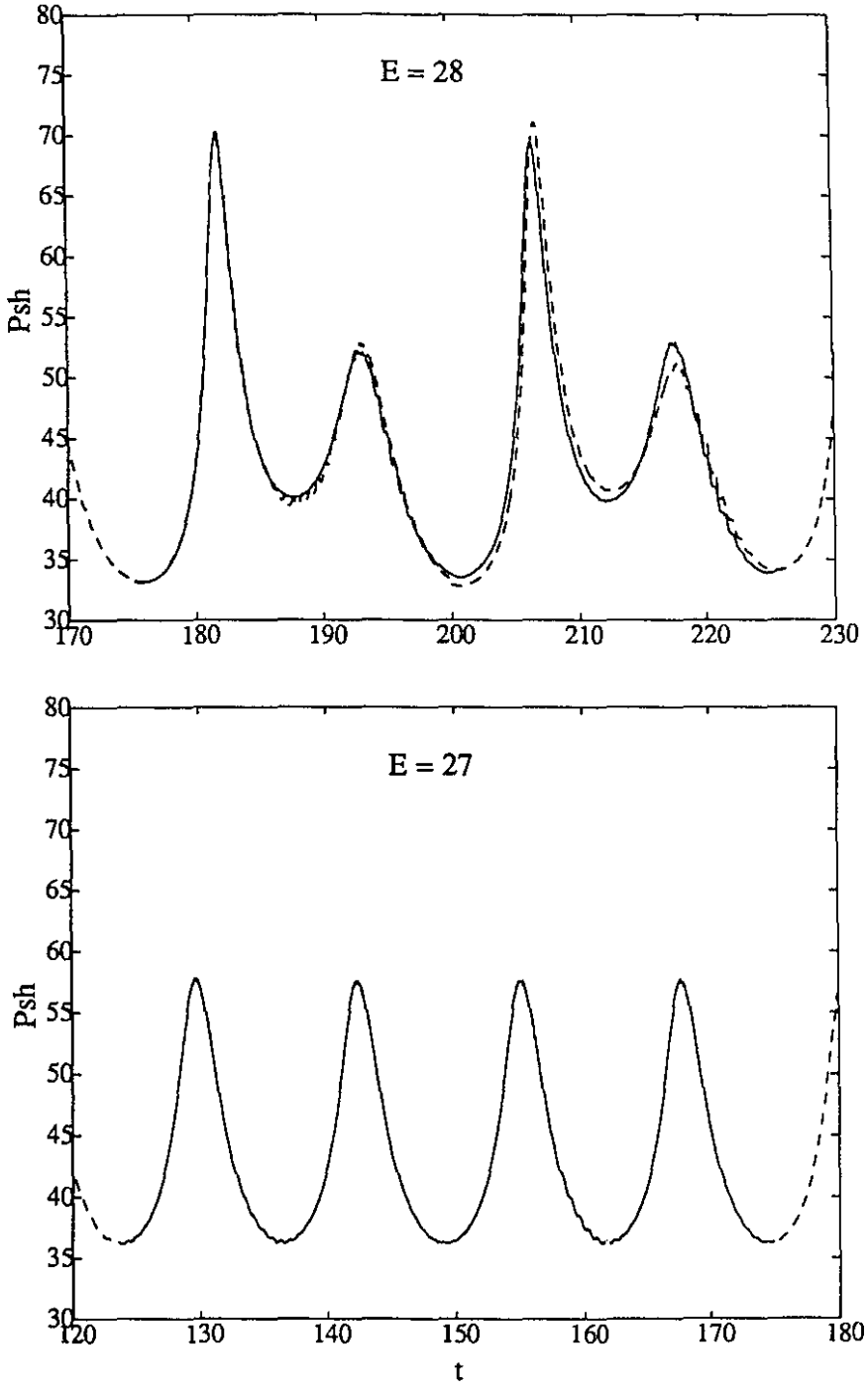

Figure 3.6: Effect of downstream boundary on the pulsating detonation. Solid line: "radiation" boundary condition, dashed line: full solution. (a) $E = 28$, (b) $E = 27$.

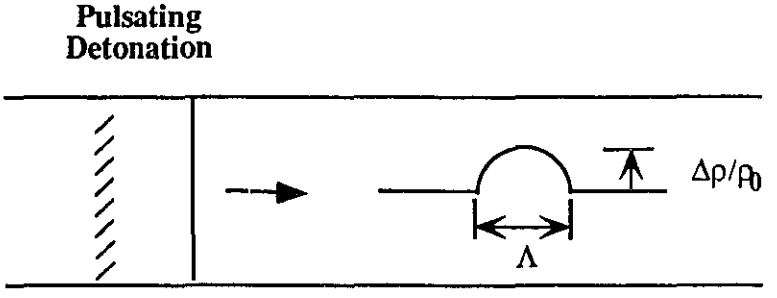

Figure 3.7: Density perturbation wave form on pulsating detonation.

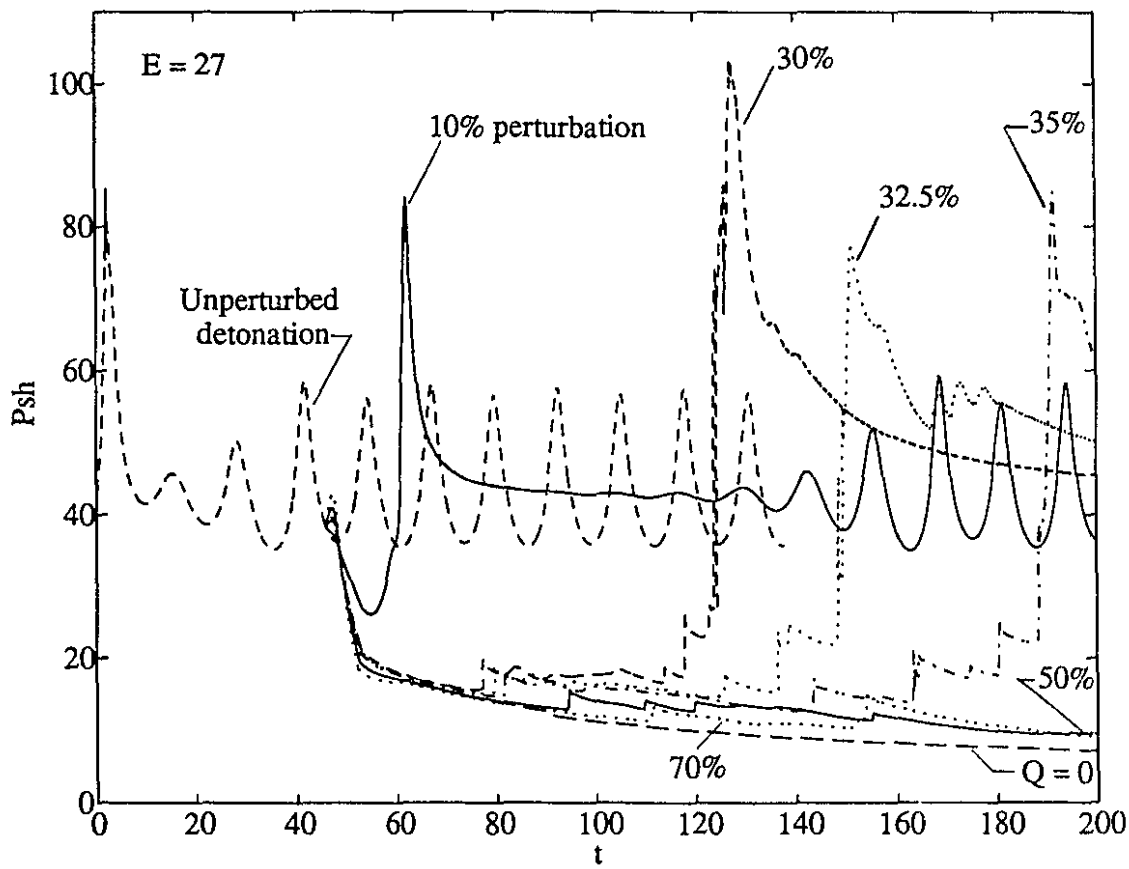

Figure 3.8: Failure of pulsating detonation for different amplitudes of density perturbation applied at $t = 46$. Amplitudes of perturbation $\Delta\rho/\rho_0$ calculated include: 10, 30, 32.5, 35, 50, 70 percent. Also plotted is the case for Q set to zero at $t = 69.6$ for a 50 percent perturbation.

(a)

(b)

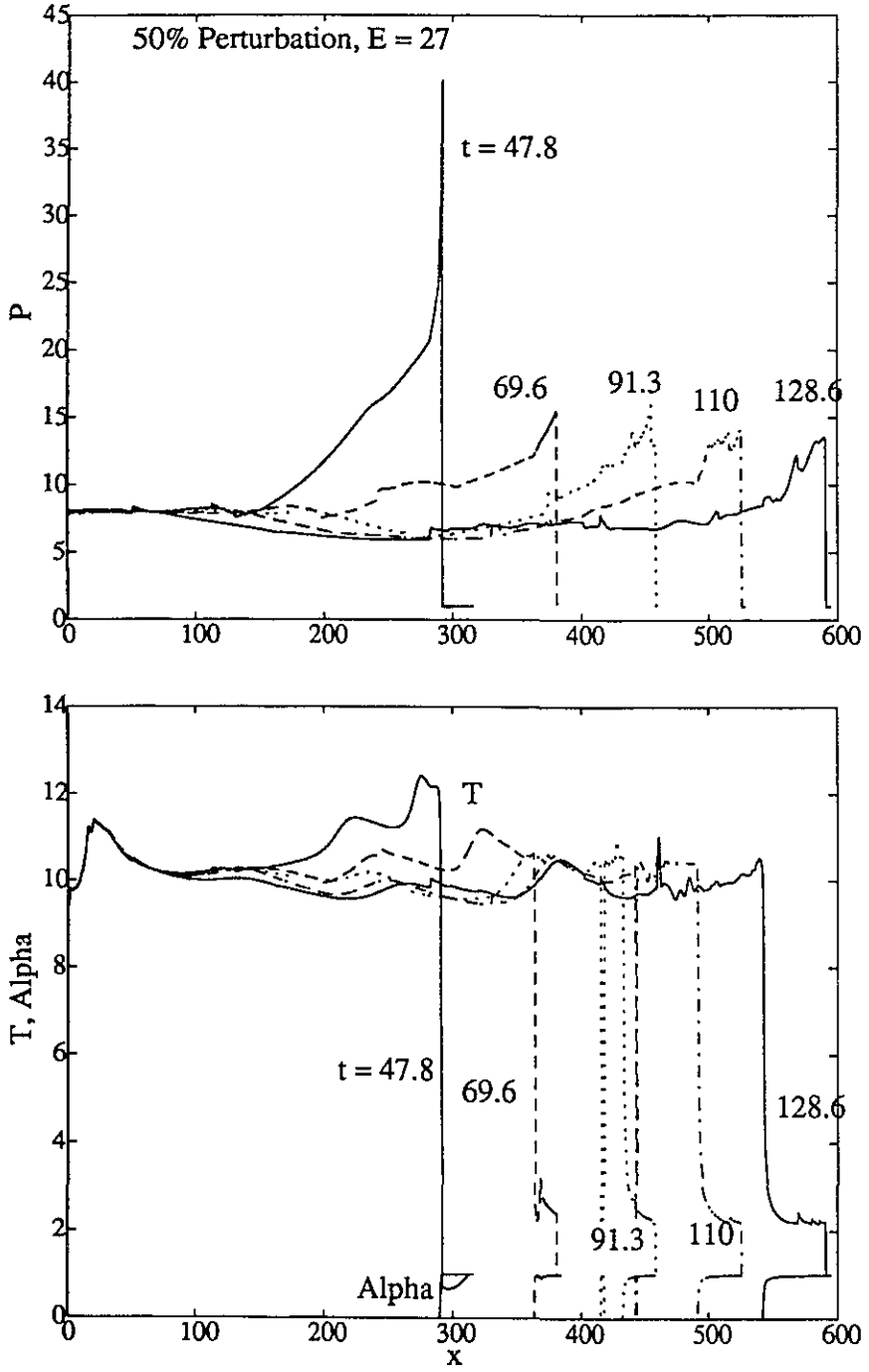

Figure 3.9: Spatial profiles of the quasi-steady shock-reaction complex at different times. $E = 27, Q = 50, \gamma = 1.2$. 50 percent density perturbation. (a) Pressure, (b) temperature and reactant mass fraction α distributions. Note that due to the initial rapid reaction at $t = 47.8$, the shock temperature ($T \simeq 4.8$) cannot be distinguished from the figure.

(c)

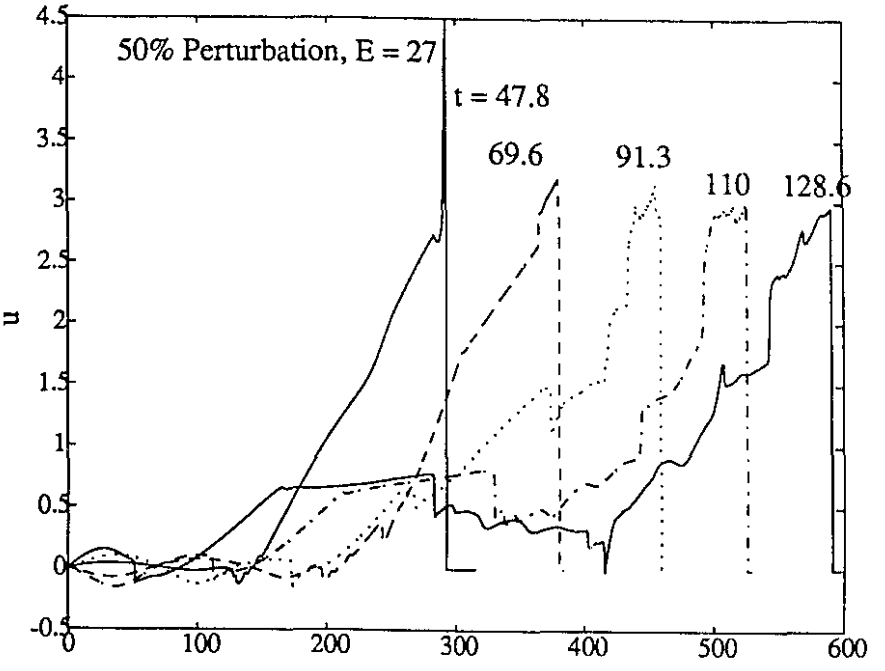

(d)

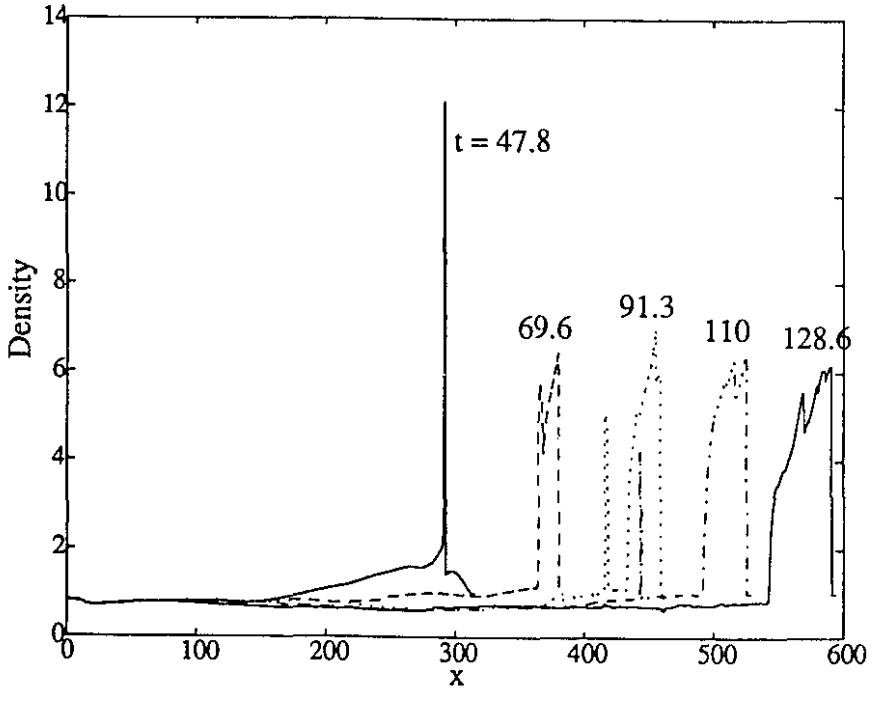

Figure 3.9: (c) Velocity and (d) density distributions.

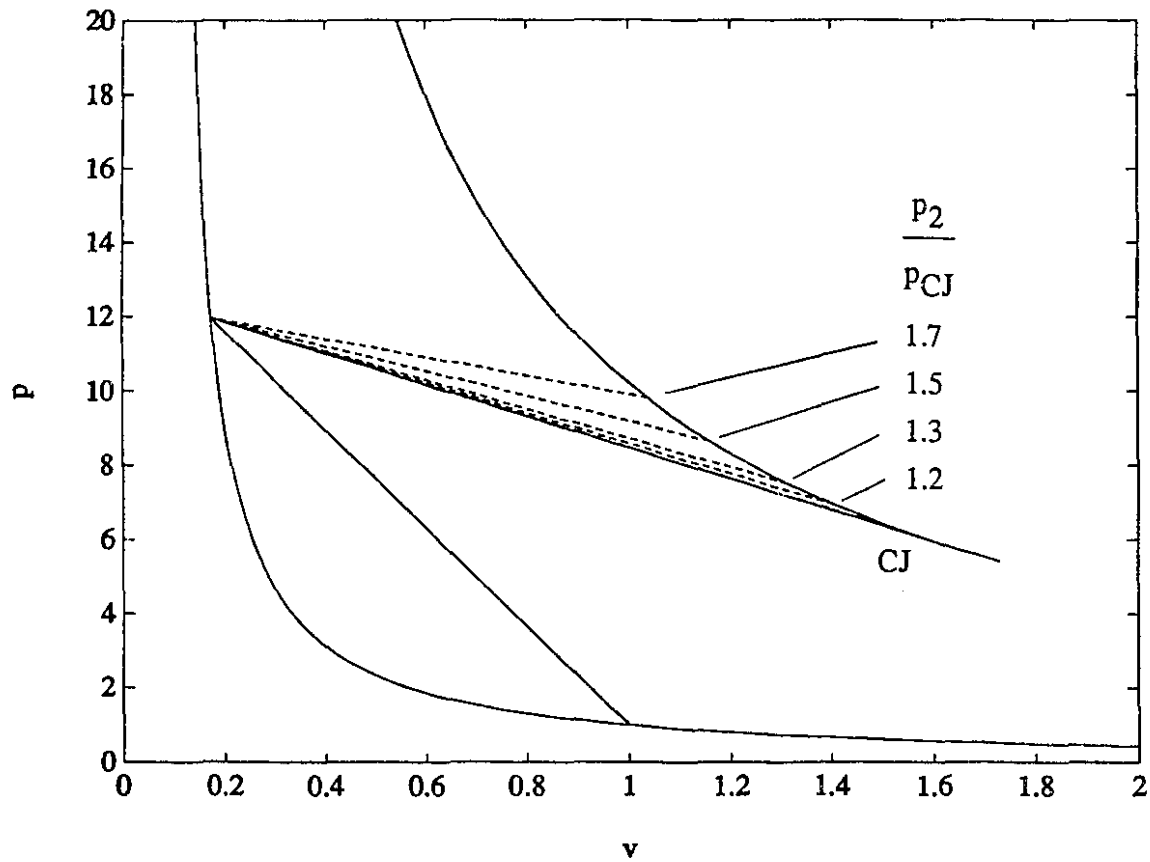

Figure 3.10: Hugoniot diagram for different possible steady deflagrations with the same Q assuming a fixed leading shock state calculated from the CJ deflagration solution.

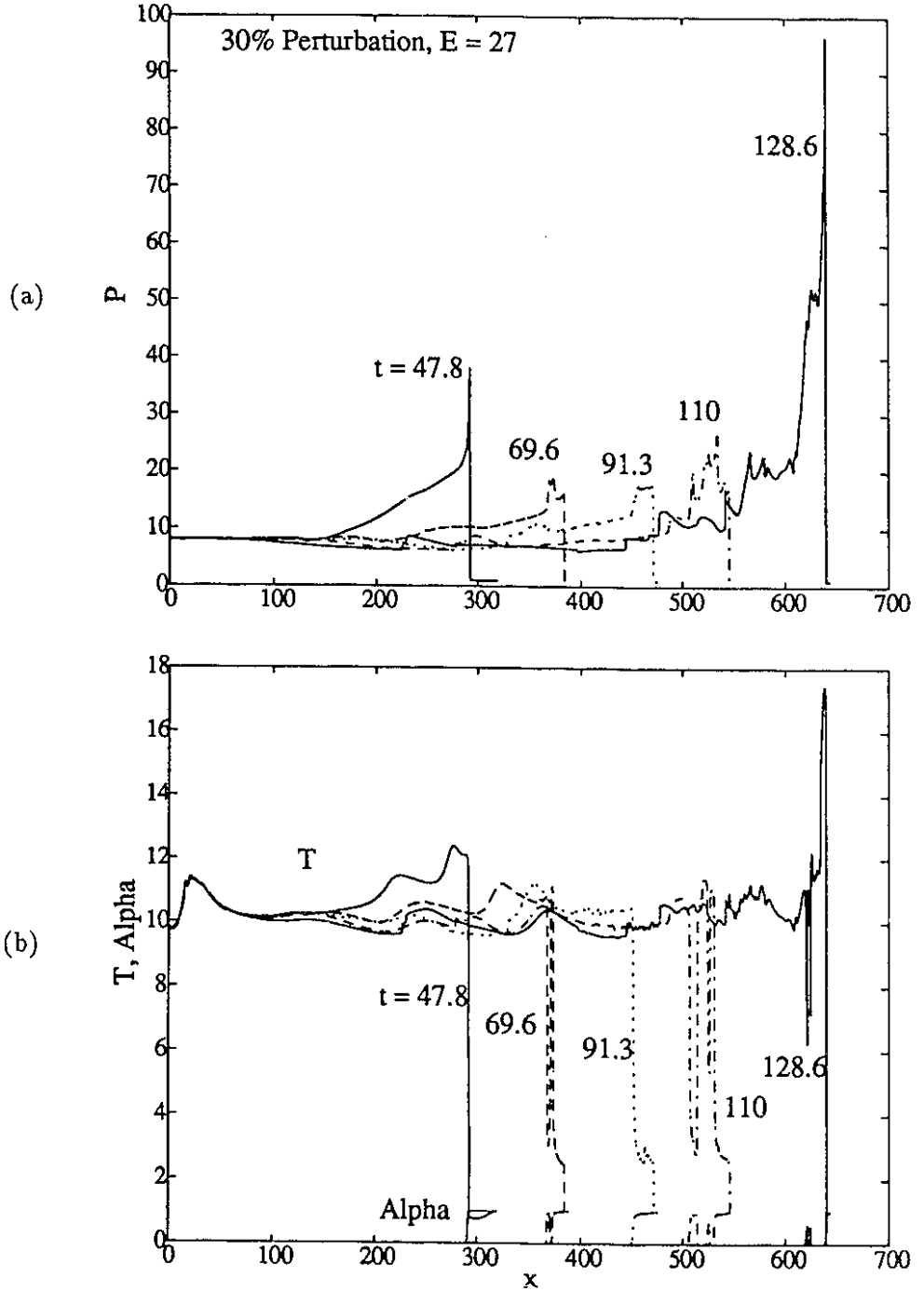

Figure 3.11: Spatial profiles of the quasi-steady shock-reaction complex and natural re-transition at different times. $E = 27, Q = 50, \gamma = 1.2$. 30 percent density perturbation. (a) Pressure, (b) temperature and reactant mass fraction α distributions. Note that due to the initial rapid reaction at $t = 47.8$, the shock temperature ($T \simeq 4.8$) cannot be distinguished from the figure.

(c)

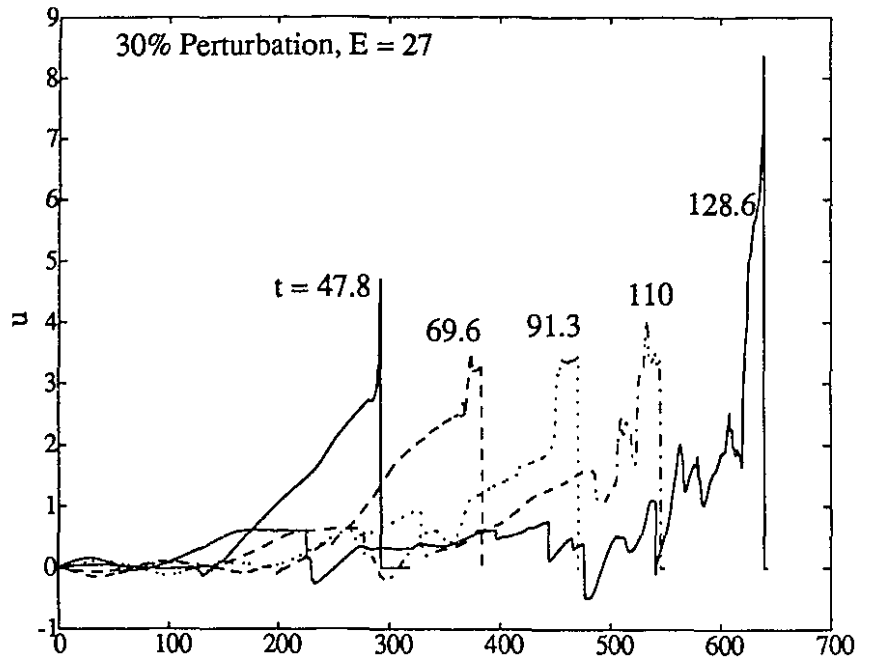

(d)

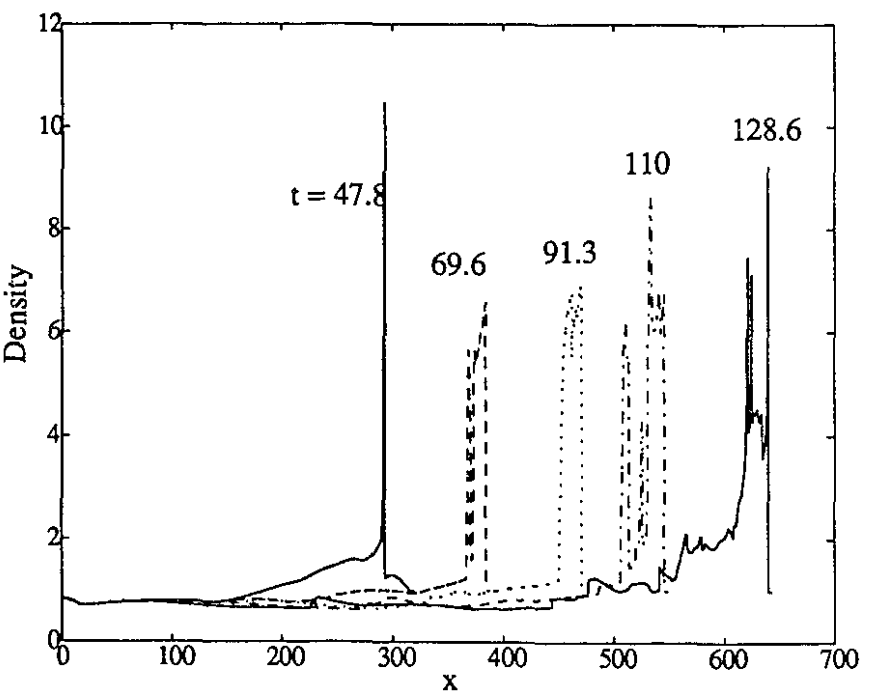

Figure 3.11: (c) Velocity and (d) density distributions.

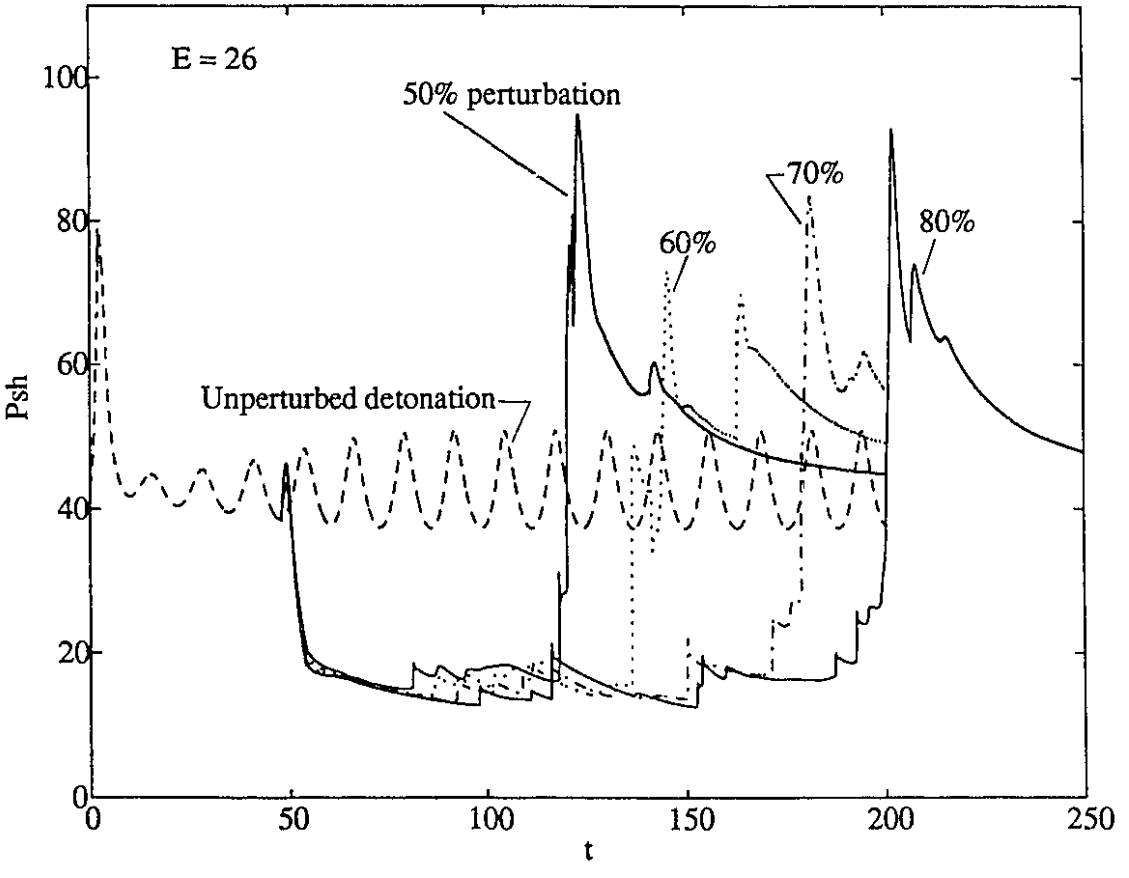

Figure 3.12: Failure of pulsating detonation for $E = 26$ with different amplitudes of density perturbation applied at $t = 47$. Amplitudes of perturbation $\Delta\rho/\rho_0$ calculated include: 50, 60, 70, 80 percent.

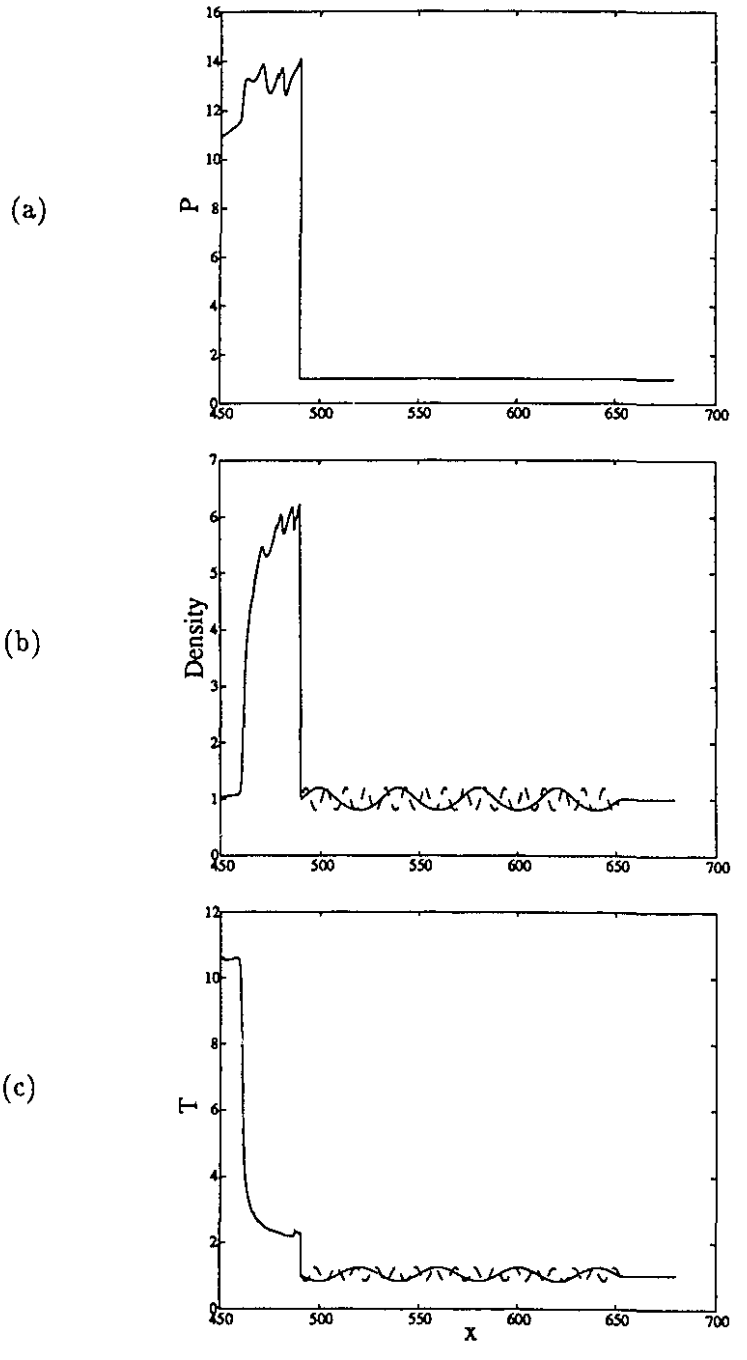

Figure 4.1: Spatial profiles of the quasi-steady shock-reaction at $t_0 = 100$ when periodic density perturbations are applied to induce transition. The form of the perturbations are shown in the density and temperature plots, where the amplitude is 20 percent of the initial density, periods of 12.7 and 3.175 are displayed. (a) Pressure, (b) density, (c) temperature.

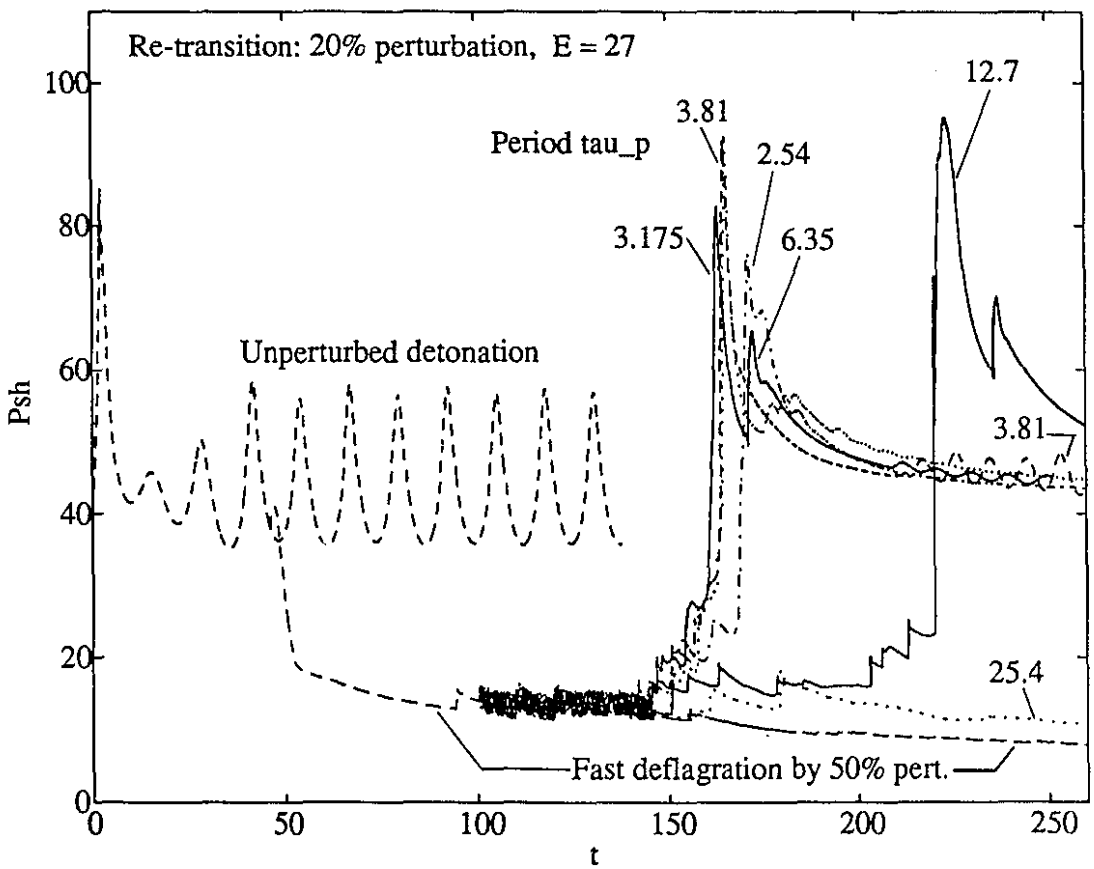

Figure 4.2: Re-transition of detonation using periodic density perturbations for $E = 27$. Perturbation periods shown are τ_p of 0.127, 0.635, 2.54, 3.175, 3.81, 6.35, 12.7, and 25.4. The solution for periods 0.127 and 0.635 are overlapped with the fast deflagration solution with no periodic density perturbation.

(a)

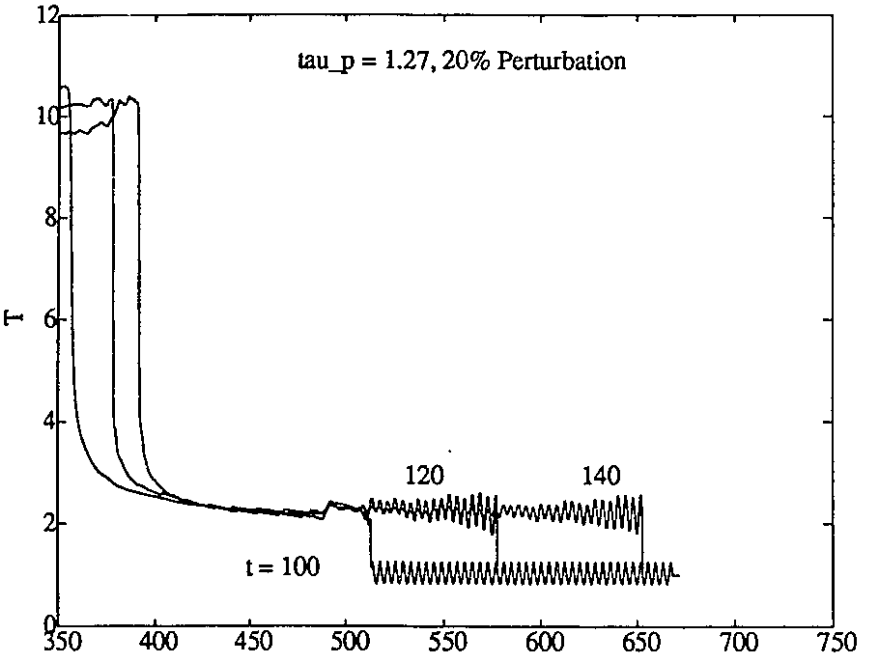

(b)

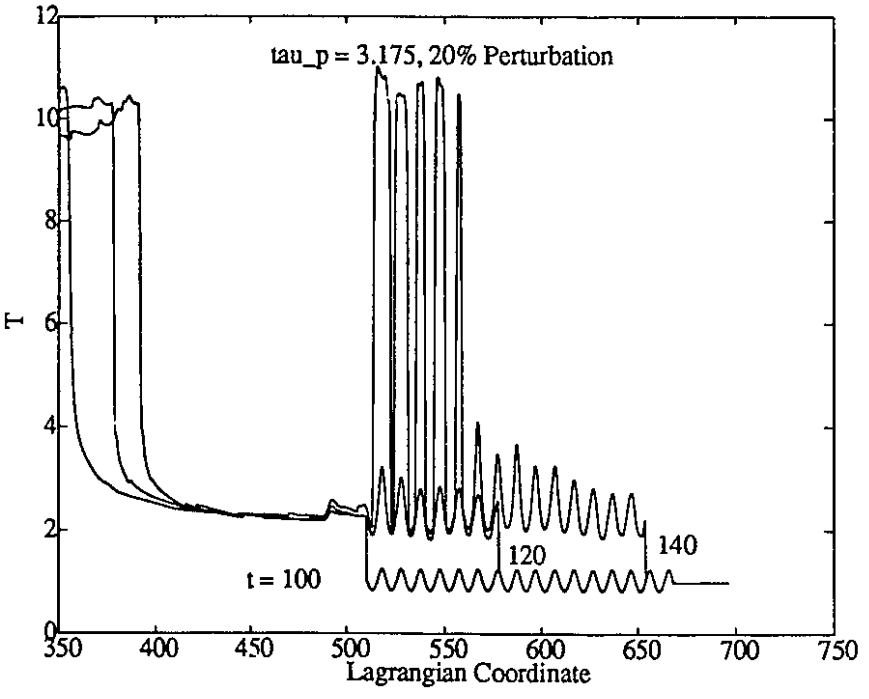

Figure 4.3: Amplification of temperature perturbations for different perturbation periods displayed in Lagrangian coordinate ξ. $E = 27$, 20 percent density perturbations. (a) $\tau_p = 1.27$, (b) $\tau_p = 3.175$.

(c)

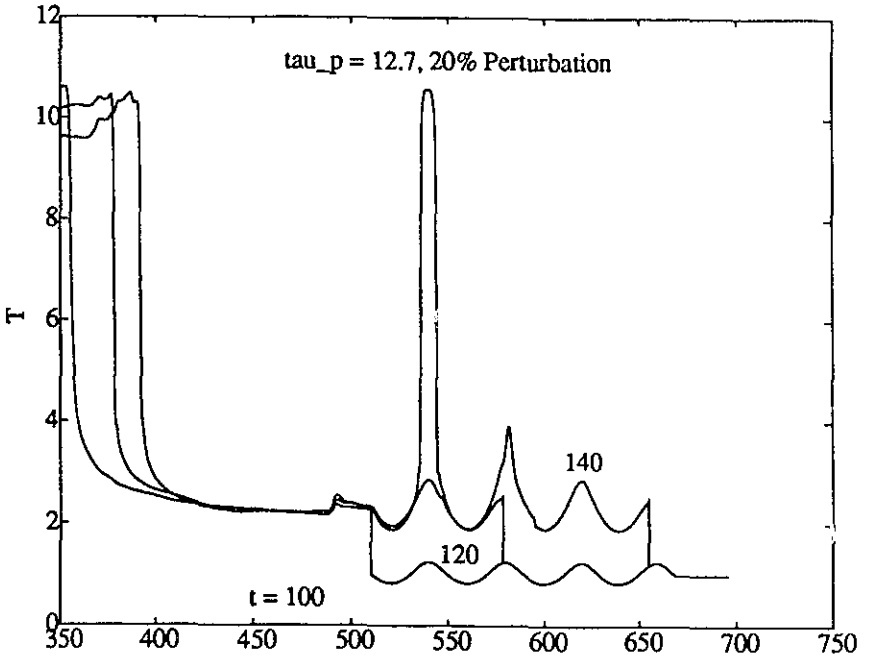

(d)

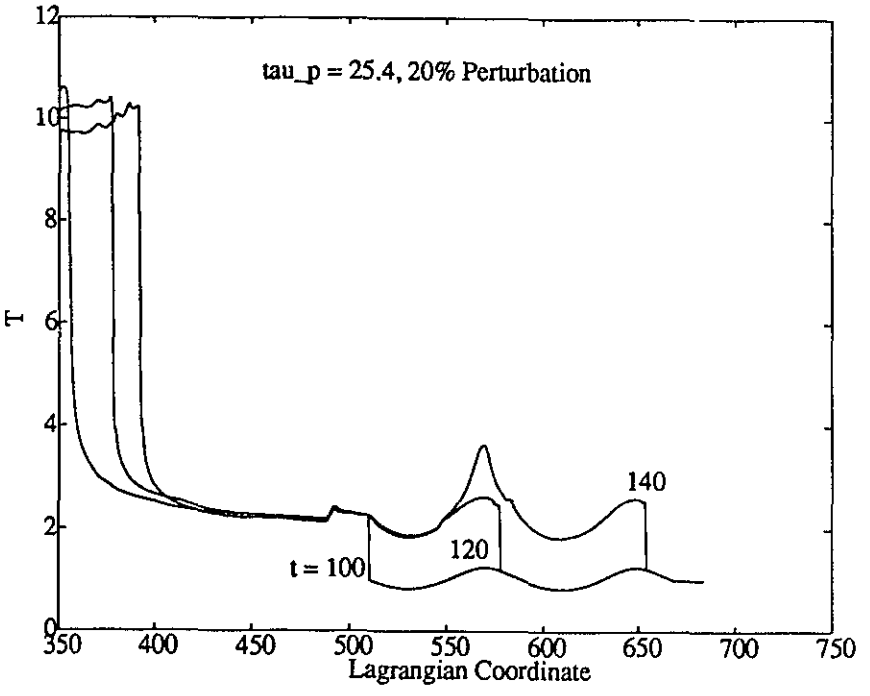

Figure 4.3: (c) $\tau_p = 12.7$, (d) $\tau_p = 25.4$.

(a)

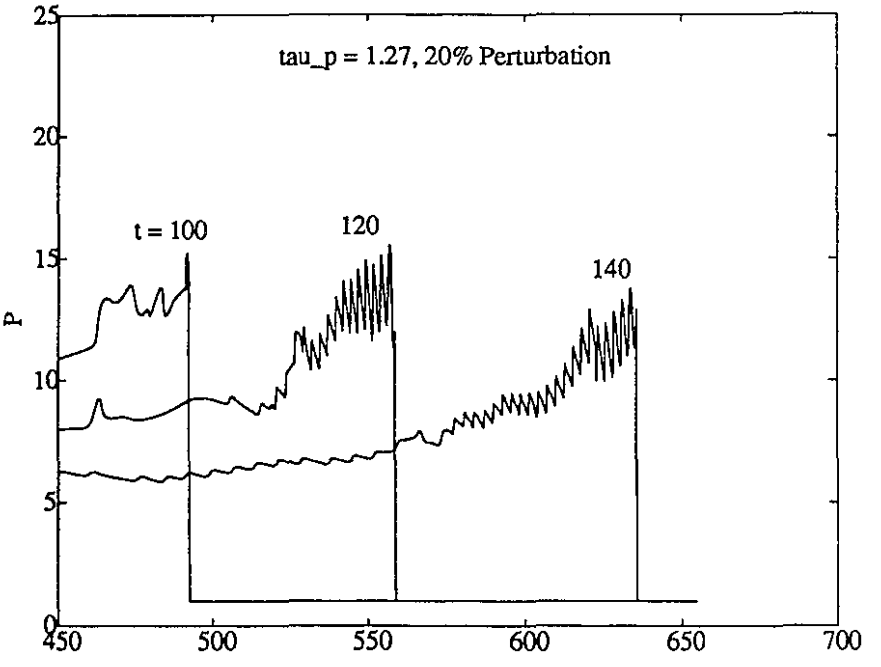

(b)

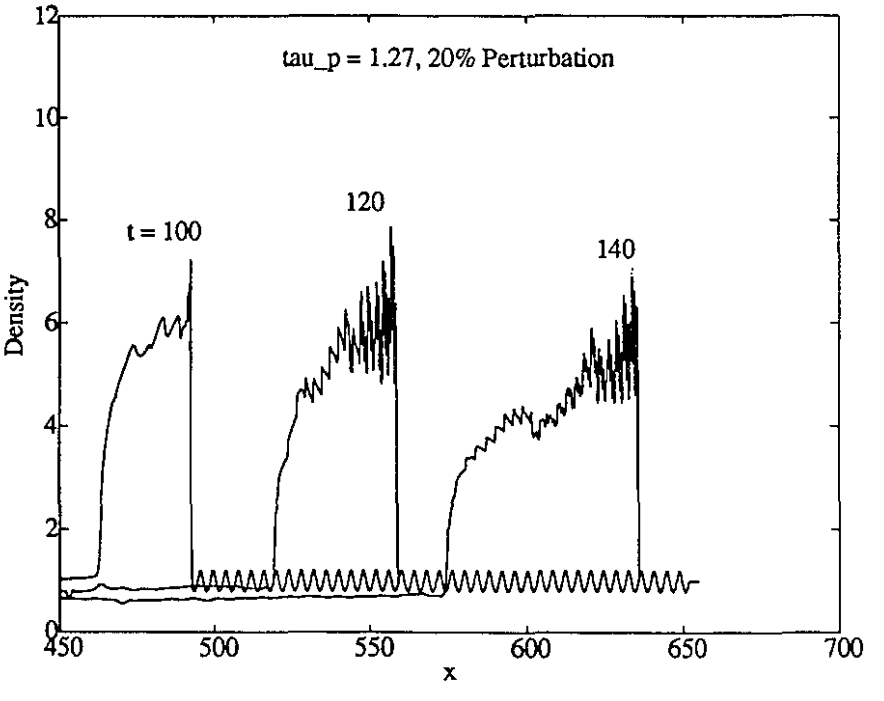

Figure 4.4: Distributions of pressure and density in physical (Eulerian) space at different times after perturbation is imposed. $E = 27, 20$ percent density perturbation, $\tau_p = 1.27$. (a) Pressure, (b) density.

(a)

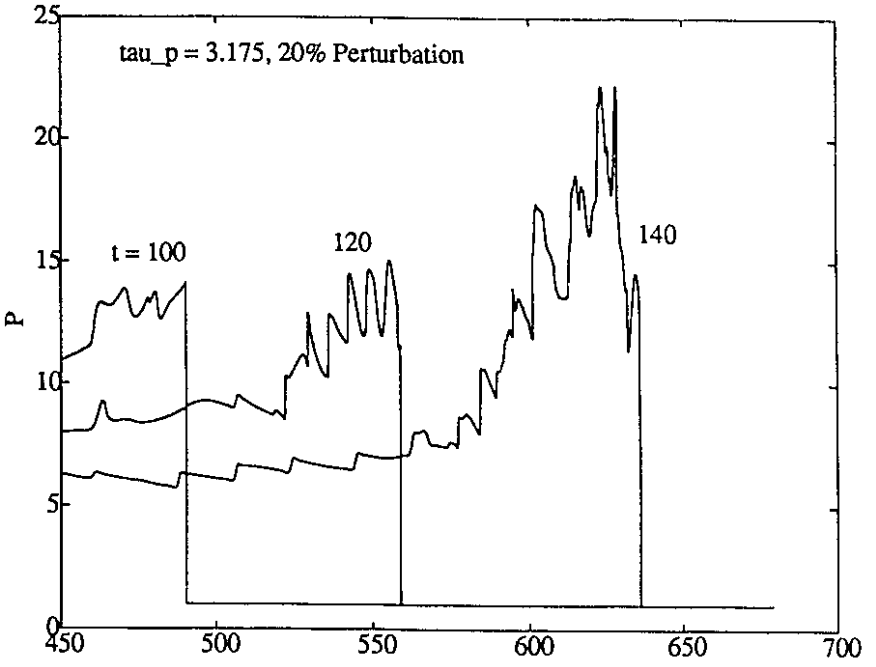

(b)

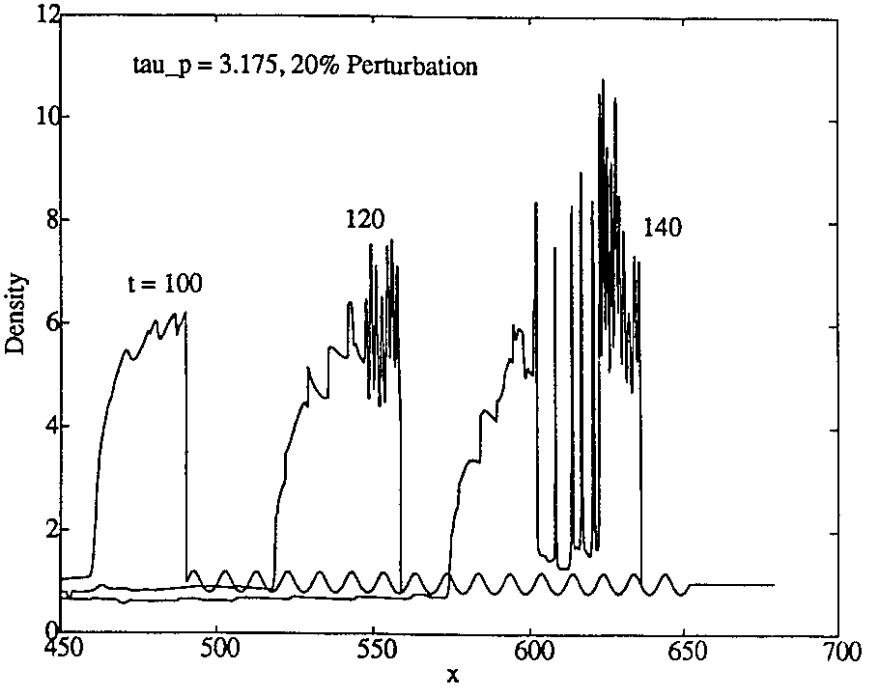

Figure 4.5: Distributions of pressure and density in physical (Eulerian) space at different times after perturbation is imposed. $E = 27, 20$ percent density perturbation, $\tau_p = 3.175$. (a) Pressure, (b) density.

(a)

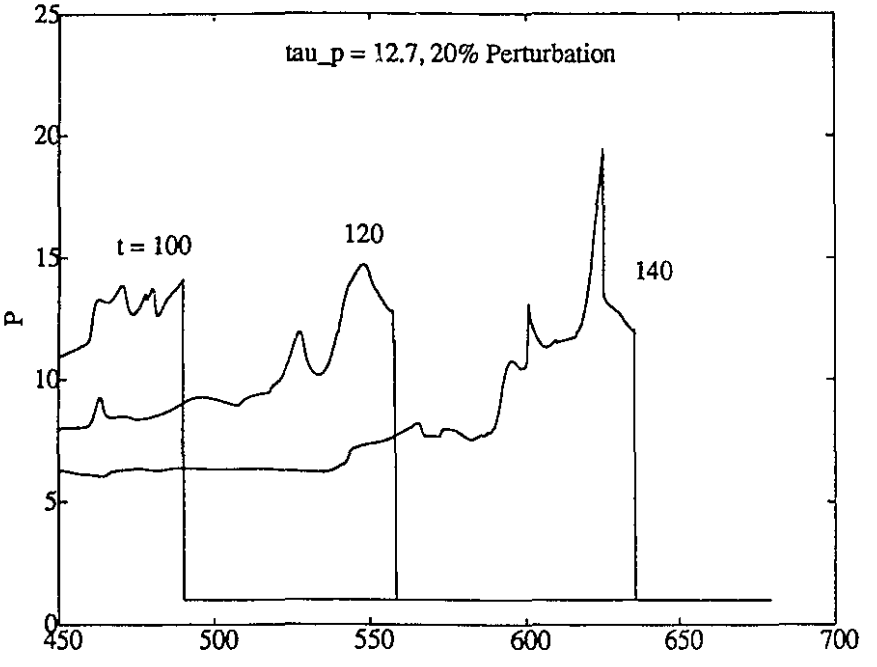

(b)

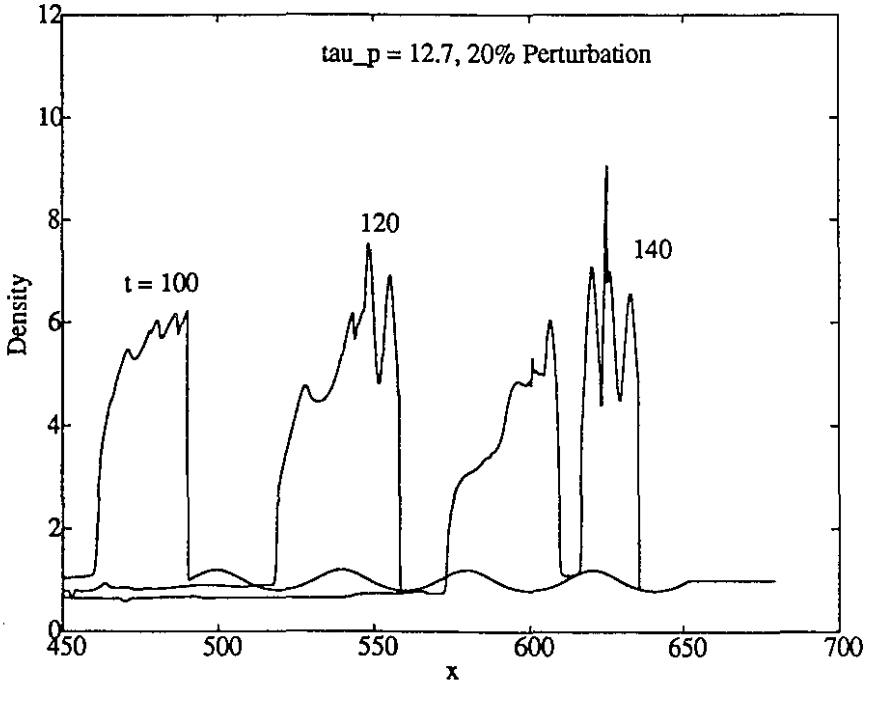

Figure 4.6: Distributions of pressure and density in physical (Eulerian) space at different times after perturbation is imposed. $E = 27, 20$ percent density perturbation, $\tau_p = 12.7$. (a) Pressure, (b) density.

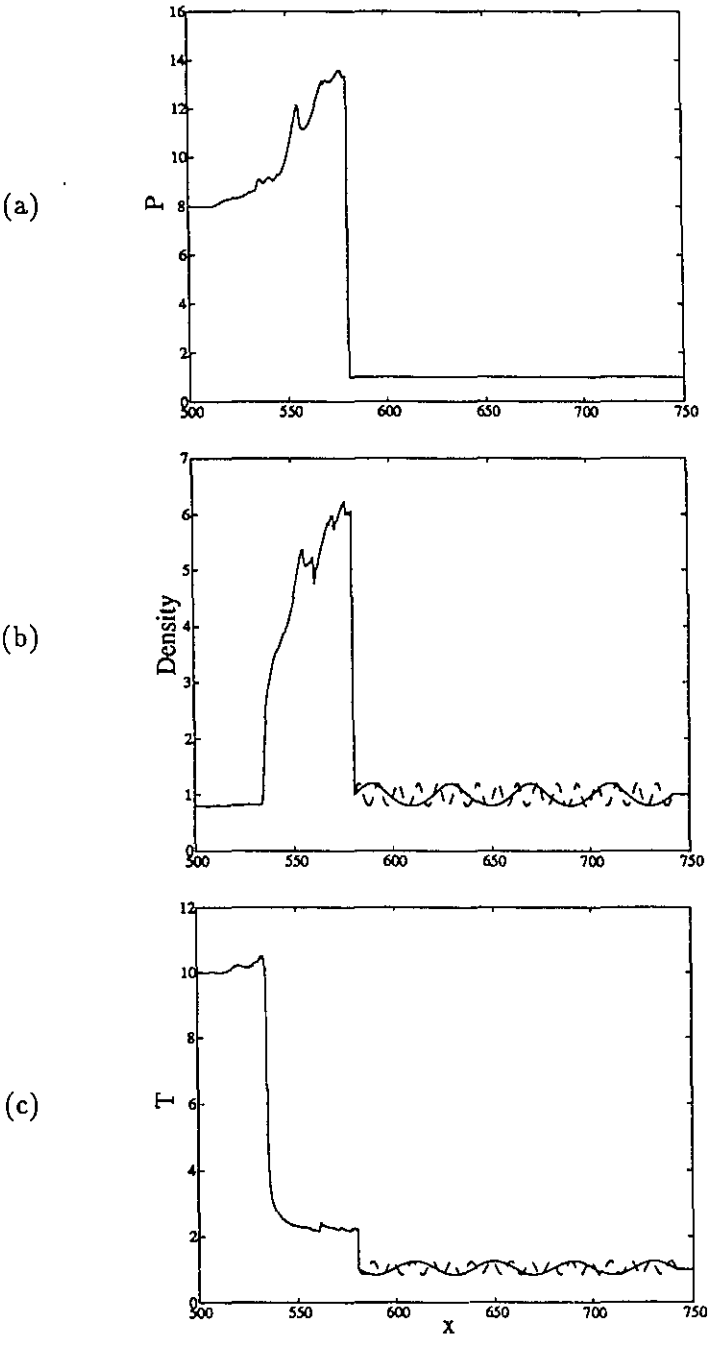

Figure 4.7: Spatial profiles of the quasi-steady shock-reaction at $t_0 = 125.5$ when periodic density perturbations are applied to induce transition. The form of the perturbations are shown in the density and temperature plots, where the amplitude is 20 percent of the initial density, periods of 12.7 and 3.175 are displayed. (a) Pressure, (b) density, (c) temperature.

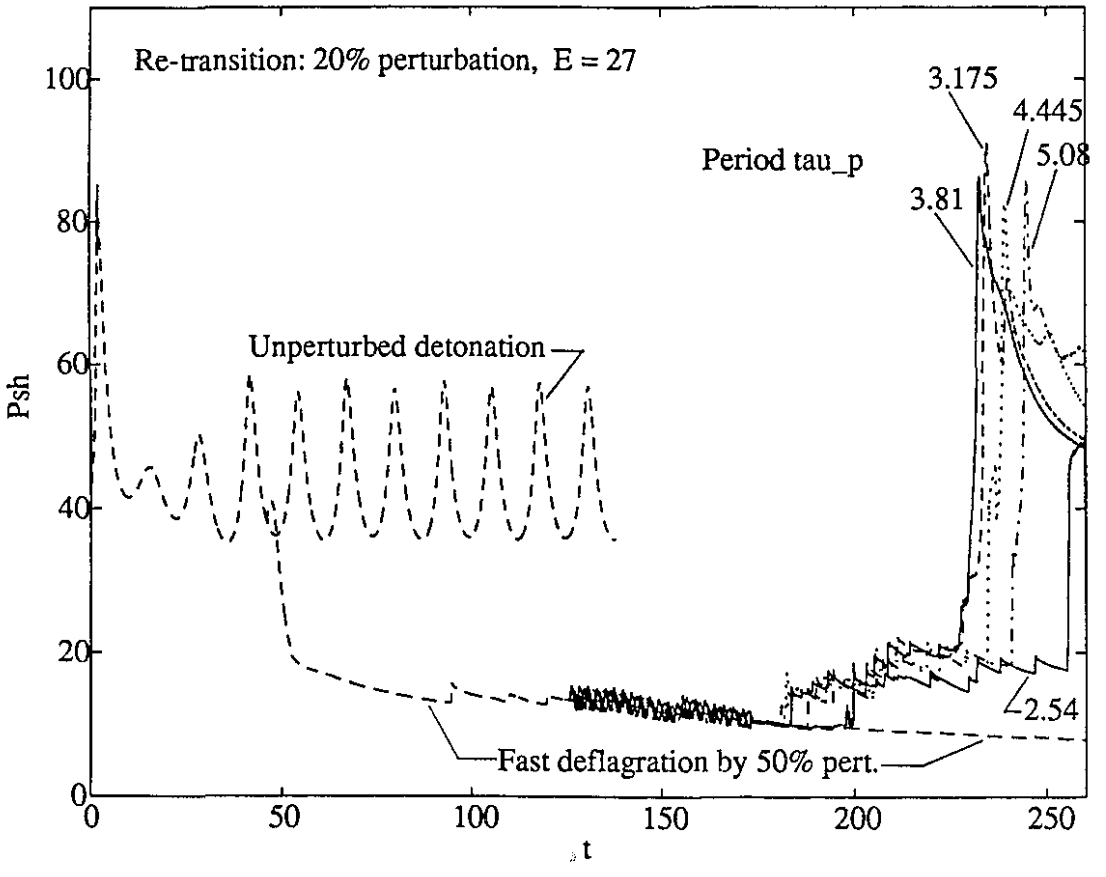

Figure 4.8: Re-transition of detonation using periodic density perturbations applied at $t_0 = 125.5$. Perturbation periods shown are τ_p of 2.54, 3.175, 3.81, 4.445, and 5.08.

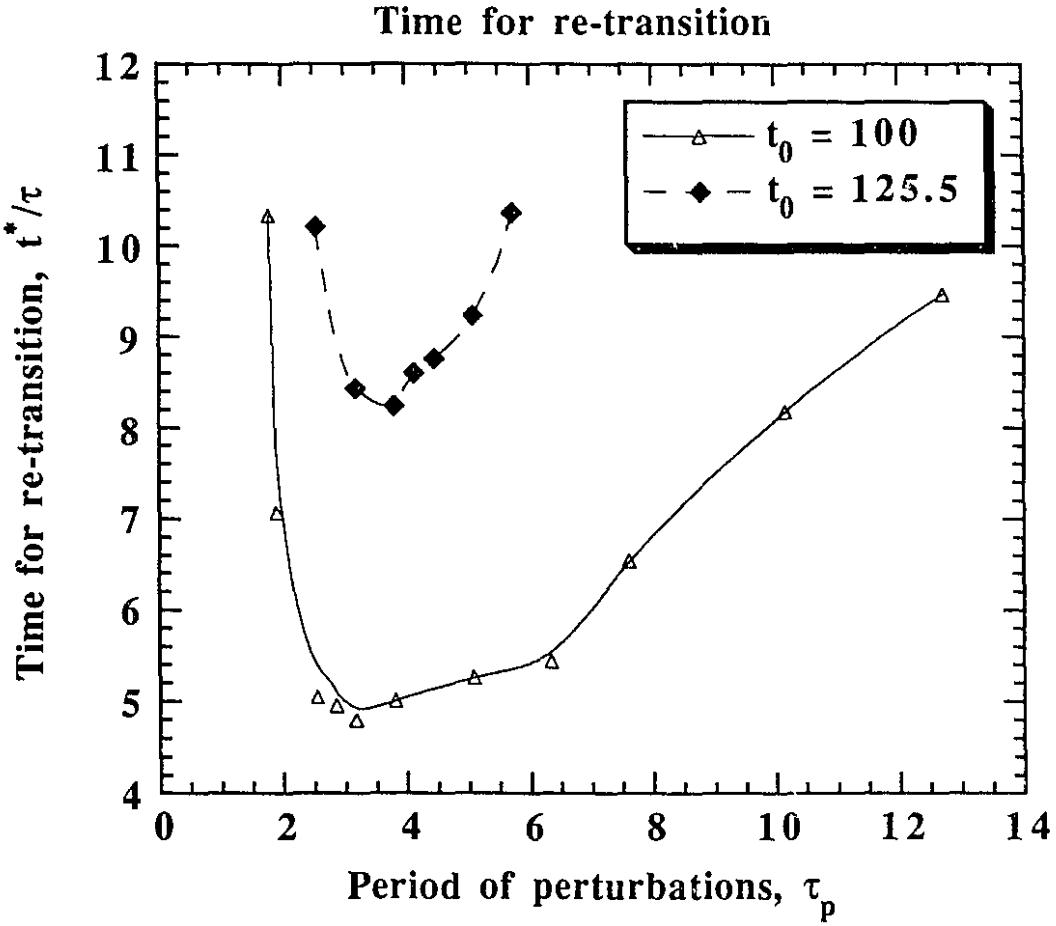

Figure 4.9: Time for re-transition versus the period of the applied perturbation for different initial time of application t_0 of the periodic density perturbation to induce transition.

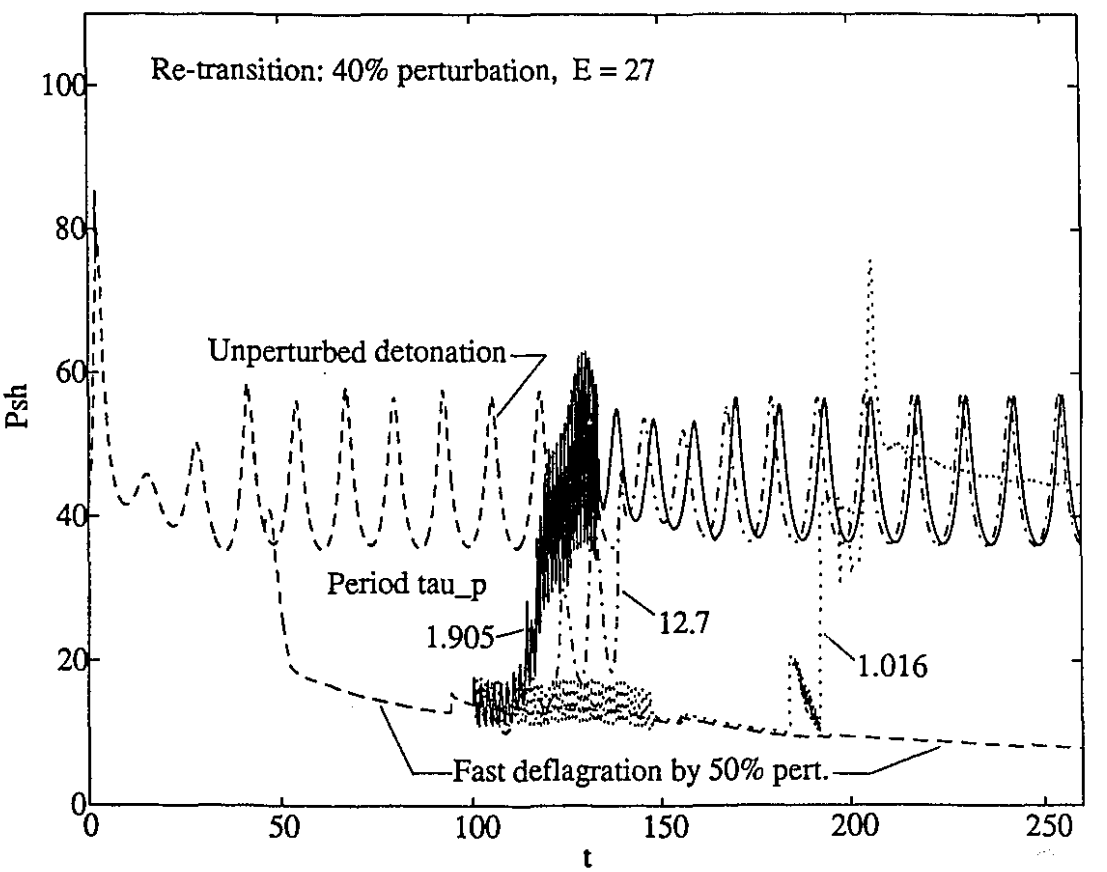

Figure 4.10: Re-transition of detonation using 40 percent periodic density perturbations applied at $t_0 = 100$. Perturbation periods shown are τ_p of 1.016, 1.905, 12.7.

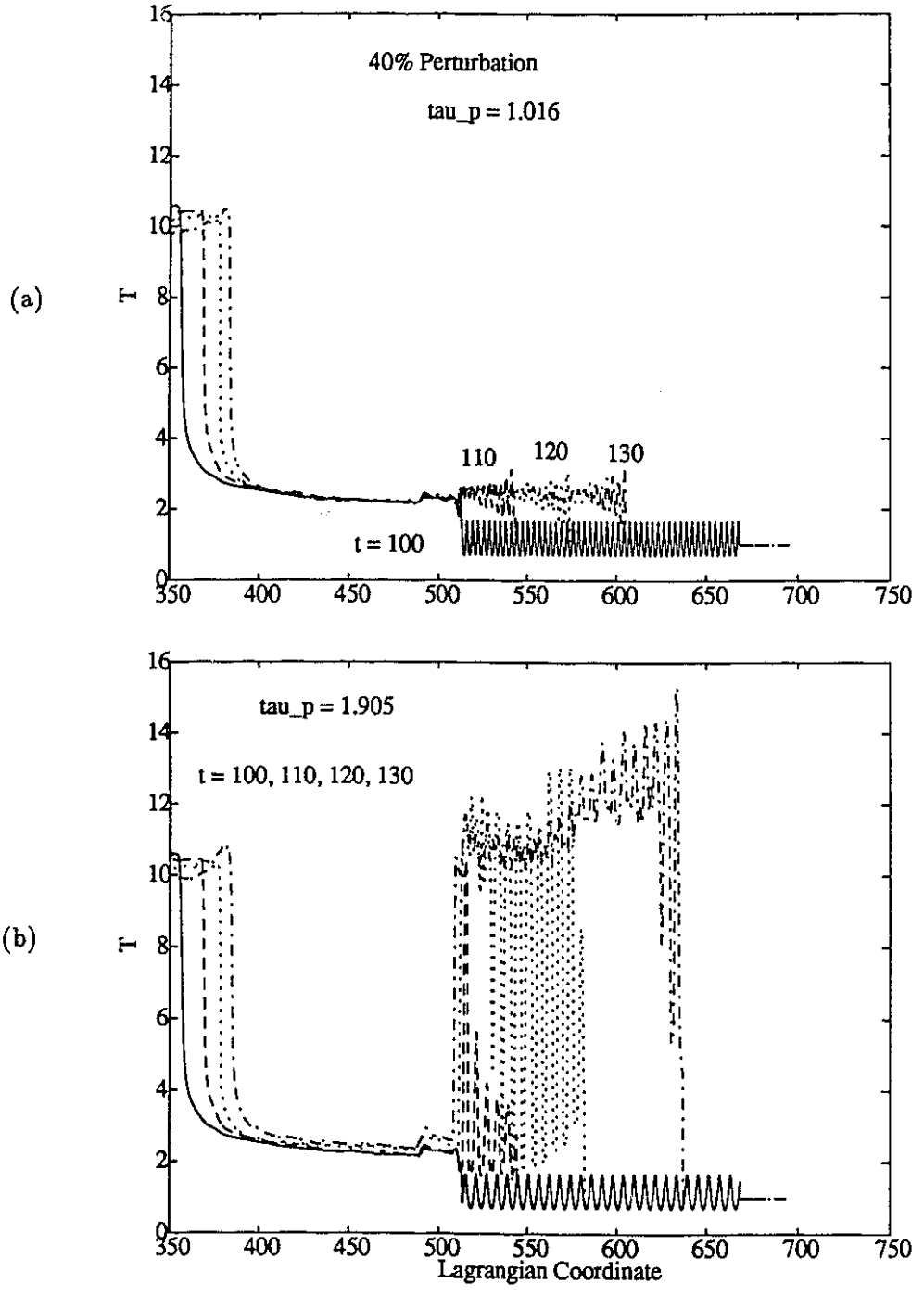

Figure 4.11: Amplification of temperature perturbations for different perturbation periods displayed in Lagrangian coordinate ξ. $E = 27$, 40 percent density perturbations. (a) $\tau_p = 1.016$, (b) $\tau_p = 1.905$.

(c)

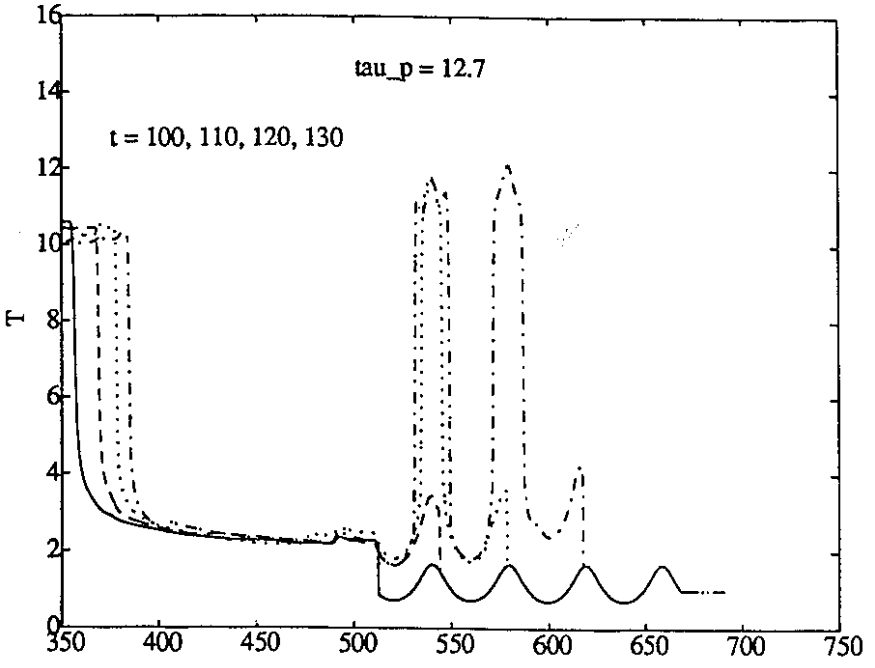

(d)

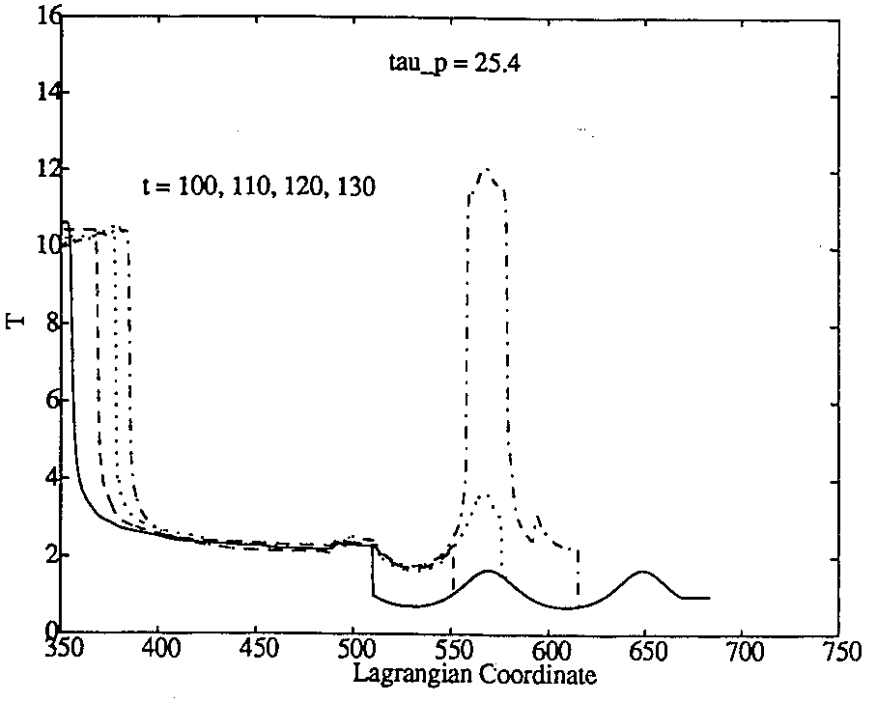

Figure 4.11: (c) $\tau_p = 12.7$, (d) $\tau_p = 25.4$.

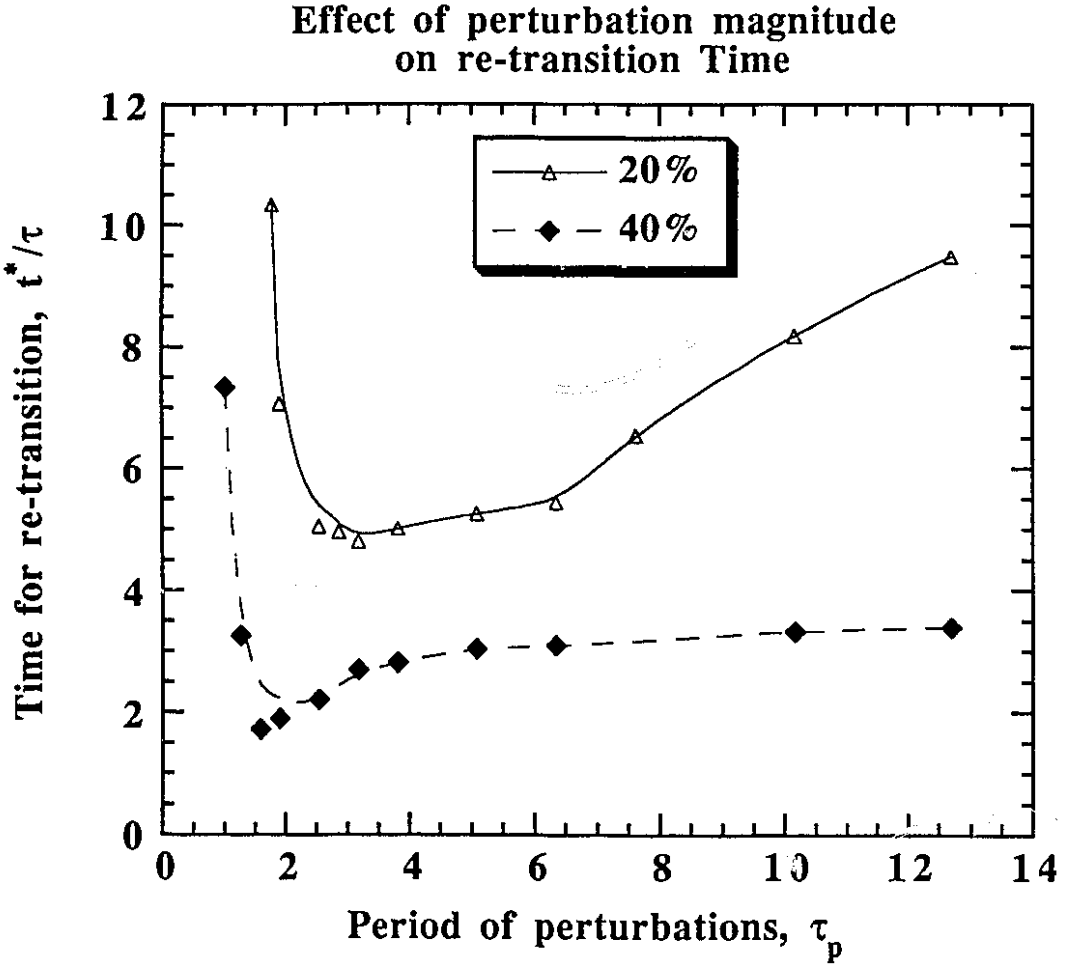

Figure 4.12: Time for re-transition versus the period of the applied perturbation for different amplitudes of density perturbation to induce transition.

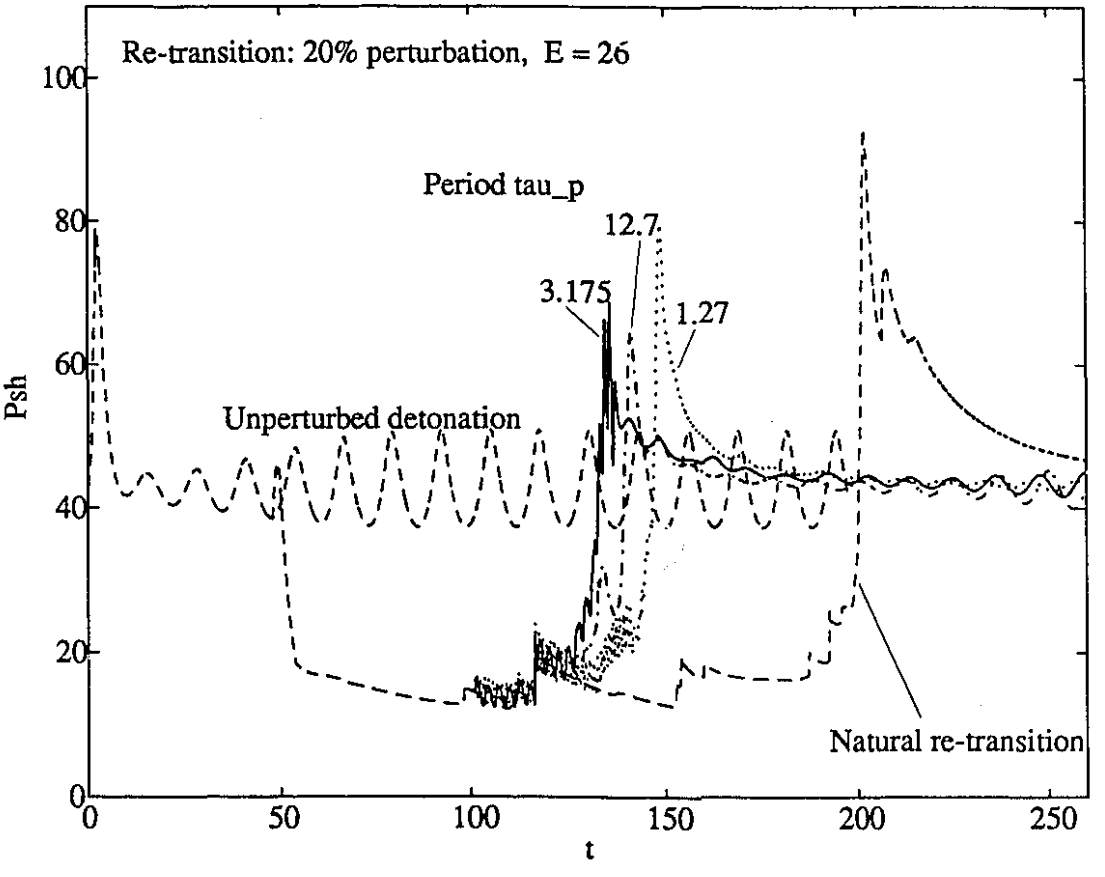

Figure 4.13: Re-transition of detonation using periodic density perturbations for $E = 26$. Perturbation periods shown are τ_p of 1.27, 3.175, and 12.7.

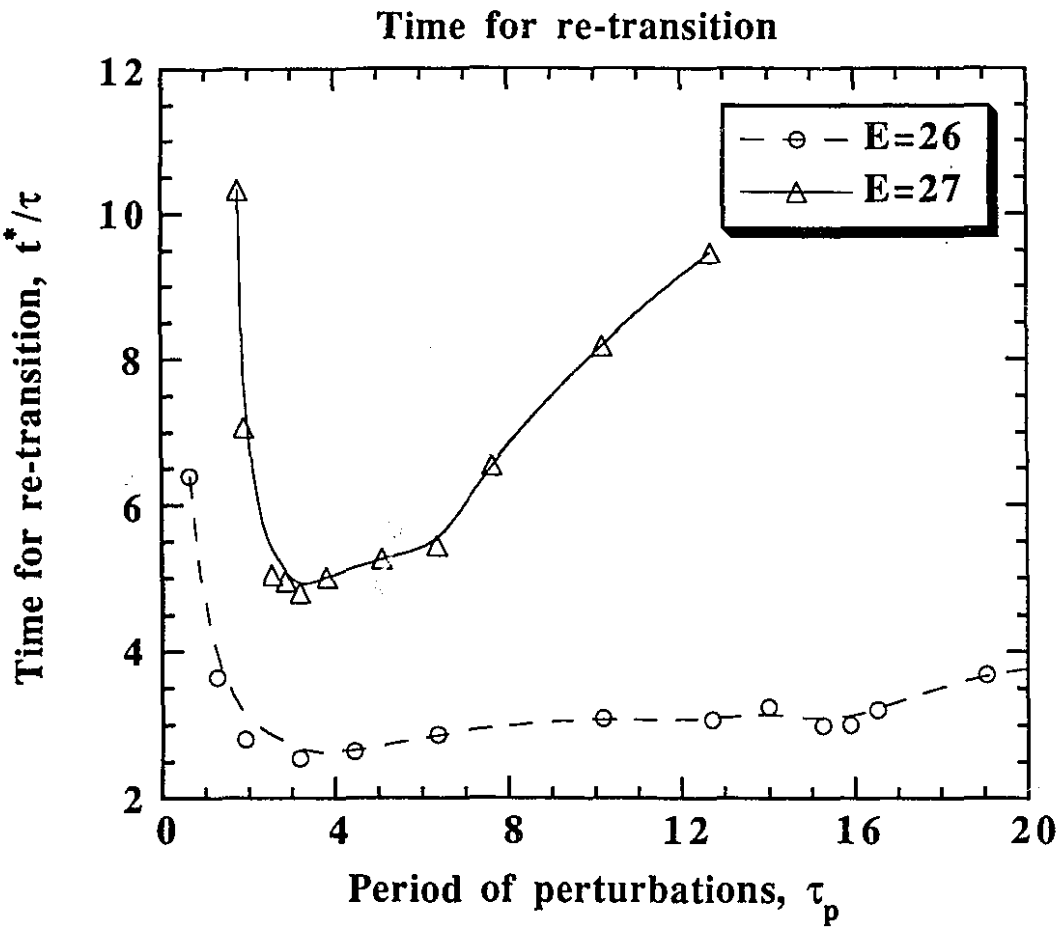

Figure 4.14: Time for re-transition versus the period of the applied perturbation for different activation energies.

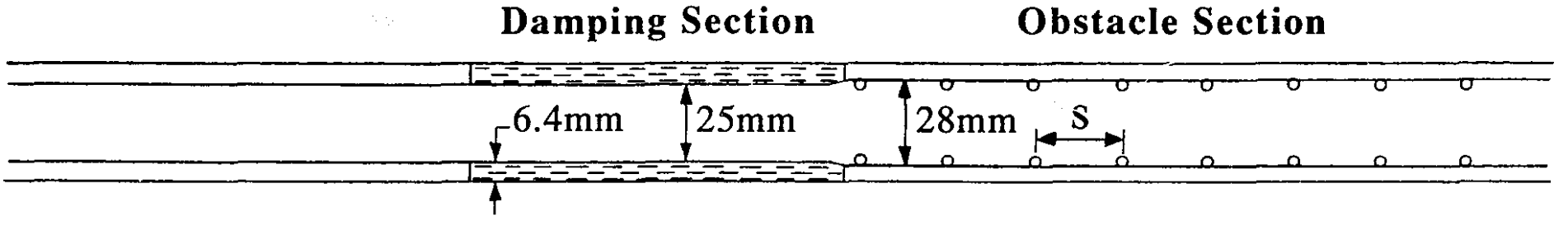

Figure 5.1: Sketch of the damping and test sections: channel width is 1.6 cm, and s is obstacle spacing.

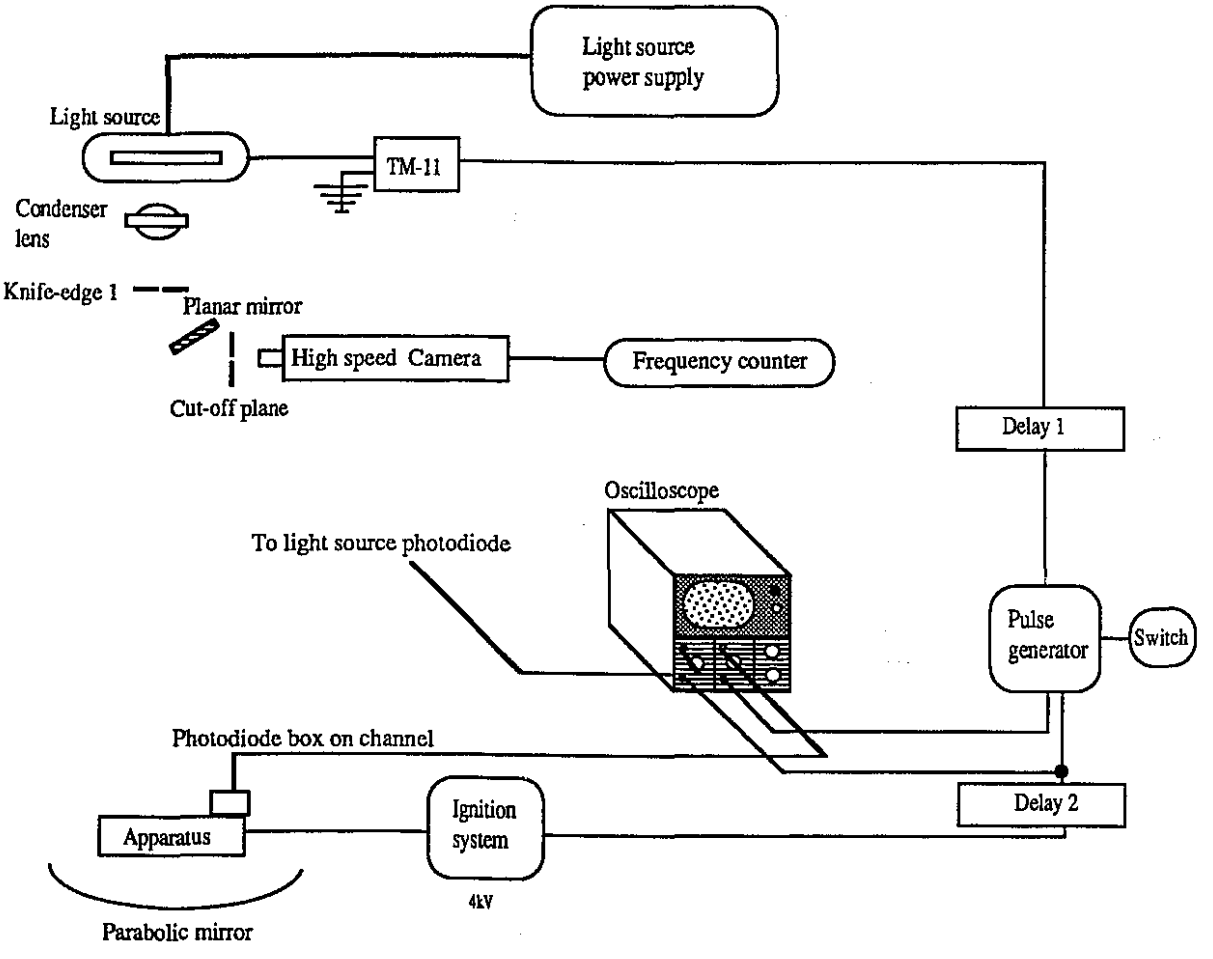

Figure 5.2: Schematic of the experimental set-up and the optical system.

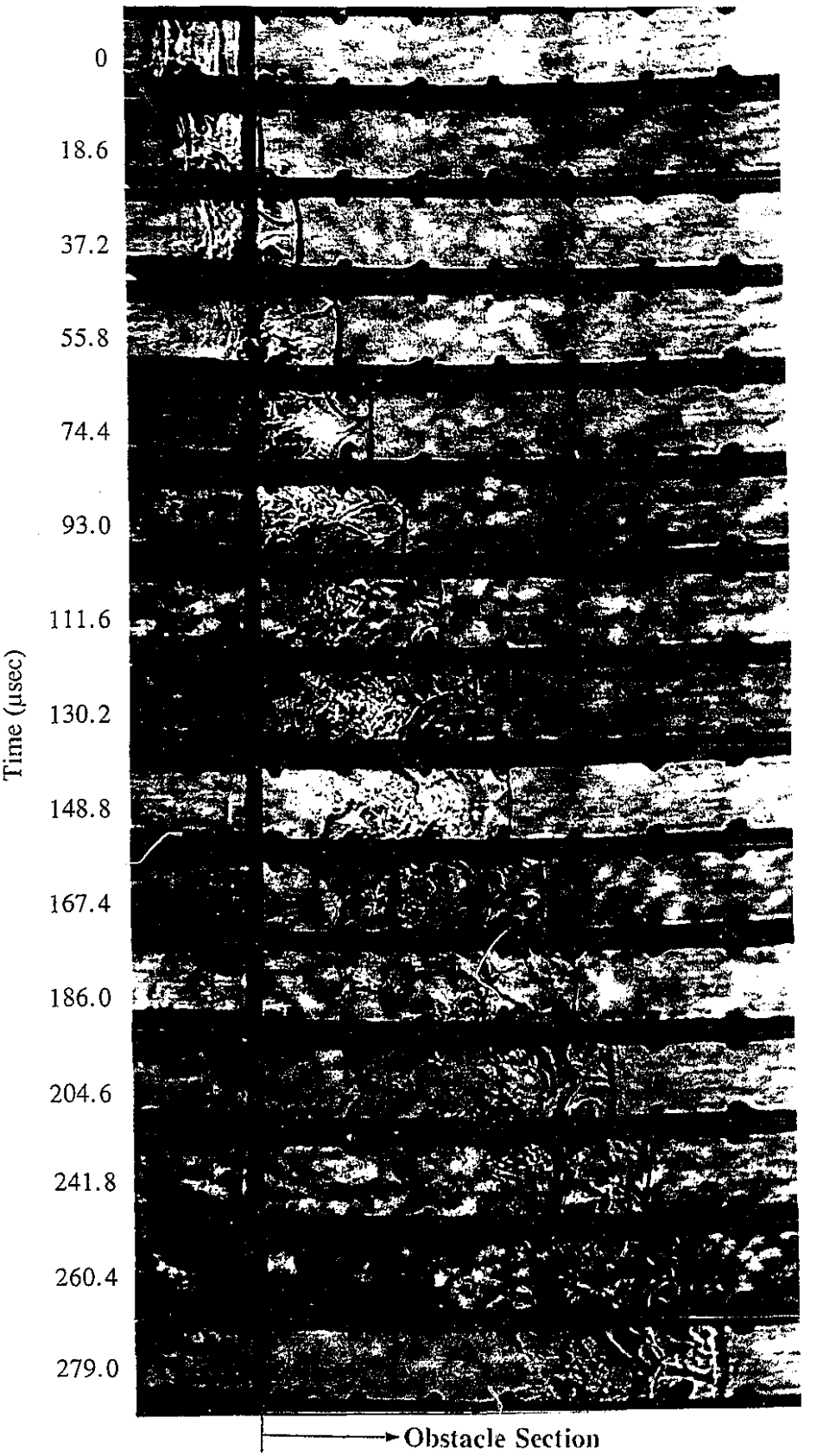

Figure 5.3: Laser stroboscopic Schlieren photographs of the propagation of the fast deflagration in the obstacle section, obstacle spacing equals channel height (28 mm), $2C_2H_2 + 5O_2 + 75\%Ar$ at 100 Torr, transition not observed: black vertical marker at the left denotes the beginning of the obstacle section, 18.6 μsec between frames, the first frame is arbitrarily labeled as time 0.

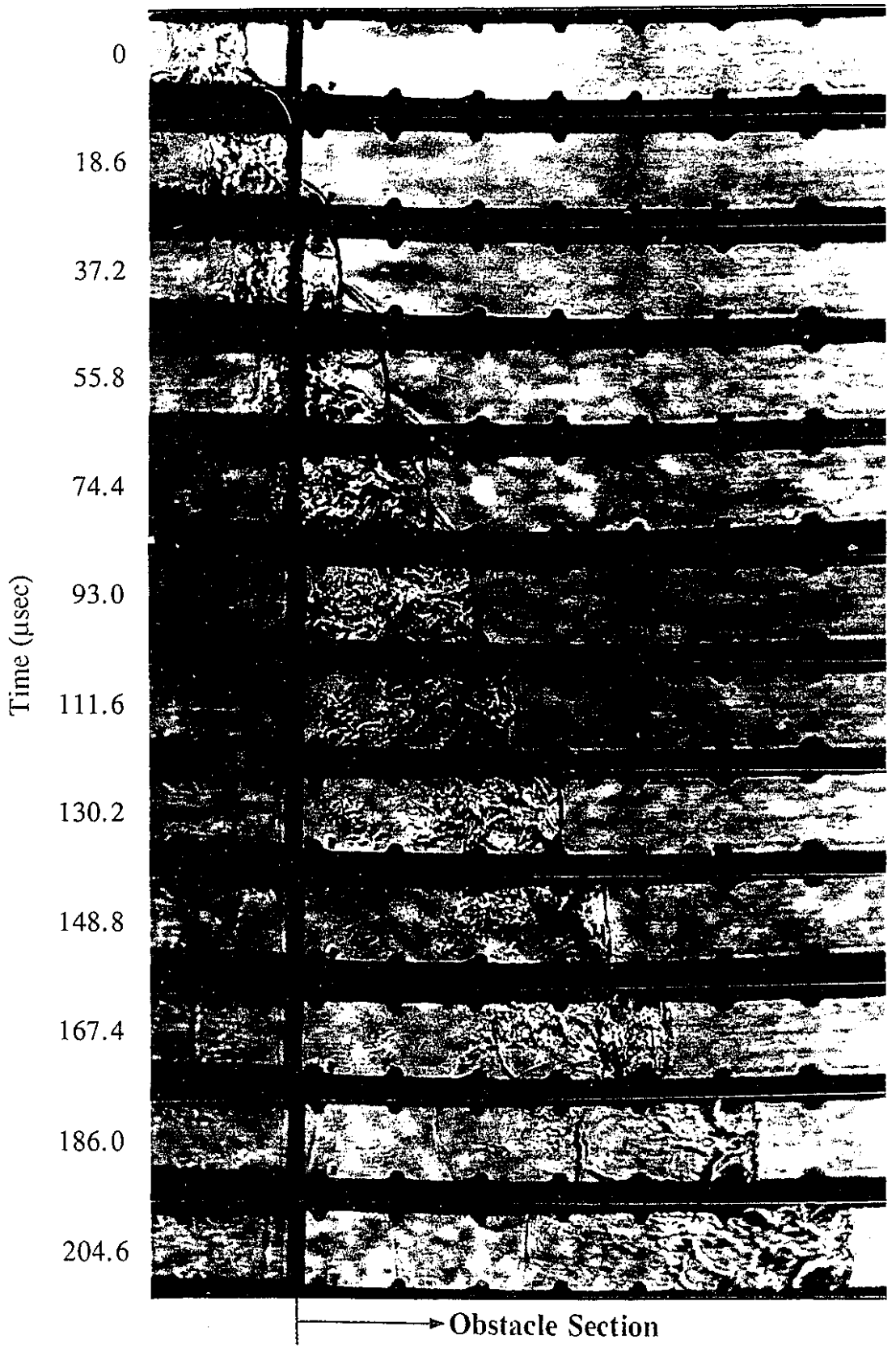

Figure 5.4: Laser stroboscopic Schlieren photographs of the transition of the fast deflagration in the obstacle section as initial pressure is increased to 140 Torr. See Fig. 5.3 for legend.

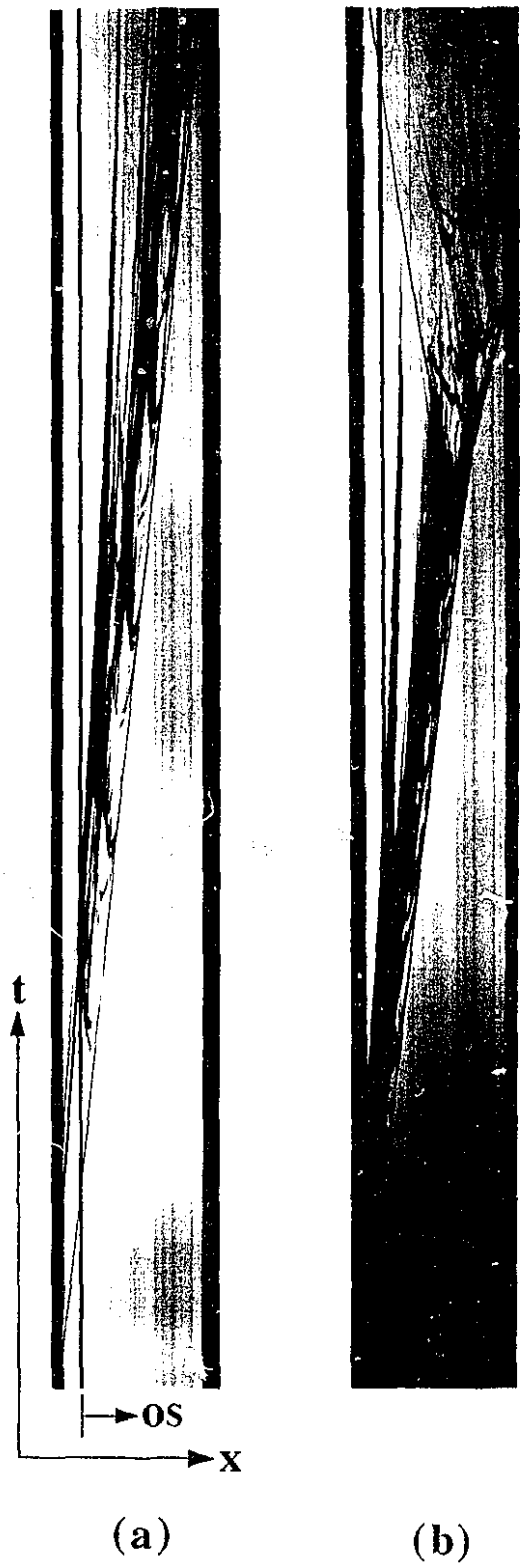

Figure 5.5: Streak photographs illustrating the effect of initial pressure on transition, $2C_2H_2 + 5O_2 + 75\%Ar$ at (a) 100 Torr and (b) 135 Torr. The thin black vertical line on the left of each photograph denotes the beginning of the obstacle section (os).

Figure 5.6: Streak photographs illustrating the effect of obstacle spacing on transition, $2C_2H_2 + 5O_2 + 75\%Ar$: (a) s = 10 mm at 122 Torr, (b) s = 20 mm at 125 Torr, (c) s = 28 mm at 127 Torr, (d) no obstacles at 160 Torr. The thin black vertical line on the left of each photograph denotes the beginning of the obstacle section (os).

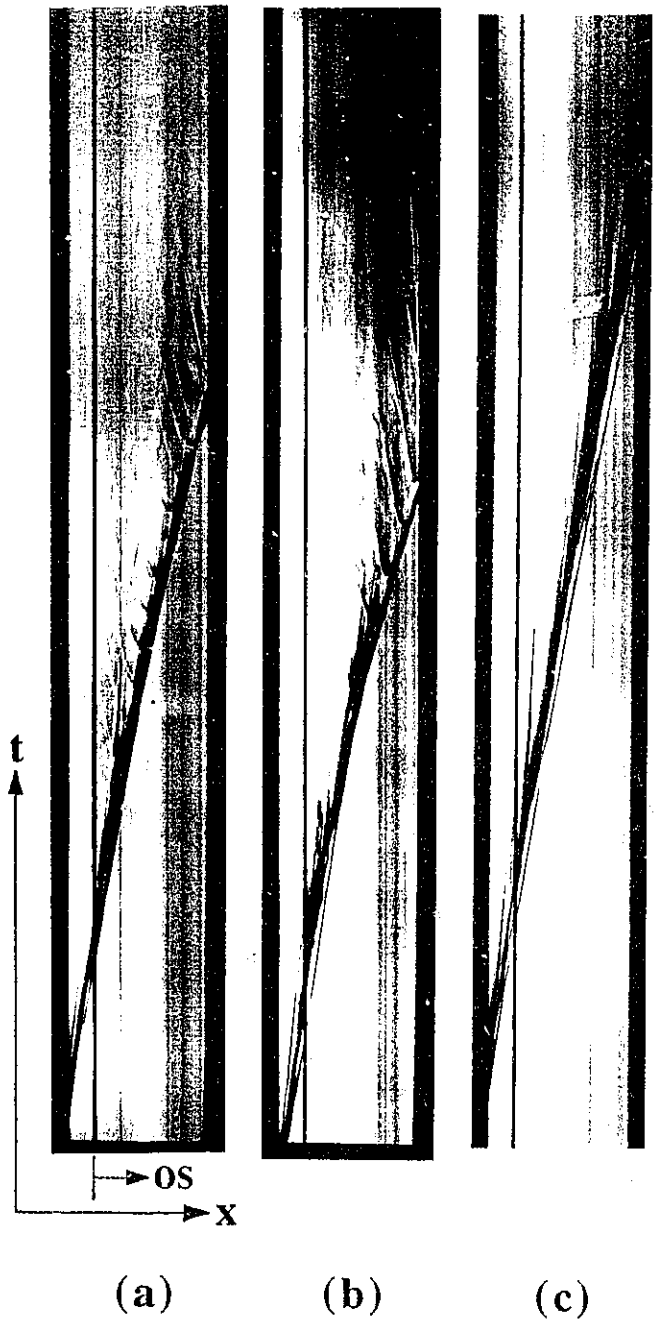

Figure 5.7: Streak photographs illustrating the effect of obstacle spacing on transition, $C_3H_8 + 5O_2$ near the initial pressure of 35 Torr: (a) s = 10 mm at 38 Torr, (b) s = 20 mm at 35 Torr, (c) no obstacles at 35 Torr. The thin black vertical line on the left of each photograph denotes the beginning of the obstacle section (os).

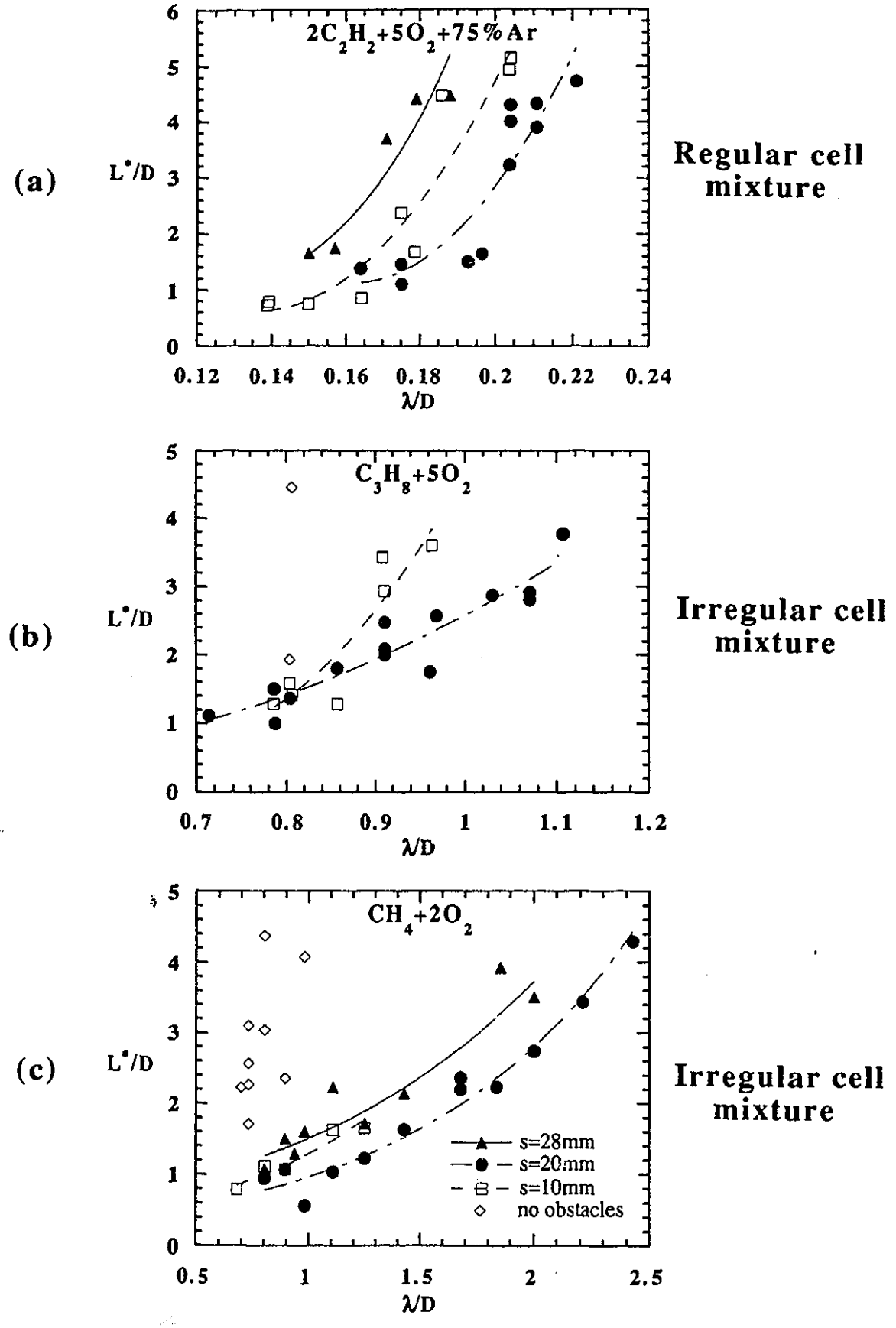

Figure 5.8: Transition distance L^* versus mixture sensitivity (cell size λ), nondimensionalized with channel height D: (a) $2C_2H_2 + 5O_2 + 75\%Ar$, regular detonation cell structure, (b) $C_3H_8 + 5O_2$, irregular detonation cell structure, (c) $CH_4 + 2O_2$, irregular detonation cell structure.

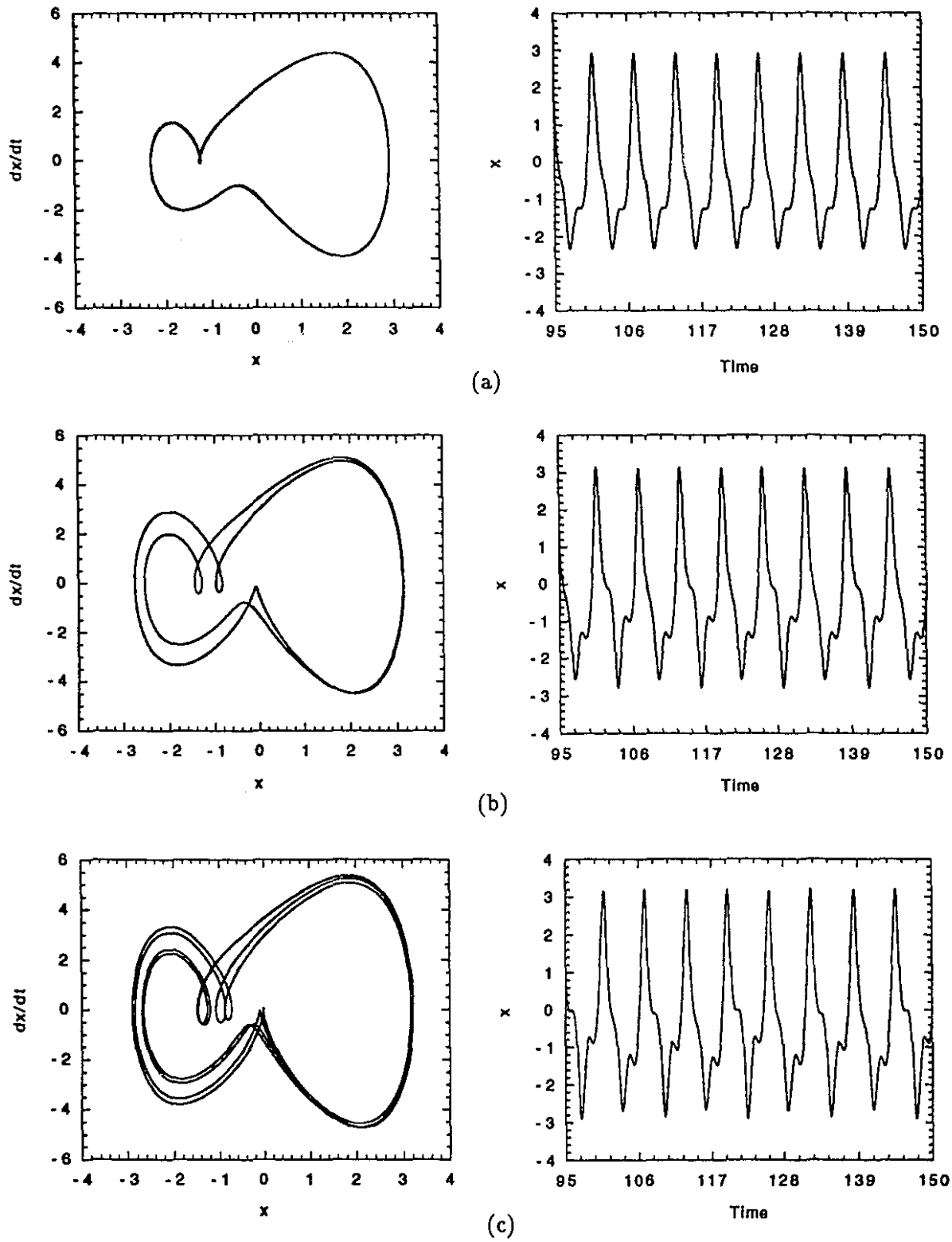

Figure 6.1: $x - \dot{x}$ phase portrait and temporal evolution of the Duffing equation. $\beta = 0.35, \sigma^2 = 0, \delta = 1, \omega = 1$. $x(0) = \dot{x}(0) = 0$. (a) $\alpha = 6.5$, limit cycle occurs, (b) $\alpha = 8.0$, period doubling has occurred, (c) $\alpha = 6.5$, period is now four times larger than the original cycle in (a).

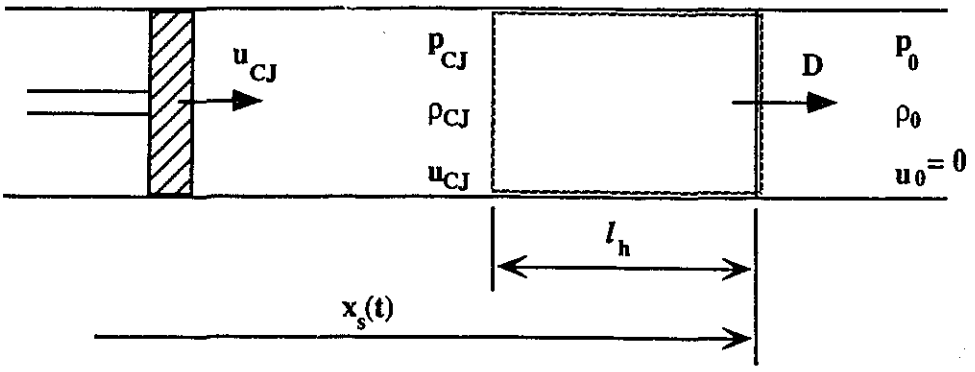

Figure 6.2: Schematic of an open system for the one-dimensional detonation bounded by the shock front and the Chapman-Jouguet surface.

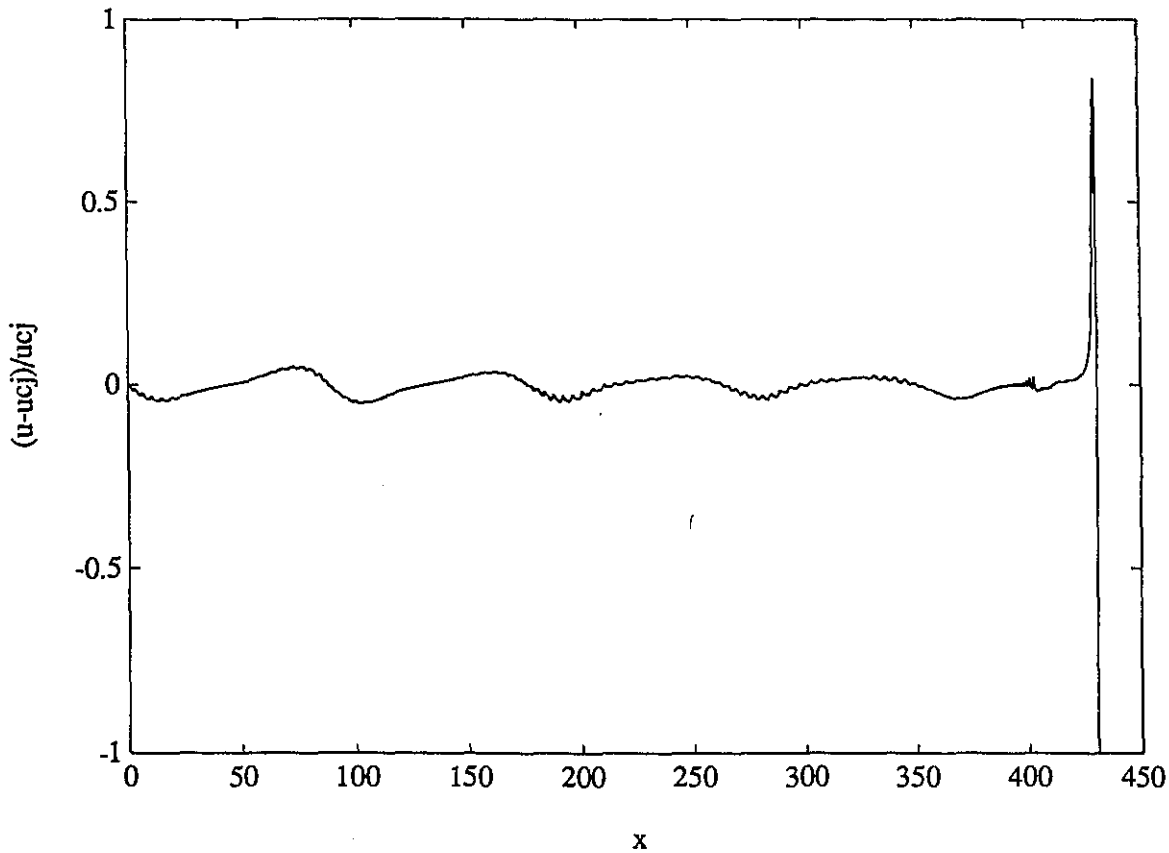

Figure 6.3: Spatial profile of particle velocity with respect to the CJ surface at $t = 124.3$, $f = 1, \gamma = 1.2, Q = 50, E = 27$.

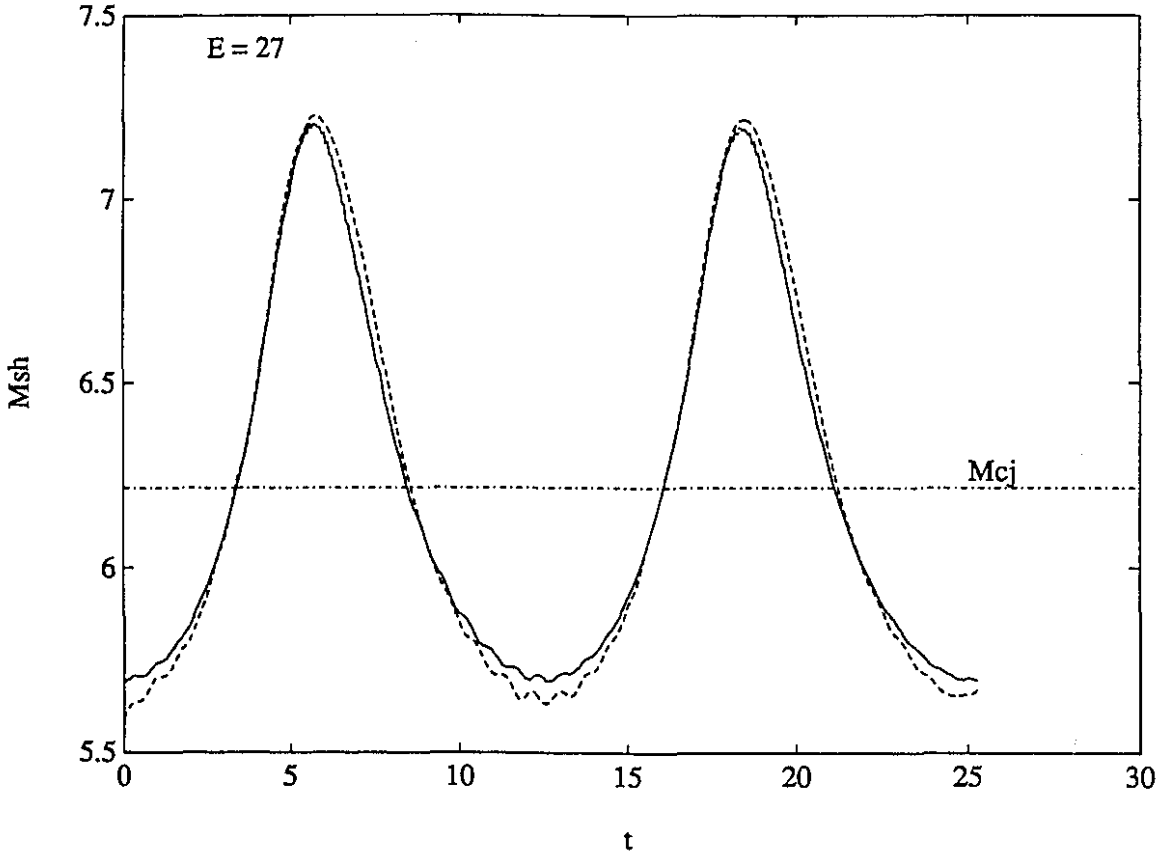

Figure 6.4: Temporal evolution of shock Mach number. $f = 1, \gamma = 1.2, Q = 50, E = 27$. —— full solution from direct numerical simulation; - - - - solution of oscillator equation (6.23) with $l_h = 20$.

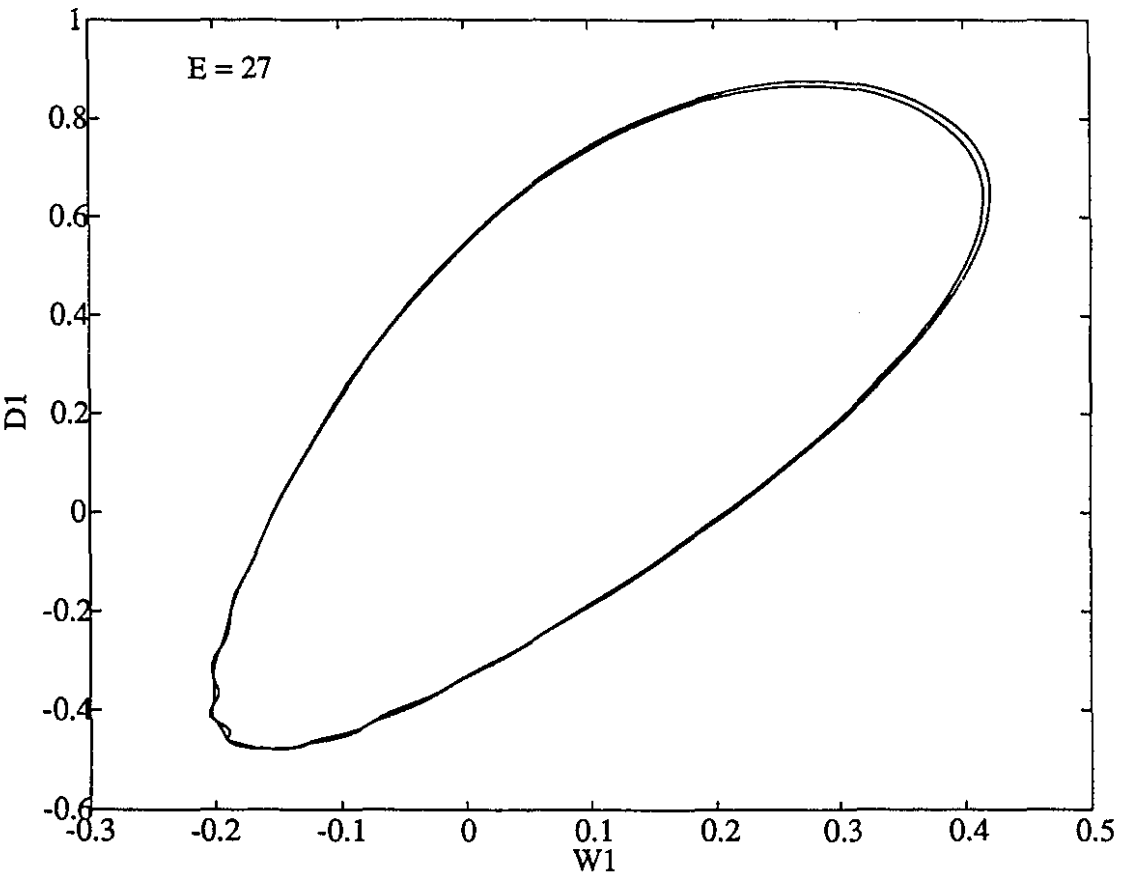

Figure 6.5: Phase protrait of shock velocity fluctuation D_1 versus fluctuation of reactant depletion rate W_1, $D_1 = \dot{F}/D_{CJ}, W_1 = W - 1, W$ given by eqn. (6.20). $f = 1, \gamma = 1.2, Q = 50, E = 27$.

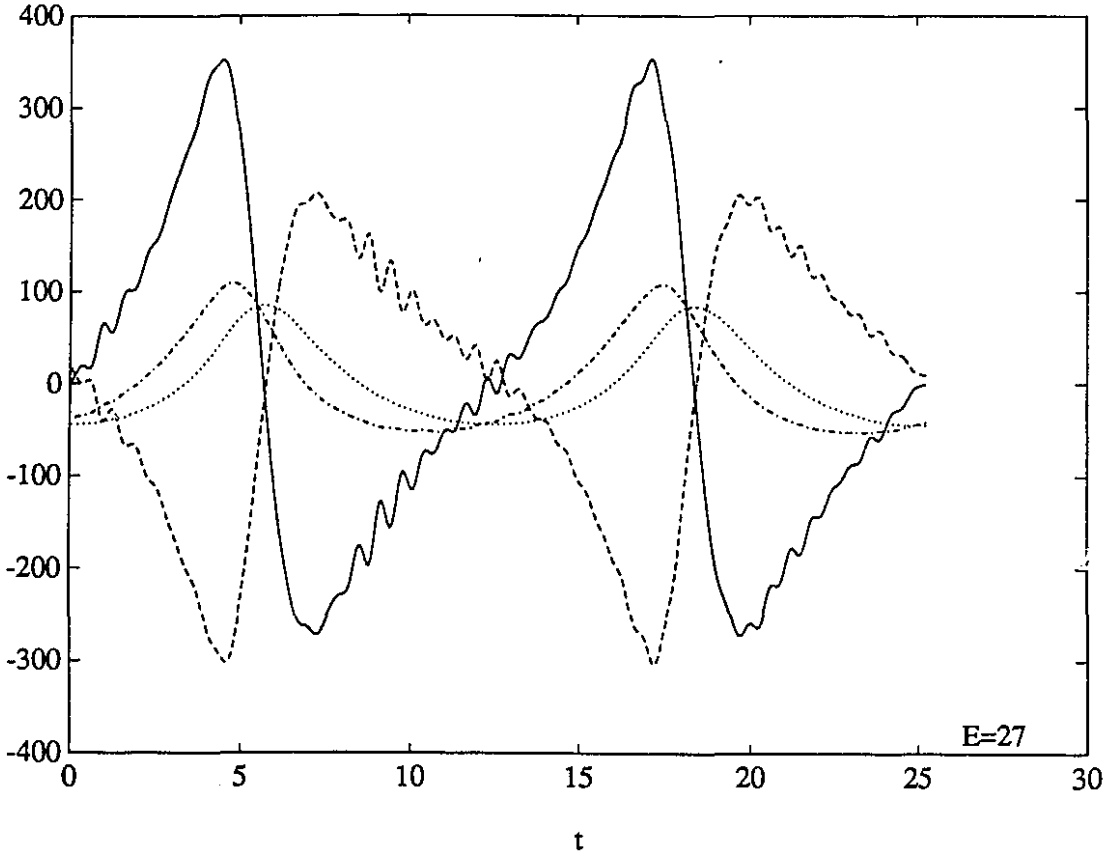

Figure 6.6: Temporal evolution of the four terms in the oscillator equation (6.23). $f = 1, \gamma = 1.2, Q = 50, E = 27$. —— $l_h I D \ddot{F}$, - - - - $l_h D^2 \dot{I}/2$, ... $\frac{\rho_{CJ}}{\rho_0} e_{CJ} \dot{F}$, ... $D_{CJ} Q W_1$.

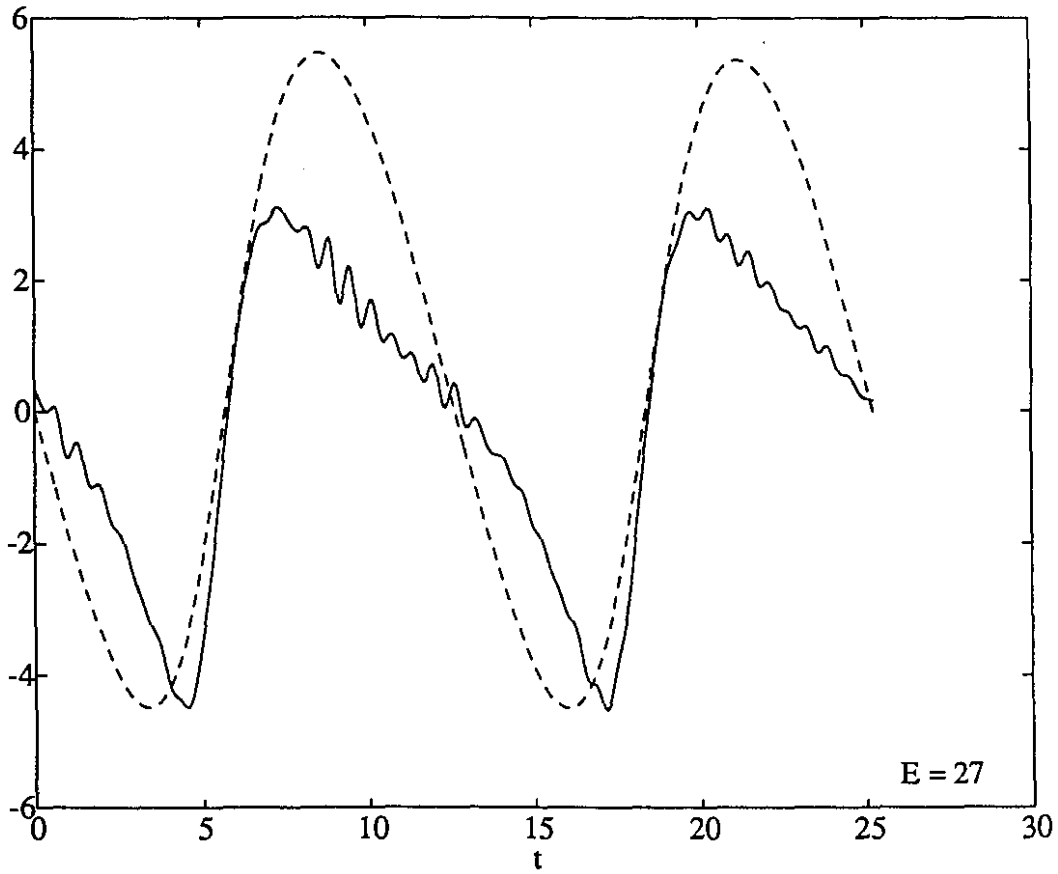

Figure 6.7: Temporal evolution of rate of internal-kinetic energy fluctuation (i.e., —— $D\dot{I}$, - - - - $4F$).

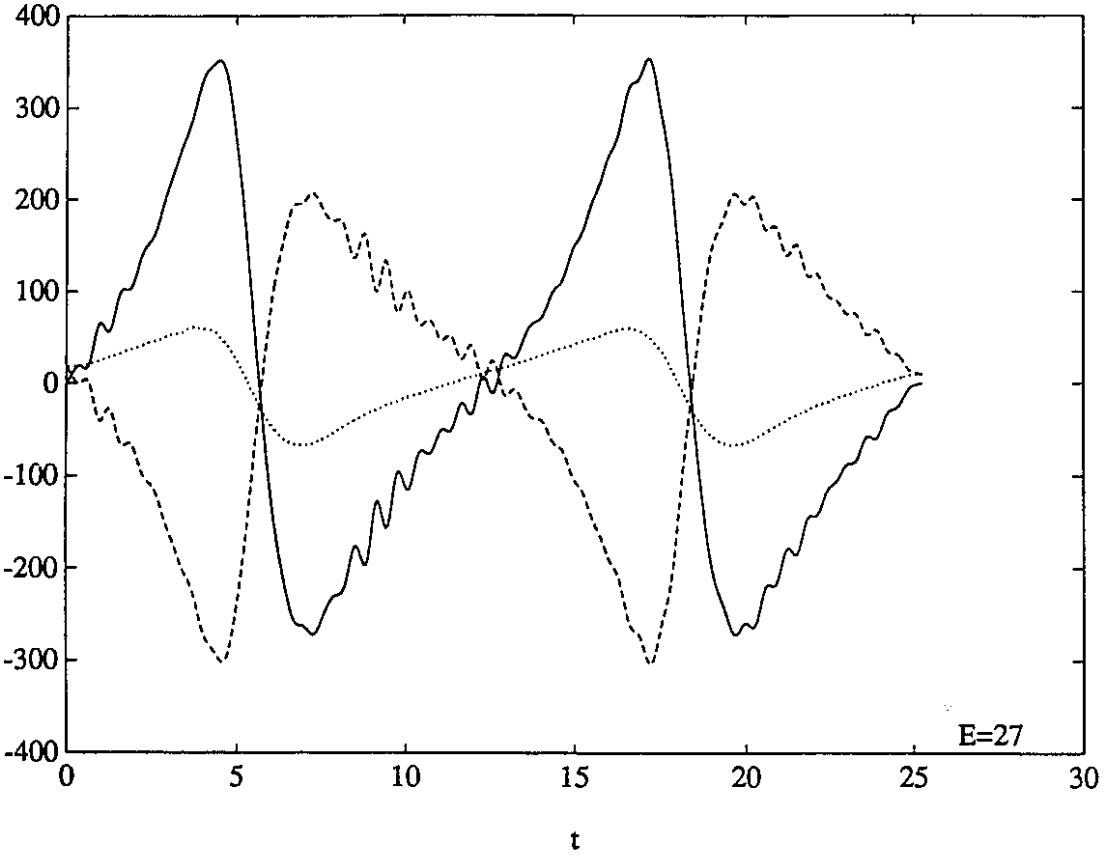

Figure 6.8: Temporal evolution of net energy input (i.e., μf) and terms of oscillator equation (6.23). $f = 1, \gamma = 1.2, Q = 50, E = 27$. —— $l_h I D \ddot{F}$, - - - - $l_h D^2 \dot{I}/2$, $\cdots\cdots \mu f(F, \dot{F})$.

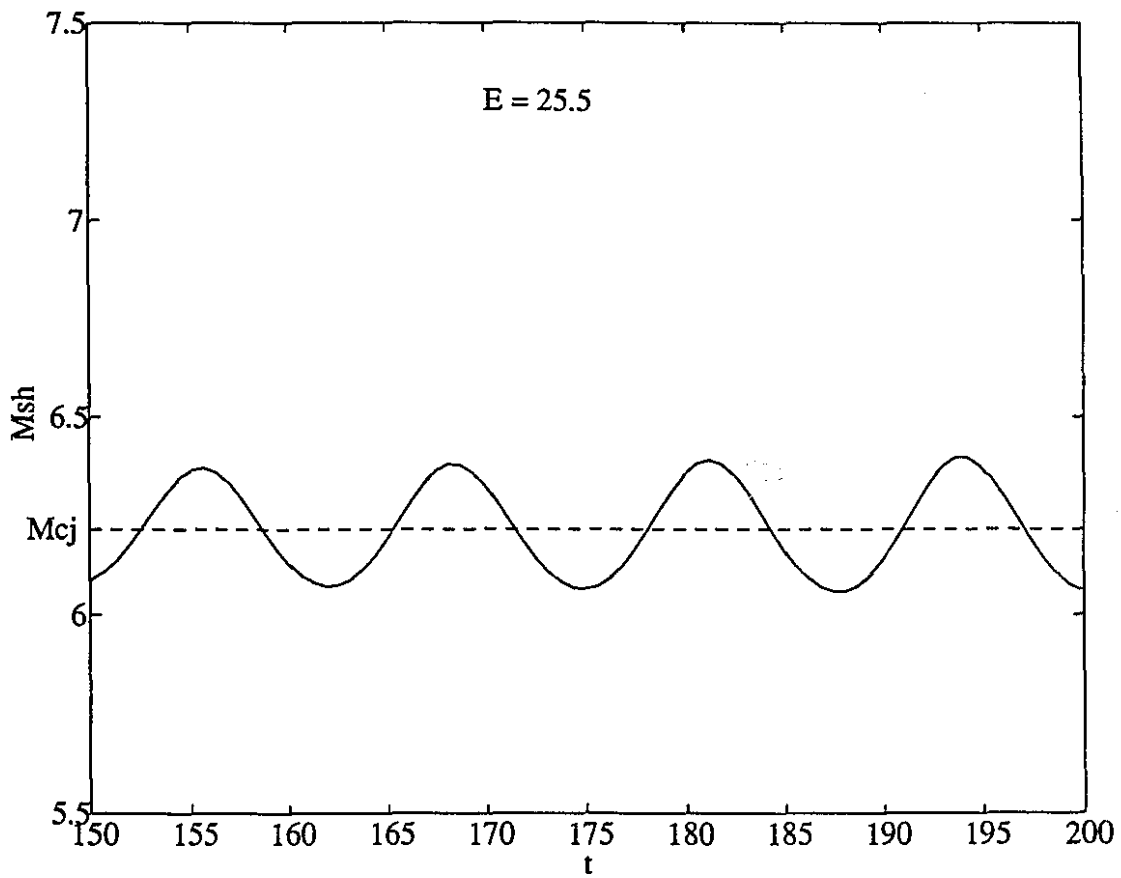

Figure 6.9: Temporal evolution of shock Mach number for $E = 25.5$.

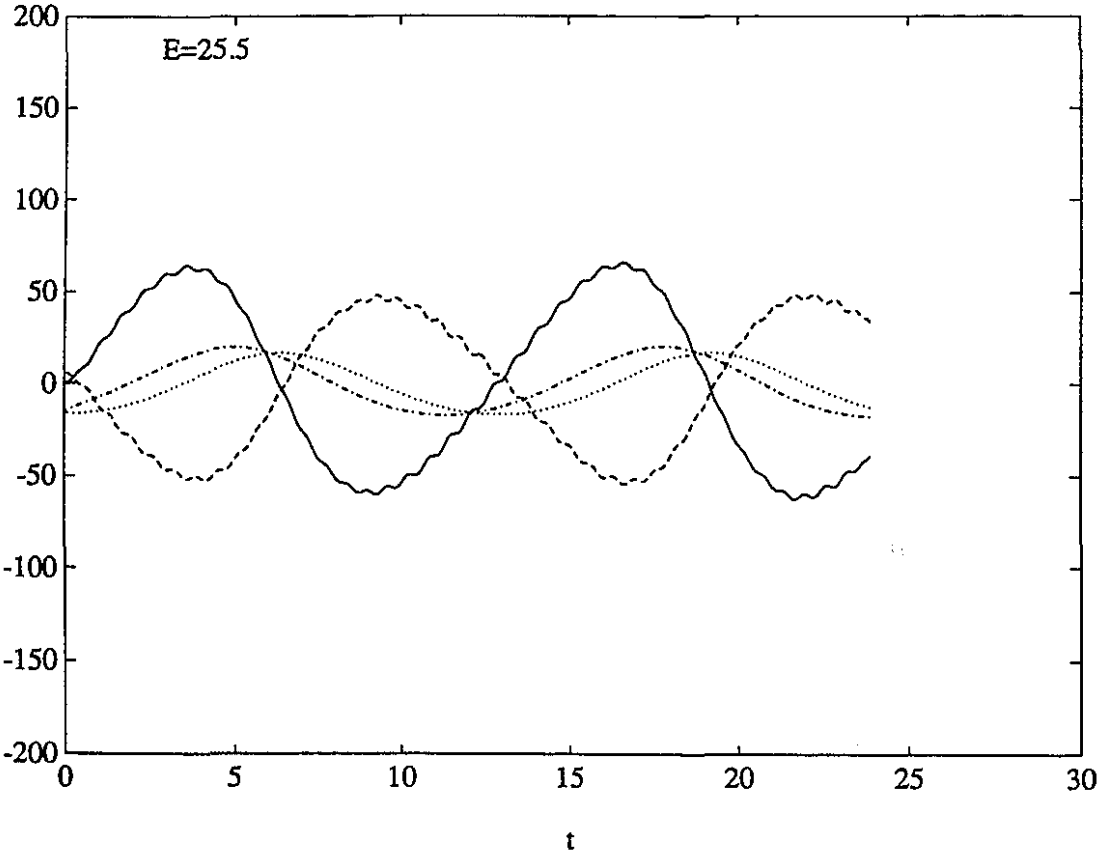

Figure 6.10: Temporal evolution of the four terms in the oscillator equation (6.23) for $E = 25.5$. —— $l_h I D\ddot{F}$, - - - - $l_h D\dot{I}/2$, · · · · · $\frac{\rho_{CJ}}{\rho_0} e_{CJ}\dot{F}$, ·-·-·-· $D_{CJ}QW_1$.

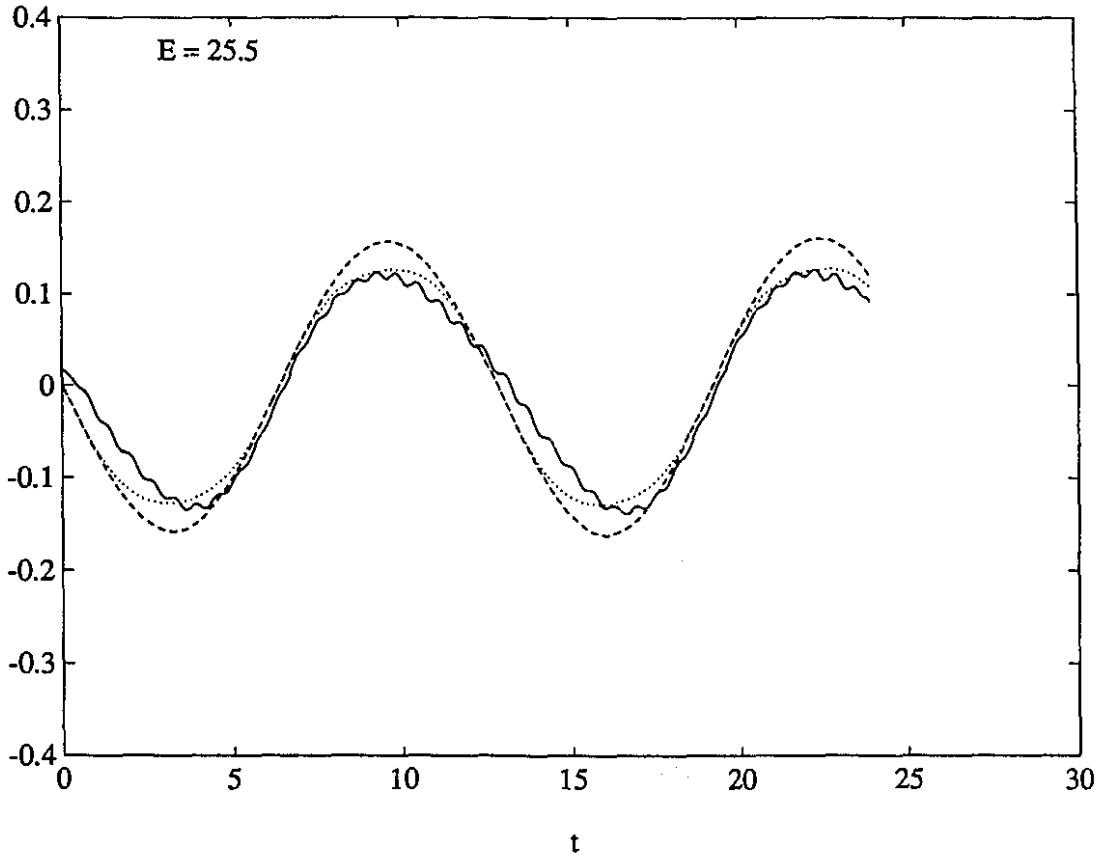

Figure 6.11: Comparison of temporal evolution of term $\dot{I}$ of oscillator eqn. (6.23) and F of eqn. (6.28). $E = 25.5$. —— $\dot{I}$, - - - - kF, · · · · $kF - 0.75F^3$, where $k = b_0/D$.

(a)

(b)

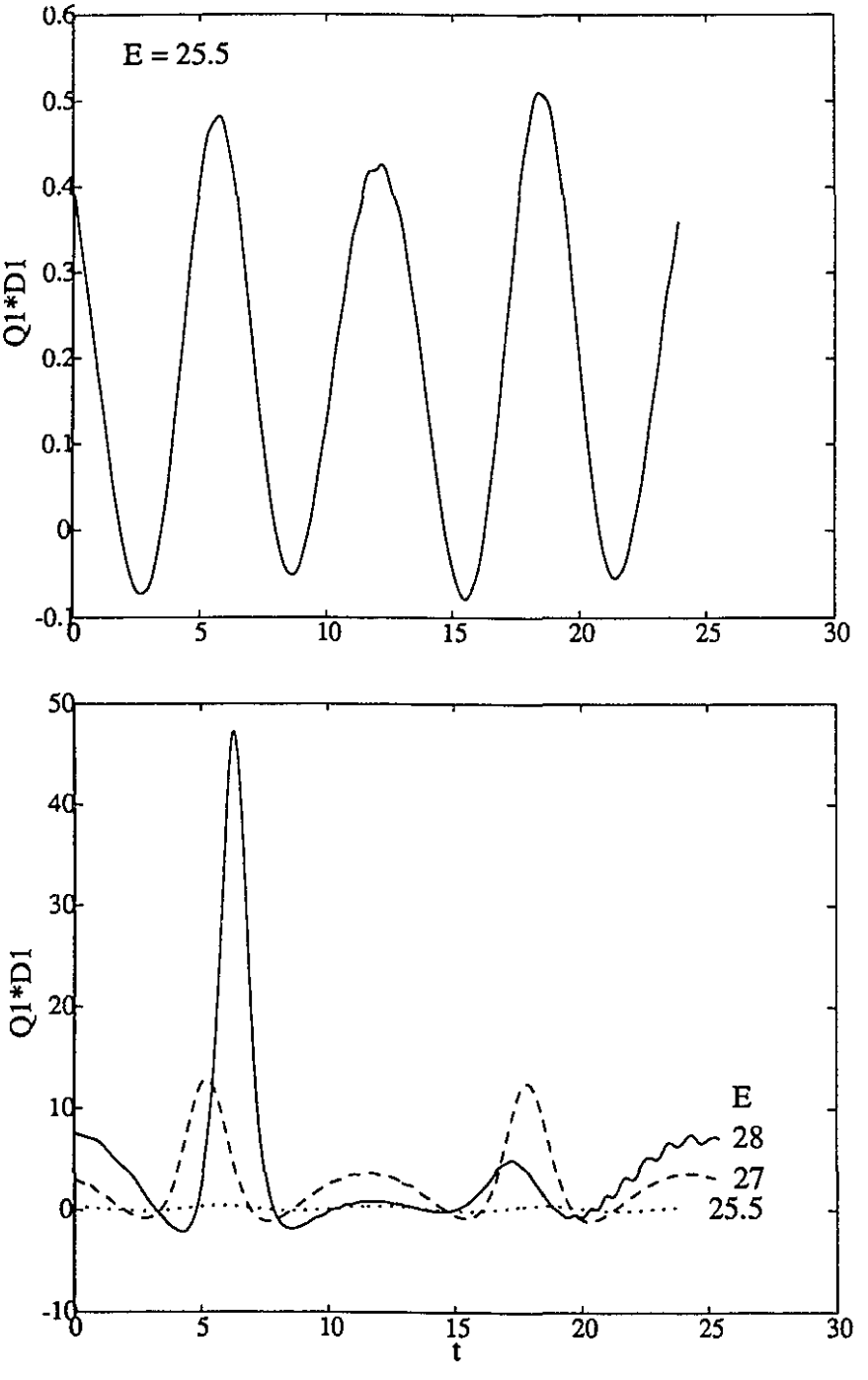

Figure 6.12: Temporal evolution of product of unsteady chemical energy release and shock velocity fluctuation (i.e., $\dot{Q}_1 D_1$). (a) $E = 25.5$, (b) $\cdots\cdots E = 25.5$, - - - - $E = 27$, —— $E = 28$.

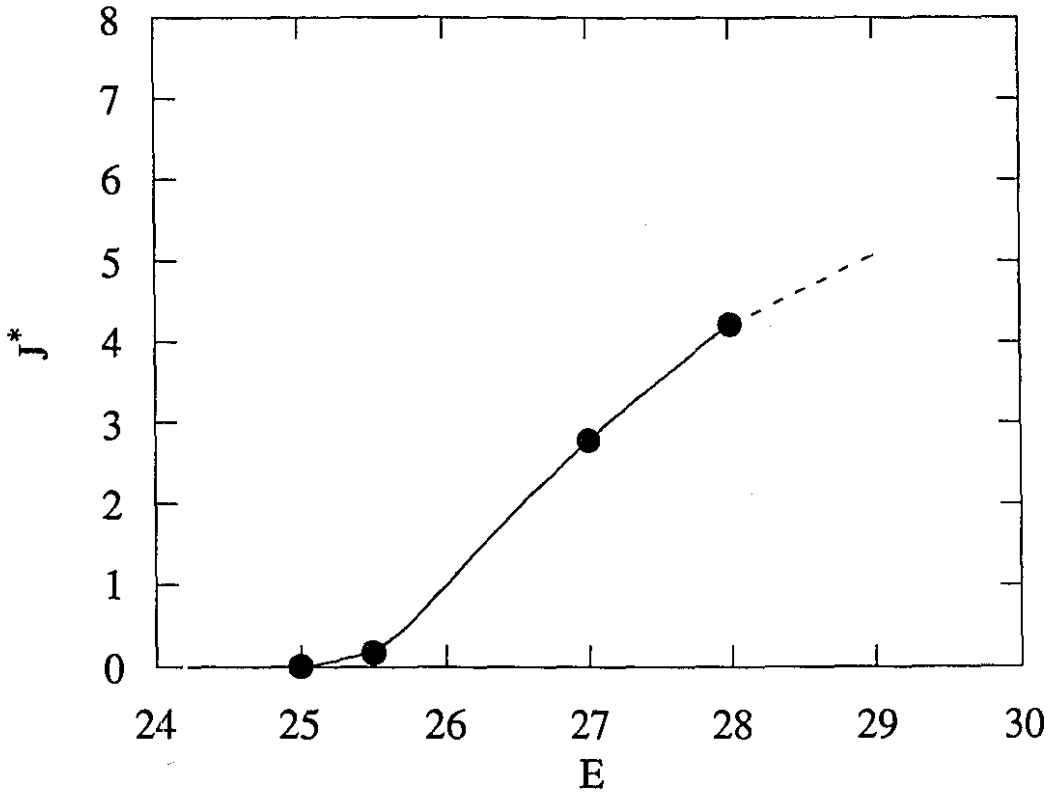

Figure 6.13: Integral value of unsteady chemical energy release and shock velocity fluctuation over a cycle (i.e., J) with respect to E. $J^* = J/(\rho_0 D_{CJ} R T_0)$.

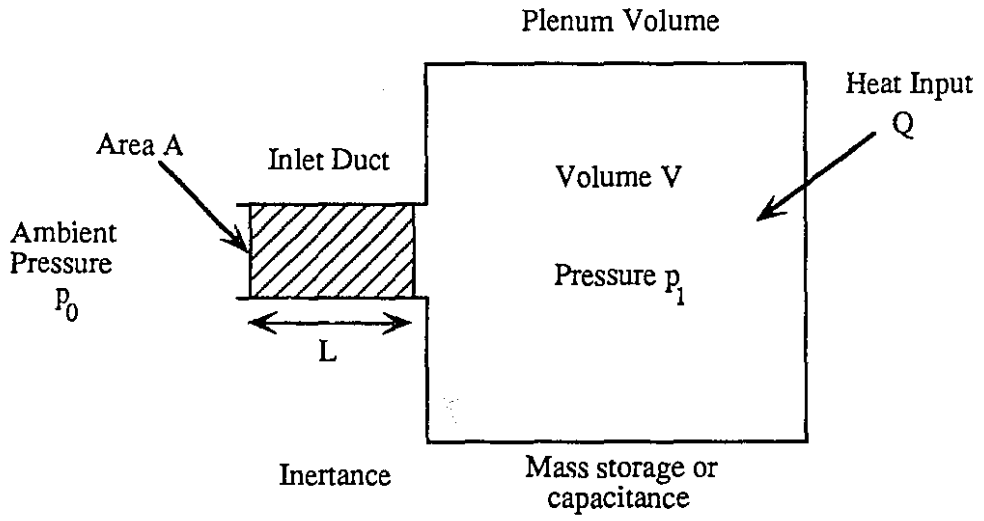

Figure B.1: Schematic of the Helmholtz Oscillator.